MARINE GROWTH AND THE HYDRODYNAMIC LOADING OF OFFSHORE STRUCTURES

by

ANDREAS THEOPHANATOS, B.Sc., M.Sc.

A thesis submitted for the degree of
Doctor of Philosophy

Ship and Marine Technology Division
Department of Mechanical and Process Engineering
University of Strathclyde

February 1988

SOME PAGES BOUND INTO/CLOSE TO SPINE.

To Helen, Anna and my parents

"...the use of dimensionless parameters reduces the number of independent coordinates required. A convenient way to realise the importance of such a reduction is to recall that a function of one independent coordinate can be recorded on a single line; two independent coordinates, a page; three require a book; and four, a library."

S.J. Kline
(Similitude and Approximation Theory)

SUMMARY

This thesis presents the results of a study on the effects of marine growth on the hydrodynamic loading of offshore structures and proposes an approach that can be adopted by designers and operators to quantify these effects. The approach is based upon the realistic characterisation of marine growth and its temporal variations during the life span of template structures.

Past research work and current design, inspection and maintenance practices are critically reviewed and their limitations with respect to marine growth are highlighted. The ecology of marine growth for a sample of North Sea platforms was examined to establish the variety and physical attributes of the fouling colonies. The traditional single-parameter characterisation of marine roughness was found to be inadequate. Appropriate parameters, verified by fluid loading experiments, are established.

Details of the laboratory experiments undertaken with both real marine growth and artificial macro-roughness on circular cylinders are given. These tests were carried out at large scale (cylinders up to 521mm diameter) in a novel "buoyant cylinder" test rig (steady flow) and in a large wave flume (regular waves). A wide range of parametric variations were undertaken for the various types of marine growth in an attempt to establish a comprehensive database from which the loading effect of any likely, practically occuring, marine growth pattern can be estimated. The extent to which this is achieved and the requirements for further research are discussed in detail.

It is concluded that the effects of marine growth are both substantial and diverse. Drag forces vary with type of fouling, overall thickness, surface cover, and distribution. Finally, detailed procedures are recommended for the design of new structures and the improved loading assessment of existing ones.

ACKNOWLEDGEMENTS

This study would never have come to fruition without the continual guidance of Dr Julian Wolfram of the Ship and Marine Technology Division. I am very grateful to Julian Wolfram not only for his keen interest and enthusiasm and his contribution to every single aspect of the project, but also because he taught me how to find practical solutions to engineering problems.

I sincerely thank Professor Chengi Kuo who initiated the "Design for Maintenance" theme from which this work emerged and who provided me with the opportunity to study for a higher degree.

I am indebted to Mr Charles Keay for his excellent technical support, dedication and physical effort in carrying out the labour intensive experimental programme. The contribution of Messrs Iain Bellingham and David Clelland is also acknowledged.

Thanks are due to the Science and Engineering Research Council and the U.K. Department of Energy who funded various stages of this project; the personnel of Britoil plc., BP Pet. Dev. Ltd, Mobil North Sea and Orca Ltd who kindly provided useful data; Dr David Edwards, Shell Expro, London and Dr Robin Wright, Shell Internationale B.V., The Hague for their valuable contribution at the earlier stages of the research.

Finally, I would like to express my gratitude to my wife Helen for her constant encouragement and well tried patience during the preparation of this thesis.

CONTENTS

CHAPTER 1. INTRODUCTION

Oil and gas platforms were first installed in the southern North Sea in the mid-1960's and they were followed a few years later by the development of the Forties field in the central North Sea. In those early days of North Sea hydrocarbon exploitation little attention was drawn to the potential problems associated with marine fouling. The design and operating experience which was available came predominantly from the moderate environment of the Gulf of Mexico and, as North Sea related data were non-existent, gross simplifications of the environmental conditions within design practices were inevitable.

Not least of these was on the effects of marine growth to the hydrodynamic loading of template structures. Whilst it was a well known fact that marine growth significantly increases hydrodynamic forces this effect, though not completely overlooked, was certainly underestimated. The principal reasons were the severe paucity of information on the fouling levels expected in the North Sea and the lack of experimental data on the drag and inertia forces for macro-roughness.

Design practice is, however, evolutionary and is based on experience and current level of technological development. Initial experience in the North Sea indicated spectacular increases in the levels of marine growth which in many cases exceeded the allowances accounted for in the design. Within 3-4 years from the installation of the first southern North Sea platforms, 200mm thick mussel beds were reported on just 300mm diameter members located in the wave affected zone (top 30m water depth). In deeper waters, up to 250mm high sea anemones and soft corals were only too common. This had two implications:

- remedial cleaning had to be regularly carried out on those structures which had been designed using low marine growth tolerance limits and low drag coefficients;
- higher fouling thickness allowances and drag coefficients should be applied to future structures.

So new design practices evolved. For example, whilst the drag coefficients used in the North Sea in the late sixties were about 0.5 to 0.6 in the late seventies they were generally 0.7 to 0.8. Meanwhile, fresh research effort was directed towards the estimation of wave forces on rough cylinders which suggested the use of even higher drag

coefficients. Some designers have since adopted drag and inertia coefficients of 1.0 and 2.0 respectively for members near the surface and in addition to depth related marine growth thickness allowances of 50-150mm. These values have been somewhat intuitively based on limited full scale field data for largely unrepresentative marine growths and on smaller scale laboratory data for artificially roughened cylinders. Marine growth allowances were also ill-defined gross estimates of thickness which were expected to parameterise roughness conditions irrespective of type of fouling, non-uniformity, distribution, surface cover etc. Therefore, it is far from certain as to whether the adopted design practices have been adequate in estimating hydrodynamic loads on marine roughened structures.

The uncertainties have been further compounded with the recent expansion to the deeper and colder waters of the northern North Sea. The emergence of new types of growth, in the form of kelp and other long seaweeds, has caused concern among designers and regulatory authorities about the wave loads on kelp fouled tubular members.

However, marine growth and force coefficients form one part of the wave loading procedure. The view has been frequently expressed that since the other part, which includes idealisations of the flow field and predictions of expected wave heights and currents, is inherently conservative then any underestimations in fouling thickness or coefficients would be eventually counterbalanced. The use of conservatism to offset uncertainties is not the solution in itself and may be inordinately expensive. Conservatism in loading estimates must be accounted for by additional structural weight. On the other hand, if loadings were underestimated the integrity of the structure would depend upon its reserve strength and redundancy or the overloaded members would be strengthened or regular cleaning would be carried out. In either case the cost penalties are substantial.

The most effective way to reduce uncertainties in estimating hydrodynamic loads on marine fouled structures would be a systematic investigation into the fluid loading effects of marine growth. This would provide a database of appropriate force coefficients and address in a realistic manner the requirements for characterising marine growth.

That approach was adopted for the research study presented in this thesis. The study addresses the paucity of force coefficients for

marine roughened tubulars and the need for extensive experiments with different types of fouling. It also addresses the complete lack of force coefficients required to assess the sensitivity of hydrodynamic loads to variations in marine fouling as they occur during the in-service life of North Sea platforms. This may be of significance to fatigue damage calculations and to the structural assessment of existing installations. That is, the study considers how marine growth develops on a typical structure from the day it is installed up to decommission, on the basis of the ecological behaviour of fouling species and of strategically selected survey data about the state of marine growth on North Sea platforms [7].

It is upon such inter-disciplinary considerations that the systematic experimental investigation was carried out through large scale tests with macro-roughened circular cylinders in steady and wave flows. The majority of the experimental work formed part of the overall research programme entitled "Fluid Loading in Offshore Engineering", which was jointly funded by the Science and Engineering Research Council (S.E.R.C.), the U.K. Department of Energy and the industry sector.

An insight into the ecology of marine growth and its importance to design and maintenance of offshore structures is given in Chapter 3. In Chapter 4, past research work and current design, inspection and maintenance practices are critically reviewed. The proposed approach and its relationship to design and maintenance are described in Chapter 5. The findings on the state of marine growth patterns on six North Sea platforms are presented in Chapter 6. In Chapter 7, the experimental facilities and procedures for the steady flow tests are described followed by a detailed presentation of the results (Chapter 8). Although some of the experimental results have been published in [1,2,3,4,6] they are presented in Chapter 8 in a more organised fashion to identify the hydrodynamic significance of those roughness parameters which are necessary for the realistic marine growth characterisation. The experiments in regular waves with an artificially macro-roughened cylinder are described in Chapter 9.

Based on the experimental results, recommendations are made for the selection of appropriate force coefficients and the characterisation of fouling through rational design and survey data interpretation procedures (Chapter 10). Finally, the research findings and outstanding uncertainties which require further research are discussed.

CHAPTER 2. AIMS

The aims of the present research study are as follows:

a) to critically review current practice and available data for the fluid loading effects of marine growth at the design and in-service stages of offshore installations;

b) to establish a rational approach for the consideration of marine growth effects both at the design stage and during the operational life of the structure;

c) to quantify the hydrodynamic effects of marine growth through systematic large scale experiments with macro-roughened circular cylinders;

d) to identify the significant roughness parameters that characterise marine growth and to classify design macro-roughness, leading to improved design and maintenance appraisal of new and existing template structures.

CHAPTER 3: MARINE GROWTH AND ITS IMPORTANCE

In the context of this study marine growth is treated from an engineering point of view. However, the biological and environmental aspects are of vital importance in understanding the nature of the problem and in realising the mechanism of succession of marine growth. A brief outline of these is, therefore, worthwhile to provide the background to a complex multi-disciplinary problem prior to any in-depth investigation of the hydrodynamic effects of marine growth on offshore platforms.

3.1. What is Marine Growth ?

Marine growth or marine fouling may be broadly defined as a biological term that encompasses all organisms colonising the surface of any man-made fixed or floating marine structure. The process of colonisation starts with the release of larval forms by adult species into the plankton. The planktonic larvae are then transported by currents and provided that they survive long enough they settle on a suitable hard surface. Survival of larvae depends primarily on the nutrition content of the inflows of surface water masses and on the length of planktonic phase of each species [8]. The North Sea provides one of the richest environments in nutrients, phytoplankton and zooplankton and the platforms are ideal surfaces for settlement since hard substrates on the seabed are scarce. So it is virtually guaranteed that every North Sea structure will be colonised by various species shortly after its installation.

The initial colonisers are bacteria forming a layer of slime over the jacket surface within two to three weeks. They cause a change in physical and chemical properties of the steel surface and pave the way for colonisation by other fouling organisms namely the 'hard fouling community' [8]. As the term suggests these organisms have calcareous protective shells or tubes which adhere firmly to the substrate. Depending on geographic location, after two to three years a secondary fouling community consisting of soft fouling organisms overgrows and usually dominates hard fouling whilst seaweeds begin to emerge on areas near the water surface.

Generally, thickness is more pronounced at the surface waters where food is plentiful and water temperature is higher. The increase in thickness is caused by the tendency of the fouling organisms to grow out of the slowly moving boundary layer towards faster moving waters which carry more nutrients [9]. For similar reasons they tend to colonise all available space starting at the top and outer faces of structural members where light conditions are more favourable and eventually covering the full surface of the members.

The dominant types of marine growth encountered in the North Sea are shown in Table 3.1 and their relevant biological characteristics are described in Appendix A. The species are classified as hard and soft marine growth and long flapping seaweeds. The latter generally fall into the soft growth category but a distinction is necessary in this context since seaweeds present their own loading characteristics.

Although all organisms are in direct competition for space, food and light in most cases each established community appears at distinct depth zones. Figure 3.1 shows a typical distribution of marine growth types on a North Sea platform. This distribution is by no means the norm as environmental, operational and other conditions vary considerably for every platform. It simply indicates at what depth range each species is likely to dominate and that several types of fouling can occur in the same location simultaneously.

Mussels, kelp and green or brown seaweeds are the most significant species occuring in the upper depth zones. Sea anemones, soft corals, barnacles, tubeworm and hydroids are dominant at greater depths i.e. over 30m. Numerous other species are present at various elevations and past marine growth surveys have recorded more than 40 attached (sessile) animal species per platform [10,11], but the majority of them is rather insignificant in terms of population and contribution to structural loading.

3.2. Factors Influencing Marine Growth

As mentioned earlier the marine fouling found on the platforms depends on several environmental and operational factors. The following paragraphs describe how these factors influence the physical characteristics of marine growth.

Hard Marine Growth	Soft Marine Growth	Long Flapping Seaweed
Mussels Barnacles Tubeworm	Sea anemones Soft corals Hydroids Tunicates Algae	Kelp Green seaweeds Brown seaweeds

Table 3.1. Classification of dominant fouling organisms.

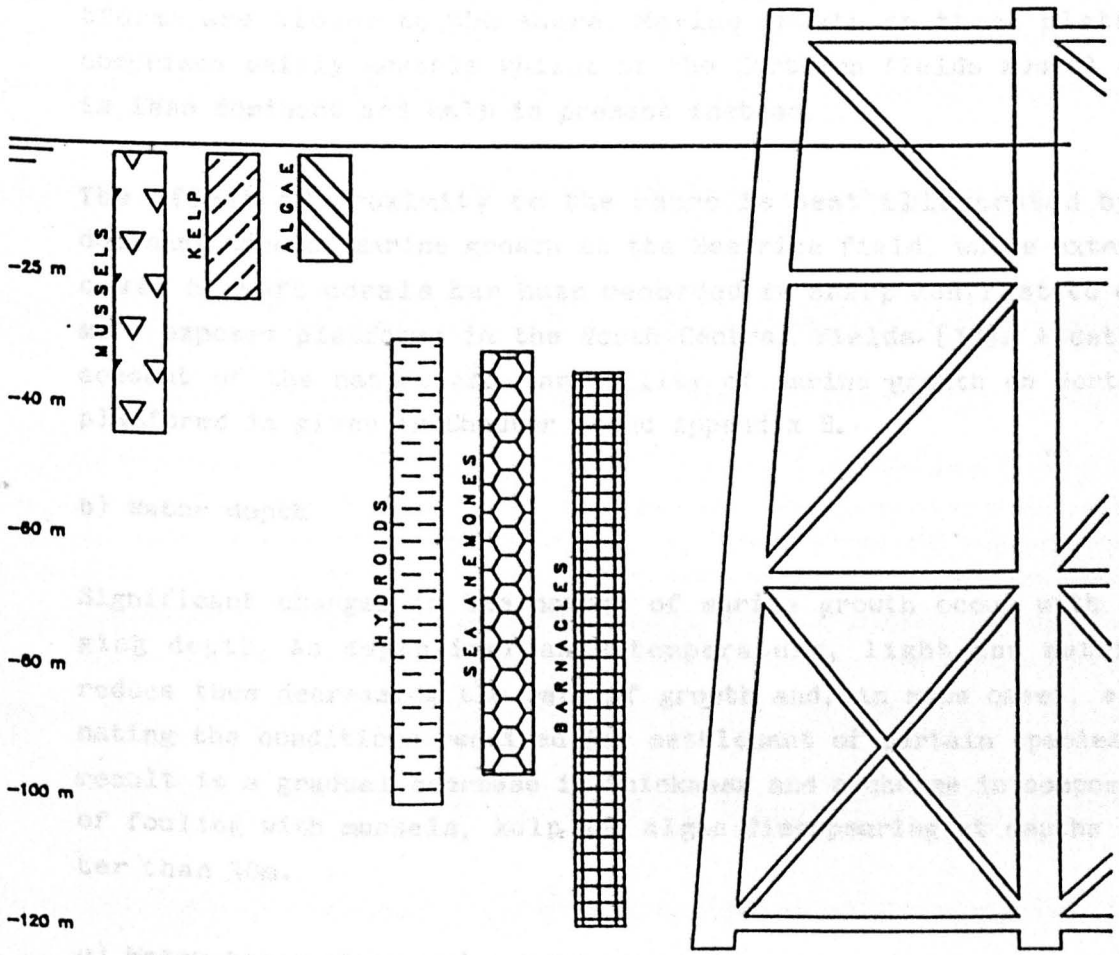

Figure 3.1. Typical marine growth colonisation pattern in the North Sea.

a) Geographic location

This factor largely dictates the species and extent of marine growth present on a structure. It encompasses secondary factors such as distance from shore, exposure and salinity which interact with temperature, food availability and light conditions to produce an overall marine growth composition. As expected marine growth on North Sea installations is dissimilar to that on platforms in the Gulf of Mexico or in the Santa Barbara Channel [13], both in terms of composition and extent of growth. Lack of broad similarity extends even among North Sea sectors and, further still, among platforms situated in the same sector. Figure 3.2 shows the North Sea divided into four areas and the location of all oil and gas fields. When compared with the Northern fields the Southern fields have smaller water depths, higher current speeds, less severe weather conditions and the platforms are closer to the shore. Marine growth on these platforms comprises mainly mussels whilst at the Northern fields mussel cover is less dominant and kelp is present instead.

The effect of proximity to the shore is best illustrated by the dominant type of marine growth at the Beatrice field, where extensive cover by soft corals has been recorded in sharp contrast to other more exposed platforms in the North Central fields [14]. A detailed account of the nature and variability of marine growth on North Sea platforms is given in Chapter 6 and Appendix B.

b) Water depth

Significant changes in the nature of marine growth occur with changing depth. As depth increases temperature, light and nutrients reduce thus decreasing the rate of growth and, in some cases, eliminating the conditions required for settlement of certain species. The result is a gradual decrease in thickness and a change in composition of fouling with mussels, kelp and algae disappearing at depths greater than 30m.

c) Water temperature and season

These two interacting factors affect rate of growth and settlement of particular fouling organisms. As temperature rises the rate of growth increases, so new settlement and high growth rates of most species

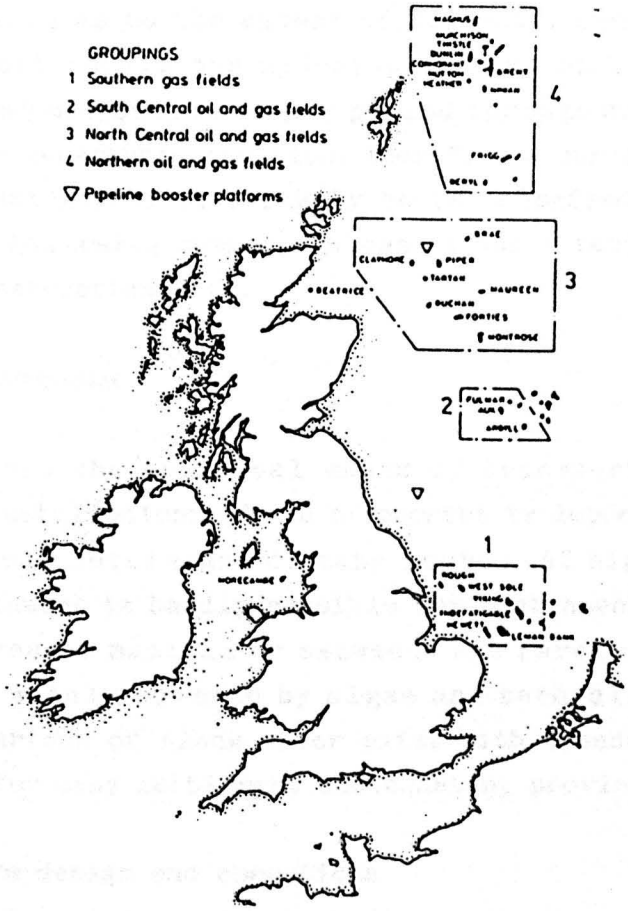

Figure 3.2. The main North Sea regions (from Oldfield [9]).

occur during the summer months. In fact growth rates of mussels may be estimated by empirical formulae which are functions of average yearly water temperature [9,12]. Other surface water colonisers such as kelp and other seaweeds settle in summer but die back during the winter period. This may be significant to hydrodynamic loading since most storms occur during winter, but as yet no definitive information is available as to the extent of die back. Some deep water species such as soft corals and hydroids are not affected by temperature changes and may settle at any period throughout the year depending largely on geographic location. Therefore a structure installed after a settlement period is unlikely to be colonised at least by mussels until the following summer, unless it was infected during tow-out or at the construction site.

d) Water currents

Currents are the principal means of transportation of larvae to offshore installations. Speed of current is important in the survival and eventual settlement of many larvae. At high speed, i.e. over 3 m/s, settlement is hardly possible for most species except barnacles. For this reason mussels or seaweeds are rarely found on ship hulls which are mainly covered by algae and barnacles. In the North Sea regular periods of slack water exist with speeds lower than 0.5 m/s, allowing for easy settlement and constant provision of nutrients.

e) Platform design and operations

Any form of crevices or appurtenances provides ideal surfaces for initial colonisation by most fouling organisms due to their sheltered safe habitat. This is noticeable particularly during the development stage when the structural members are partially covered. The areas around nodes and anodes are more densely populated and subsequent settlements result in large undulations in marine growth thickness. By the very nature of their design secondary structural elements such as conductor guide frames, hot and cold marine risers, and fenders are also prone to heavy localised concentration of marine growth. The type of corrosion protection systems appears to influence growth rates too as platforms protected by the impressed current system are more heavily fouled than those with sacrificial anodes [9].

In terms of production and drilling operations it has been established that discharges of oil related chemicals and production water containing toxic substances reduce or even eliminate the fouling population in the vicinity of outlets [15,16]. Underwater repair and maintenance operations involving cleaning for structural relief or inspection usually lead to rapid regrowth and may be considered as influencing factors in predicting future levels of marine growth.

It must be realised that the unpredictable complex interaction of the above factors allows only for generalisations in forecasting future marine growth levels. Specific and important differences exist between offshore installations so the best line of action is to consider each platform on its own.

3.3. Consequences

It is common knowledge that fouling on marine structures affects adversely their perfomance and operation in many ways. Marine roughness on ship hulls and propellers has been well documented and its effect on resistance and propulsion efficiency is significant [17,18,19,20]. However, preventive and remedial measures such as drydocking and antifouling paints - whose effective lifetime ranges from 2 to 5 years - can be readily adopted for floating vessels, whilst the same cannot be said about permanently located offshore installations.

Marine fouling on offshore structures:

- increases structural loading
- impedes underwater inspection and maintenance operations
- enhances corrosion
- limits topside weight
- obstructs seawater intakes.

Consideration of structural loading entails questions of design philosophy and regulations, hydrodynamic behaviour and fatigue analysis. Therefore designers ought to address the following effects due to marine growth:

a) **Higher drag coefficients;** marine growth alters the surface roughness characteristics of tubular members increasing overall and local hydrodynamic loading. Appropriate selection of drag coefficients is important as the level of increase depends on parameters such as type of growth, distribution, area cover and others.

b) **Increased structural member projected area and displaced volume;** direct loading also increases through this effect. In estimating projected area and volume the thickness of accumulated growth is added to the nominal "clean" member diameter leading to the rather ambiguous term of "effective member diameter" [69]. Normally, thickness of fouling ranges from a thin layer of slime to over 200mm, whilst in the case of soft growth it may exceed this figure.

c) **Increased structural weight;** type of fouling, growth rate and extent of cover are the governing parameters. Weight of fouling may reach appreciable proportions. For example, the weight of mussels on the first horizontal framing in a Forties platform was estimated at 12.5 tonnes [21].

d) **Higher mass and hydrodynamic added mass;** the platform natural frequency is reduced by concentrated mass of fouling around the splash zone.

e) **Reduced fatigue life;** can be significant for critical joints in the wave affected zone. Depends on loading from waves of moderate period.

Oldfield [9] showed that the increase in direct loading arising from higher drag coefficients, member projected area, added mass and structural weight is by far the most important. It affects both the ultimate limit state stress estimates and the stress range resulting from waves of moderate period which contributes to fatigue life estimation. The same study demonstrated that assuming a 30m design wave, marine growth thickness of 50mm and C_d of 0.8, the total base shear for a jacket at water depth of 100m would increase by 5-10%, while fatigue life would reduce by 15%. To accommodate such increases it requires either a heavier structure or a rigorous cleaning programme which may prove expensive and difficult to implement.

Cleaning of marine growth is associated with the majority of underwater inspection and maintenance tasks constituting up to 40% of actual diver working time [22]. Complete removal of marine growth is required prior to the implementation of such tasks as close visual survey and Non-Destructive Testing. Other effects include concealing possible weld cracks, obscuring platform reference signs, blocking inlets of seawater intakes and creating a hazardous working environment for divers [23].

Finally marine growth may enhance corrosion through Sulphate Reducing Bacteria (SRB) activity, that is by creating anaerobic conditions under the layer of fouling which provides an ideal habitat for sulphate reducing bacteria. An insight to corrosion enhancement is given in [24,25].

CHAPTER 4. CRITICAL REVIEW

To assess the hydrodynamic loading of a structure one must consider the mechanics of fluid flow past rough cylinders, the data available on force coefficients and the design, inspection and maintenance approaches to marine growth. In this chapter all three aspects are reviewed highlighting the present state of affairs and identifying shortcomings in each case.

4.1. Experimental Approaches

Wave forces are the most significant form of environmental loading on any marine structure. For space-frame structures the established method of determining these forces is by Morison's equation [26]. It expresses the total force acting on a tubular element of unit length as the sum of the drag and inertia forces,

$$\text{i.e.} \qquad F(t) = 0.5C_d\rho Du|u| + 0.25C_m\rho\pi D^2\dot{u} \qquad (1)$$

where, $F(t)$ = instantaneous wave force,
C_d = drag coefficient,
ρ = density of sea water,
D = element diameter,
C_m = inertia coefficient,
and $u, \dot{u}$ = horizontal components of water particle velocity and acceleration respectively.

Morison's equation is only valid if it is assumed that the water particle motion is not affected by the presence of the structure itself. Therefore, it may be safely applied to the majority of template structures with elements whose principal diameter does not exceed 0.2 x wavelength. For larger diameter members, diffraction wave theory is used to allow for wave scattering arising from the presense of the structure.

Despite its simplicity, Morison's equation poses a number of practical problems which influence the accuracy of computed wave forces. The most important ones are the use of appropriate time-invariant force coefficients and the definition of wave kinematics. Further problems associated with Morison's equation are discussed in [27,65].

It would be apt at this stage to define drag and inertia forces. Drag is the in-line component of the fluid force on a body and in phase with the ambient flow velocity, whilst inertia force is in phase with the acceleration of the undisturbed fluid flow. It should be noted that the transverse force component, i.e. normal to the drag, termed as "lift" is not considered by Morison's equation.

The concept of drag and inertia forces has been established over the past three centuries. Hogben [28] has comprehensively reviewed classical research developments for idealised cases such as smooth cylinders, spheres and discs. A useful reference source for fluid dynamic coefficients for various bodies and flow conditions is the data compiled by Hoerner in 1958 [29].

Substantial fundamental and applied research has been devoted to fluid flow past smooth and rough circular cylinders, particularly since the advent of offshore structures. Because of the complex aspects of the flow field a numerical solution for credible prediction of hydrodynamic coefficients is not known, however great the advances in numerical hydrodynamics may have been in the last decade. Therefore, the coefficients are determined experimentally. Such experimental programmes may be broadly classified into laboratory and field tests. The former aim primarily towards understanding the underlying flow phenomena, whereas the force coefficients derived from field tests reflect the combined effects of multi-directional waves, currents, scale etc. and include the much publicised shortcomings of the generalised Morison's equation [54].

In the following sections the results and observations from previous experiments are reviewed. It would be an immense task to review all the published work on smooth and rough circular cylinders here. Attention is focused only on work of relevance to macro-roughened cylinders.

4.1.1. Laboratory experiments

The hydrodynamic coefficients are functions of the following non-dimensionalised parameters,

- Reynolds number, $Re = U_m D/\nu$

- Keulegan Carpenter number, $KC = U_m T/D$
- relative roughness, k/D
- Strouhal number, $S = fD/U_m$

where, U_m = maximum horizontal water particle velocity,
D = element diameter,
T = wave period,
k = mean roughness height,
f = vortex shedding frequency,
ν = kinematic viscocity of water.

In an attempt to model these parameters in the laboratory various experiments have been conducted with smooth and rough cylinders in steady, planar oscillatory or wave flow in wind tunnels, wave flumes or pulsating water channels.

One valid concern with most experiments is that of scale. In the North Sea waves of 30m in height and 15 seconds period are possible. They result in water particle velocities of 6m/s which, when coupled with currents of up to 0.5m/s, produce Reynolds numbers for typical jacket structures in the range

$$10^5 < Re < 10^7$$

The Keulegan Carpenter numbers, which represent the significance of amplitude in harmonic flow past cylinders [30], range between 2 and 80 subject to wave kinematics and element diameter. Strouhal number, a dimensionless measure of vortex shedding frequency, is approximately constant at around 0.2 at high Reynolds numbers [27,32].

The final parameter is the relative roughness, k/D. The dependence of steady flow C_d on surface roughness is shown in Figure 4.1. The range of "in-service" marine roughness is generally within the following range,

$$0.0006 < k/D < 0.03.$$

This range should be treated as speculative because of ambiguities in measuring and characterising marine growth in terms of thickness. Surely roughness parameters such as shape, distribution, density and type of fouling would also have to be characterised as will be discu-

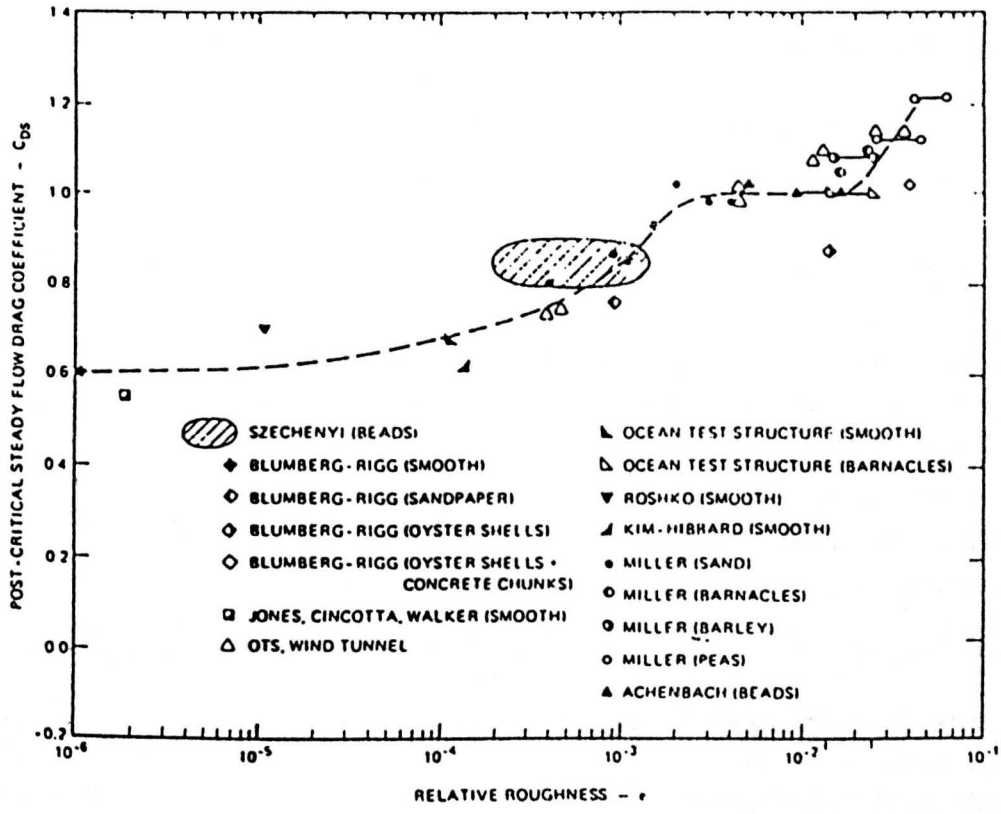

Figure 4.1. Dependence of post-critical steady flow C_d on surface roughness.

ssed later in detail. At this stage, it is adequate to consider marine fouling as a form of macro-roughness.

To meaningfully model full scale conditions, laboratory tests must be performed within the above mentioned ranges. Modelling of KC numbers alone presents little difficulty since appropriate combinations of planar oscillatory or wave flow kinematics with cylinder diameter should yield full scale KC numbers. However, for time-dependent flows at KC lower than 60 the Reynolds numbers achieved through this type of experiments generally do not exceed 5×10^5. This is illustrated in Figures 4.2 and 4.3 where the variation is shown in force coefficients with Re and KC for smooth cylinders in harmonic flow [35].

Higher Reynolds numbers have been achieved through tests in steady flow, albeit in wind tunnels. Steady flow represents a limiting case of unsteady flow where temporal variations approach zero [36]. That is, drag is similar in magnitude to that experienced under oscillatory flow conditions at very large KC numbers. Therefore, steady flow C_d data are important in ultimate limit state design of offshore structures whose member diameters are relatively small and in fatigue design since most damage accumulates in storms when KC numbers will also be large [37,38].

Several researchers [e.g. 34,39,40,41,42,43] have studied the variation of cylinder drag at high Re in steady flow. Achenbach [39] has described this variation and the transition from laminar to turbulent flow around cylinders by considering four flow regions as indicated in Figure 4.4.

The smooth cylinder drag coefficient changes from 1.2 for subcritical Reynolds numbers ($Re<10^5$) to a minimum of 0.2-0.4 in the critical range ($2 \times 10^5 < Re < 4 \times 10^5$) and up to 0.6-0.7 at postcritical Re ($Re>3.5 \times 10^6$). Any further changes in Cd are unlikely at Reynolds numbers greater than 3.5×10^6 [40]. This sequence of changes is due to laminar separation and turbulent reattachment of the boundary layer causing variations in base pressure (i.e. pressure at the rear of the cylinder) and in wake width. These variations are outlined below in connection with surface roughness effects.

In 1929, Fage and Warsap [46] examined the influence of surface roughness on drag at low Re by attaching various grades of sandpaper on

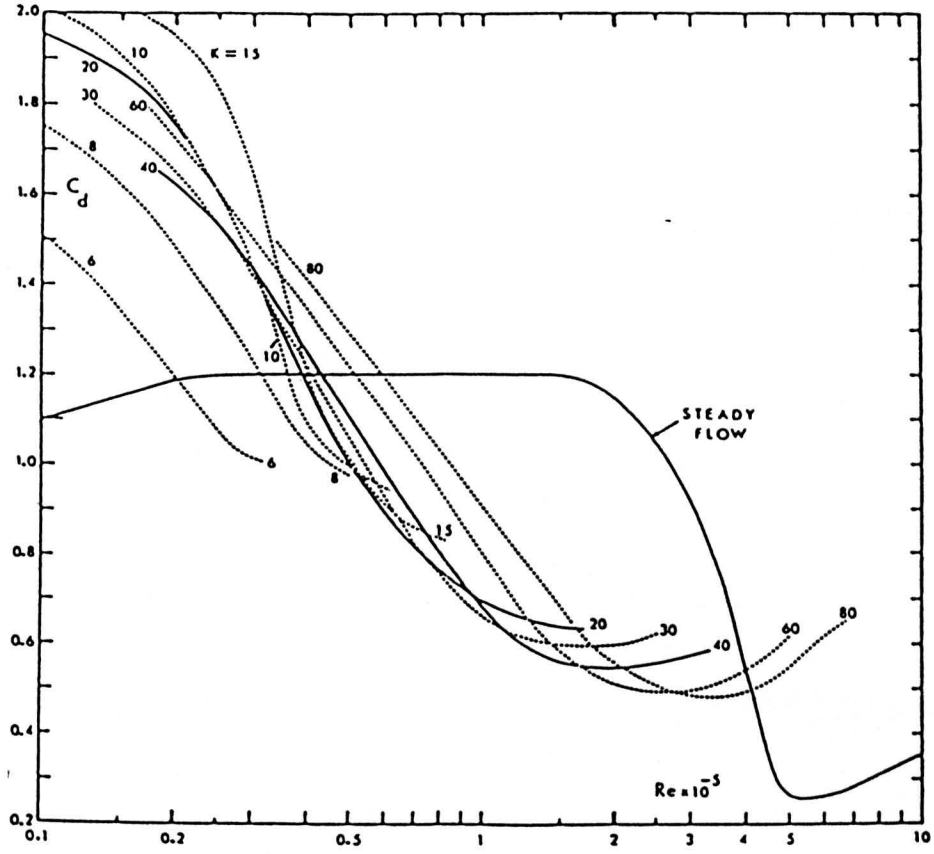

Figure 4.2. Drag coefficient versus Reynolds number for smooth cylinders in harmonic flow at constant KC values [35].

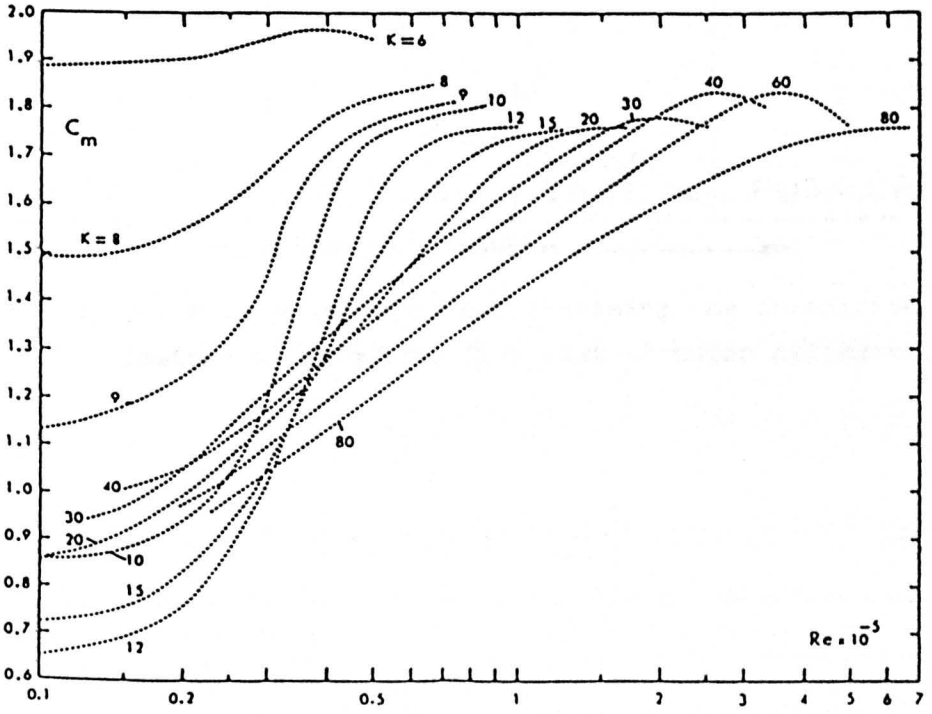

Figure 4.3. Inertia coefficient versus Re for smooth cylinders in harmonic flow at constant KC values [35].

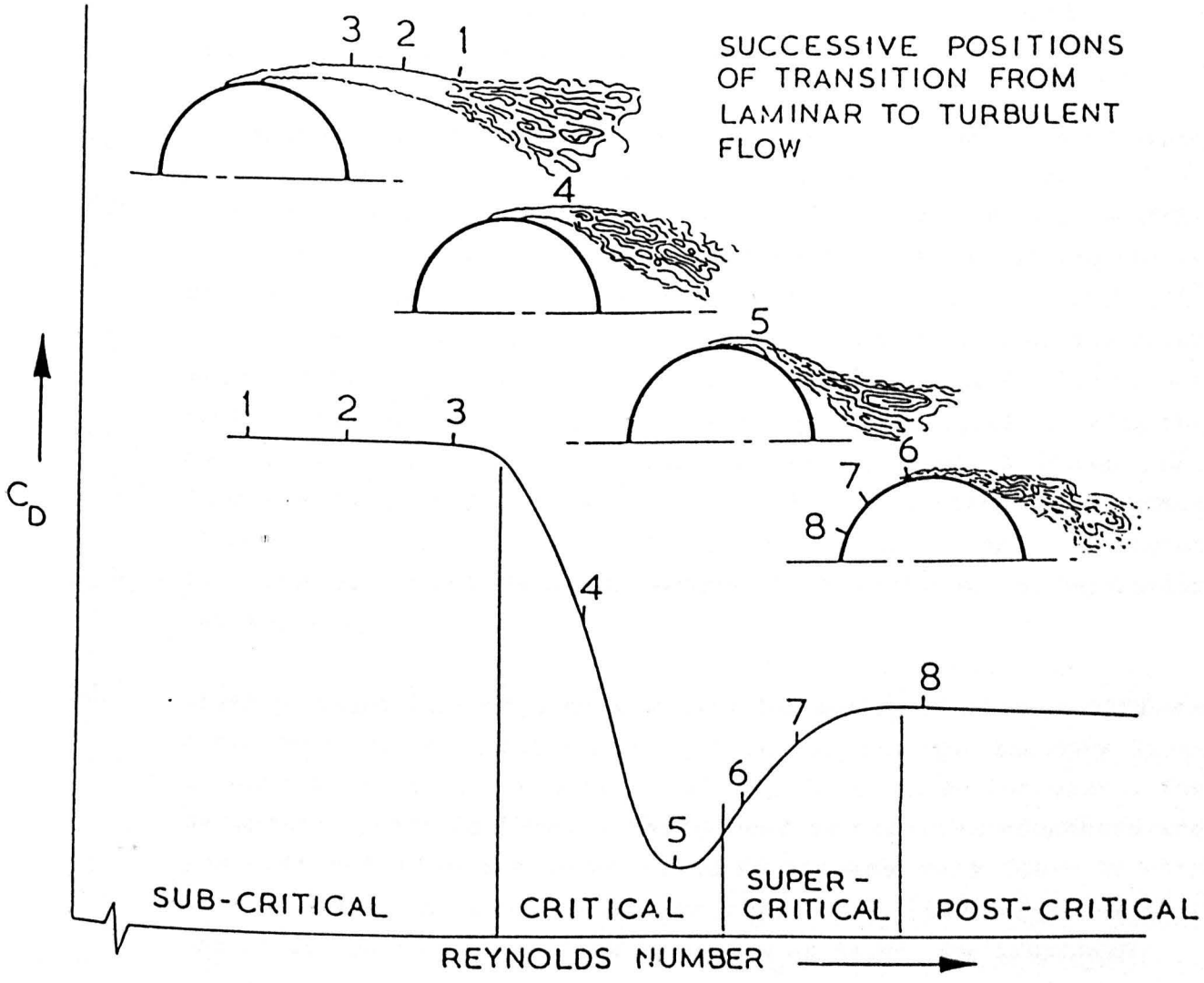

Figure 4.4. The four Re regions characterising the transition from laminar to turbulent flow past circular cylinders.

circular cylinders. They found that by increasing relative roughness the critical regime shifted towards lower Reynolds numbers and minimum C_d increased. Their results are shown in Figure 4.5 together with those of Achenbach [39] who also examined the influence of skin friction drag. He found that it accounts for only 0.5-3% of the total drag depending on Reynolds number. Thus, C_d is almost entirely influenced by changes in pressure drag.

For cylinders in subcritical flow, the laminar boundary layer separates at approximately 80^o from the front stagnation point. Base pressure is low and the wake is wide resulting in high drag coefficients which are nearly independent of Reynolds number. In the critical flow regime the separation point moves downstream to about 110^o and the initially laminar boundary layer forms a free stream shear layer which undergoes transition to turbulent flow. The turbulent shear layer reattaches to the cylinder almost immediately forming the so called "separation bubble" and finally separates at around 140^o. As a result base pressure increases, the wake structure becomes narrower and drag decreases rapidly. The flow at the critical regime is essentially unsteady due to asymmetric formation of the separation bubbles [47].

Under post-critical flow conditions which are applicable to offshore structures, the transition from laminar to turbulent boundary layer is direct and occurs progressively upstream as Re increases. The separation point is largely influenced by relative roughness and postcritical flow can be achieved at successively lower Re with corresponding increases in k/D. Pearcey et al. [48] suggested that the Re for post-critical flow is as low as 3×10^5 for k/D=0.0028.

Achenbach [44] and Schezhenyi [41] suggested that an upper relative roughness limit exists beyond which no further increase in C_d occurs at postcritical Re. However, Figure 4.5 shows different magnitudes of C_d for rough cylinders with k_s/D of 0.0011 and 0.0045 - Achenbach defined "equivalent" sand grain size, k_s, through Nikuradse's roughness [39]). Further experiments by Achenbach using spherical beads (k/D=0.016 or k_s/D=0.009) resulted in similar drag coefficients to those obtained for k_s/D=0.0045 [39]. In an attempt to correlate his results with those of Fage and Warsap, Achenbach defined k_s for the spherical beads as,

$$k_s = 0.55\ k$$

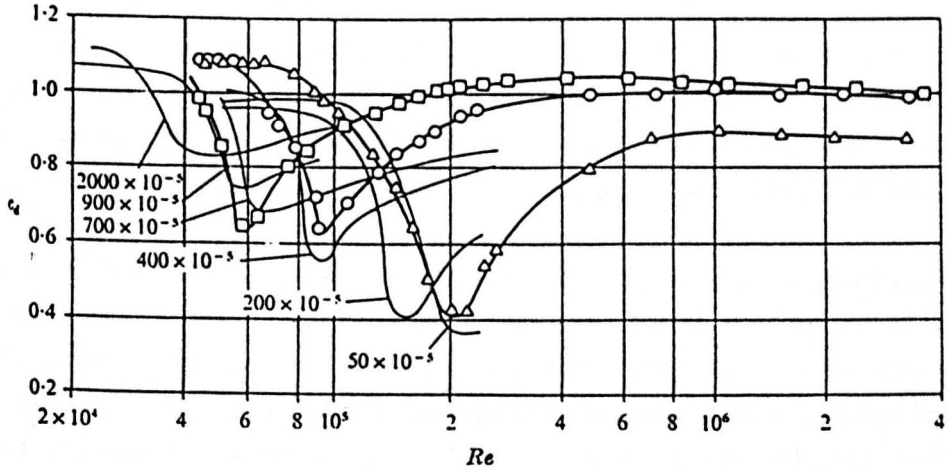

Figure 4.5. Drag coefficients for rough circular cylinders in steady flow (from Achenbach [39]):

- △ $k_s/D=1.1\times10^{-3}$
- o $k_s/D=4.5\times10^{-3}$
- □ $k_s/D=9.0\times10^{-3}$
- —— Fage & Warsap [46]

In a generalised form, Achenbach adopted an approximate relationship between the critical Reynolds number and k_s/D [44,45], i.e.

$$Re_{crit} = \frac{6000}{(k_s/D)^{0.5}}$$

However, in experiments with cylinders covered by regular arrays of pyramids (k_s/D=0.009) Achenbach obtained drag coefficients which were 10% lower than those obtained with spherical beads at the same k_s/D; the maximum difference occuring at subcritical/critical Re [45]. He cited as possible reasons the method of determining C_d (integration of static pressures) and the difference in roughness types. This suggests that roughness size alone, no matter in what form it is expressed, cannot characterise roughness accurately; particularly marine roughness, which exhibits not only a variety in types of fouling but also in distribution, density, area cover, shape etc.

So far, wind tunnel tests with rough cylinders at low k/D ratios have been discussed. These have provided the framework for describing the basic flow mechanisms and the influence of surface roughness on C_d and Re. However they are not fully applicable to marine fouled cylinders. As stated in Chapter 3, marine growth can be either hard or soft and flexible or indeed a mixture of both, it is very irregular and much thicker than any sand roughness tested giving rise to thicker boundary layers.

Surprisingly limited amount of published data exists for marine fouled cylinders bearing in mind the extensive research on smooth and rough cylinders. This is summarised in Table 4.1. To the author's knowledge, the only in-depth systematic investigations on the subject have been undertaken by Nath and to a lesser extent by Miller.

Miller [34] performed tests in wind tunnels with cylinders covered by uniformly distributed artificial roughness or by naturally grown barnacles. He inferred that local drag increases by 50-70% for heavily fouled tubulars over that for smooth ones after allowances in effective member diameter. He also observed differences in C_d arising from roughness density variations. However, the study was limited to roughness types which do not fully represent the predominant forms of fouling on offshore structures, i.e. mussels and kelp.

REFERENCE	TYPE OF FLOW	ROUGHNESS	k/D	Re(x10^5)	KC	C_d	C_m
Nath [52]	Steady	Artificial	–	0.2–4.2		1.5–4.0	
	Waves	kelp	–	0.4–2.5	3–25	1.5–6.0	2.5–4.0
	Waves+current		–	1.0–6.0	4–28	1.3–3.5	2.2–4.0
Nath et al. [51]	Steady	Barnacles	0.11	0.4–4.5		1.2–1.4	
	Waves			1.2–1.7	8–25	1.1–1.5	1.5–2.3
Nath [51]	Steady	Mixed hard	0.037	0.8–7.0		1.04	
	Waves+current	fouling		0.8–5.0	15–25	1.0–1.5	1.2–2.2
Nath [32,50]	Steady	Artificial	0.09	0.4–4.0		1.2–1.4	
	Waves	marine					
	Horizontal cyl.	roughness			15–25	1.52	1.73
	Vertical cyl.				15–25	2.4	3.02
Miller [34]	Steady (wind tunnel)	Barnacles	0.048	1.0–16.0		1.16	
Cash [48]	Waves	Plastic seaweeds			2–15	55–120% of C_d smooth	
Norton et al.[56]	Steady	OTS–barnacles	0.024	3.0–12.0		1.2	
Blumberg & Rigg [57]	Steady	Oyster shells	0.015	10.0–60.0		0.88	
		Oysters and concrete chips	0.04	10.0–60.0		1.02	
Sarpkaya [58]	Harmonic	Barnacles	0.02	0.3–8.4	4–60	1.42–2.42	0.49–1.48
Rodenbusch & Gutierrez [59]	Harmonic/ 2–D random	Conical frusta	0.02	4.4–17.5	3–90	0.85–2.5	0.96–2.0

Table 4.1. Summary of past laboratory work on the fluid loading effects of marine growth.

Nath [32,49,50,51,52,53] carried out extensive wave flume tests with simulated hard and soft flexible marine roughness in steady tow, regular waves and combined waves plus towing. In-line and transverse forces were measured on horizontal and vertical cylindrical elements up to 200mm in diameter in periodic waves. The same cylinders were also towed by a carriage in still water or in waves. Nath et al. [52] found that for cylinders fully covered with plastic seaweeds the steady flow C_d ranged between 1.5 and 4.0; a significant increase over the average C_d of 1.22 for his artificially marine roughened cylinder (k/D>0.1) [50]. In wave or combined wave and current flows, similar increases in drag were observed and also in lift and inertia force coefficients [50,52]. The increase in C_m for flexible growths is important since hard roughness causes marginal reduction in inertia [35,54]. It suggests higher added mass due to entrained water among the kelp fronds.

Drag coefficients from steady flow tests by Nath with barnacle encrusted (k/D=0.11) and sand roughened (k/d=0.02) cylinders were lower than Miller's data (see Chapter 8 for further comments). Drag coefficients of the same horizontal cylinders in waves plus towing compared well with steady flow data despite some scatter [53]. This observation is plausible since the presence of a current increases the drag component of the total force at the expense of inertia. Therefore, such data are better conditioned for drag loading estimation in unsteady flow. Wherever relevant, the experimental results presented here will be compared with those obtained by Nath although the latter generally fall within a lower Re range.

Other contributions are those by Cash [48] and Matten [55]. Both compared total wave force coefficients between smooth cylinders and cylinders covered with simulated roughness, i.e. plastic strips representing seaweed and garnet paper simulating rigid growths (k/D=0.02) respectively. Cash - who did not report on the length or density of the plastic seaweed - suggested that C_d increased by 50% to 120% but exhibited large scatter. Matten estimated that hard roughness produced about 60% higher drag over that for the smooth cylinder. Matten also claimed that high transverse forces experienced by smooth cylinders in irregular waves were not increased further by the addition of roughness. Both experiments were carried out at low Re and no attempt was made to derive C_d and C_m from measured kinematics and forces.

Norton and Mallard [56] tested barnacle encrusted tubular members of the Ocean Test Structure (OTS) in a wind tunnel at various inclinations. They found that the "flow independence" principle - which states that normal drag forces are proportional to the normal velocity component squared and are independent of the axial velocity component - is valid for cylinder inclinations up to 40^{o} in post-critical steady flow.

Results from an earlier study by Blumberg and Rigg [57], though included in Figure 4.1 and Table 4.1, should be treated with caution because of discrepancies between their quoted data and previous results and strong evidence of free surface and tank boundary interference effects.

Finally, recent research that should be mentioned includes tests in harmonic flow by Sarpkaya [58], with a sand roughened and a barnacle encrusted cylinder, and periodic and random oscillatory cylinder motion tests by Rodenbusch and Gutierrez [59] with a 1000mm diameter cylinder covered with conical frusta (k/D=0.02). Both studies are extensively refered to in Chapter 9.

4.1.2. Field tests

A number of ocean projects have been undertaken since 1976 in an attempt to evaluate wave force calculation procedures and generally to improve offshore structural design. Force coefficients from instrumented piles attached to offshore structures have provided a standard source of design information in the offshore industry. Table 4.2 lists these projects and the data collected under various environmental conditions.

A large scale investigation was undertaken by Exxon Production Research Co. using a scaled jacket, the Ocean Test Structure (OTS) situated in the Gulf of Mexico [60]. Although the ranges of Re and KC numbers were not fully representative of extreme environmental conditions, it is believed that by means of the reduced scale the OTS data are useful in design load predictions for small structures. As shown in Figure 4.6, large data scatter was obtained particularly at KC<20. Also the marine growth comprised almost exclusively barnacles, thus the applicability of the results to other forms of growth is limited.

REFERENCE	PROJECT	ROUGHNESS	k/D	Re(x10^5)	KC	C_d	C_m
Helderman et al.[33]	OTS–Gulf of Mexico	0.5–1" barnacles	0.025	2–6	6–45	0.3–3.0	1.25–1.43
Bishop [62]	C.B.T.	Granite chips	0.033		10–15	C_f=1.56–2.18	
Bishop et al. [63]	C.B.T.	Kelp	0.8–1.7		10–30	1.05–1.2	1.75–2.4
Ohmart & Gratz [64]	Gulf of Mexico, Hurricane Edith	38mm at –8.5m	0.09	3–30	-	0.7	1.7–2.0
Lloyds' R.S. [31]	Forties FB	clean	–	2.25–3.4	5–12	0.9–2.0	0.95–2.05

Table 4.2. Summary of field experiments.

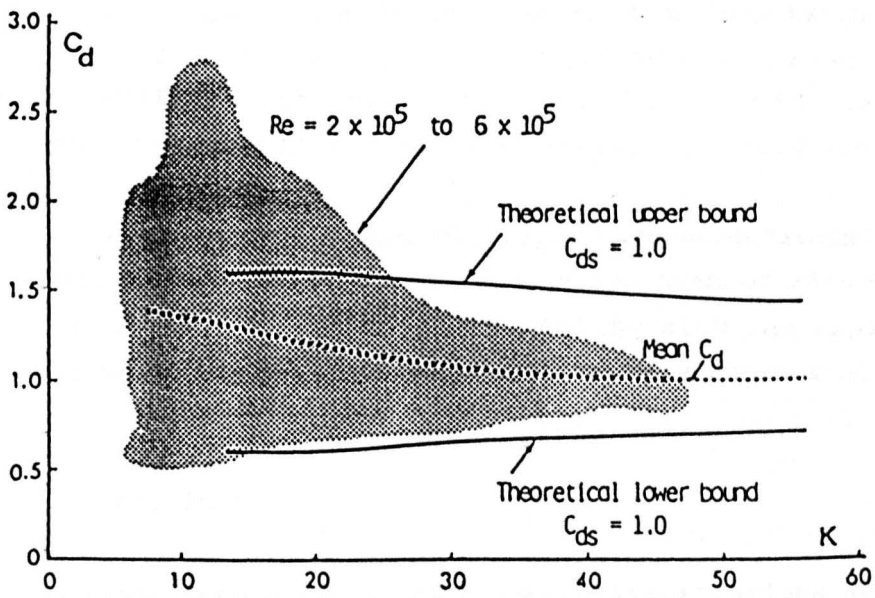

Figure 4.6. Ocean Test Structure results (adapted from [54]).

Another investigation carried out by Lloyd's Register of Shipping involved the instrumentation of the Forties FB fixed steel platform [31]. Marine growth on the instrumented members was cleaned off. Therefore only clean cylinder force coefficients are available.

A major field study currently in progress, is that conducted by British Maritime Technology Ltd. at the Second Christchurch Bay Tower (CBT) [61]. The CBT experiments, being undertaken in real sea conditions, include all the irregularities of wave height and directional spread. Initial results with clean cylinders correlated well with the OTS data, whilst experiments with simulated hard fouling (k/d=0.033) showed a 20% increase in total force coefficient, C_f, over the clean cylinder [62]. Further systematic tests with kelp covered horizontal and vertical tubular elements were carried out in 1986 [63]. For the horizontal cylinder the total force increased by 29% at KC=30 compared to the smooth cylinder. For the vertical cylinder C_f increased by 83% and C_d more than doubled at KC=30. In both cases C_m was higher than the smooth cylinder values. Surface cover and length of plants did not have a significant influence on the force coefficients.

Through the CBT study it is hoped to obtain valuable force coefficient data in real sea conditions. It would not however be possible to isolate all the environmental and surface roughness parameters and interpret their significance in the manner laboratory tests do. It is therefore necessary to have laboratory procedures whereby different roughness configurations may be tested and from which data can be obtained for characterising roughness relative to fluid kinematics.

Parameters such as aspect ratio, blockage, three-dimensional flow and free surface effects which may influence the drag of circular cylinders are discussed in the chapters dealing with the experimental results. Güven et al. [42] review compehensively these aspects.

4.2. Design Practices

The design requirements for fixed offshore installations are similar to those for any industrial space-frame structures. The first step in the design is to develop a concept of the structure based on its functional requirements, environmental constraints, construction and installation methods and anticipated maintenance needs. The function

of an offshore structure is to provide a safe working platform adequate to support the operational and environmental loads throughout its life.

It is not proposed to review all design aspects and the reader should refer to numerous publications available on these [27,66]. Instead, this section is concerned with the consideration of hydrodynamic loading due to marine growth by currently adopted design methods.

Two types of wave induced loading are normally considered in structural design:

a) the "design wave" with at least 50-year recurrence period to determine ultimate limit state stress,
b) cyclic loading for estimation of fatigue.

4.2.1. Limit state

The estimation of maximum design loads using Morison's equation requires reasonable descriptions of the following:

a) Water particle kinematics

In the past, the kinematics have generally been obtained from theories such as Stokes' Fifth Order, Airy etc., depending on water depth, significant wave height and wave steepness [67]. Water particle velocities and accelerations are computed as derivatives of the wave potential or stream function. The horizontal particle velocities are calculated by adding vectorially the wave component to the velocity imposed on water particles by current.

However, increasingly available wave records for various sea states have paved the way for more realistic design approaches in determining the particle kinematics and correlating with force coefficients [e.g. 68].

b) Morison force coefficients

The selection of appropriate force coefficients is essential in estimating hydrodynamic forces which are the most important sources

of overturning moments and shears on an offshore structure. All Classification Societies [69,70,71] recommend values for C_d and C_m to be used in the calculation of wave loads. As shown in Table 4.3 significant differences exist between the values suggested by each authority. The influence of marine growth, Re and KC numbers or interference between elements is weakly reflected in the recommended coefficients and no account is taken of transverse loading. Yet it has been suggested through sensitivity studies [72] that the drag coefficient has by far the strongest effect on overturning moment and horizontal base shear of typical North Sea platforms (see Figure 4.7). The inertia coefficient is also shown to be a major influence on fatigue calculations.

The implications for wave loading estimates that arise from adopting different force coefficients have been quantified by Abdelradi and Miller [73]. They showed that maximum stresses on individual members calculated using the coefficients recommended by three Classification Societies differed by up to 60% approximately. Comparisons of computed wave loads using the Lloyd's coefficients and those of Sarpkaya [74] for two levels of roughness indicated large differences in forces and moments particularly when lift was included.

The question that arises is: "If such discrepancies exist among recommended design procedures are the structures already produced unsafe?". The excellent safety record of North Sea platforms suggests otherwise. Safety factors introduced at the various design stages and the ovepredictiion of combined wave and current kinematics from wave theories more than compensate for the uncertainties surrounding force coefficients. That is not to say that designers and platform operators are not concerned with the issue. After all, the design responsibility lies with the operators who generally introduce more stringent requirements than the minimum recommendations of the Certifying Authorities.

The force coefficients adopted by platform operators depend firstly on whether the computed loading is to be used for global or local design and, secondly, on expected marine growth levels. In local design, all wave and current load components on individual members are estimated. Global design involves the temporal summation of local loads when the structure experiences maximum deformation. In global design lower drag coefficients are adopted since the coherence of

Classification Society	C_d	C_m
Lloyds'.R.S.	> 0.7	2.0
Det norske Veritas	0.5 to 1.2 subject to Re & k/D >0.7 for $Re>3x10^5$	1.5 for (2R/L)>1.0 2.0 for (2R/L)>0.1 Intermediate values by interpolation
Bureau Veritas	0.75	1.5 for R<725 $C_m = 1+\log_{10}20R-0.8$ for R>725

N.B. R = Radius of structural member (mm)
L = Member length (mm)

Table 4.3. Minimum design force coefficients recommended by classification societies.

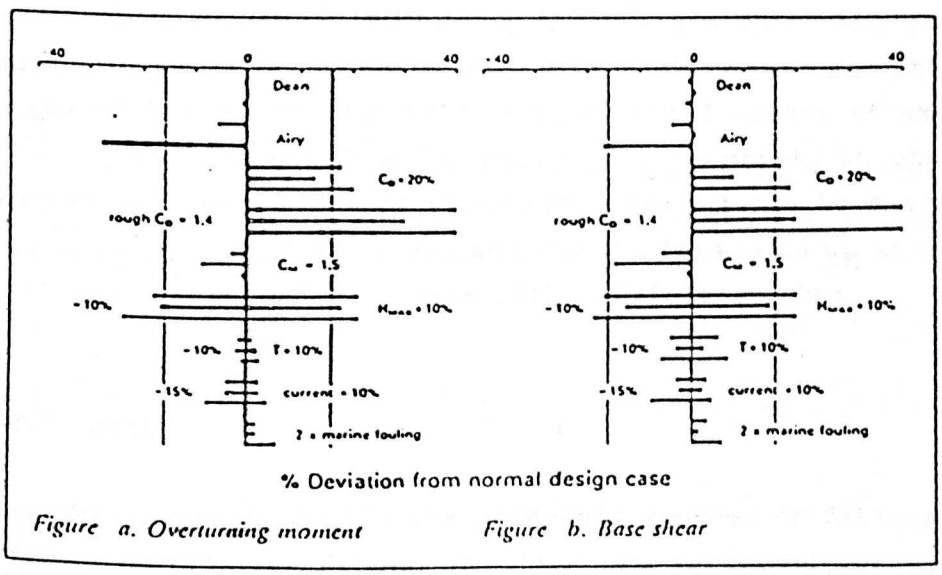

Figure a. Overturning moment *Figure b. Base shear*

Figure 4.7. Sensitivity of overall loadings to variations in design parameters.

loading assumed for all members at the design stage will never occur in practice [75]. Typical values of design force coefficients adopted in industry are [75]:

	Local design	Global design
C_d	1.0	0.7
C_m	2.0	2.0

c) Marine growth design allowance

Compared with experimental data, the above C_d design values are still low. It is claimed that marine growth thickness allowances in member diameter should adequately compensate for this difference [69]. Typical "design allowances" for marine fouling are shown in Table 4.4. These are predicted from marine growth survey data for specific North Sea locations and water depth ranges. The validity of such figures is debatable due to ambiguities in growth characterisation and the variability in local environmental conditions.

It has been suggested that the effects of different types of growth may be "normalised" to produce an "equivalent thickness index" which would incorporate the composition, surface cover and thickness or length of fouling species [16]. A substantial amount of experimental data would be required to validate this approach, which after all ignores the inducement of transverse forces due to uneven growth around cylindrical elements and the variation in C_M which reduces with hard fouling but increases with flexible growths.

4.2.2. Fatigue

Wave forces are generally the principal sources of fatigue damage in offshore structures. Fatigue analyses are performed for all tubular joints using fracture mechanics or results from fatigue tests (SN curves). Long term stress distributions are established using deterministic or spectral approaches.

Operator	Southern fields
1	At sea level 50mm on legs, 90mm on bracings
2	100 to 125mm
3	100mm
4	50mm all over but in reality 100mm at sea level
5	50 to 75mm
	Central and Northern fields
1	80mm on upper part of structure
2	100mm
3	100mm in upper part of structure, 25mminlower parts
4	0 to -40m, 50mm; -70m and deeper, 0mm
5	0 to -35m, 50mm; -35m and deeper, 25mm

Table 4.4. Summary of fouling levels tolerated by operators in the North Sea [9].

The effect of marine growth on fatigue is threefold:

a) increase in structural mass,
b) increase in hydrodynamic added mass due to higher displaced volume,
c) increase in fluid loading.

As marine growth distribution is not uniform over the whole structure but is instead concentrated on the top elevations, it tends to increase the natural period and dynamic amplification factor of the platform. This results in fatigue life reductions by 30-50% from those for clean structural elements [9]. Increased fluid loading results in higher stress ranges, S, and reduces fatigue life significantly since,

$$\text{Fatigue life} \propto \frac{1}{(\Delta S)^m} \quad \text{, where } 2<m<4.$$

Added mass is the major hydrodynamic parameter in fatigue calculations. However recent studies have shown that most fatigue damage occurs during storms [37,38]; so the rough C_d is also important. In estimating fatigue lives designers normally adopt the same force coefficients used for ultimate limit state calculations. This may result in fatigue estimates which would significantly differ from estimates where temporal and topological variations in C_d and C_m are considered.

4.3. Inspection and Maintenance Practices

According to the 1974 Offshore Installations Act [76] every offshore installation must comply with minimum statutory requirements. It is the responsibility of the operator to carry out routine inspections of each platform for the award of 5-year Certificates of Fitness by Certifying Authorities on an agreed inspection schedule. Monitoring of marine growth forms a small part of the overall legislative survey requirements.

4.3.1. Marine Growth Surveys

Before considering marine growth survey practices for offshore structures one should perhaps ask: "Why perform marine growth surveys?". The answer is that they are essential for the following reasons:

- to comply with certification requirements;
- to identify any need for structural cleaning;
- to regularly assess structural loading caused by changes in the extent and nature of marine growth;
- to forecast with reasonable confidence future levels of fouling.

To fulfill these objectives the survey data should produce a reasonably accurate mapping of marine growth based on:

- type of individual species present;
- average and maximum sizes of each type;
- percentage surface cover by dominant fouling species;
- overall extent, distribution and composition of hard and soft growth;
- weight of marine growth.

The quality of such data depends on the methods of measurement, analysis and interpretation employed by the operator as no official code of practice exists. This may be attributed to the inaccurate assumption made in the early days of North Sea activity that marine growth would not reach significant levels due to the cold environment inhibiting growth as opposed to the temperate waters of the Gulf of Mexico. This assumption was reflected not only in the low marine growth allowance used in the design of first generation jackets but also in the Guidance Notes on surveys [77] where the only reference to marine growth states that:

> **"An assessment should be made of the thickness of marine growth on typical members or areas of the structure".**

This guideline focuses solely on thickness as the singular parameter for marine growth characterisation ignoring growth type, distribution, area cover and structural element topology.

However, it was soon realised that marine growth on North Sea platforms could indeed pose problems to structural loading and to underwater inspection and maintenance operations. In 1978 the Department of Energy initiated the establishment of a Working Party on Marine Fouling to consider the problems arising from the build-up of marine growth on offshore structures [78]. Among its recommendations the Group called for improvements in collection and interpretation of data on the nature, extent and rate of development of marine growth. Existing data were collated and analysed to provide tentative forecasts of future fouling levels [9,79], while most operators introduced systematic explicit procedures for marine growth surveys within their inspection programmes [10,15].

The general framework of adopted practice is broadly similar among all operators, with some differences in process implementation and data interpretation according to the inspection objectives of each operator. The following two types of survey are carried out:

a) Video survey

Video surveys are performed during General Visual Inspections and produce an overall impression of growth through the use of cameras mounted on Remotely Operated Vehicles (ROV's). They provide a clear perception of fouling distribution on most structural elements and risers, a regular update on significant changes in character of growth and rough estimates of size of dominant fouling species. However, data accuracy may be impaired due to equipment operability and quality of vision. ROVs cannot operate in the splash zone which is of primary importance to marine growth assessment and, not all operators utilise high resolution colour video cameras, thus being severely limited in quality of visual perception. The most serious drawback though is the inability to obtain precise measurements of thickness and length of fouling species.

b) Diver survey

Additional data are obtained through diver surveys which include on-site thickness and length measurements, close-up photographs for estimation of percentage surface cover and sample collection. The methods employed are as follows:

Size measurements: Probably the most ambiguous aspect of marine growth assessment is the definition of size. For hard growth such as mussels and barnacles thickness or, strictly speaking, height of the layer is the appropriate size. In the case of soft growth thickness tends to vary for reasons associated with species responce to environmental changes. Sea anemones, for example, retract when disturbed and reduce considerably in height (see also Appendix A), thus rendering virtually impossible an accurate measurement through mechanical means (e.g. depth gauges).

The highest degree of uncertainty occurs with flexible growths such as kelp and hydroids. Should the size of each individual be defined in terms of its extended length or in terms of thickness when wrapped around the member by wave or current action? Is the width of the kelp fronds significant? And what is the effect of stipe length and its flexibility? No satisfactory answers exist on these aspects, although Picken [80] suggests that, in the absence of experimental evidence which would indicate an appropriate measure, the fully extended length of each plant should be measured.

Measurements are taken either in-situ by scaled depth probes or tapemeasures or onshore from stereo photographs; the selection of the most suitable technique being dictated by the type of growth. Depth probes are not suitable for soft growth and seaweeds. They may lead to inaccurate thickness estimates of hard growth layers due to lack of penetration right down to the substrate and at least three spot checks are required to derive an average. The latter drawback can be overcome by using a tapemeasure wrapped around the member to estimate the increase in circumference and from this to deduce the average thickness of growth. However, by this method it is **not possible:**

- to estimate hard fouling thickness variations which occur among member faces;
- to differentiate between types of fouling when mixtures of hard and soft growth exist on different faces;
- to account for undulations in the layer of growth unless many closely spaced measurements are taken;
- to measure either soft growth, such as sea anemones and soft corals, or seaweeds since the tape will either fall in between some individuals or it will compress the plants onto the substrate in an unpredictable manner.

It appears, therefore, that stereo photography is the most reliable technique as almost all types of growth can be measured with reasonable accuracy from photographs which include size and colour scales. It is not intended to describe this technique here and for details the reader is refered to [24].

Percentage surface cover: As will be seen in later chapters, the effect of marine growth surface cover is a significant factor in hydrodynamic loading. Therefore it is important to obtain proper estimates on overall percentage cover and on distributions of dominant fouling over each member. All adopted practices on data interpretation fall short of this objective. The most common approach by the industry is to estimate approximately the percentage of hard and soft fouling from stand-off photographs, without specifying how it is distributed or what is the contribution of each species. Density of cover, particularly for kelp plants, is also rarely reported. Thus, the engineer does not have a clearly defined mapping of marine growth.

Sample collection: The main objective of live sample analysis is to identify the fouling species present at different locations on the structure, Thus, maximum sizes, longevity and reproduction capacity are established for predicting the future development of fouling. Qualitative data of this nature can only be tentatively used in characterising marine fouling as they do not define growth configurations and thickness variations.

The practice adopted by one operator consists of two diver surveys within a five-year certification period [81]. Emphasis is given on vertical sampling of a representative structural member at approximately ten depth elevations with more frequent sampling near the water surface. Additional information is obtained from marine fouled steel and concrete A4 size plates which are suspended at different depths from various platforms [82]. Thus settlement and growth rates can be regularly monitored at a fraction of diver deployment costs. Although this approach is regarded as most comprehensive the sampling rate is low and concentrates on vertical members. Picken [80] and Ralph [83] suggest higher sampling rates and thickness measurements and photographs of the top and bottom faces of major horizontal and inclined members. Whilst information is thus maximised it is not always feasible to incorporate such extensive surveys in the overall annual

inspection programme but, whenever possible, this practice is followed by most North Sea platform operators.

Further limitations regarding diver surveys arise from adverse weather conditions as no marine growth surveys are conducted in winter. There are strong indications that fouling, particularly kelp, dies back in winter possibly resulting in lower force coefficients. It has been suggested, but not validated by quantitative data, that die back may be up to 50% in length for kelp and hydroids at the splash zone, whilst minimal die back occurs at mid-water assemblage (-10m to -70m) [14].

4.3.2. Cleaning

Marine growth is removed from a structure either for inspection and repair purposes or, if design thickness tolerances are exceeded, to relieve structural loading. The cleaning requirements are different for each operation. Cleaning prior to inspection is carried out over small areas (e.g. nodes) and must produce 100% bare metal finish. A cleaning programme to relieve loading entails the removal of bulky fouling from large sections of the structure leaving only hard calcareous growth, i.e. tubeworm and barnacles. It is the latter type of operations that this study is concerned with. The reader should refer to other published material for further information on cleaning to facilitate inspection [e.g. 84,85,86].

The decision to clean part or the whole of a structure is based upon design thickness allowances and survey data which are reported to the Certifying Authority. If thickness levels exceed the tolerance limits pertaining to the structure the Certifying Authority may request cleaning prior to re-certification. Marine growth thickness thresholds vary among platforms. According to Lloyd's R.S. [69], typical hard growth limit thickness on North Sea platforms ranges between 50mm and 100mm down to -12m water depth gradually reducing to 25mm at the seabed, while soft fouling is reduced to equivalent hard growth by considering its thickness when compressed onto the member surface. However, the results from a survey among operators [9] shown in Table 4.4, illustrate the diversity of opinion in marine growth levels tolerated before remedial cleaning is deemed necessary. The contradictory figures indicate the confusing state of affairs which arises

from the following:

- inadequately defined marine growth levels,
- uncertainties to its effects on fluid loading,
- low design allowances for some of the earlier platforms.

The latter is particularly true for most Southern North Sea installations and some Central sector ones. Operators of these platforms have adopted a 'clean' policy which is sometimes based on two-year cleaning intervals [21,84]. Such high frequency is not only due to low design allowances but is also attributed to dominant mussel growth, which quickly re-establishes in multiple layers at the 0 to -20m depth range. Frequent cleaning is therefore concentrated on the upper parts of the structure the rest being cleaned less frequently, if at all. Scheduling is critical as cleaning ought to be done after the spawning period to eliminate possible resettlement shortly after removing established growth. However, the experience of one operator [16] indicates that mussel growth after cleaning tends to fluctuate in thickness over the years without exceeding critical levels. This suggests that if design thickness limit was high enough no remedial cleaning would be required.

This is certainly the case for Northern and Central sector installations. Conservative designs, higher fouling allowances coupled with non-abundant mussel growth have led to the adoption of a 'no-clean' policy for most structures. Watson [21] suggests that no cleaning need will arise in future due to stabilisation and self limiting thickness of growth. However, indications are that some cleaning may be required in the light of likely future domination of Northern sector installations by kelp growth in the wave affected zone.

Marine growth is removed almost exclusively by divers, the utilisation of ROV's or purpose built devices [87,88] being still minimal. The operational hazards and high costs of diver cleaning are widely acknowledged and well documented [84,89,90]. Cleaning for structural relief by ROV's would therefore be an attractive solution if such vehicles had the capability to operate and maintain station in the wave affected zone where loading due to marine growth is most critical. As it happens, and despite advancements in ROV technology, the operator still relies on divers. The cleaning techniques for steel structures are determined by [90]:

- operating depth, i.e. air or saturation diving
- deployment method, i.e. support vessel or platform spread
- type of marine growth
- size of area to be cleaned
- access to worksite and rigging requirements
- water visibility and tides.

Details on available techniques, their limitations and associated cleaning rates information are given in [9,78,84,90] and in relevant trade literature.

4.4. Antifouling Techniques

Cleaning of marine growth is only a temporary cure to a recurrent problem. Possible prevention of fouling may be achieved through various antifouling techniques but, as far as it is known, only a couple of the U.K. sector installations has any means of combating marine growth exclusively on the primary structure. This is attributed to the restricted lifetime of most antifoulants, the high material and application costs and the ensuing environmental consequences arising from the release of toxins [78]. Also, it is not unconnected with traditional design practice where underwater maintenance has been overlooked at the design stage.

Operators have realised the benefits of antifouling measures for new designs or even for existing installations. But due to the above stated reasons few applications have been carried out and these are concerned with conductors and risers [91]. One notable exception has been the installation of Cu-Ni sheathing on the legs of several platforms in Morecambe Bay primarily for corrosion protection in the splash zone [92].

Currently available antifouling methods are comprehensively reviewed by Sell [93] and Swain [94], so they are only briefly dealt with here. The methods may be classified into non-toxic and toxic ones. Non-toxic techniques are still at the development or trials stage. They include brush or spray applied epoxy resins [e.g. 95], oil based 'fouling release' cast coatings [91] and abrasion hoops driven by current action along the member [96].

Toxic compounds involve the gradual release of biocides into the water and encompass all commercial antifouling paints and Cu-Ni alloys [97,98,99]. Paints have been successfully applied on ship hulls but they rely on high release rates of toxins and reapplication every two to three years. Cu-Ni cladding possesses lower toxicity levels and lifetime is claimed to be more than 20 years [98]. It is available in various forms depending on type of application.

The use of Cu-Ni sheathing at the design and construction stages may lead in substantial cost savings. Reduced hydrodynamic loads have direct impact on steel weight, number of piles required, fabrication and installation costs. Barger et al [100] suggest potential cost savings up to 9% for typical North Sea platforms just by sheathing all conductors and members at the top two bays without though considering sheathing material and application costs. For retrofit applications a suitable product are the flexible composite panels where a 90:10 Cu-Ni matrix is embedded in neoprene backing. Each panel is wrapped round member sections which are free from appurtenances, and secured with fasteners along the seam. Experiments to assess the hydrodynamic effects of retrofit cladding indicated that drag coefficients are low despite the added panel thickness to the original member diameter [101]. These tests are described in Chapter 8.

4.5. Summary

From the preceding sections it is evident that:

- Force coefficient data from previous research are limited to largely unrepresentative forms of fouling.

- The hydrodynamic effects due to real long flapping weed and soft fouling have not been quantified.

- Most experiments have been performed at small scale without fully covering the in-service Reynolds number, KC number and relative roughness ranges.

- No systematic examination of marine roughness parameters other than thickness has been carried out.

- A high degree of uncertainty is associated with thickness tolerances and the use of "effective" member diameters at the design stage.

- Current marine growth survey procedures do not characterise adequately fouling for fluid loading assessment.

In the following chapter a new approach is described addressing the above mentioned problem areas and establishing the basis of the work presented here.

CHAPTER 5. A SYSTEMATIC EXPERIMENTAL APPROACH

Previous research has conclusively proved that marine roughness significantly increases hydrodynamic loading. Yet a number of questions remain unanswered. Has, for instance, past experimental work realistically represented full scale conditions? Are there differences between types of fouling in terms of loading and, if so, are they significant? What are the effects of mixed fouling or partial surface roughness? Do relative roughness and "effective" member diameter adequately define marine fouling? Could the apparent decrease in inertia forces compensate for the higher drag forces? And, how would the potential use of variable coefficients influence the design and maintenance processes?

Only a systematic experimental investigation could provide some of the much needed answers to those questions. The basic concept and the implementation of such an approach is described in this chapter and the likely advantages to the design and maintenance of offshore installations are highlighted.

5.1. Basic Concept and Specification

The principal objective of this study was to develop a methodology for the realistic assessment of hydrodynamic loading on marine roughened template platforms. In order to provide a framework for the proposed approach it is worthwhile to recall how marine growth develops during the in-service life of a platform.

Over a typical 25-year life span, several fouling types accumulate on the structure in varying rates, distributions, thicknesses, densities and surface cover. That is, marine growth undergoes temporal and morphological changes and it is reasonable to anticipate corresponding variations in hydrodynamic loading. More important still, are the maximum wave induced loads on heavily fouled structural members.

To improve on existing practices in estimating extreme and nominal hydrodynamic loads on marine fouled tubular members a realistic approach ought to address the following:

a) to characterise marine growth in terms of those "hydrodynamically significant" roughness parameters which adequately describe the marine growth development process;

b) to use force transfer coefficients which are directly related to the pertinent marine fouling and wave flow conditions;

c) to apply a rational methodology for the marine growth appraisal at the design and maintenance stages.

The above requirements are equally valid for the prediction of design loads and for the structural monitoring of existing platforms. However, a distinction is necessary in applying the approach to new designs and existing platforms due to differences in the levels of available information and in objectives sought in each case.

In the design of new structures it is required to predict under **assumed** marine roughness and wave flow conditions:

- the extreme overall and local loads that the structure is likely to experience when heavily fouled by certain species;
- the nominal loads acting on individual members throughout the operational life of the structure;
- the structural responce (e.g. member stresses in a joint) which, when combined with member sizing procedures and criteria, result in the acceptable level of platform strength.

In the assessment of existing structures it is required:

- to estimate the overall and local loads on the structure using **available** marine growth survey data and **given** structural member geometry;
- to compare the above estimates against design loads and assumptions and, if necessary, to re-assess fatigue damage and cleaning requirements.

The relationship of the proposed approach to new and existing structures will be further discussed in Section 5.4. Based on the foregoing, the strategy adopted in formulating and implementing the approach is illustrated in Figure 5.1 and its key elements are described in the following sections.

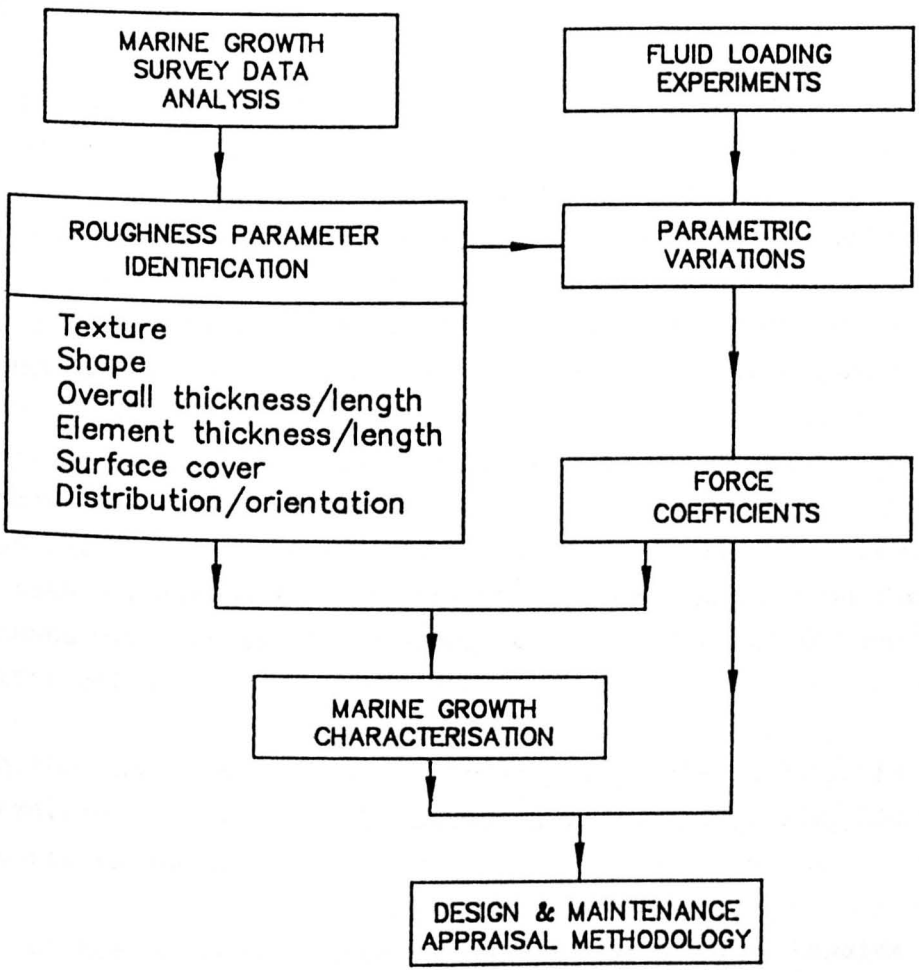

Figure 5.1. The proposed approach.

5.2. Marine Growth Characterisation

Evidently there exist infinite marine fouling configurations on offshore structures and it would be an impossible, if not meaningless, task to assess the fluid loading effects for specific geometries. On the other hand, it would be inappropriate to oversimplify a highly diverse and complex situation by describing roughnesses of different nature by a single independent thickness parameter or in terms of equivalent sand grain size.

The problem is therefore reduced to the pragmatic definition of marine roughness; pragmatic, since apart from the hydrodynamic aspects it must also reflect the constraints imposed by design, inspection and maintenance objectives and procedures. For instance, while say, the radius of curvature of roughness peaks may influence the drag of a tubular, it cannot be estimated by underwater survey techniques nor can it be predicted with any degree of accuracy. Desirable as it may be from a hydrodynamics viewpoint, to include this parameter in the characterisation of fouling it would be redundant information for the engineer with no relevant survey data at his disposal. That is, one must identify those roughness parameters which are both "hydrodynamically significant" and feasible to forecast and estimate with reasonable accuracy at the design and inspection stages respectively.

With the above in mind and as indicated by Figure 5.1, six roughness parameters were selected to characterise marine growth. The selection criteria included:

a) the potential contribution to hydrodynamic loading either by individual parameters or by a combination of two or more;

b) temporal and spatial variations of fouling established from marine growth surveys (see Chapter 6) and from information on the ecological behaviour of the dominant species;

c) constraints in measurement and control of each parameter by underwater surveys and under laboratory conditions.

Texture, shape and, to a large extent, mean element size are dictated by the physical characteristics of the fouling species. For the sake

of simplification, texture and shape were considered to be inherent characteristics of the species and could be defined simply by identifying the species. Mean element size was defined in terms of height for hard fouling (mussels, barnacles) and some soft fouling (sea anemones), and in terms of extended length for kelp and other seaweeds.

Surface cover, distribution and overall thickness are highly variable parameters being governed by several environmental, biological and geographical factors. They were defined through trends derived from survey data on a platform by platform basis as described in Chapter 6 and Appendix B.

Thus, marine roughness k_r could be represented by the function:

$$k_r(t,d_w) = G\{N_i, k_m, k, \lambda, D_r\} \qquad (5.1)$$

where, t = platform in-service time,
d_w = water depth at member location,
N_i = fouling species,
k_m = maximum overall thickness or length of fouling,
k = mean roughness element size,
λ = rough surface area/total surface area,
D_r = roughness distribution.

It goes without saying that any attempt to evaluate the above function (e.g. by assigning weighting factors) would require extensive systematic experimental verification, a methodology for which is described in the next section.

5.3. Systematic Experiments

The objectives of the experiments were:

a) to obtain a compehensive set of hydrodynamic force coefficients for marine roughened circular cylinders which would reflect with sufficient accuracy full scale conditions;

b) to identify the significant roughness parameters leading to effective characterisation of marine growth;

The first objective was the essential prerequisite for characterising fouling since the force coefficients formed the criterion in determining the hydrodynamic significance of marine roughness parameters.

The salient features of the experimental approach were as follows:

a) Flow conditions of similar scale to real sea kinematics

To a large extent, the relevance of laboratory experimental data to the design of offshore structures depends on whether the experiments have been carried out at a scale which is large enough to ensure their applicability to full scale conditions. It is noted that for the vast majority of template structures the "design wave" refers to post-critical Reynolds numbers ($Re>5x10^5$) and to KC numbers in excess of 50.

Steady flow presents a limiting case of time dependent flow at KC tending to infinity. Therefore, steady flow drag coefficients are well conditioned for design applications at high KC wave flows or combined wave and current flows. An added attraction lies in the relatively simple characterisation of steady flow compared to more complex wave or harmonic flows, which allows one to emphasise the comparative effects of marine roughness primarily on drag forces, without having to cope with uncertainties arising from complex flow fields.

The majority of the present experiments were carried out in steady flow at postcritical Reynolds numbers (up to $1x10^6$). The test procedure involved accelerating the cylinder from rest to a plateau of steady velocity in a vertical trajectory by means of its own buoyancy force. The test facility and procedures are described in Chapter 7.

What the steady flow tests could not provide was an absolute measure of the in-line and transverse force variations over the full range of KC and Re numbers pertaining to fixed steel structures. To this end, large scale tests were performed in regular waves past an artificially macro-roughened vertical cylinder with mean k/D of 4% at KC between 3 and 25 and Re up to $7x10^5$.

b) Simulation of the marine growth development process

As shown in Figure 5.2, experiments were carried out with marine and artificially roughened cylinders. It is apparent though that even such a limited number of roughness parameters as those indicated by Figure 5.2 cannot be modelled through artificial means without having some previous knowledge of the quantitative fluid loading effects of marine fouling. By using real fouling as the roughness agent it is possible to reduce the uncertainty related to roughness definition, particularly for texture and shape. However, artificial roughness offers the advantages of idealisation and close control of each parameter ,i.e. it allows for extensive parametric investigations and provides a reference comparative measure for marine roughness. It was therefore necessary to strike a balance between tests with artificially roughened and marine fouled cylinders.

Fouling patterns directly comparable to those encountered offshore were achieved in two ways. Firstly, by deploying cylinders of various diameters at selected offshore locations where fouling was allowed to accumulate on the cylinder surface and secondly, by artificially attaching real fouling to cylinders in a systematic manner.

Through the first method it was possible to simulate the fouling development process as it occurs on offshore structures, with the added advantage of higher growth rates. For example, typical mixtures of hard and soft fouling were obtained in longitudinal strips spanning the full cylinder length. Such patterns are among the commonest ones in the early development stages (first 3-5 years) of marine growth on structural members. Though this is the most realistic method it was not possible to attribute fluid loading variations to a particular species or roughness parameter, or even to obtain climax fouling in a short time period. Also, it was not possible to perform extensive experiments due to fouling deterioration, hence the need for artificial roughness.

Most of these problems were overcome by the second method where adult species were artificially attached to form the desired roughness geometries. This allowed for the systematic variation of the roughness parameters indicated by Figure 5.2 and for close control of each parameter, whilst ensuring that the developed patterns did not significantly deviate from the realistic fouling patterns found of-

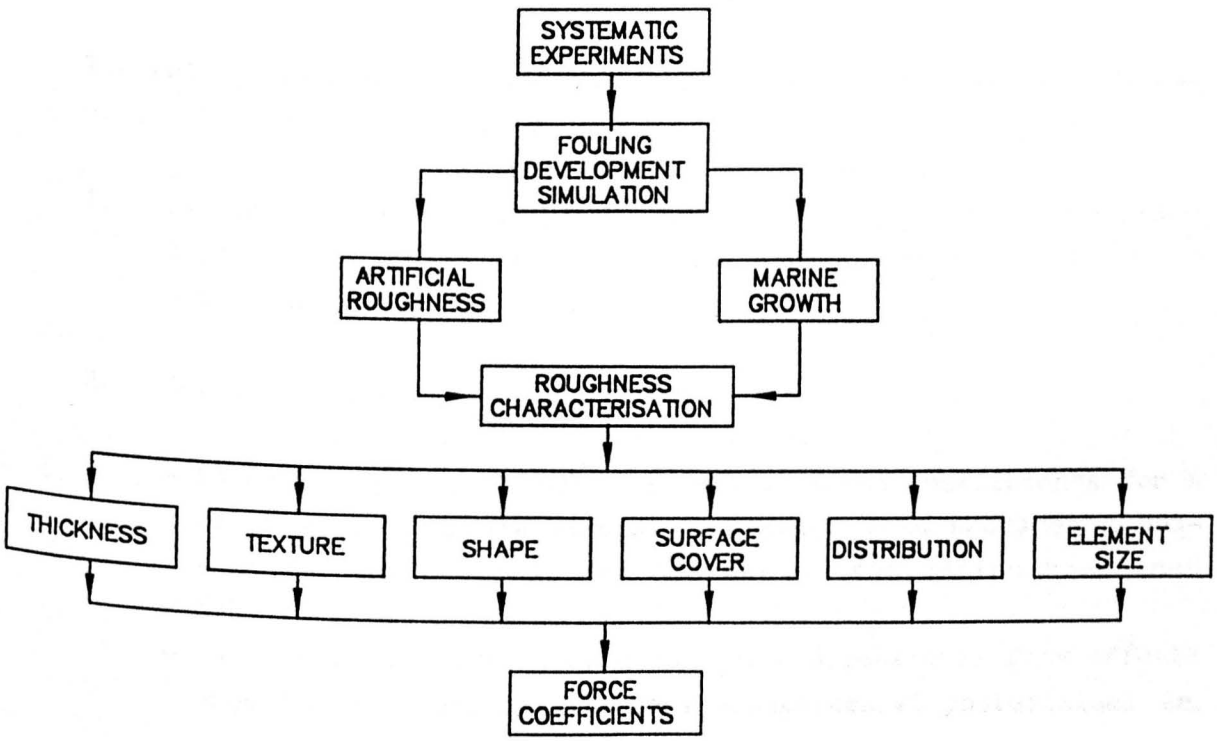

Figure 5.2. The systematic experimental investigation.

fshore. Details on the roughness configurations tested are given in the chapters dealing with the experimental procedures and results.

Perhaps the most significant parameter is the overall thickness of fouling. To obtain realistic relative roughness ratios, k/D, the test cylinders had diameters similar to those of platform members. Cylinder diameters ranged from 160mm up to 521mm without allowances for effective increase due to roughness. Thus scaling problems, a common drawback of many experimental studies of forces on rough cylinders, were effectively overcome. This advantage was further exploited by the experimental techniques to produce flow kinematics parameters which approximated the design environment of offshore structures.

The full programme of tests may be classified into the following categories each one aiming at specific goals:

1. **Calibration "smooth" and roughened cylinders;** to check the validity of test procedures and data analysis through a comparison with other published data.

2. **Artificially roughened cylinders;**

   - to establish a base reference set of force coefficients for a readily reproducible standard roughness that provides a context for the presentation of results for marine roughened cylinders;
   - to examine the aspect ratio and three dimensional flow effects upon drag coefficients for macro-roughness at postcritical Re.

3. **Marine roughened cylinders;**

   - to estimate the hydrodynamic forces due to different types of marine fouling;
   - to quantify the influence of marine growth thickness (or length for kelp) upon the fluid loading of cylinders;
   - to evaluate the drag coefficients for cylinders covered by naturally accumulated mixed fouling.

4. **Partially roughened cylinders;**

   - to assess how force coefficients vary with percentage surface

cover and distribution of roughness;
- to examine whether artificial roughness can represent with sufficient accuracy marine growth at reduced surface cover;
- to investigate whether a cylinder which is free from marine growth, apart from concentrations of heavy roughness in isolated circumferential bands, can be treated as a series of segments when estimating overall force coefficients.

5. **Pyramid roughened cylinders;**

- to test well defined and reproducible roughness in the form of standard shaped pyramids in steady flow and in regular waves.
- to compare with results obtained for marine roughened cylinders at similar relative roughness and to correlate with other published data from tests in regular wave and harmonic flows;

6. **Cylinders covered with antifouling cladding;**

- to assess the potential reduction in fluid loading arising from retrofit sheathing of tubulars;
- to investigate the effects of spanwise protrusions due to fitting appurtenances.

5.4. Relationship to Design and Maintenance

As stated earlier, the proposed approach distinguishes between new designs and existing platforms. In the following paragraphs this distinction is further clarified by outlining the basic philosophy of the marine growth orientated appraisal methodology in terms of its application to design and maintenance.

a) New designs

In view of the inherent uncertainties arising from sketchy historical environmental and loading data the hydrodynamic and structural design process is a simplified set of analytical models and parameters intended to arrive at given maximum and nominal levels of loading on the platform. The derived acceptable levels of platform strength must comply with the strategic objectives of the design process which is

to develop and maintain good performance and adequate safety at equitable cost. This may be best achieved through feedback of information between the fundamental stages in the life cycle of the platform. As illustrated in Figure 5.3 these stages are the design, fabrication and in-service maintenance.

The proposed approach enhances the interactions between the three stages through the following:

- interpretation of historical marine growth survey data in a form conditioned for the prediction of hydrodynamic loads;
- use of hydrodynamic force transfer coefficients which are directly related to the predicted marine growth levels.

Marine growth and design force coefficients are thus more accurately defined and the associated uncertainties are reduced. Therefore, it is possible, through a rigorous approach based on marine growth development scenarios, to evaluate alternative equivalent designs and to improve: firstly, on estimates of extreme structural responce and fatigue lives; secondly, on structural weight and first cost estimates; and thirdly, on forecasts of maintenance requirements in terms of cleaning intervals.

A detailed procedure on the selection of design force coefficients is described in Chapter 10. Also in the same chapter a computer application of the appraisal methodology is presented where its impact on materials, fabrication and maintenance requirements is assessed through techno-economic criteria.

b) Existing platforms

Being data dependent the approach is arguably better conditioned for the assessment of existing platforms which aims to maintain safety levels and structural integrity. The life cycle in this case is modified to one of "structural assessment-inspection-maintenance" as depicted in Figure 5.4.

Structural design and fabrication information is given in this case resulting in reduced uncertainties. As more data become available for the platform location through routine inspections and, possibly, wave and current monitoring, the assessment capability is continuously

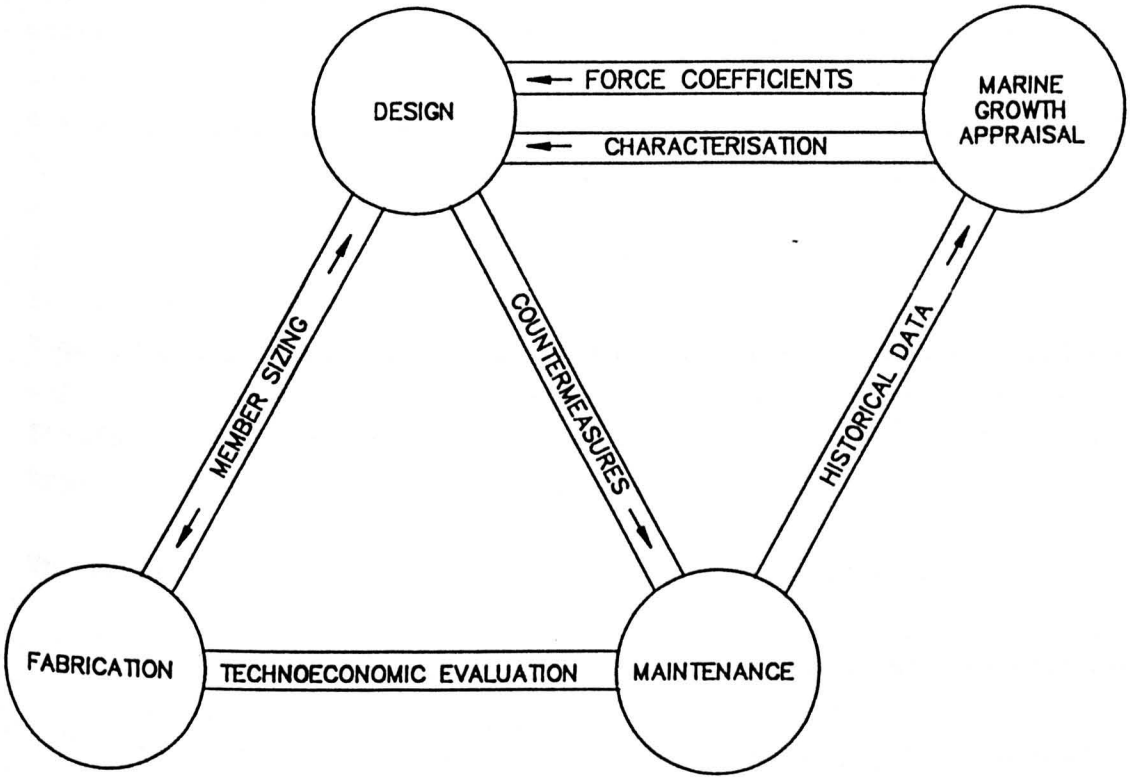

Figure 5.3. The key stages and interactions for new designs.

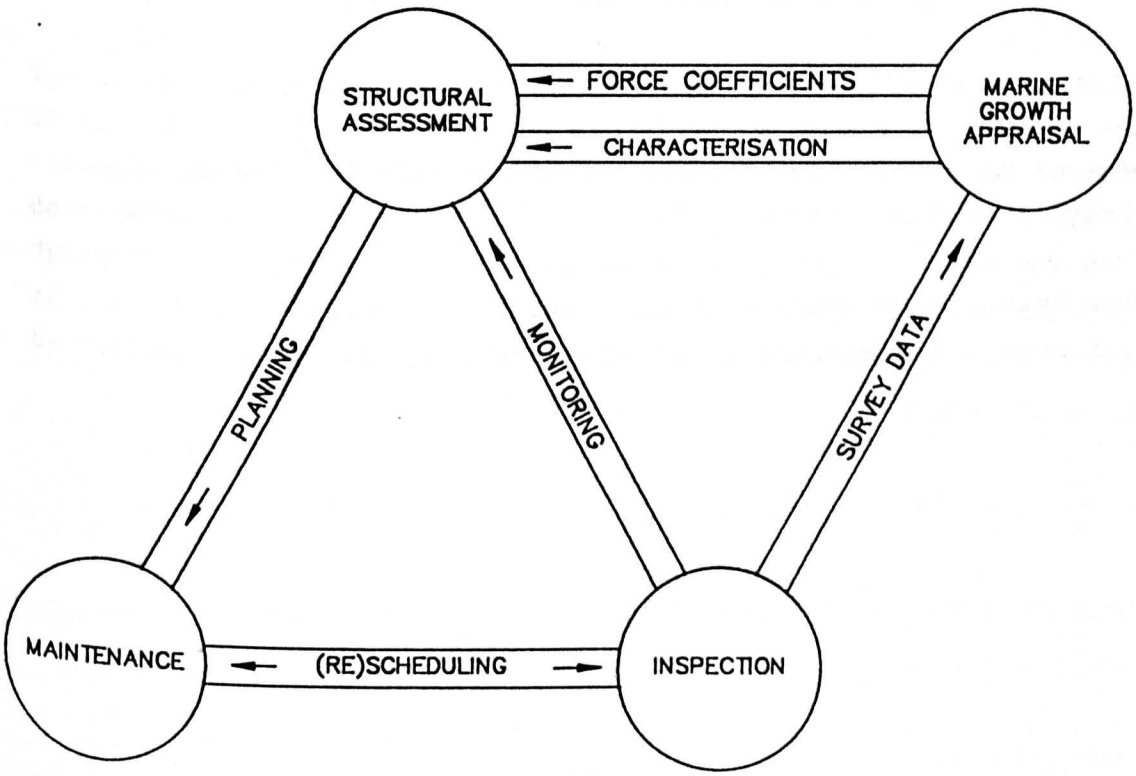

Figure 5.4. Key stages and interactions for existing platforms.

upgraded by abstracting information for characterising marine growth which is sufficiently accurate and applicable to structural re-analysis. The information requirements include all significant roughness parameters characterising the fouling of individual members at the time of inspection and the corresponding hydrodynamic force coefficients.

It is therefore feasible to revise the coefficients during the life time of the platform and, subject to flow kinematics and structural topology, to adopt different ones for tubulars with different marine fouling configurations as will be illustrated in Chapter 10 through typical applications to structural members.

The potential benefits can be realised in the following:

- fine-tuning of platform strength and joint fatigue life re-analysis;
- improved planning and re-scheduling of inspection and maintenance activities;
- rational interpretation of survey data leading to reduced inspection requirements;
- evaluation of alternative maintenance strategies;

The dependence of the proposed methodology to tangible data as well as to policy objectives by the platform operators cannot be more strongly stated. For this reason the present work is geared towards developing a comprehensive and constantly updated database of hydrodynamic coefficients. It is acknowledged that this is only one part of the loading estimation procedure and that other "grey areas" must be refined before the approach can be fully implemented in practice.

CHAPTER 6. MARINE GROWTH CHARACTERISATION

As explained in Chapter 5, the systematic experiments on marine roughened cylinders relied heavily upon the realistic reproduction of fouling. To this end, marine growth surveys for various North Sea platforms were reviewed. This exercise was carried out in parallel with the experiments and provided the information required to produce the test cylinders. Also, through the interaction with the experimental results, the survey data requirements were identified for characterising marine growth in the context of hydrodynamic loading.

The main review findings for six representative fixed steel structures are presented in this Chapter. They are based on a survey data collection and interpretation procedure which was largely developed in the light of the experimental findings. However, it seems appropriate to include them before discussing the experimental procedures and results to provide a reference context for the tested marine roughness configurations.

6.1. Data Requirements and Interpretation

Inspection specifications call for marine growth data where type, range of overall thickness and extent of the predominant form of growth are recorded for each structural member and, in some cases, live samples are collected. Such data are useful in monitoring fouling throughout the life span of the structure and in predicting future trends. However, for fluid loading purposes, they are often inadequate. The experimental results, presented in later chapters, suggest that additional data are needed for characterising marine growth. For example, the hydrodynamic loading on a member covered by sea anemones can be lower than that for a kelp covered tubular, yet higher than the loading expected due to hydroid cover. However, all three species are commonly classified as soft growth. Similar arguments apply to reported figures on average thickness and percentage surface cover without due consideration of uniformity or roughness distribution.

For hydrodynamic loading estimates, a comprehensive marine growth should be characterised through the detailed surface mapping of the member. Most data may be retrieved from ROV general visual survey

video recordings and stereo photographs. Supporting information obtained through diver surveys, strategic sampling, historical records and forecasting can verify and complement data on weight of fouling and size of individual species.

It is clear from the above, that all the required data can be retrieved from existing survey records, provided that the resolution quality of the visual records is high. What is important, therefore, is to interpret this existing information in a suitable format for characterising marine fouling. This should include the following:

- type and location of structural member
- identification of all significant fouling species, in terms of population and surface cover
- distribution and spatial arrangement of patterns for each fouling type over the outer, inner, top and bottom member surfaces (Appendix B, Figure B.1)
- maximum and average sizes of individuals on outer, inner, top and bottom faces of the member
- overall thickness of hard fouling layer recorded at regular intervals along the member and around its circumference
- composition and density of plants/animals per unit area.

The above procedure was applied to a review of visual inspection records for primary structural members of six representative platforms located in different sectors of the North Sea [7].

6.2. Survey Data Review for North Sea Platforms

The six platforms were selected according to their age and geographic location. It was therefore possible to examine marine growth both at the early stages of development and in the "climax" condition, and to identify the fouling species which dominate particular North Sea areas, or are likely to dominate in the future.

One platform (SNS1) is located in the Southern North Sea, three (NCNS1, NCNS2 and NCNS3) in the North Central sector and two recently installed platforms (NN1 and NN2) in the Northern sector. For a quick reference, the general marine growth characteristics are shown in Table 6.1. Although an overall impression of the growth was obtained

for each entire structure, only the members located within the wave affected depth zone were studied in detail. The data pertaining to each structural member are classified in Appendix B. Detailed descriptions are also included since they are considered an essential complement to the raw data and allow one to perceive a clearer picture of the marine roughness characteristics.

Despite the variety of the observed marine fouling configurations, some commonly encountered patterns were established through this review. Typical examples are illustrated in Figures 6.1 through 6.7. The main findings are summarised as follows:

a) Predominant marine growth on the SNS platform consisted of mussels and sea anemones, each type colonising over a distinct depth range. Heavy mussel growth dominated all members at the splash zone (Figure 6.1). Mussels grew in multiple layers or clusters and new growth was evident over older settlements resulting in average thickness of 60mm. Even heavier growth was concentrated around stubs or similar appurtenances. At depths below 12m, fouling consisted of randomly distributed patches of sea anemones and hydroids (Figure 6.2).

b) On platforms located in the Northern Central sector, various types of marine growth were present including kelps. Because of the age of the platforms, fouling should be expected to have reached a "climax" condition. However, there was evidence that the composition of fouling continued to change from hard to soft growth, with sea anemones expanding into the wave affected zone. Two examples of marine growth on NCNS platforms are shown in Figures 6.3 and 6.4. Members at the -25m elevation were 85-100% covered by sea anemones, the growth being heavier along the bottom face. At -5m a mixture of kelp, green weed and mussels covered the top and outer faces of bracings and small sea anemones covered the bottom face.

c) Marine growth on the recently installed NNS platforms was not fully established over the 0-30m depth range, and was insignificant at greater depths. Predictably, hard fouling (mussels, barnacles and tubeworm) colonised the top or outer sections of horizontal or inclined members respectively either in elongated strips or in randomly distributed clusters. Size of individuals varied with member location and face. Figure 6.5 shows a typical member

of platform NN1 fully covered by mussels along the top half with only small randomly distributed patches of mussels along the bottom half of the tubular. Similar patterns and types of growth were recorded on platform NN2 (Figures 6.6 and 6.7). In addition, low density cover by green weed and isolated kelp plants was evident among mussel beds, whilst the bottom and inner faces were dominated by hydroids.

d) Fouling distribution and surface cover varied along the span of inclined members, primarily due to water depth changes. Both parameters varied even among platform faces highlighting the influence of currents, light conditions and production water discharges. However, surface cover was always dense around anodes and other appurtenances and near the nodes resulting in overall thickness undulations.

e) For the majority of the inspected members it was not possible to assign relative roughness values due to the variability of fouling. Therefore, approximate k/D ratios are quoted only for those members which were almost fully covered by fouling of nearly uniform thickness. Relative roughness was based on the average overall thickness of growth and the nominal clean member diameter. For platform SNS1 k/D ranged from 0.07 to 0.17, whilst for the platforms located in the Northern sectors k/D was between 0.01 and 0.04.

Within the bounds of feasibility, every effort was made to incorporate the pertinent roughness parameters in the reproduction of marine fouling configurations on test cylinders. As will be seen in the next chapters, the relative hard roughness range encountered on offshore structures was adequately represented; as was the ratio of roughness element size to member diameter for both hard and soft fouling. Also the tested roughness densities, distributions and orientations to the principal direction of flow represented commmonly encountered fouling patterns offshore. The two reproductions which fell somewhat short of a realistic representation were the roughness by sea anemones and by mixed hard and soft growth for reasons given in Appendix C.

Platform	Water Depth (m)	Dominant Marine Growth
SNS1, > 15 years in service	MSL to -1.5	Mussels, 100% cover, 60mm thickness, all members
	-1.5 to -12	Mussels, 60-90%, 60-80mm thickness, all members
	-6 to -12	Hydroids, 20-90%, 10-50mm length, mainly on inclined members
	-12 to -25	Sea anemones, 30-90%, 20-100mm Thickness, 90% of members
		Mussels, 20-80%, 15-50mm thickness, south face only
NCNS1, NCNS2, NCNS3, > 10 years in service	MSL to -5	Kelp, 20-70% of top and outer faces, 60-900mm length, varying with platform face
		Green weed, 30-80% of top and outer faces, 30-150mm, 80% of members
		Mussels, 10-90%, 20-40mm thickness, 60% of members
		Sea anemones, 20-90% of bottom faces, 10-40mm, 60% of members
	-5 to -24	Sea anemones, 60-100%, 20-120mm, 100% of members
		Green weed, 20-30% of top and outer faces, 50-130mm, 30% of members
		Hydroids, 20-70%, 20-50mm, 40% of members
	-24 to seabed	Sea anemones, 70-100%, 60-120mm, 100% of members
NN1 > 3 years in service	MWL to -12	Mussels, 30-90% of top, outer and inner faces, 20-30mm thickness, all members
		Green weed, 30-80% of outer or inner faces, 20-40mm length, 70% of members
	-12 to -38	Hydroids, 90-100%, 20-30mm, 100% of members
	-38 to seabed	Hydroids, 10-40%, 20-30mm, 60% of members
		Tubeworm 10-30%, 2-6mm thickness, 80% of members
NN2 > 3 years in service	MSL to -16	Mussels, 60-80% of top, outer and inner faces, 25mm thickness, 60% of members
		Isolated kelp and green weed, up to 60% 100mm length, 80% of members
	-16 to -45	Hydroids, 50-100%, 20-60mm, 100% of members
		Mussels, 10-70% of top, outer or inner faces, South face only
	-45 to seabed	Hydroids, 60-100%, 20-80mm, 100% of members
		Solitary sea anemones and tubeworm

Table 6.1. General characteristics of marine growth of the six reviewed North Sea platforms.

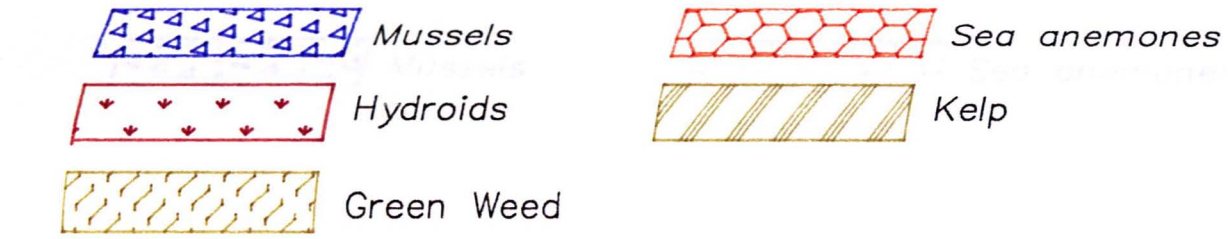

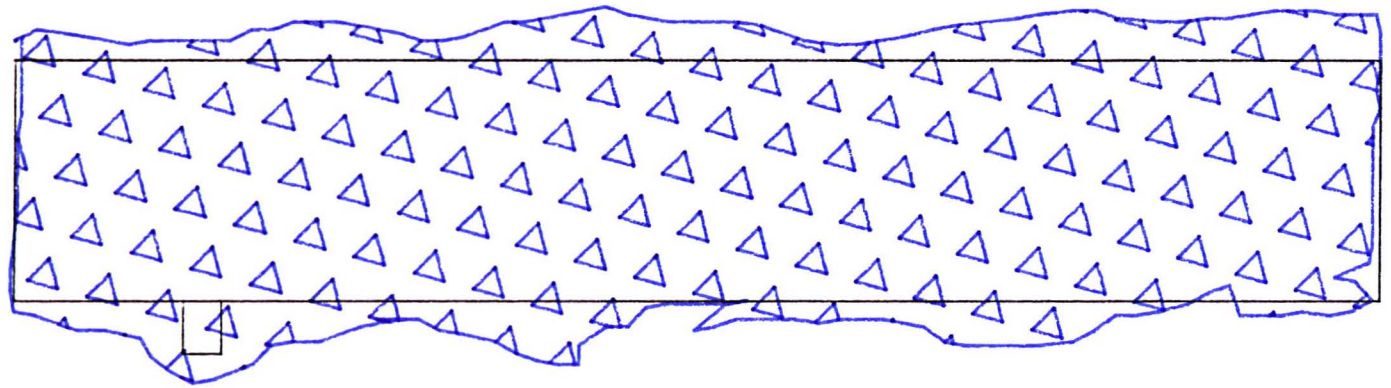

Figure 6.1. Mussel growth on platform SNS1 at −1.5m.

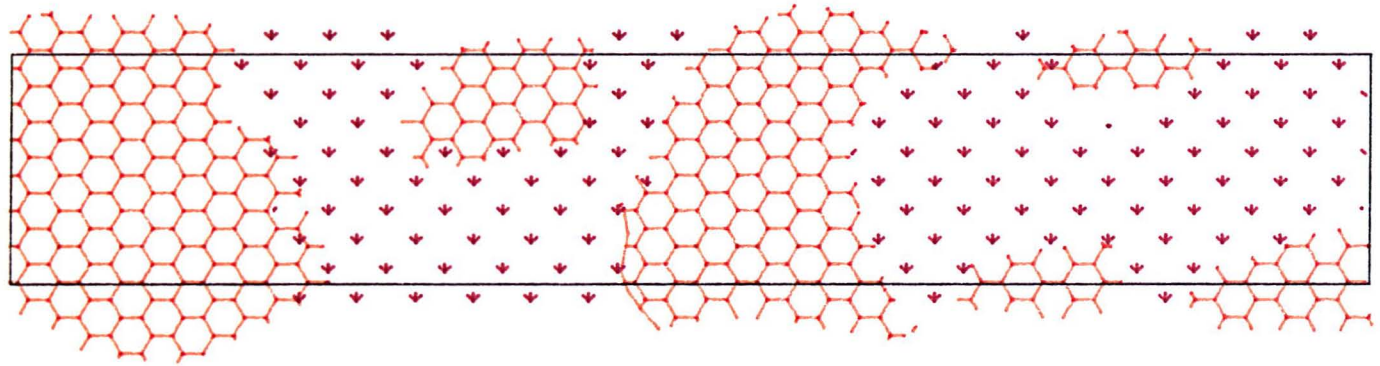

Figure 6.2. Patches of sea anemones and hydroids on platform SNS1 at −12m.

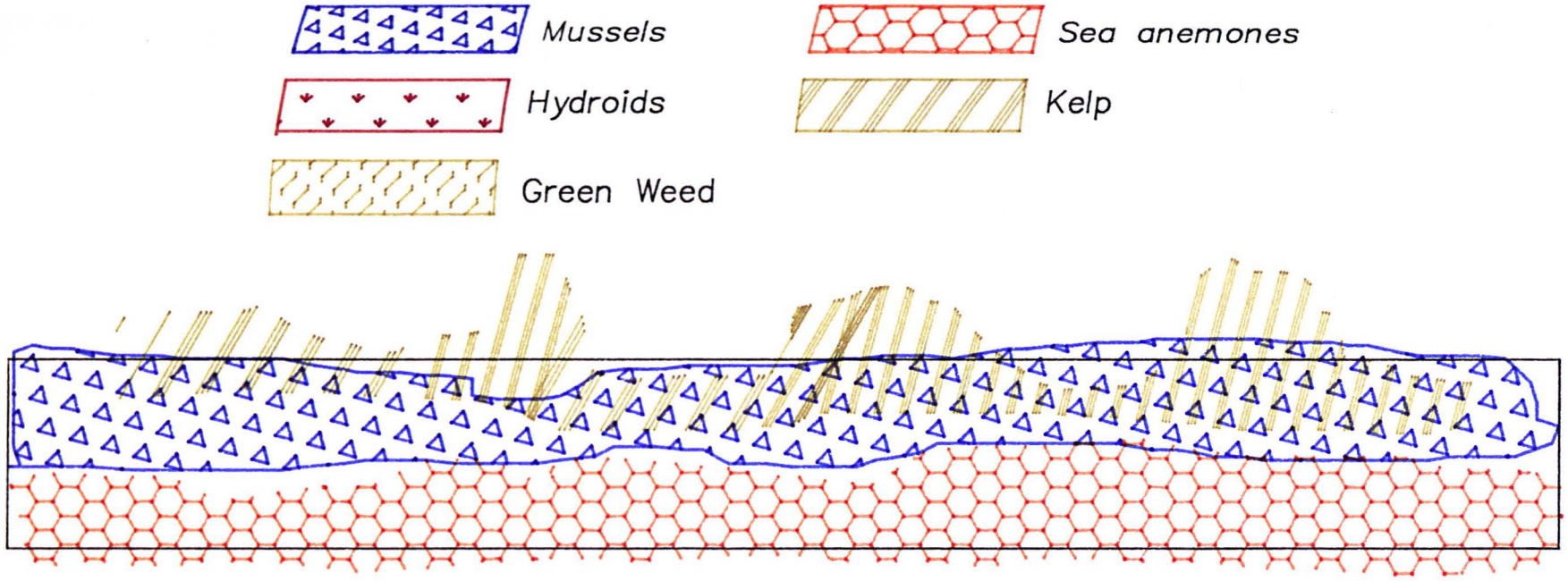

Figure 6.3. Typical fouling pattern on NCNS platform at −5m elevation.

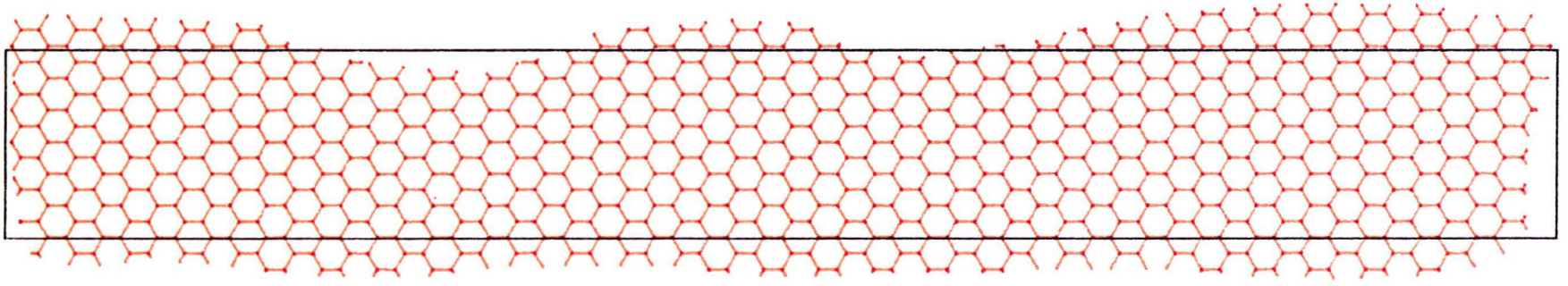

Figure 6.4. Sea anemones growth on NCNS platform at −25m elevation.

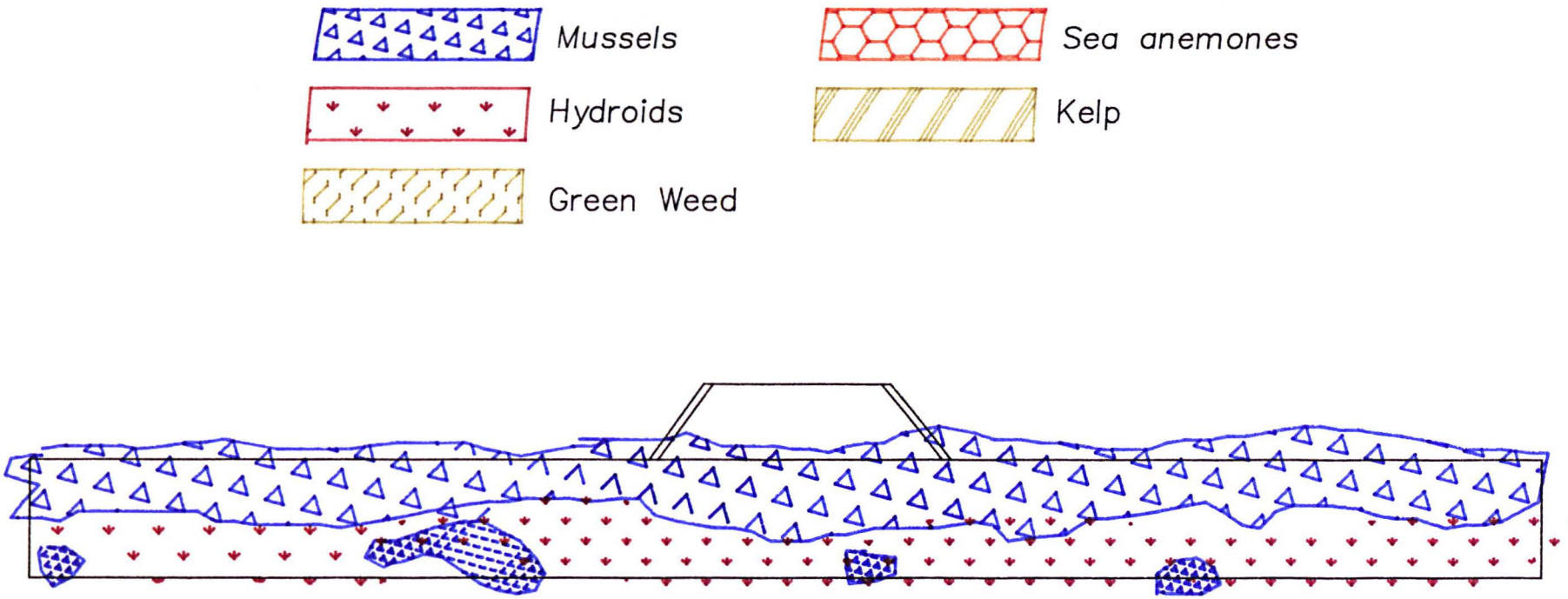

Figure 6.5. Partial mussel cover of horizontal bracing of platform NN1 at the splash zone.

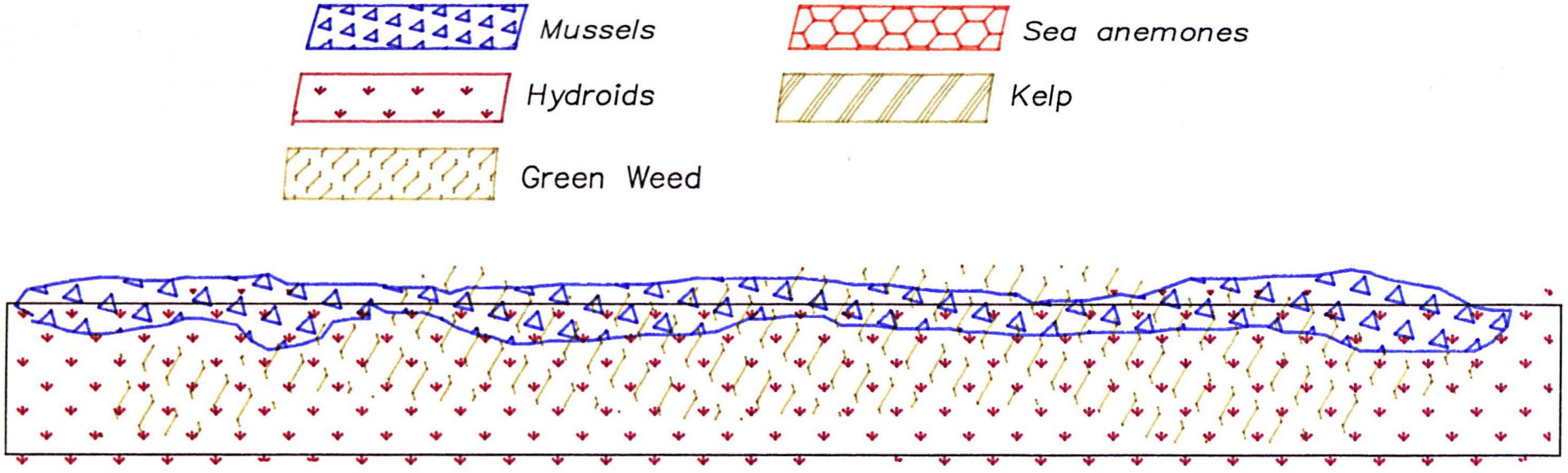

Figure 6.6. Marine growth on outer face of horizontal bracing of platform NN2 at the splash zone.

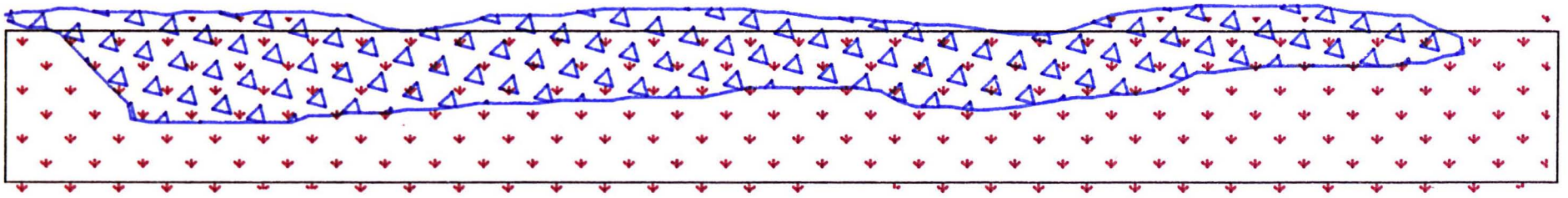

Figure 6.7. Marine growth along the inner face of the same member.

CHAPTER 7. EXPERIMENTS IN STEADY FLOW

As explained in Chapter 5, the experimental determination of hydrodynamic coefficients for macro-roughened cylinders formed the major item of the present study. The full programme of steady flow tests is outlined here and the experimental arrangement, test and analysis procedures are described for the steady flow experiments.

7.1. The Test Cylinders

For the steady flow experiments, several PVC and perspex circular cylinders were used. All cylinders were 1500mm long and ranged in nominal diameter from 150mm to 400mm. Each cylinder was fitted with a polyurethane foam core to provide the necessary buoyancy. Two wooden plates, of diameter equal to the inner cylinder diameter, were flush-fitted at either cylinder end and were secured by means of a threaded rod along the cylinder axis. Water leakage was negligible and the cylinders were assumed watertight during the data analysis.

The cylinders were roughened by marine growth or by artificial means. The types of fouling included mussels, kelp, sea anemones, tunicates and mixtures of hard and soft growth. Graded sand or gravel and pyramids were used for the artificially roughened cylinders. Mean element size, overall thickness, surface cover and distribution of roughness were systematically varied as shown in Tables 7.1 through 7.3. Relative roughness, k/D, is based on the mean roughness element height and the nominal "clean" cylinder diameter, except for pyramid roughness where an allowance is made for the base panel thickness. For partially roughened cylinders and only for reference purposes "local" k/D ratios are quoted. The quoted values of cylinder mass include the whole assembly of the test cylinder plus the mass of attached roughness measured in air.

The various techniques employed in preparing the roughened cylinders are described in Appendix C, which also includes photographs showing typical macro-roughened cylinders.

Nominal Diameter(mm)	Roughness Height k(mm)	k/D	Aspect Ratio L/D	Mass (kg)
400	1.95	0.005	3.75	46.5
200	1.5	0.0075	7.5	15.1
160	1.5	0.0094	9.375	10.0
400	3.9	0.0097	3.75	49.0
200	1.95	0.0097	7.5	15.5
150	1.5	0.01	10.0	N/A
160	1.95	0.012	9.375	12.5
315	3.9	0.012	4.76	38.5
400	7.5	0.0185	3.75	57.5
200	3.9	0.0195	7.5	18.5
160	3.9	0.024	9.375	14.5
315	7.9	0.025	4.76	46.0
400	10.0	0.025	3.75	65.0
160	10.0	0.062	9.375	19.0
Pyramids				
408	20.0	0.049	3.7	N/A
408	40.0	0.098	3.7	N/A

Table 7.1 Artificially roughened cylinders.

Roughness Type	Test Condition	Surface Cover (%)	Roughness k (mm)	Mass (kg)	
MUSSELS	Random patches single layer	5	29.5	42.4	
		10	29.5	44.0	
		20	29.5	48.0	
		25	8.0	42.0	
		25	24.0	49.5	
		25	34.0	51.5	
		50	8.0	44.5	
		50	24.0	59.5	
		50	34.0	61.5	
	Random patches, multiple layers	25	26.0	26.0	*
		50	26.0	32.5	*
	Strips	20	29.5	48.0	
KELP (L.Digitata)	Strips	20	1000	54.0	
KELP (L.Saccharina)	Random patches	25	1000	48.5	
		25	500	45.5	
		25	250	43.5	
		50	1000	57.5	
		50	500	52.5	
GRAVEL	Random patches	5	8	41.4	
		10	8	42.2	
		20	8	43.9	
		25	7.5	44.0	
		50	7.5	50.5	
	Strips	20	10.0	43.0	
		20	4.0	6.7	**

N.B. Nominal diameter of all cylinders was 400mm except for:
(*) 200mm diameter, (**) 160mm diameter.

Table 7.2. Partially roughened cylinders.

Type of Fouling	D(mm)	% Surface Cover	k(mm)	k/D or 1/D	Mass (kg)
MUSSELS					
-single layer	400	100	8.0	0.02	47.0
-single layer	400	100	24.0	0.06	78.5
-single layer	400	100	27.0	0.067	83.0
-single layer	400	100	34.0	0.085	82.0
-multiple layers	200	100	43.0	0.215	44.0
KELP					
-L. Digitata	400	100	500	1.25	62.0
-L. Digitata	400	100	1000	2.5	64.5
-L. Saccharina	400	100	500	1.25	63.5
-L. Saccharina	400	100	1000	2.5	67.0
SEA ANEMONES					
distribution:					
- non-uniform	400	40	60	0.15	N/A
- uniform	400	25	60	0.15	N/A
MIXED FOULING					
-Sea anemones and tunicates	315	70	20-80	0.16	44.5
-Barnacles,mussels and seaweed	315	35	24	0.076	39.5
-Barnacles,mussels and seaweed	400	45	24	0.06	50.5

Table 7.3. Marine roughened cylinders.

7.2. Experimental Facility and Instrumentation

The test rig is depicted schematically in Figure 7.1. It comprised a tall scaffolding tower the lower part of which stood in a tank of fresh water 3.8m deep. The overall tank dimensions were:

- length = 3.80m,
- width = 3.20m,
- depth = 3.80m,

with a floor opening of 2.70m by 3.20m i.e. spanning the full tank width. The scaffolding tower was 1.68m long by 2.20m wide by 8.0m high and was rigidly jacked against opposite tank walls and also against the tank floor and laboratory ceiling.

The technique involved accelerating cylinders from rest to a steady velocity in static water by means of buoyancy forces. Plastic cylinders were pulled to the bottom of the tank and then released. Figure 7.2 shows a plan view of the tank indicating the relative position of a 160mm diameter cylinder. The test cylinder was attached horizontally between two continuous loops of wire rope which acted as guides constraining the cylinder to rise vertically from the bottom of the tank. The cylinder was attached to the wire loops via four strain gauge transducers which measured the external forces applied to it. Two transducers were placed at each end of the cylinder; one at the top and one at the bottom. In addition to the buoyancy force provided by the foam core, weight pans were introduced in the upper half of the wire loops to allow the applied force and the speed of ascent to be varied by adding weights on either side of the loops.

To ensure the cylinder maintained a horizontal attitude the wire loops, which passed through low friction pulley blocks at the top and bottom of the rig, were wound around two drums several times. Both drums were rigidly connected to a single solid axle. To eliminate any transverse movement of the cylinder the wire loops were kept under constant tension. For symmetrical cylinders no transverse movement was observed. However, for cylinders with asymmetric appurtenances or fouling some transverse movement occured due to biased lift forces (see also Chapter 8).

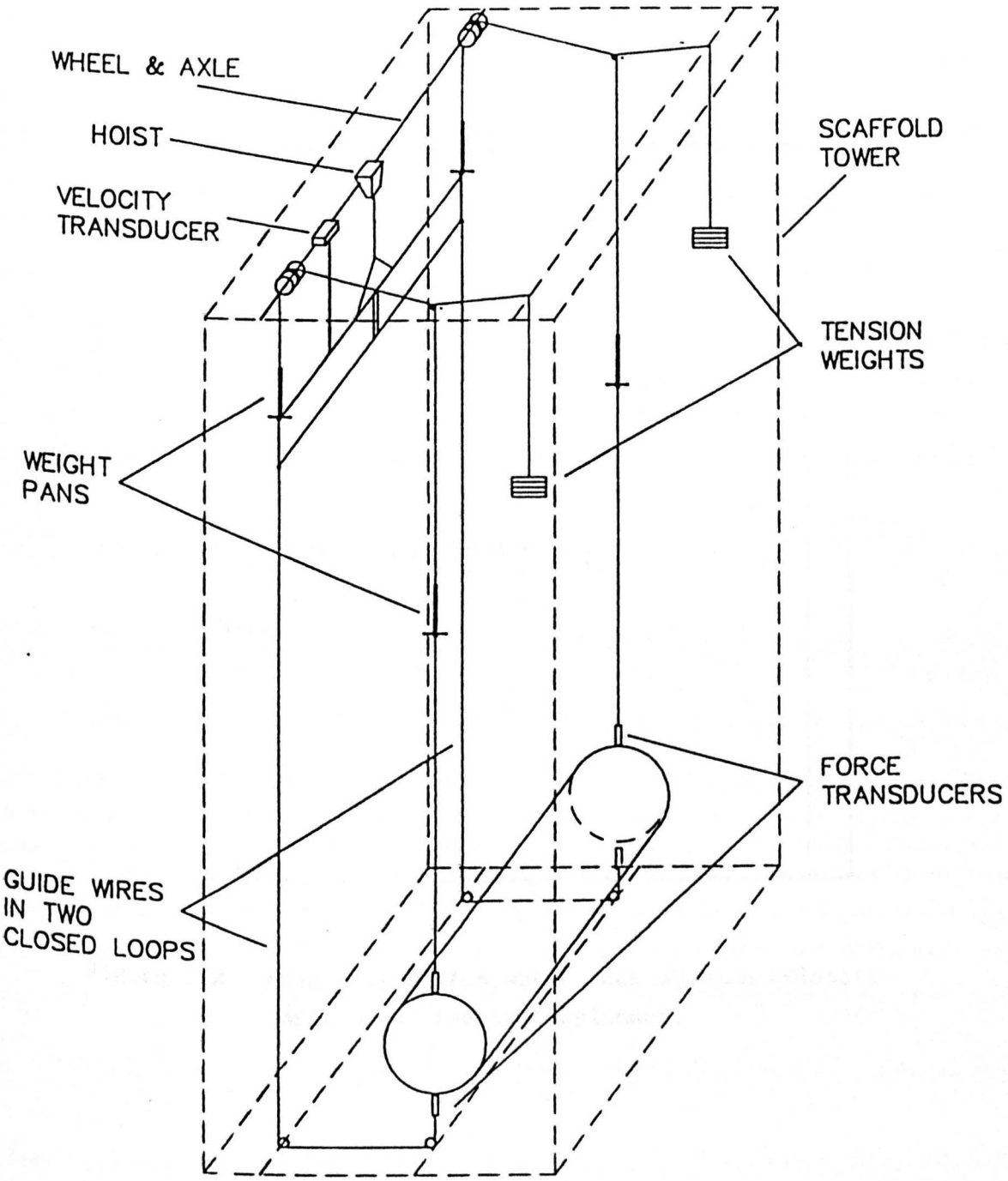

Figure 7.1. Schematic view of the test rig for "buoyant cylinder" tests.

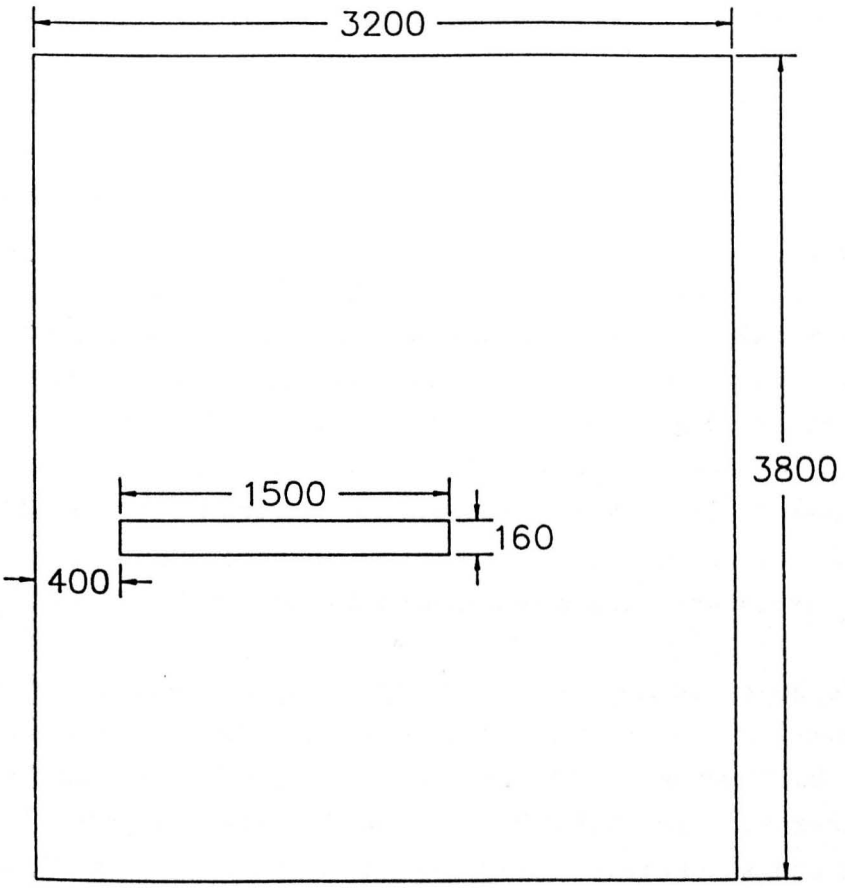

Figure 7.2. Plan view of the water tank showing relative position of the test cylinder.

The displacement and velocity of the cylinder were measured from the instant of release until the end of the test run by a position transducer and a tachogenerator. The output signals of the force and position transducers and tachogenerator were sampled at a rate of 40Hz per channel and digitised by a Tektronix computer through an analogue/digital converter. The data, which were stored in binary form on tape, could be displayed graphically on the screen.

The instrumentation used for the data acquisition is outlined in Figure E.1, Appendix E.

7.3. Test Procedure

Before the start of a set of experiments the force and position transducers and tacho were calibrated and the zero readings were checked. The foam filled cylinder was then attached into the wire loops and pulled beneath the water surface to determine the net buoyancy force. During this operation the parts of the wire loops above the cylinder were kept slack. The outputs from the tacho and position transducer were checked at the begining, centre point and end of a trial run to establish end points and check linearity.

The cylinder was pulled to the bottom of the tank by means of an electric hoist. After allowing for the water to settle, the transducer readings at the equilibrium (static) position were recorded. The computer data logging was started and the cylinder was released. At the end of the 3.0m long run the cylinder was retarded by the combined brake action of elastic ropes and of buoyancy loss as it broke through the water surface. The measurements of force, velocity and acceleration were being displayed on the screen for visual checking, and Reynolds number and force coefficients were estimated using typical data points to provide an instant check on the validity of the run.

The cylinder was then pulled back down to the bottom of the tank and the water was allowed to settle for at least 10 minutes before the next run. By appropriate use of weights a typical set of experiments with a smooth 400mm diameter cylinder would start at Re around 7.5×10^5 rising over three or four runs to 1×10^6 and then reducing to 3×10^5 approximately, filling in at intermediate speeds with four or

five more runs. The Re range covered by each test cylinder obviously varied with diameter. Figure 7.3 shows the final stages of a typical test run sequence.

At the begining and end of each set of tests the cylinder was photographed, usually in four orientations, to obtain a complete picture of the roughness pattern.

7.4. Data Analysis Procedures

The force on the cylinder at every sampled position during a run was obtained from the difference between the sum of the two top transducer signals and the sum of the two botttom ones giving the net force applied to the cylinder whilst in motion. The static force was measured in the same way in still water just before the cylinder was released. The total force was then the difference of the net dynamic and net static forces.

The instantaneous velocities and accelerations were either the derivatives of consecutive displacement readings taken through the position transducer or direct velocity measurements and their derivatives taken from the tacho. Although no discernible differences were found between the two measurement techniques the latter was used during most data analyses for faster computation.

All data were filtered using a simple running average process to remove noise. The filtered force, velocity and acceleration curves for a typical run are graphically illustrated in Figure 7.4 together with the regions used in calculating the drag and inertia coefficients. The data for the same test run are listed in Table 7.4. Typical graphical illustrations of other test runs are included in Appendix E.

The steady velocity region was selected over a range where acceleration became negligibly small. Care was taken to disregard the part of the run where the cylinder was approaching the water surface to exclude any free surface effects from all calculations. The total force corresponding to the steady velocity region was estimated and the arithmetic means of both force and velocity were used to obtain the drag coefficient C_d.

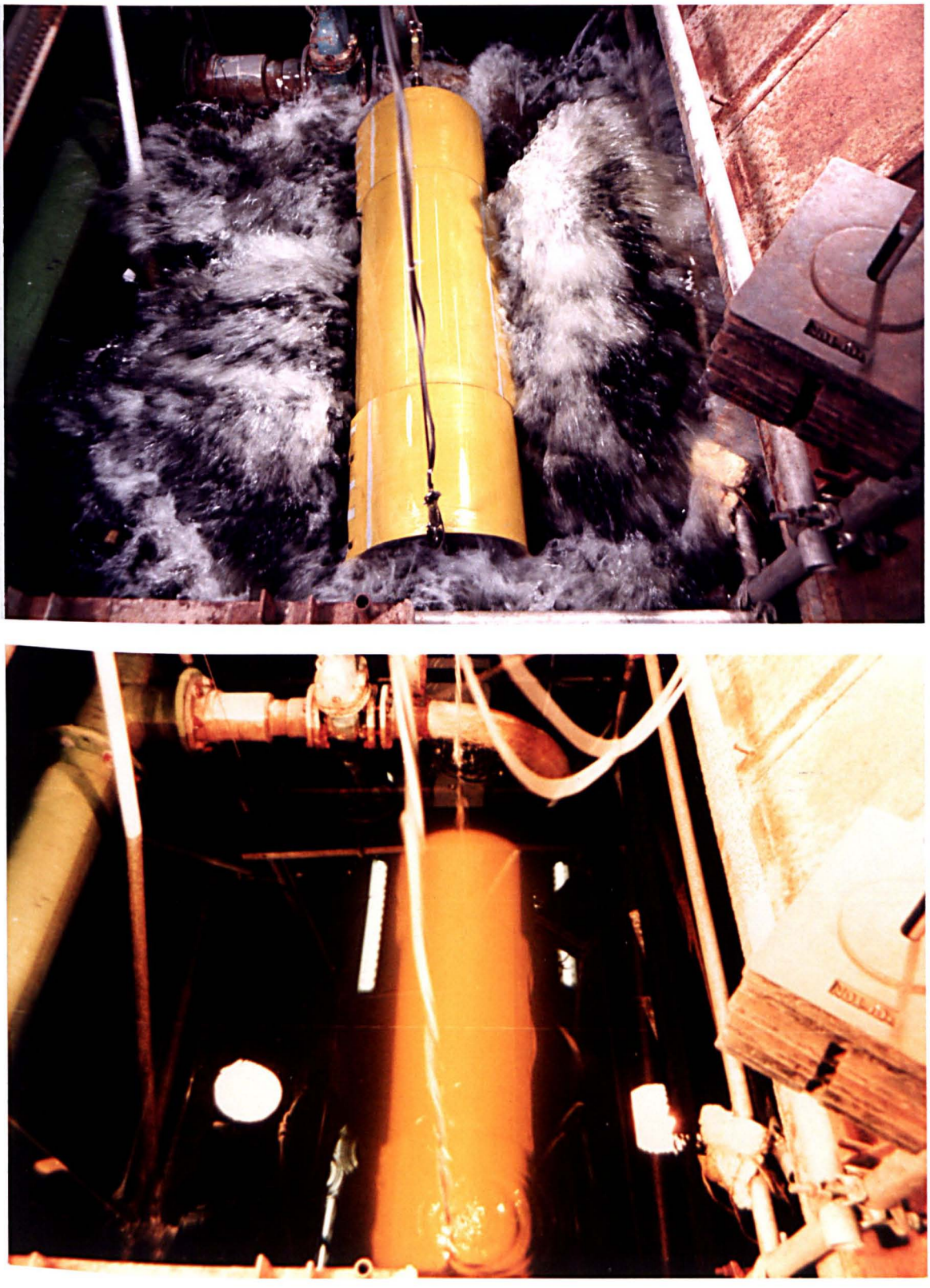

Figure 7.3. Final stages of a test run showing the cylinder approaching and finally breaking through the water surface.

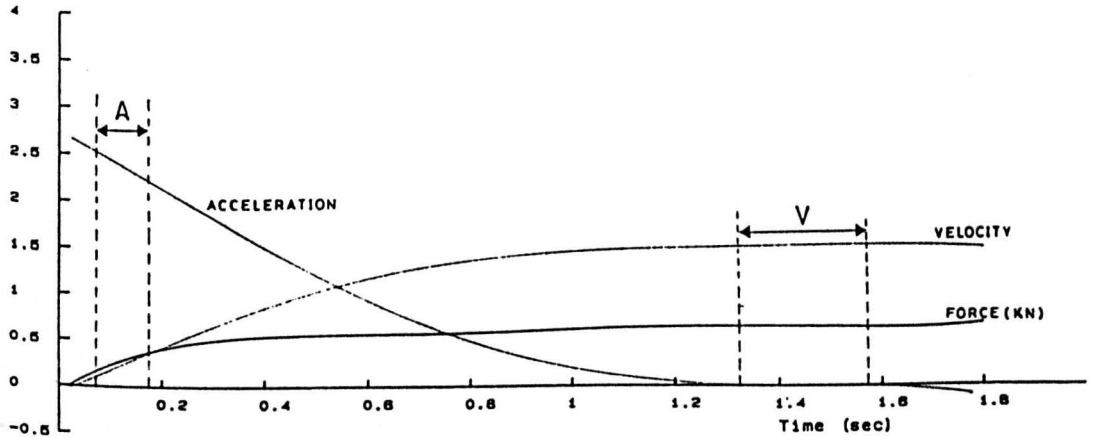

Fig. 7.4. Graphical output of time history for typical test run.

VELOCITY =1.506975113289 M/S
ACCELERATION =2.366427736122 M/S2
DRAG FORCE =635.257292197 N
INERTIA FORCE =27.66576714 N
REYNOLDS NUMBER =0.269102702302 X E6
DRAG COEFFICIENT =1.86485997605
INERTIA COEFFICIENT =2.44466427107

TIME (sec)	FORCE(N)	VELOCITY(M/S)	ACCELERATION(M/S2)
0.025	11	-0.026	2.663
0.050	32	0.038	2.592
0.075	163	0.102	2.519
0.100	245	0.165	2.444
0.125	288	0.228	2.368
0.150	327	0.291	2.291
0.175	368	0.353	2.212
0.200	401	0.411	2.133
0.225	433	0.473	2.053
0.250	458	0.531	1.972
0.275	479	0.588	1.893
0.300	497	0.644	1.814
0.325	511	0.697	1.734
0.350	523	0.749	1.655
0.375	532	0.799	1.577
0.400	539	0.847	1.499
0.425	545	0.893	1.423
0.450	549	0.938	1.347
0.475	553	0.980	1.274
0.500	555	1.020	1.201
0.525	557	1.058	1.130
0.550	558	1.094	1.061
0.575	560	1.126	0.993
0.600	561	1.160	0.928
0.625	562	1.190	0.864
0.650	563	1.219	0.802
0.675	564	1.245	0.744
0.700	565	1.269	0.687
0.725	567	1.292	0.632
0.750	569	1.313	0.580
0.775	572	1.332	0.530
0.800	574	1.350	0.482
0.825	577	1.366	0.437
0.850	581	1.381	0.394
0.875	585	1.394	0.354
0.900	589	1.406	0.316
0.925	593	1.417	0.281
0.950	597	1.427	0.248
0.975	601	1.436	0.217
1.000	606	1.444	0.189
1.025	610	1.451	0.163
1.050	615	1.458	0.140
1.075	619	1.463	0.118
1.100	623	1.468	0.099
1.125	627	1.473	0.082
1.150	630	1.477	0.067
1.175	633	1.481	0.054
1.200	636	1.484	0.042
1.225	638	1.487	0.032
1.250	640	1.490	0.024
1.275	641	1.493	0.017
1.300	642	1.495	0.011
1.325	642	1.497	0.007
1.350	642	1.500	0.003
1.375	641	1.502	0.001
1.400	640	1.504	-0.001
1.425	638	1.506	-0.003
1.450	636	1.508	-0.004
1.475	634	1.510	-0.006
1.500	632	1.511	-0.007
1.525	629	1.512	-0.009
1.550	627	1.513	-0.011
1.575	624	1.514	-0.012
1.600	622	1.515	-0.014
1.625	619	1.516	-0.015
1.650	616	1.516	-0.016
1.675	613	1.517	-0.017
1.700	610	1.517	-0.018
1.725	606	1.517	-0.019
1.750	603	1.517	-0.020
1.775	599	1.517	-0.021
1.800	595	1.517	-0.021

Table 7.4. Tabulated data for the same run.

$$\text{i.e.} \quad C_d = \frac{F_d}{0.5\,\rho\,D\,L\,u^2}$$

where, F_d = drag force,
ρ = fresh water density,
D = nominal cylinder diameter,
L = cylinder length,
u = velocity.

The added mass coefficient, C_a was calculated at the start of the run when the velocity was negligible. For a cylinder accelerating in still water C_a is given by:

$$C_a = \frac{F_i - m_c\,\dot{u}}{0.25\,\rho\,\pi\,D^2\,L\,\dot{u}}$$

where, F_i = inertia force,
m_c = mass of cylinder including dry mass of fouling or artificial roughness,
$\dot{u}$ = acceleration.

The corresponding inertia force coefficient for a stationary cylinder in fluid flow, C_m, is then:

$$C_m = 1 + C_a$$

Due to data fairing and also possibly due to wire stretch the derived accelerations were not always a maximum at the start of the run but a fraction of a second later as can be seen from the time series of typical runs shown in Figures E.2-E.7 , Appendix E. The measured total force also showed the same characteristics. Some inertia coefficients were, therefore, calculated using the mean acceleration up to the point of maximum acceleration and the corresponding mean force. The related velocities over this inertia dominated regime were low and the drag component was minimal. An allowance for the drag force was calculated, following the method by Kim and Hibbard [102], using the steady state C_d and the mean velocity at the inertia dominant region for each run. The effect of this minor correction was found to be small as can been seen from results presented in Chapter

8, where both corrected and uncorrected C_m values are reported.

The Reynolds number for all the results was calculated using the average steady velocity. The diameter used in all calculations was that of the "clean" cylinder unless stated otherwise.

An alternative way to calculate C_a would be to include the added volume of fouling or artificial roughness by introducing an allowance to the cylinder diameter. This would result in lower C_a values for marine roughened cylinders by about 4-5%. The C_a values presented here do not include this allowance which is significantly less than the data scatter in C_a obtained through the "buoyant cylinder" experimental technique.

CHAPTER 8. STEADY FLOW EXPERIMENTS - RESULTS AND OBSERVATIONS

The results from the unidirectional steady flow tests are presented in this chapter according to roughness type and surface cover. Hydrodynamic drag is considered in detail whilst only the trends in inertia coefficients are discussed. The flow conditions under which the inertia forces were measured using the "buoyant cylinder" technique are not fully representative of those for waves or planar oscillatory flows. Despite the fact that few significant conclusions can be drawn for the various roughness parameters, it is reasonable to assume that the inertia coefficients presented here may at least provide some trends. Detailed C_m data are given in [1,5,6].

8.1. Calibration Smooth and Rough Cylinders

Nominally smooth and lightly abraded cylinders of diameter ranging from 160mm to 400mm were tested at various stages of the experiments. No surface preparation of the "smooth" cylinders was carried out as these tests were only intended for calibration of the test apparatus and data acquisition system and to check for data repeatability. Also the surface roughness was not measured due to non-uniform surface irregularities caused by scratches or by the PVC extrusion process. A more uniform roughness was achieved with the abraded cylinders and the measured roughness height averaged 0.4mm resulting in the following k/D range:

Cylinder diameter (mm)	k/D
160	0.0025
200	0.002
400	0.001

The variation in C_d with Reynolds number for smooth and abraded cylinders is shown in Figures 8.1 and 8.2 respectively. The drag coefficients show reasonable correlation with earlier work [34,48] as illustrated in Figure 8.3 and suggest that the roughness of the nominally smooth cylinders is of the order of 0.02mm although this estimate should be qualified as potential three dimensional flow effects for smooth cylinders cannot be discounted (see Section 8.2). The corresponding C_m values correlate reasonably well with potential flow theory despite some scatter (Figure 8.4).

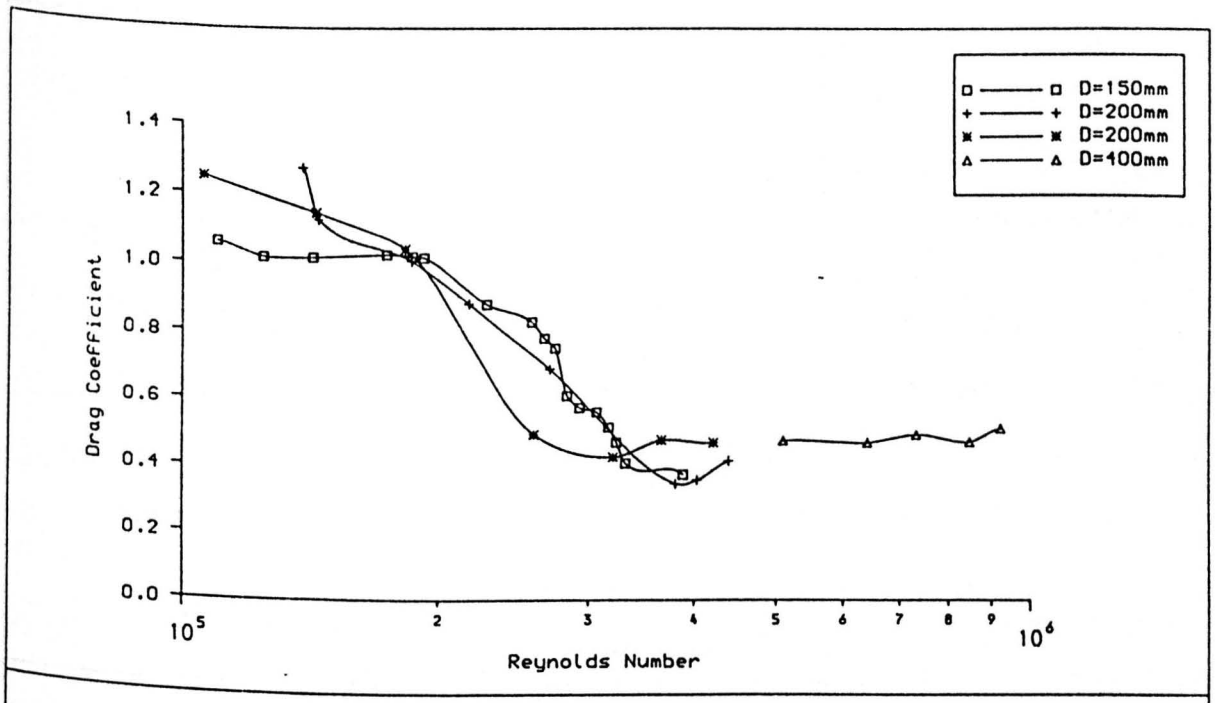

Figure **8.1.** Drag coefficients for nominally smooth cylinders.

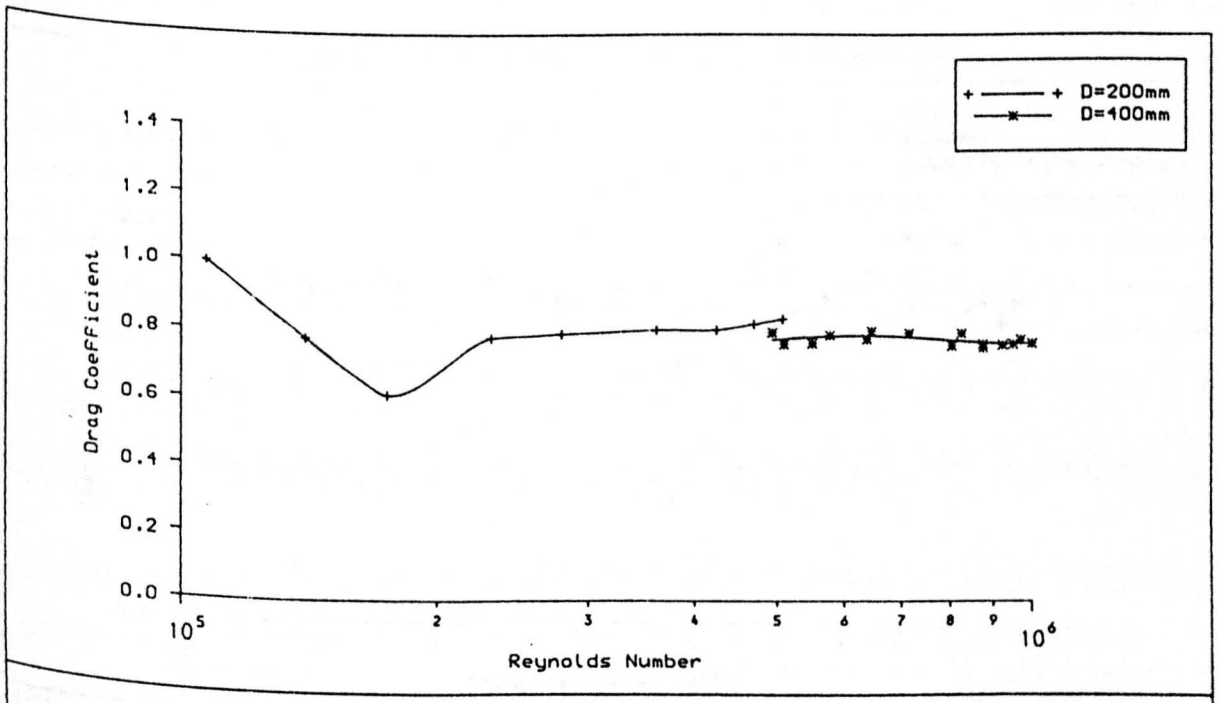

Figure **8.2.** Drag coefficients for abraded calibration cylinders.

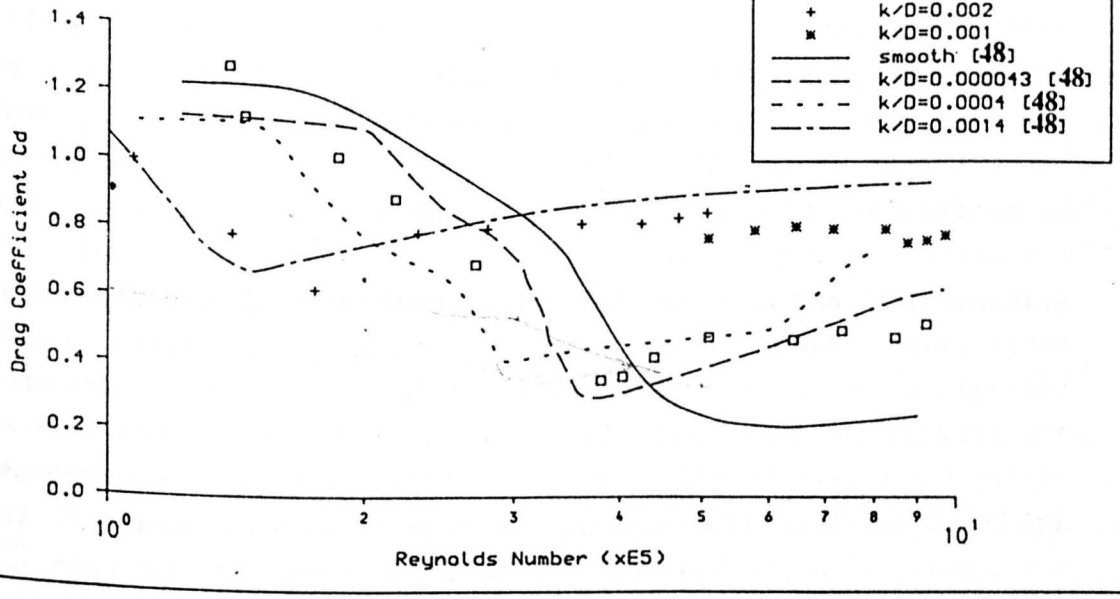

Fig. 8.3. Cd of nominally smooth and abraded calibration cylinders.

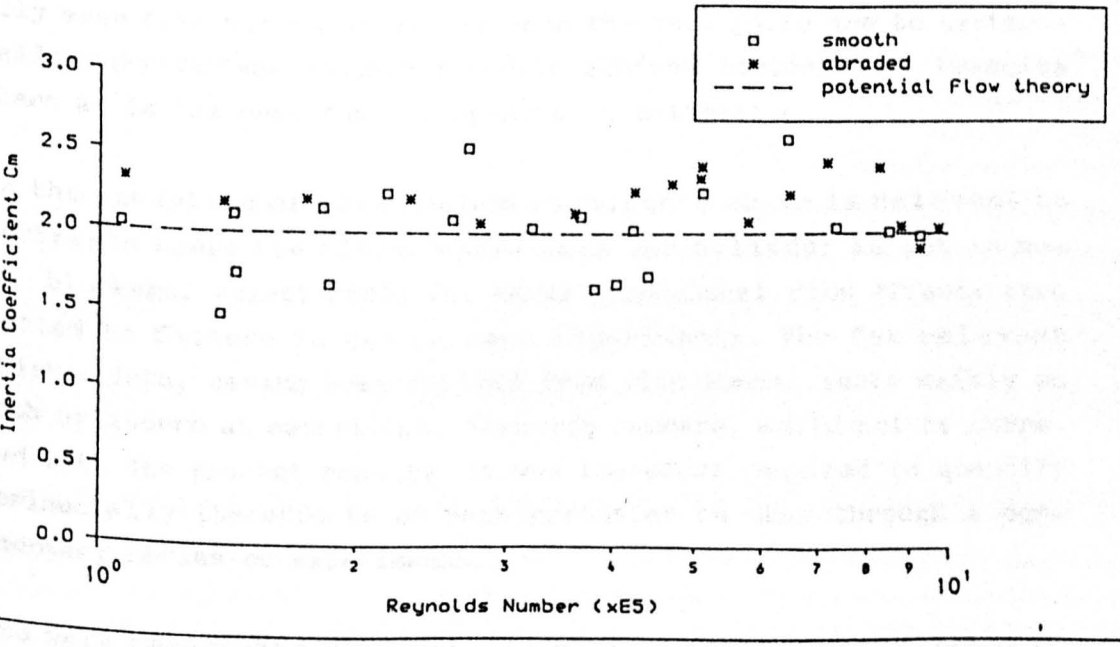

Fig. 8.4. Cm of nominally smooth and abraded calibration cylinders.

8.2. Artificially Roughened Cylinders

As listed in Chapter 7, Table 7.1, fourteen sand roughened cylinders were tested covering a k/D range of 0.005 to 0.062 and a Re range between 1.2×10^5 and 1×10^6 approximately. Also tests were carried out with two pyramid roughened cylinders at k/D=0.049 and 0.098 respectively. The results are summarised in Table 8.1. In the absence of any C_d dependence on Reynolds number the mean drag coefficients can be presented in a Re independent form together with the corresponding standard deviations. Any significant trend with Reynolds number tends to decrease as k/D is increased beyond 0.002. All the tests reported here were carried out at much higher k/D values and the results are in agreement with previous findings which suggested that the postcritical Re regime is shifted down to approximately 3×10^5 at k/D>0.002 [48]. However the uncertainty about the definition of roughness height is fully realised.

Apart from surface roughness, several secondary parameters influence the flow structure and hence the pressure drag for circular cylinders. These are the blockage, aspect ratio, free end effects and free-stream turbulence and are present to a greater or lesser extent in all experimental studies. All parameters interact with each other and, unless they are closely controlled, the effects of one may be masked by the others. However, close control of all parameters is hardly ever feasible particularly when the main goals are to systematically vary surface roughness and to achieve postcritical Reynolds numbers as is the case for the present investigation.

With the exception of free-stream turbulence which is relevant to experiments where the fluid rather than the cylinder is set in motion, blockage, aspect ratio and three-dimensional flow effects were expected to feature in the present experiments. The few relevant published data, having been derived from wind tunnel tests mainly on smooth cylinders at subcritical Reynolds numbers, could not be correlated with the present results. It was therefore required to quantify experimentally the effects of each parameter on drag through a complementary series of experiments.

Tests were undertaken with two sets of sand roughened cylinders of length-to-diameter ratio ranging from 3.75 up to 10. Relative roughness was approximately constant for each set at k/D of 0.0094-0.01

and 0.025 respectively. Roughness was chosen to be sufficiently large such that the mean flow became independent of Reynolds number and no dramatic changes would occur in the position of separation. Thus it was possible to concentrate on the secondary parameters and to ensure compatibility with the experiments on macro-roughened cylinders.

The results are discussed in the following paragraphs together with a brief description of the flow mechanism associated with each parameter.

Blockage

The confinement of the flow past symmetric bodies arising from the dimensional constraints of the experimental facility is termed as **blockage.** Blockage is usually expressed as the ratio of the model frontal area (A) normal to the flow over the cross-sectional area of the test facility (C), i.e. B=A/C. The two main types of constraint for circular cylinders are the **solid** and **wake blockage.** Solid blockage arises from the lateral restriction of the flow to expand as freely as it would if unconfined. Higher velocities are induced in the vicinity of the cylinder causing a rise in absolute base pressure and in the drag coefficient. Pressure drag increases further due to wake blockage. It is caused by the velocity deficit within the wake which implies that the velocity outside the wake must be larger than that in unconfined flow such that mass continuity is maintained.

Both effects alter substantially the pressure distribution around the cylinder by shifting the points of separation and transition, the net effect being the increase in C_d with increasing blockage ratio. Since in high Reynolds number steady flows past rough cylinders it is the surface roughness which triggers early transition, one would expect a minimal effect at least for low blockage ratios. The results of Farrel et al. [103] and West and Apelt [104] indicated that C_d is hardly affected at blockage less than about 6%. In the present experiments blockage varied between 1.8% and 4.9% depending on cylinder diameter suggesting that there was no need to subject the data to correction procedures whose applicability to this technique is at any rate doubtful.

The few available correction procedures (e.g. Allen and Vincenti [105], Maskell [106]) have been developed almost exlusively for wind tunnel flow conditions at subcritical Reynolds numbers and for smooth bluff bodies. However, for the sake of completeness, the Allen and Vincenti correction formulae were applied to the mean drag coefficients obtained from this series of tests. The procedure is described in Appendix F and the corrected values are plotted in Figure 8.5. Although blockage varied with aspect ratio resulting in a combined effect which might be different had aspect ratio been kept constant, the "corrected" C_d values for the highest blockage are lower by only 3%. It was therefore concluded that no correction was required to the drag coefficients.

Aspect Ratio and Three-Dimensional Flow Effects

A main objective of these experiments was to examine the effects of 3-D flow and aspect ratio, L/D, upon cylinder drag for large surface roughness in the postcritical Re regime. The "buoyant cylinder" technique implied the use of finite length cylinders with free ends where the flow was expected to be quasi two-dimensional.

Most of the flow past an infinitely long cylinder is two-dimensional. As the cylinder length becomes shorter, the flow becomes increasingly three-dimensional since a larger proportion of high pressure fluid leaks past the free ends of the cylinder and forms a pair of vortex sheets. The resulting higher base pressure recovery causes a decrease in C_d. The lower the aspect ratio the greater the drag reduction, which may be up to 38% for L/D=3 according to Goldstein [107] and Farivar [108]. Both reported on wind tunnel experiments with smooth cylinders in laminar flow (Re up to 8.8×10^4) where L/D was varied by altering the cylinder length. However, spanwise irregularities in pressure distribution arising from unstable flow due to increasing cylinder length could influence the drag coefficient.

Stansby [109] suggested that nearly uniform spanwise base pressure distribution and two-dimensional flow conditions may be aproached by introducing optimally designed end plates. Nominally smooth and sand roughened cylinders (k/D=0.01) were tested with and without such end plates to quantify the three-dimensional flow effects. The test rig dimensions and the size of plates required to ensure geometric simi-

larity with Stansby's experiments restricted the upper limit of Reynolds numbers to $4x10^5$ and the greatest possible cylinder diameter to 150mm (see Appendix C). Therefore, it was not feasible to test the smooth cylinder at postcritical flows. The results shown in Figure 8.6 suggest that this limitation was not critical for the purpose of the experiments. At subcritical Reynolds numbers, the "two-dimensional flow" drag coefficient, $C_{d(2D)}$, for the smooth cylinder is higher by about 18% to that obtained for the same cylinder without end plates. However, the same effect is absent from the rough cylinder data where, irrespective of end conditions, all data collapse at values around 1.04.

Whilst it is not claimed that three-dimensionality in flow and spanwise pressure irregularities are absent, the results indicate that higher spanwise coherence is achieved with macro-roughened cylinders of finite length. It appears that surface roughness triggers postcritical turbulent flow conditions at much lower Reynolds numbers and establishes such coherence in vorticity dispersion which overshadows 3-D flow effects. One should expect this trend to extend at Re above $4x10^5$ although experimental verification would be desirable.

With respect to aspect ratio the opposite trend on C_d has been observed in essentially two-dimensional flow conditions to that obtained with finite length cylinders with free ends. From wind tunnel tests on smooth cylinders fitted with end plates, West and Apelt [104] inferred that at subcritical Re the drag coefficient increases as L/D decreases. They systematically varied aspect ratio and blockage such that each parameter could be independently assessed. The data of Farrel et al. [103] for rough cylinders, Achenbach [110] for smooth cylinders at postcritical Re and Sarpkaya [58] for smooth and rough cylinders in harmonic flow exhibited similar trends. Sarpkaya and Farrel et al. cited the better correlation of flow along shorter cylinders as a possible reason for the drag increase.

The data obtained from the present tests show little evidence of aspect ratio effect. This can be seen in Figures 8.7 and 8.8 where C_d values are plotted for cylinders of similar k/D and varying L/D. Figure 8.5 summarises the variation in mean C_d with L/D at two k/D ratios; also plotted are the C_d values corrected for blockage. Only a slight increase in C_d is noted at L/D=3.75. It amounts to less than 3% and could be equally well attributed to higher blockage.

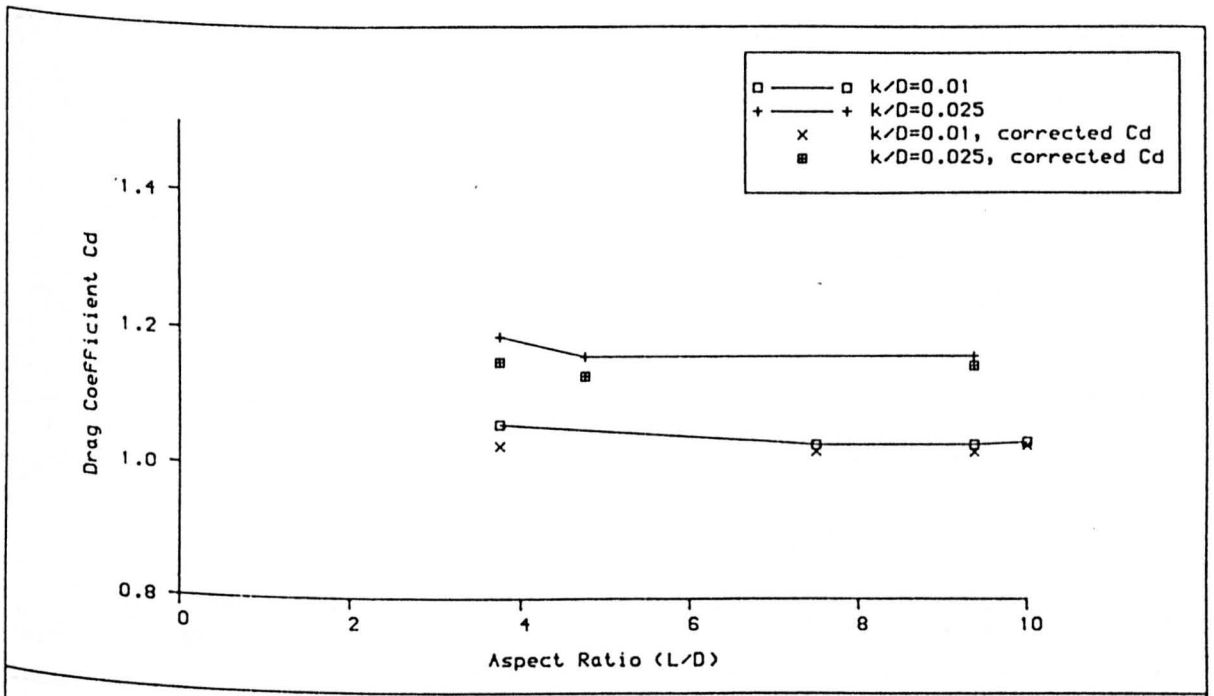

Figure 8.5. Blockage and aspect ratio effects on Cd.

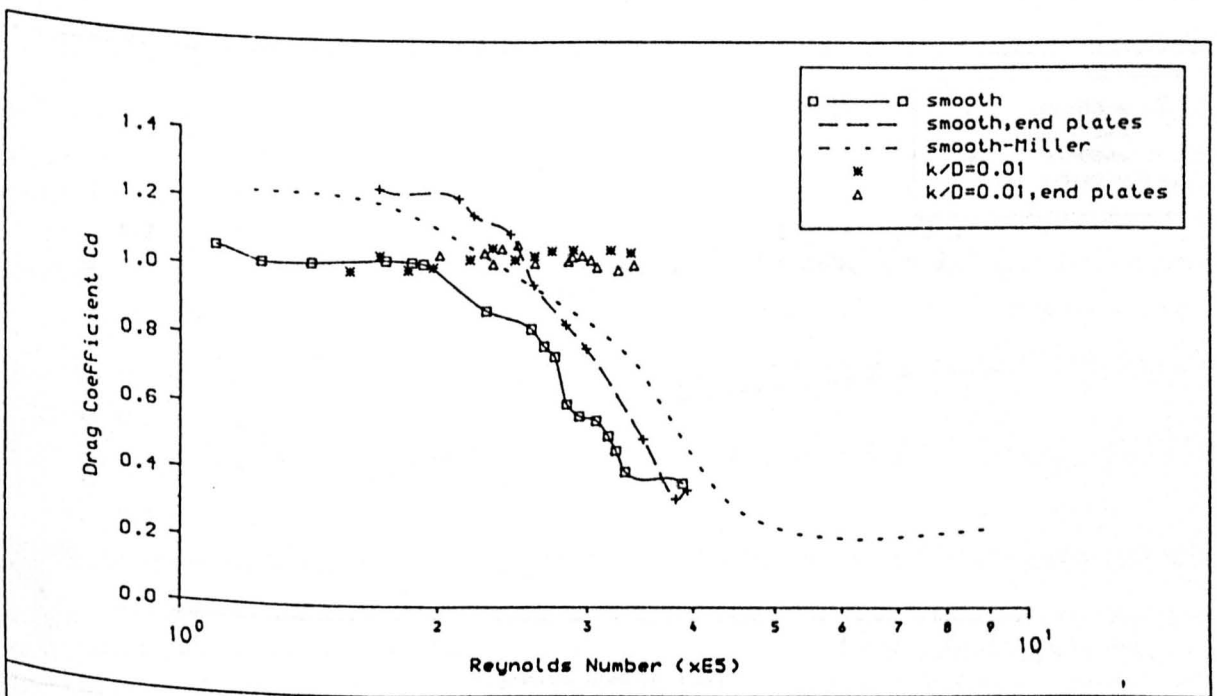

Fig. 8.6. Cd of cylinders with and without end plates.

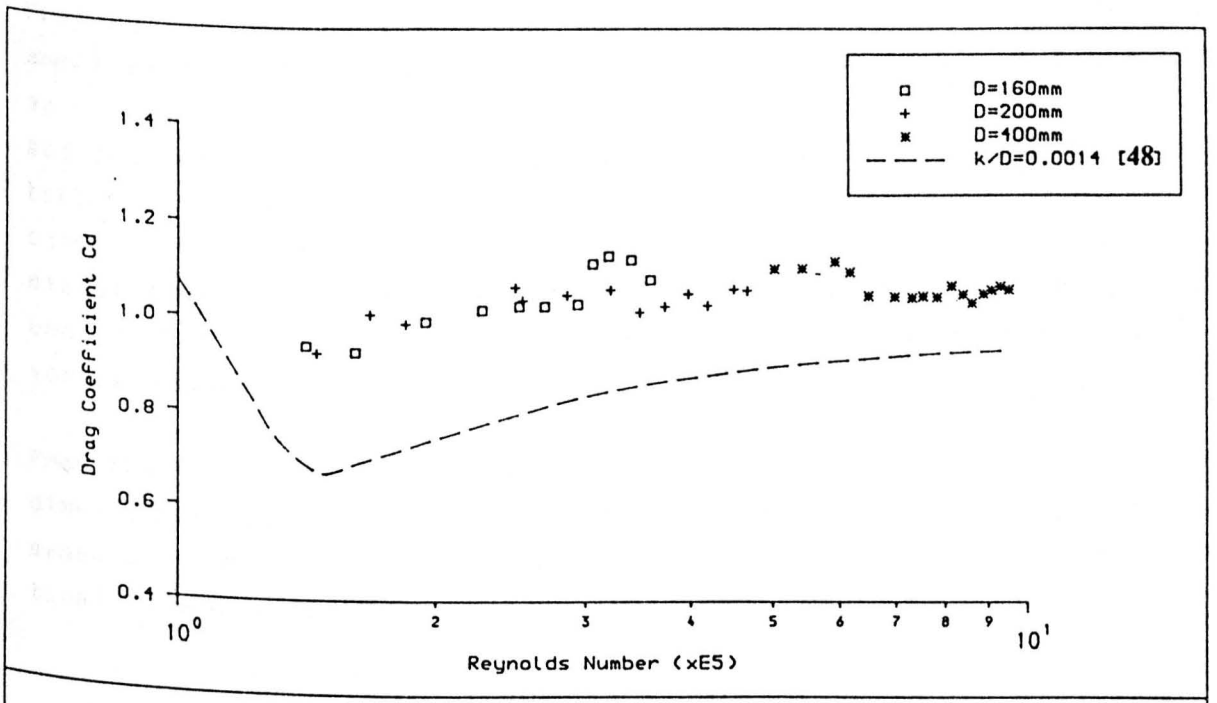

Fig. 8.7. Cd of sand roughened cylinders with k/D=0.0094-0.0097.

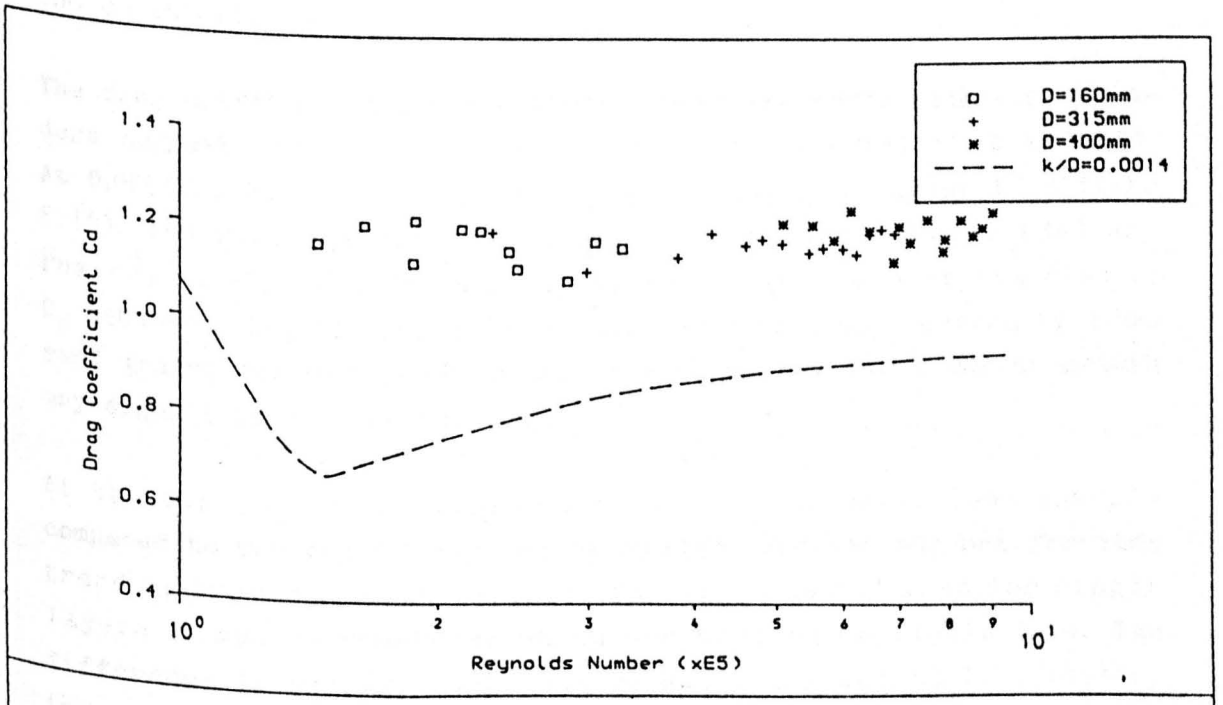

Fig. 8.8. Cd of gravel roughened cylinders with k/D=0.025.

From physical considerations the lack of variation in C_d with L/D for small aspect ratio cylinders is attributed to the shorter cylinder span which inhibits the development of spanwise velocity gradients and the free end vortices collapse, i.e. the velocity correlates better along the cylinder length [111]. Even more so in the present experiments, firstly because the aspect ratio was varied through the diameter whilst cylinder length was kept constant and secondly, because the roughness induced turbulent flow and higher spanwise vortex coherence.

From the preceding it is concluded that neither blockage nor three-dimensional flow or aspect ratio effects merited corrections of the measured drag coefficients for macro-roughened cylinders in postcritical flow conditions.

Influence of Relative Roughness

Figures 8.9-8.12 show the influence of relative roughness on the drag coefficient. No significant conclusions can be drawn from Figure 8.9 which shows results for the 160mm diameter cylinders. Non-circularity, averaging 4mm for these cylinders, induced biased transverse and fluctuating in-line forces resulting in scatter and uncertainty in the computation of C_d.

The drag coefficients for the 200mm, 315mm and 400mm diameter cylinders suggest a consistent marginal increase especially at $k/D>0.01$. At $0.005<k/D<0.01$ the C_d values lie on a plateau of about 1.0 (Figure 8.13). The findings are consistent with those of Miller [34] and Pearcey et al. [48]. It is interesting to note the distinct rise in C_d between a lightly abraded cylinder and a cylinder covered by 1.5mm sand grains ($k/D=0.005$) which suggests that very light marine growth may significantly increase drag.

At the top end of the roughness scale, C_d increases less sharply compared to the trend suggested by Miller. Further support for this trend is provided by the results for pyramids and also for single layers of mussel roughness which are plotted in Figure 8.14. The difference in pyramid roughness height is reflected in a mean C_d increase of 10%.

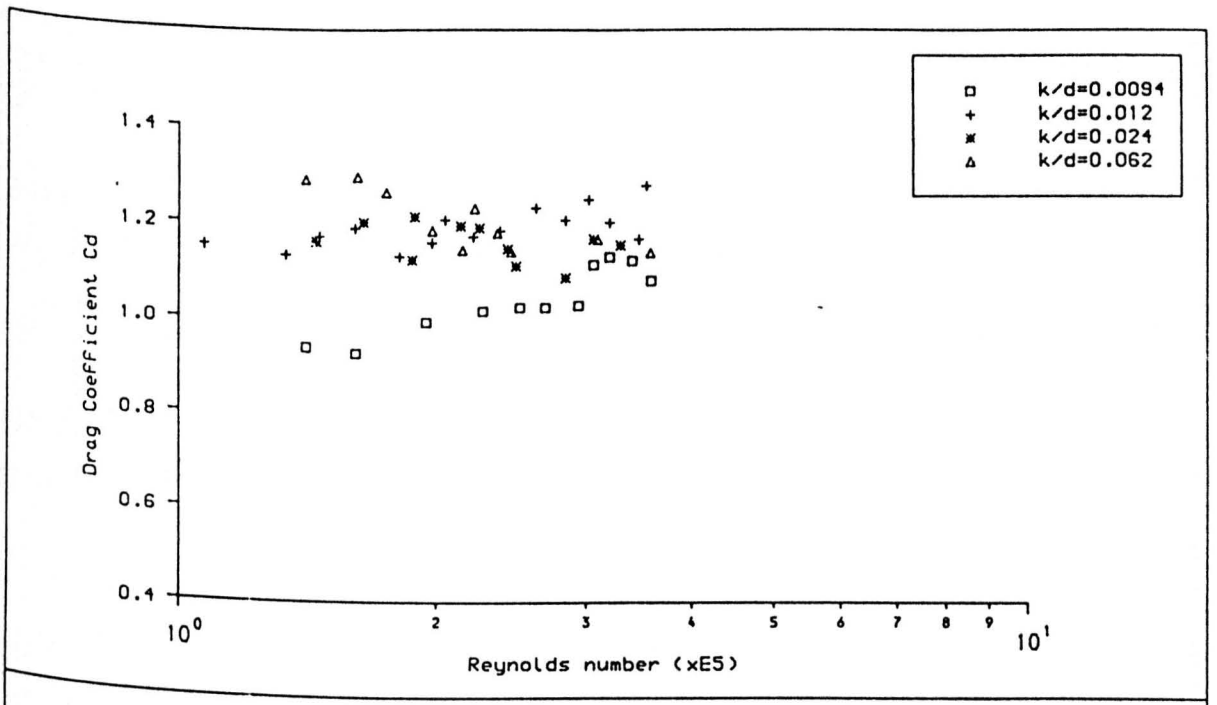

Fig. 8.9. Cd of 160mm OD cylinders - Aspect Ratio=9.375

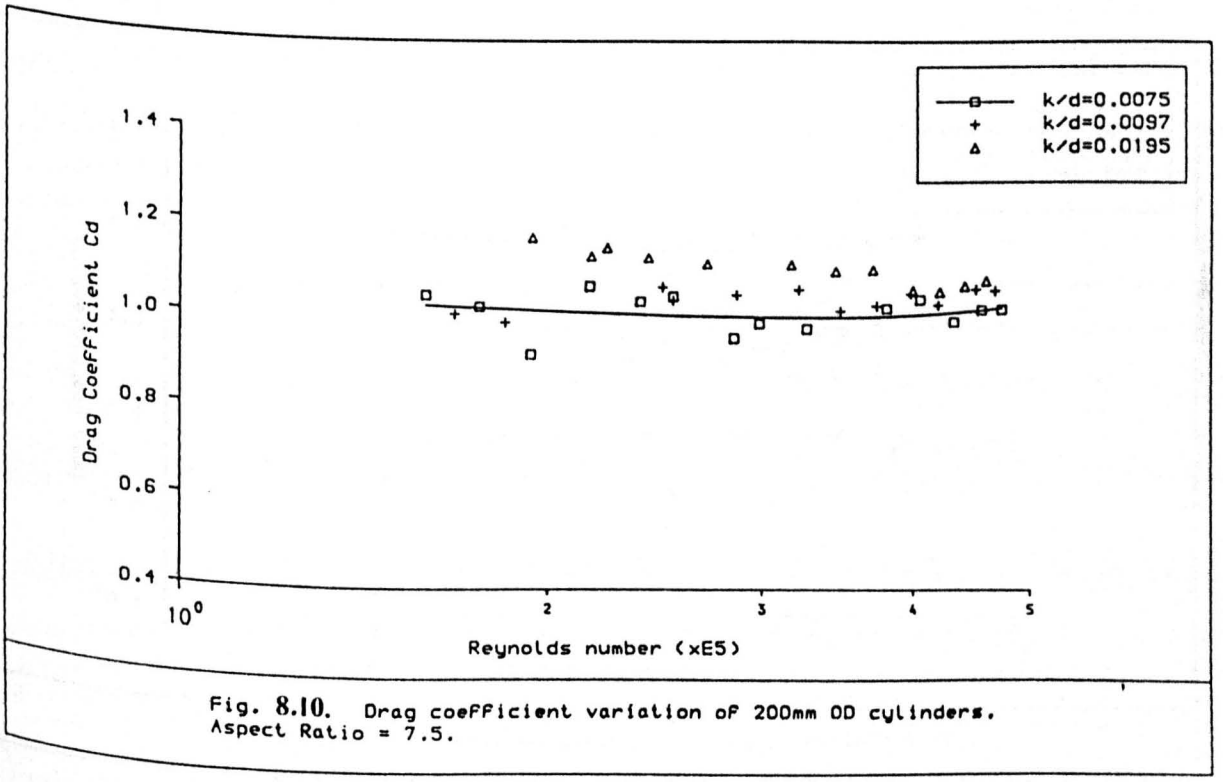

Fig. 8.10. Drag coefficient variation of 200mm OD cylinders. Aspect Ratio = 7.5.

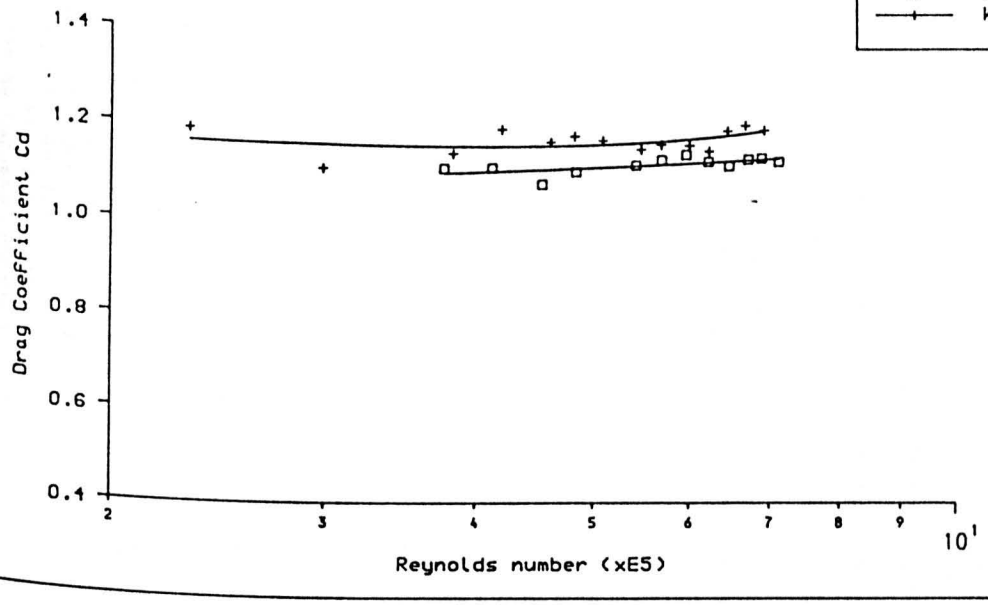

Fig. 8.11. Cd of 315mm OD roughened cylinders - Aspect Ratio=4.76

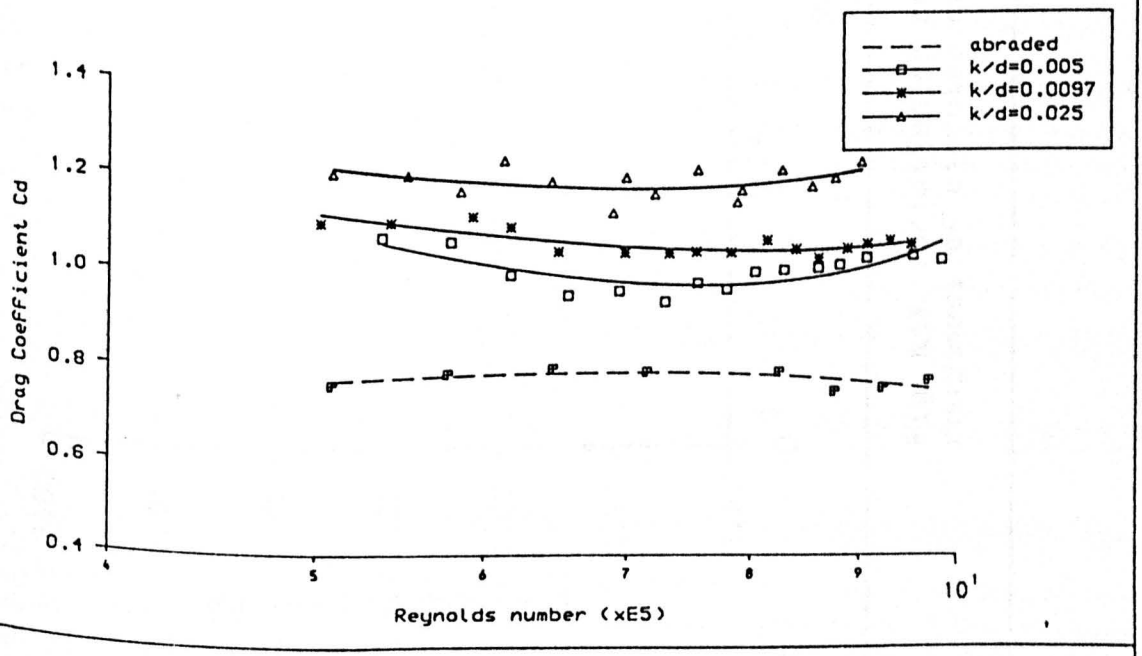

Fig. 8.12. Cd of 400mm OD cylinders - Aspect Ratio = 3.75.

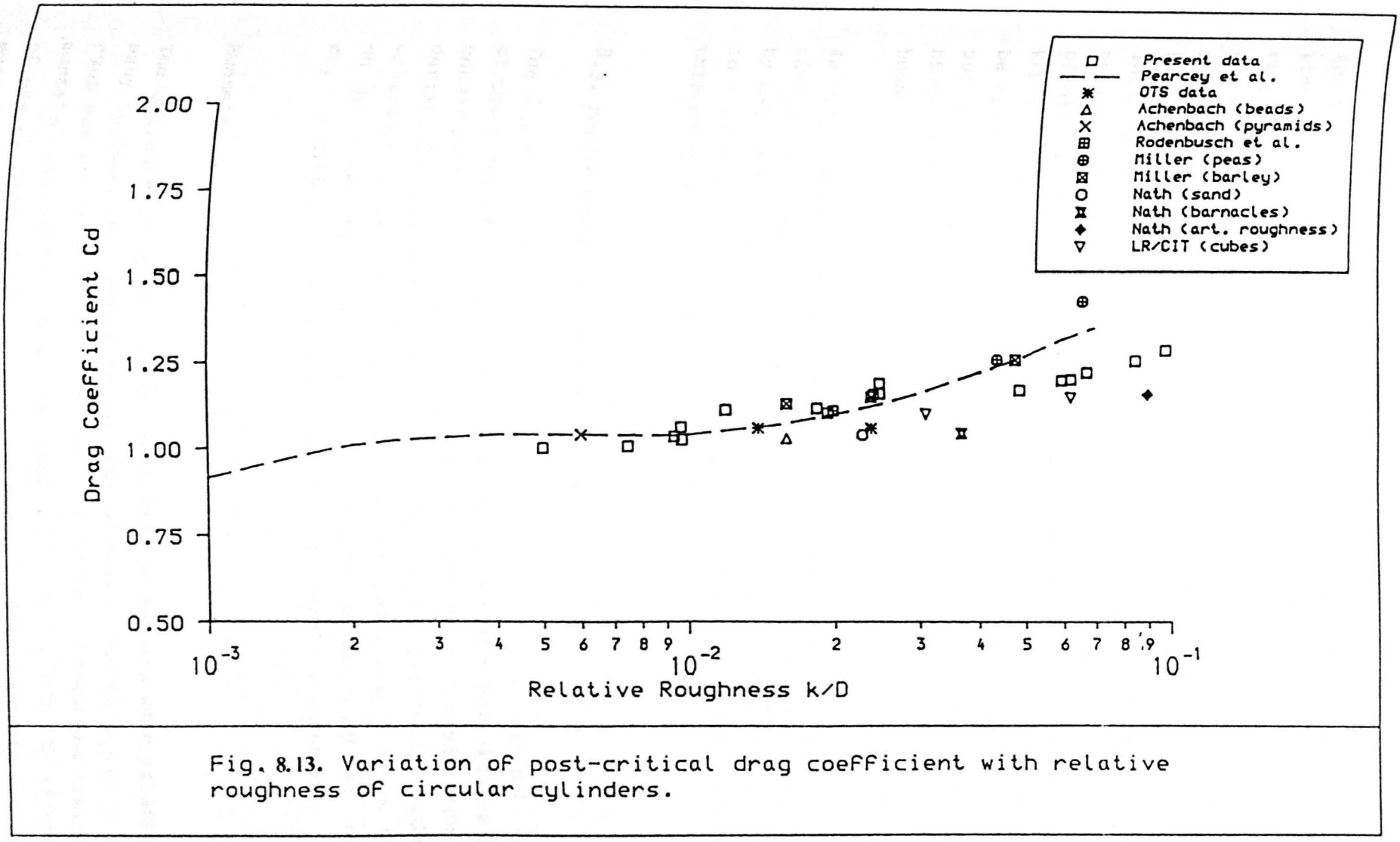

Fig. 8.13. Variation of post-critical drag coefficient with relative roughness of circular cylinders.

Apart from the present data for hard roughness, Figure 8.13 includes other published results for rough cylinders in steady flow in the k/D range 0.005 to 0.1. To allow for direct comparison all previous data have been modified according to the k/D definition adopted in the present study. The experimental results of Achenbach [39,45], Rodenbusch and Gutierrez [59] and Lloyd's R.S./C.I.T. [112] are in excellent agreement with the 'buoyant cylinder' drag coefficients. Nath's results are consistently lower particularly at higher k/D; and those of Miller and Pearcey et al. are considerably higher than the rest at k/D>0.03. Many uncertainties related to experimental procedures could be cited for these differences. However, the good correlation of all published data at k/D<0.02 as opposed to the diversity of C_d at higher k/D illustrates the difficulty in characterising macro-roughness and appears to be the main reason for these discrepancies.

As will become evident from the following sections, the drag coefficients for fully roughened cylinders by multiple layers of mussels or by kelp should not be assessed in the same context due to ambiguities in roughness height definition and the substantial departure from uniform cylindrical shape.

8.3. Marine Roughened Cylinders

The results for the marine roughened cylinders are presented in terms of the types of fouling used throughout the tests. For all the test conditions the mean C_d and C_m values together with their standard deviations are summarised in Tables 8.3-8.5. For partially roughened cylinders "local" k/D ratios are quoted for reference. They are based on the "clean" cylinder diameter and on mean element height or length or, for multiple roughness layers, on mean overall thickness.

Mussels

The cylinders roughened by single layers of mussels were relatively easy to test. They showed no tendency to drift laterally during test runs and on inspection at the end of each set of runs the number of mussels that had fallen off was negligibly small. With the exception of one cylinder which was fully roughened by 27mm barnacle encrusted mussels, all the other cylinders were also tested at reduced surface

covers of 25% and 50%, the roughness being pseudo-randomly distributed. The results for all cases are plotted in Figures 8.14 through 8.16 and tabulated in Table 8.3. The drag coefficients show no variation with Reynolds number and very little scatter; the coefficients of variation (c.o.v.) for all sets of data being less than 4%. The inertia coefficients exhibit greater scatter with c.o.v. up to 12% and consequently the effect of roughness parameters is not clear.

Figure 8.14 includes results for the two pyramid roughened cylinders (k/D=0.049 and 0.098). Their respective drag curves envelop the C_d data for mussel roughness at intermediate k/D ratios and suggest that hard fouling may be adequately modelled by artificial macro-roughness. The variation in mean C_d with k/D is better illustrated by Figure 8.17. No roughness shape effect is discernible; the mean C_d values for pyramids, gravel and mussels being well correlated. A small but consistent increase in C_d is observed with increasing size of mussels, though not to the degree indicated by Miller's data [34].

A notable exception to this trend is the mean C_d of 1.20 obtained for the 8mm mussel roughness (k/D=0.02) (see Table 8.2 and Figure 8.17). It suggests that "k" should be more like 24mm rather than 8mm. This is because uniform overall thickness of roughness was not achieved for this test cylinder, with several clusters being up to three layers thick. No circumferential measurements were carried out and therefore the data are presented based on available information. However, directly comparable tests with a uniformly roughened cylinder by 7.5mm gravel chips provided further evidence for this discrepancy. As shown in Figure 8.16 the drag coefficients for the gravel roughness, at 100% cover, are consistently 5-7% lower than for the mussels.

The 200mm diameter cylinder covered by multiple layers of 26mm mussels produced significantly higher drag coefficients (Figure 8.18). This is due to two reasons; the large increase in mean cylinder diameter and the non-uniform overall thickness which induced additional drag forces. From circumferential measurements the mean overall diameter of the fully roughened cylinder was 285mm with standard deviation of 6.7mm. To compare this roughness condition to single layered mussel roughness an "effective diameter" allowance is in order.

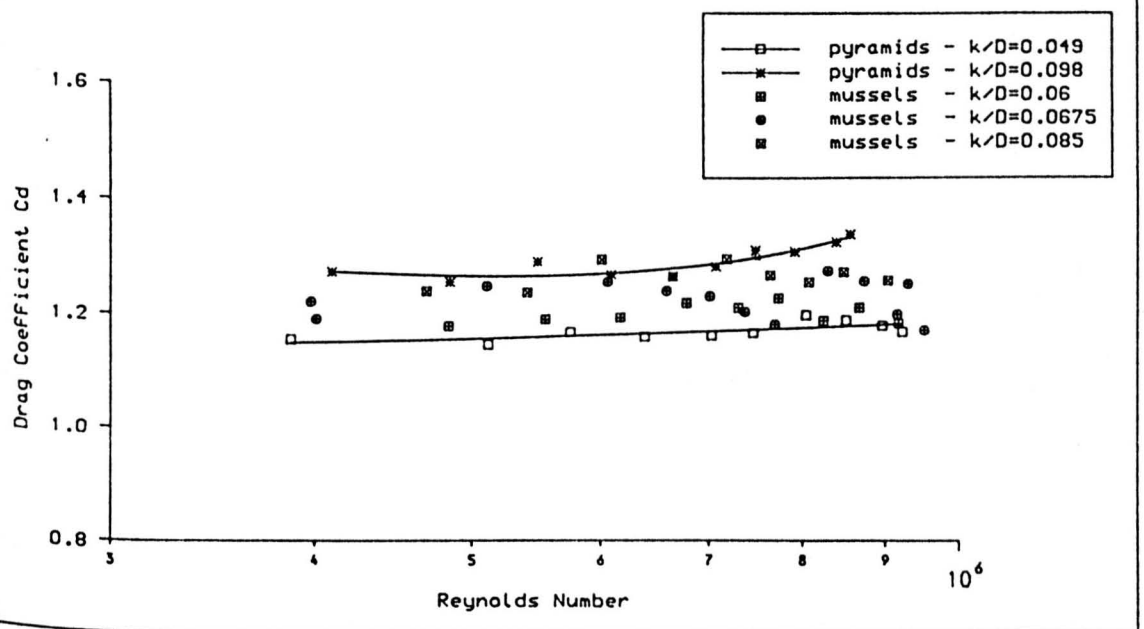

Figure 8.14 Comparison between fully roughened cylinders by mussels and pyramids.

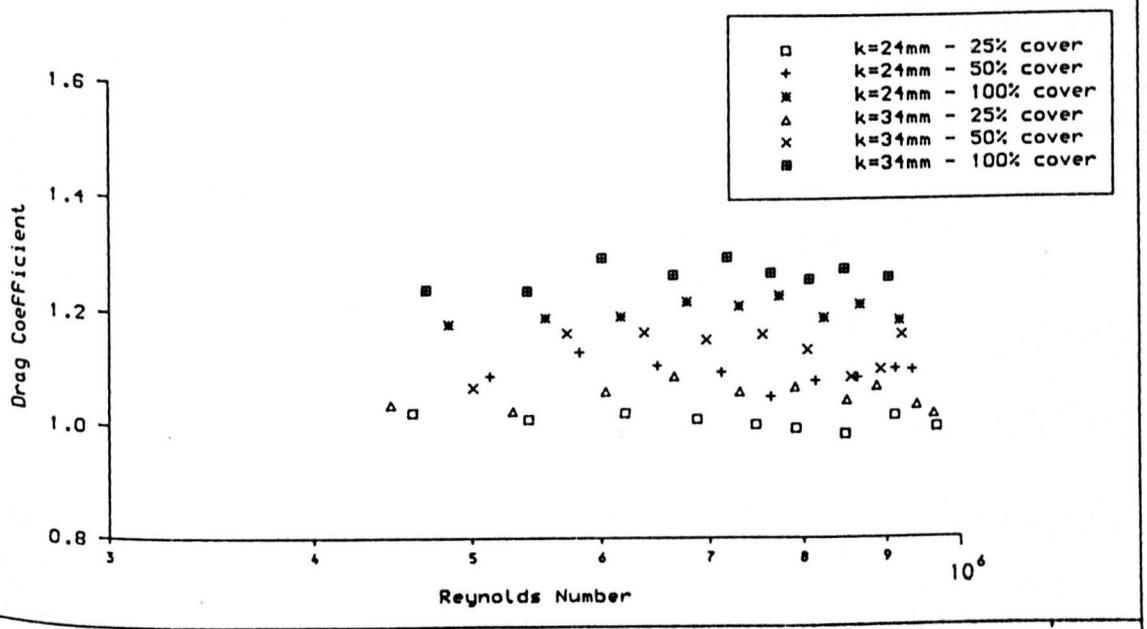

Figure 8.15 Drag coefficients for cylinders roughened by 24mm and 34mm mussels.

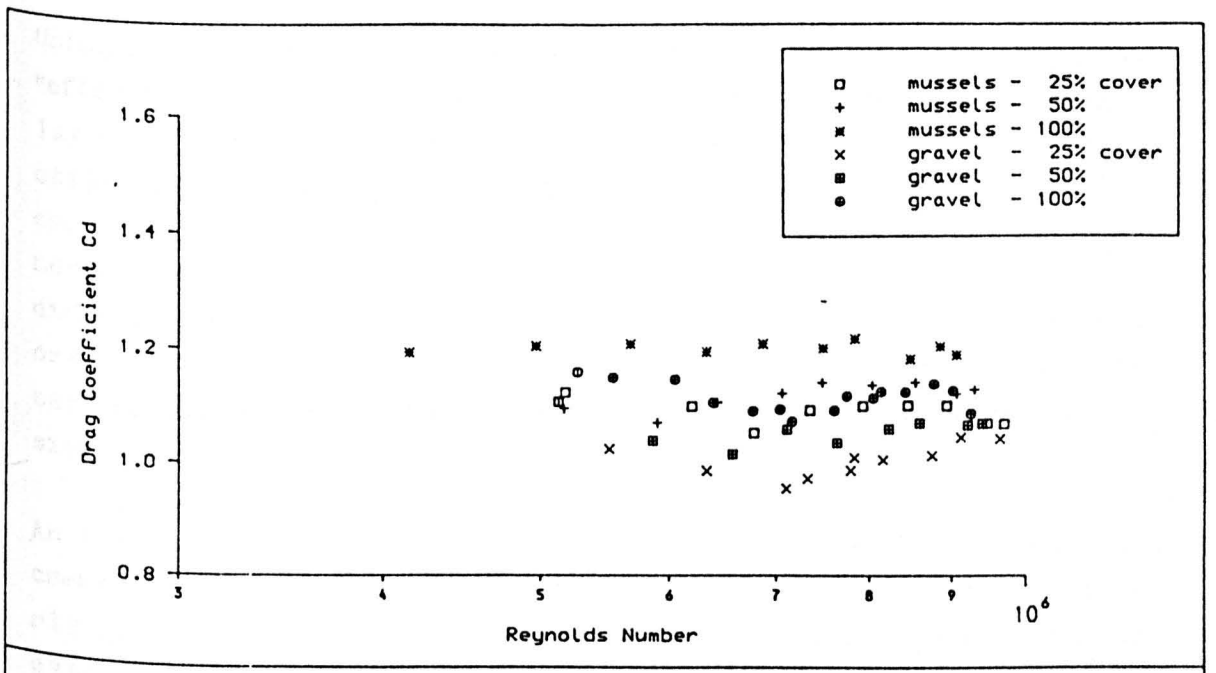

Figure 8.16 Drag coefficients for cylinders covered by mussels (k/D=0.02) and gravel (k/D=0.0185).

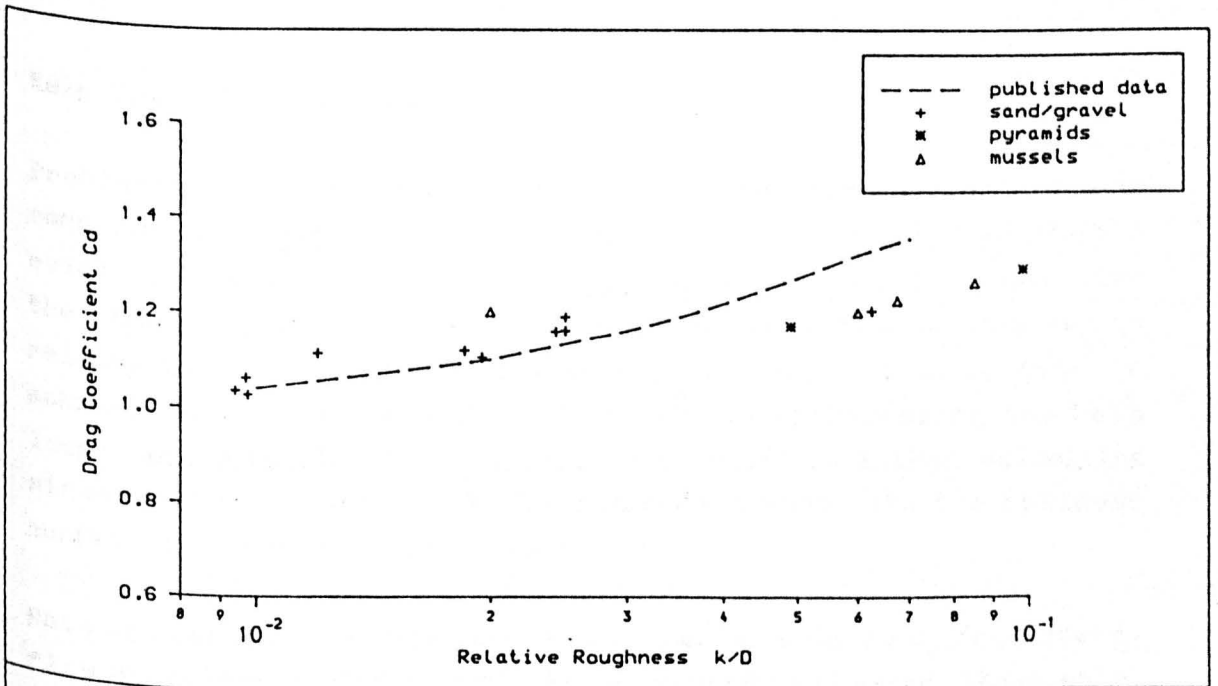

Figure 8.17 Drag coefficient variation with relative macro-roughness.

Using D=285mm and k=26mm results in "effective" k/D of 0.091 and mean "effective" C_d of 1.3. If the closest comparable data for the single layer of 34mm mussels were subjected to the same procedure the "effective" k/D and mean C_d would be 0.073 and 1.08 respectively. The corresponding C_d curves are depicted in Figure 8.18. The 20% difference in mean drag coefficients is too large to be attributed to the different relative roughness ratios and is more likely due to induced drag by non-uniform roughness. If this is so, the "effective diameter" design procedure is of limited predictive value even for the simplest forms of hard fouling.

An interesting feature of all the results is that C_d does not increase linearly with increasing percentage cover (Figure 8.19). Clearly just a few patches of fouling on the cylinder disturb the flow over a considerable part of the surface. All the mean C_d curves increase sharply from the "clean" rough cylinder condition to 25% mussel density and from then on the increase is smaller. As there were significant differences in the spatial distribution of the patches for each cylinder, it was not clear, through these tests alone, how C_d varies with partial surface cover alone. Results from further experiments on partially roughened cylinders provided an insight to this. They are discussed in Section 8.4.

Kelp (Long Flapping Seaweed)

Problems were experienced in the tests with kelp roughness due to some plants pulling off at high Reynolds numbers. Apart from visible evidence in loss of kelp, check runs repeated at reduced speeds after the highest speed runs produced lower drag coefficients. This may be related to the test rig which required accelerations up to $4m/s^2$ to achieve Reynolds numbers of about $1x10^6$. Notwithstanding the kelp loss, some reduction in C_d should be expected at higher velocities since the kelp plants would be compressed more onto the cylinder surface resulting in lower projected area.

Nath and Wankmuller [52] observed a similar drop in C_d from steady flow experiments with plastic kelp covered cylinders. Their data, which are included in Figure 8.20, tend to decrease at lower Reynolds numbers than those pertaining to the present tests. Possible reasons are the different moduli of elasticity of artificial and real plants

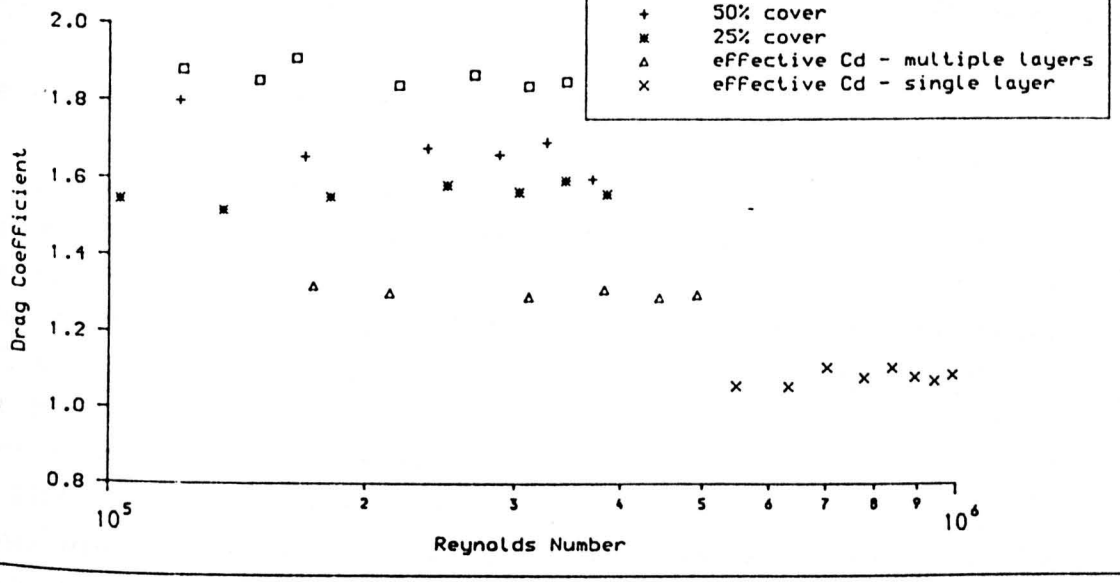

Figure 8.18 Drag coefficients for cylinder covered by multiple layers of mussels and comparison with single layered mussel roughness.

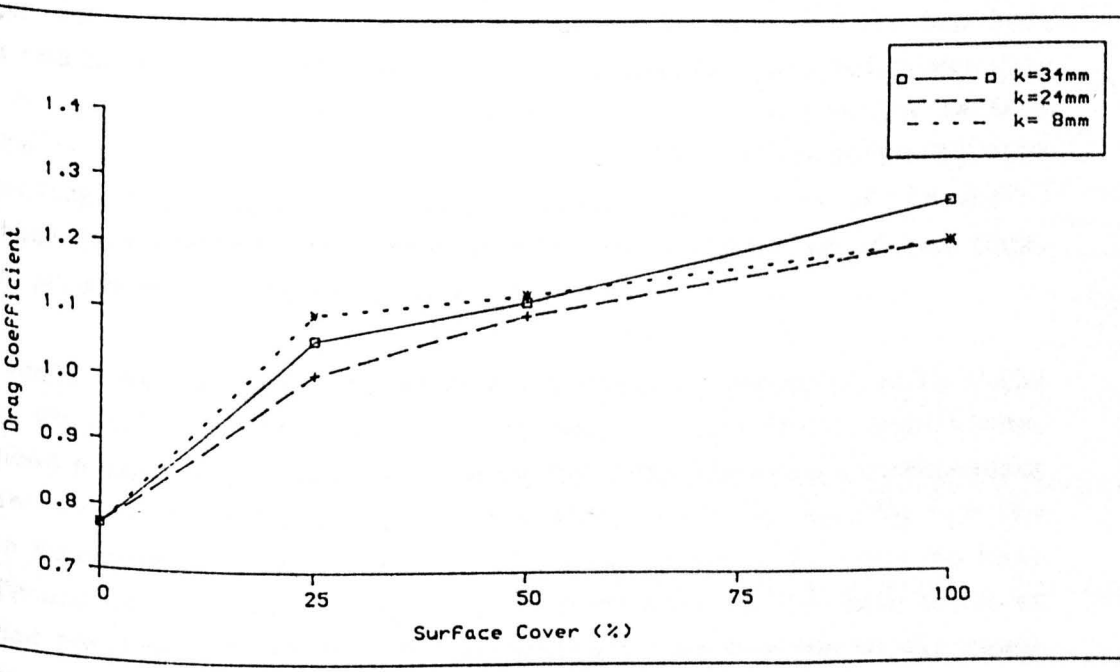

Figure 8.19. Drag coefficient versus roughness density for mussel roughened cylinders at various k/D.

and the kelp loss sustained during the present tests. It should be noted however, that Nath's hard roughness data are also consistently lower than other published results and those presented herein for hard roughness (Figure 8.13).

The variation in mean C_d with percentage cover is illustrated in Figure 8.21. It shows the same type of non-linear trend that was observed for the mussels. The increase in drag coefficients from 50% cover to full cover is significant only for the 1.0m long kelp, whilst all the mean drag coefficients at 25% and 50% covers remain more or less constant. However, the relationship is subject to uncertainties due to the large scatter of the data (Figure 8.22). Kelps are difficult to handle and there is great variability between individual specimens as not only overall length varies, but also aspect ratio, surface texture, stipe length and, in the case of L. digitata, the number of fronds per plant. This is illustrated in Table D.3 (Appendix D) for a sample of 30 plants. The coefficients of variation for both force coefficients are high because of this and also because of the kelp loss and "compressed" projected area at high Re.

The effects of kelp type and length on C_d appear to be small. It must be remembered that the short kelps were obtained by cutting back the longer kelps in length only. The aspect ratio is therefore smaller, with the breadth, thickness and surface undulations being greater than would normally be expected for kelps of this length. The pattern of the results would indicate a weak non-linear trend in C_d with increasing kelp length which must be qualified, in view of the uncertainties introduced by the sheer number and variability of the roughness parameters characterising kelp growth.

The tests, at 50% density, with a cylinder covered in kelp 0.25m long, which to all intents and purposes was just roots and stipes, produced a mean drag coefficient only 25% less than the corresponding value for 1m long kelps, yet 55% higher than the mean C_d for the clean roughened cylinder. This would tend to support the view that the fronds do not make a very large contribution to the drag force at reduced roughness densities. The situation could however be different in wave flows where the delayed flapping action of the fronds would effectively increase the projected area.

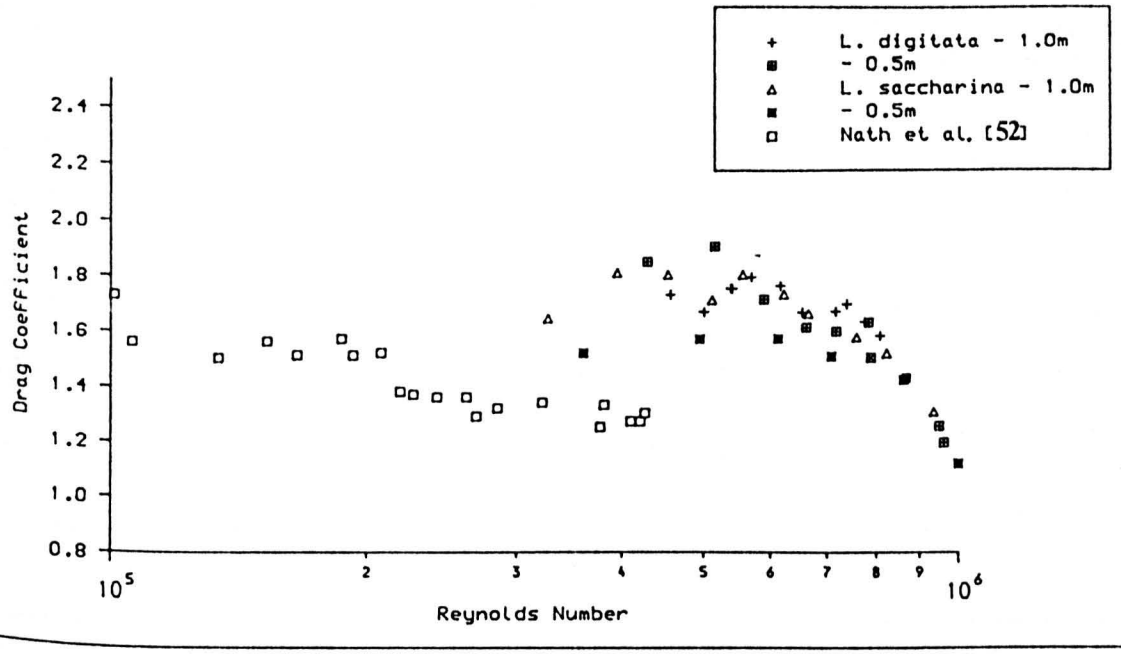

Figure 8.20 Drag coefficients for kelp covered cylinders (100% cover).

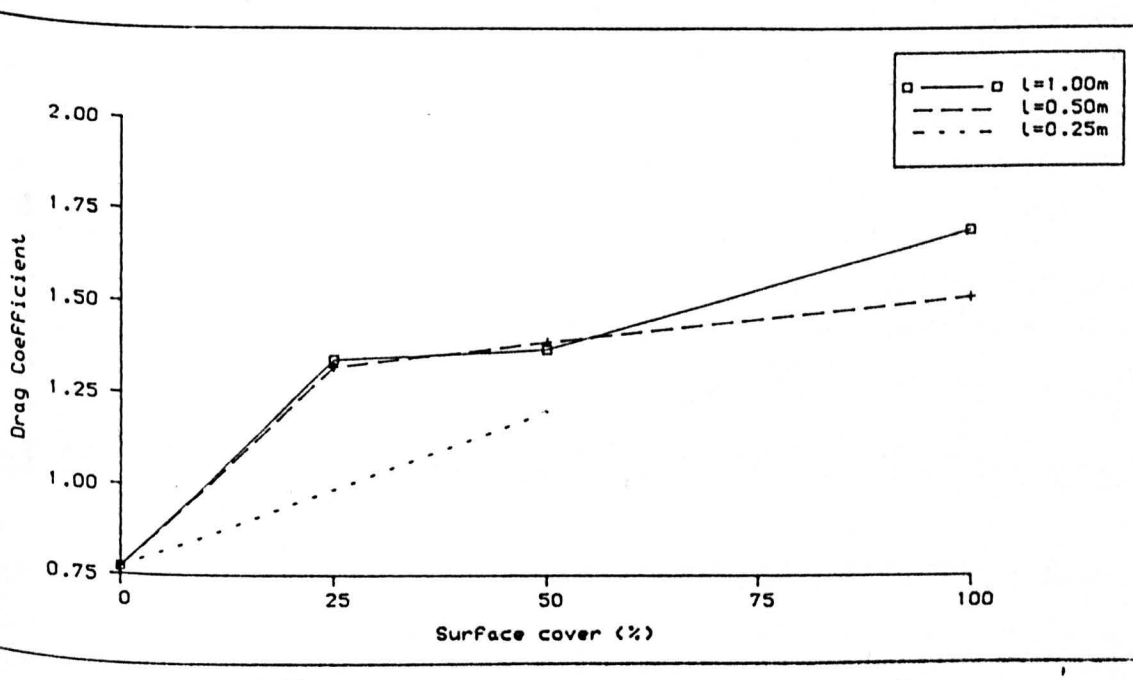

Figure 8.21. Variation in mean Cd with surface cover by the kelp "Laminaria saccharina".

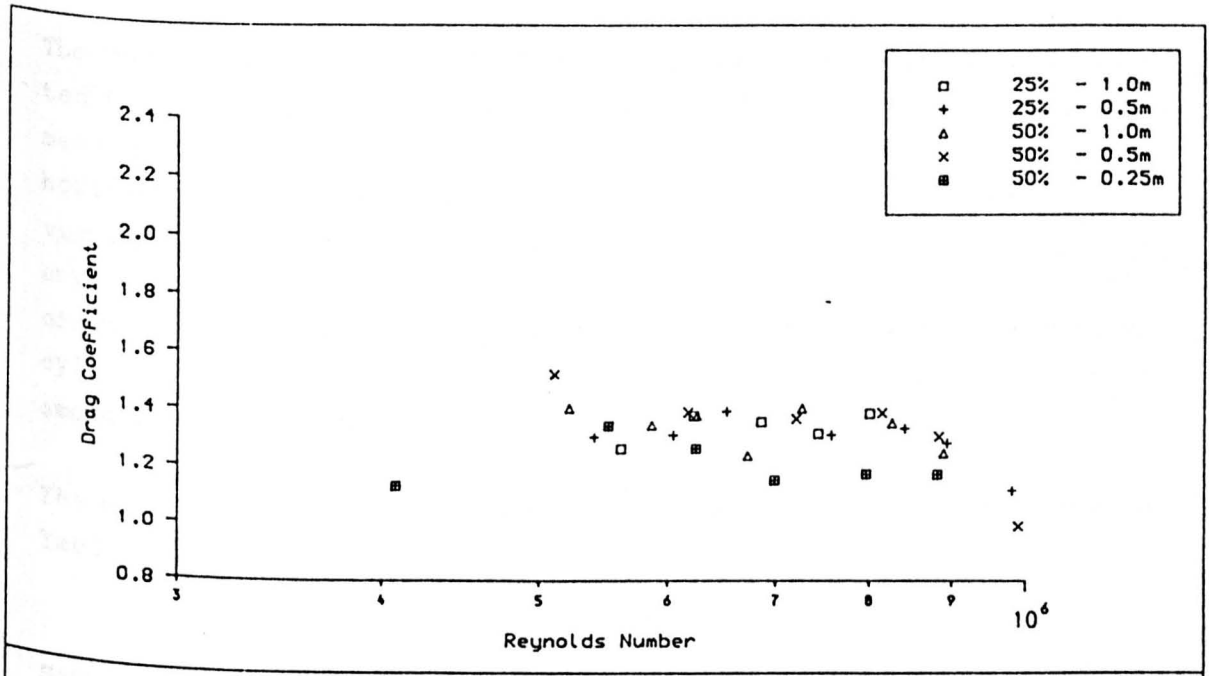

Figure 8.22 Drag coefficients for partially roughened cylinders by kelp of various length.

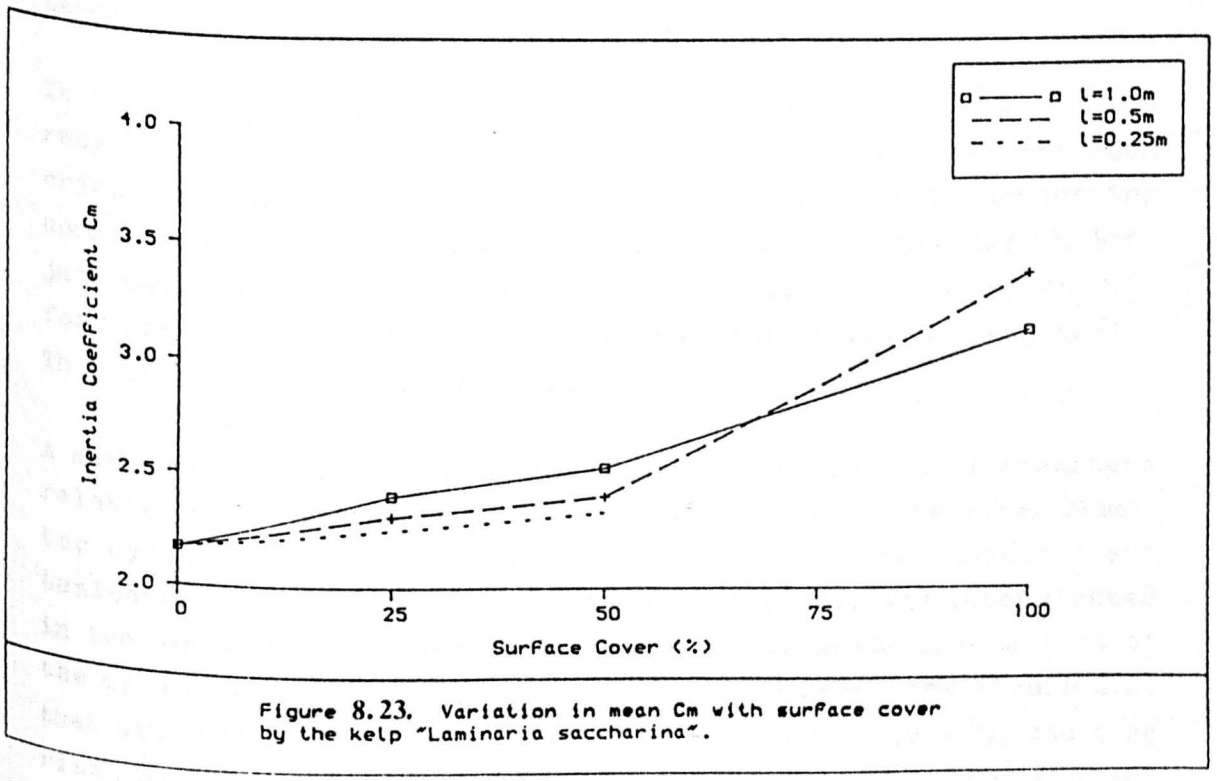

Figure 8.23. Variation in mean Cm with surface cover by the kelp "Laminaria saccharina".

The mean inertia coefficients for the **Laminaria saccharina** are plotted in Figure 8.23. C_m tends to increase with roughness density and mean values of about 3.4 were obtained at 100% cover. There is, however, considerable scatter in the results with coefficients of variation up to 25%. The effect of kelp length is not clear, nor is any variation with Reynolds number. Generally, the added mass coefficients have nearly doubled compared to those obtained for clean rough cylinders implying a considerable mass effect due to entrained water among the kelp fronds.

The mean C_d and C_m for the kelp fouled cylinders are summarised in Table 8.4.

Soft fouling

Apart from the roughness characterisation problems discussed in Appendix C, there was no difficulty in testing the cylinders covered with sea anemones and/or tunicates (sea squirts). The fouling remained attached throughout the period of tests although towards the end of each set of tests the sea anemones had visibly deteriorated. The results for both cylinders are very consistent and show no clearly perceptible Reynolds number trend.

In the first condition, at 40% surface cover by sea anemones, the roughness distribution was not uniform and the cylinder was such orientated that the regions of dense population were projecting normal to the direction of motion (see Figure C.11, Appendix C). When just under half the sea anemones were removed to obtain a more uniform distribution the change in the force coefficients was small. This is illustrated in Figure 8.25.

A marked effect of the orientation and concentration of roughness relative to the direction of flow was obtained with the 315mm diameter cylinder which was covered by a mixture of sea anemones and tunicates (Figure C.13, Appendix C). The roughness was concentrated in two diametrically opposite elongated strips spanning over most of the cylinder length (Figure 8.24). It can be seen from Figure 8.25 that with the fouling projecting normal to the flow ($\theta=90^o$), the drag rises by 24% on average. This is not surprising since the apparent projected area of the cylinder increases.

Compared to mussels, the drag forces due to soft fouling are higher. It was not possible, through these tests, to quantify the drag of fully roughened cylinders by soft fouling and there are no relevant published data. It appears though, that drag should continue to increase with increasing density in a similar manner to hard fouling. Inertia should also increase due to entrained water mass effects and flexibility of fouling in a similar manner to kelp fouling. The reason that the mean C_m values obtained for soft fouling (Table 8.5) are lower than the 'clean' or sand roughened cylinder ones is because the sea anemones remained contracted throughout the tests thus behaving almost like hard fouling.

Mixed Fouling

A similar orientation effect as above was observed with the two naturally fouled cylinders predominantly by barnacles (Figure C.12, Appendix C). Their respective roughness distributions and orientations are depicted in Figure 8.24. The drag coefficients are plotted in Figure 8.26 and the means are included in Table 8.5.

From the data refering to the 400mm cylinder, it is shown that drag is higher when the region of fouling faces the oncoming flow rather than trailing in the wake. The results for a 315mm diameter cylinder with broadly similar roughness characteristics is not conclusive at this point. This is not attributed to some experimental error. Instead, it is due to different roughness distributions and to non-uniform thickness of fouling. The distribution effects are discussed below in more detail.

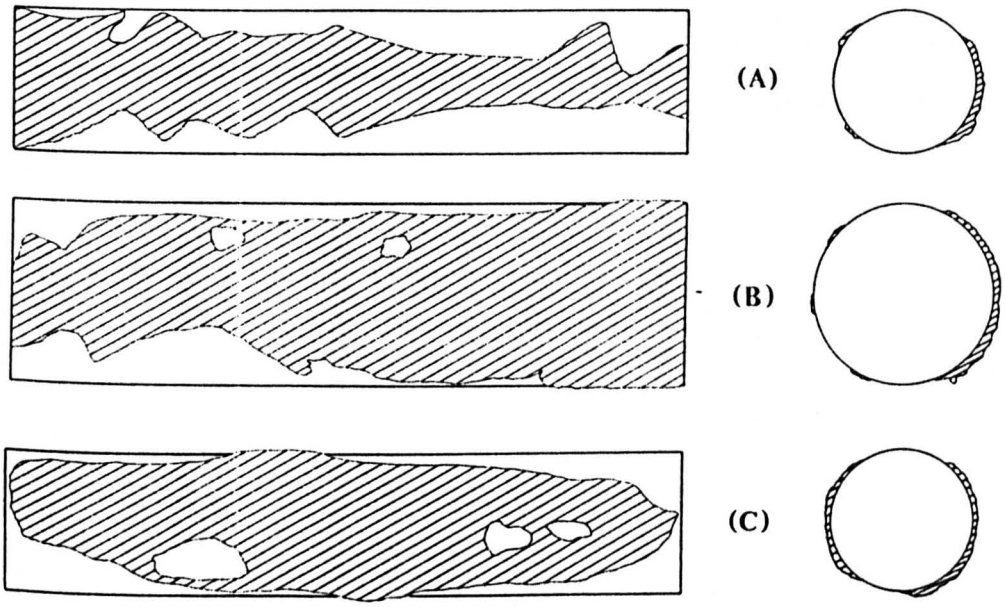

Figure 8.24(a). Distribution of mixed hard and soft growth on naturally fouled cylinders;
(A) 315mm OD; mussels and barnacles
(B) 400mm OD; mussels and barnacles
(C) 315mm OD; sea anemones and tunicates.

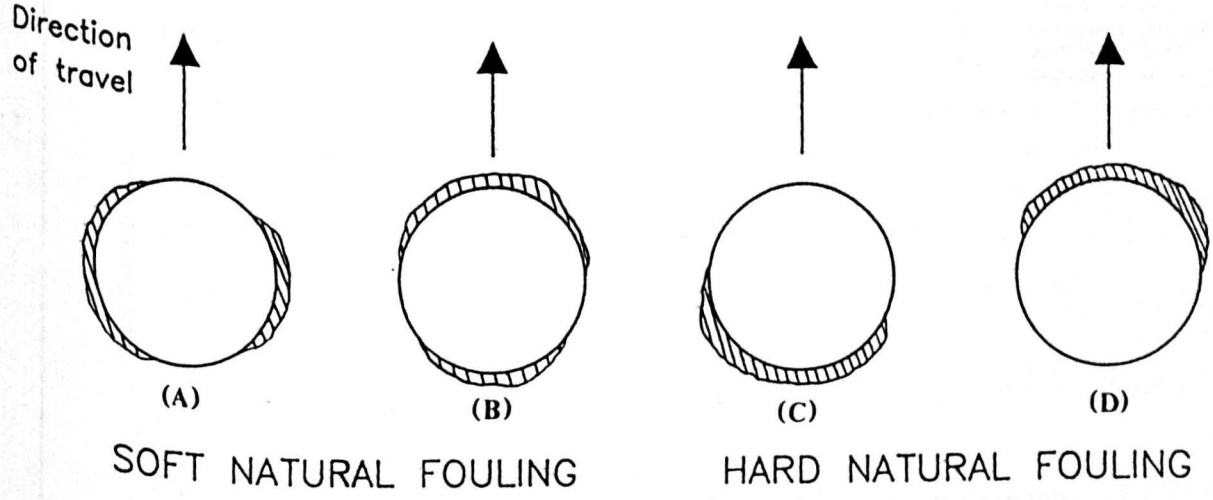

Figure 8.24(b). Orientations to direction of motion at which the above cylinders were tested;
(A) $\theta=0^{o}$, (B) $\theta=90^{o}$,
(C) $\theta=0^{o}$, (D) $\theta=180^{o}$.

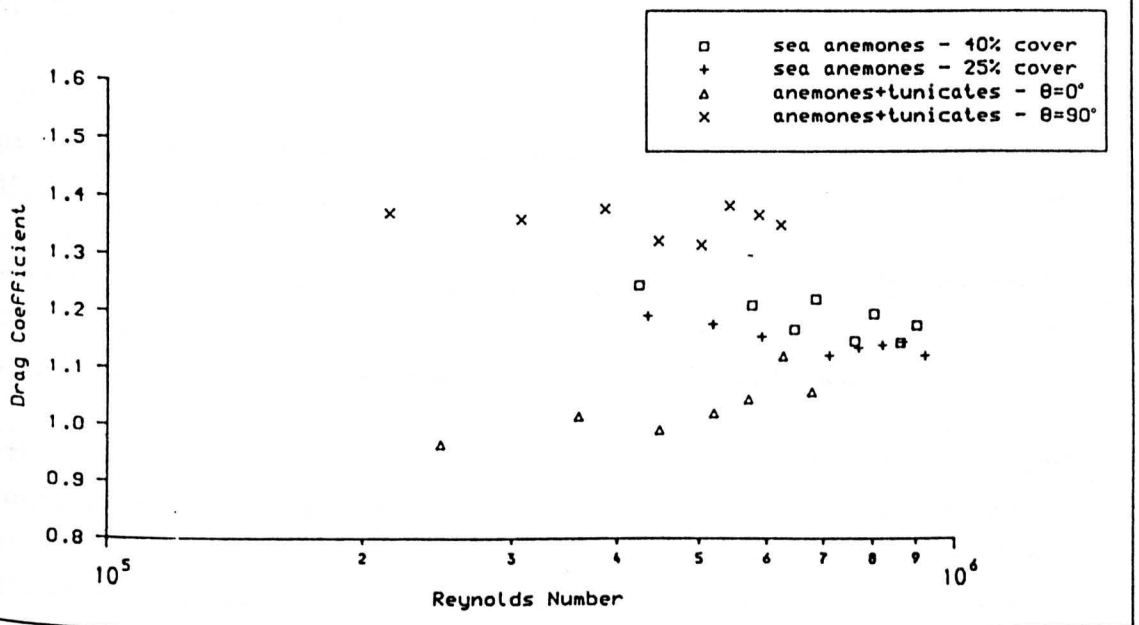

Figure 8.25 Drag coefficients for cylinders partially covered by soft marine fouling.

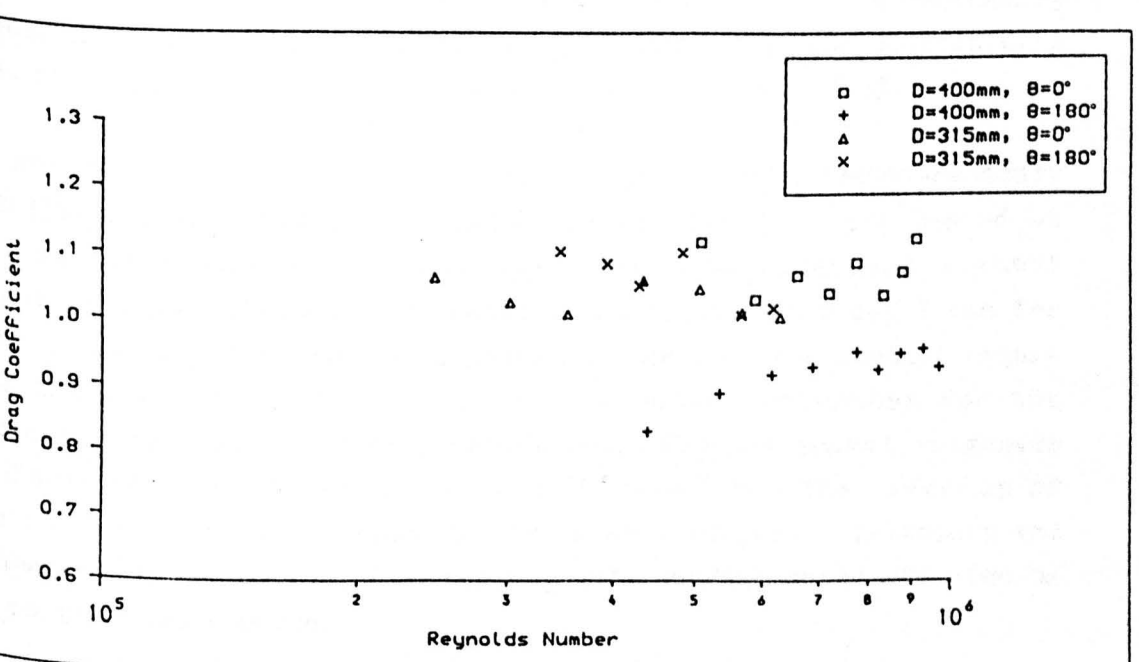

Figure 8.26 Drag coefficients for cylinders partially covered by six-month accumulated marine growth.

8.4. The Effects of Partial Roughness

In the previous section it was shown that non-uniform roughness density has a profound influence on hydrodynamic drag. It was also indicated that C_d varies with roughness distribution relative to the principal direction of flow. However, neither parameter was systematically controlled; nor was the observed non-linear variation in C_d with surface cover fully sustantiated, as most data refered to just two intermediate percentage covers, that is 25% and 50%.

Further tests were carried out where roughness type, distribution and density were independently varied. Some tests extended to densities down to 5%, since earlier experiments had shown that non-linear variation in C_d is most pronounced with the onset of just 25% roughness cover. Two distributions were examined; pseudo-random patches and circumferential roughness strips, the latter only at 20% density.

Two 400mm diameter cylinders each roughened with identical pseudo-random distributions of patches of mussels and gravel were tested at 5, 10 and 20% surface cover. The mean roughness size of mussels and gravel was 29.5mm and 8.0mm respectively. The variation in C_d for all test conditions is illustrated in Figure 8.27. For the respective surface cover conditions tested, the average C_d values are remarkably close. Maximum differences between corresponding drag coefficients (i.e. at approximately the same Re) are of the order of 5%.

Two more cylinders, also identically roughened with pseudo-randomly distributed mussel and gravel patches respectively, were tested at 25% and 50% densities. In this case, the mean roughness element height was approximately the same; 7.9mm for mussels and 7.5mm for gravel. However, for reasons explained in the previous section regarding the uncertainty in characterising mussel roughness for the particular cylinder, the drag coefficients for the gravel roughness are lower than those for the mussels (Figure 8.16). The overlap of data at lower Reynolds numbers for the mussel roughened cylinders and the comparatively small increase in C_d with surface cover may also be due to the same reasons.

The drag coefficients for cylinders with circumferential strips representing 20% surface cover are plotted in Figure 8.28. As anticipated, kelp exhibits higher drag values compared to mussels or gra-

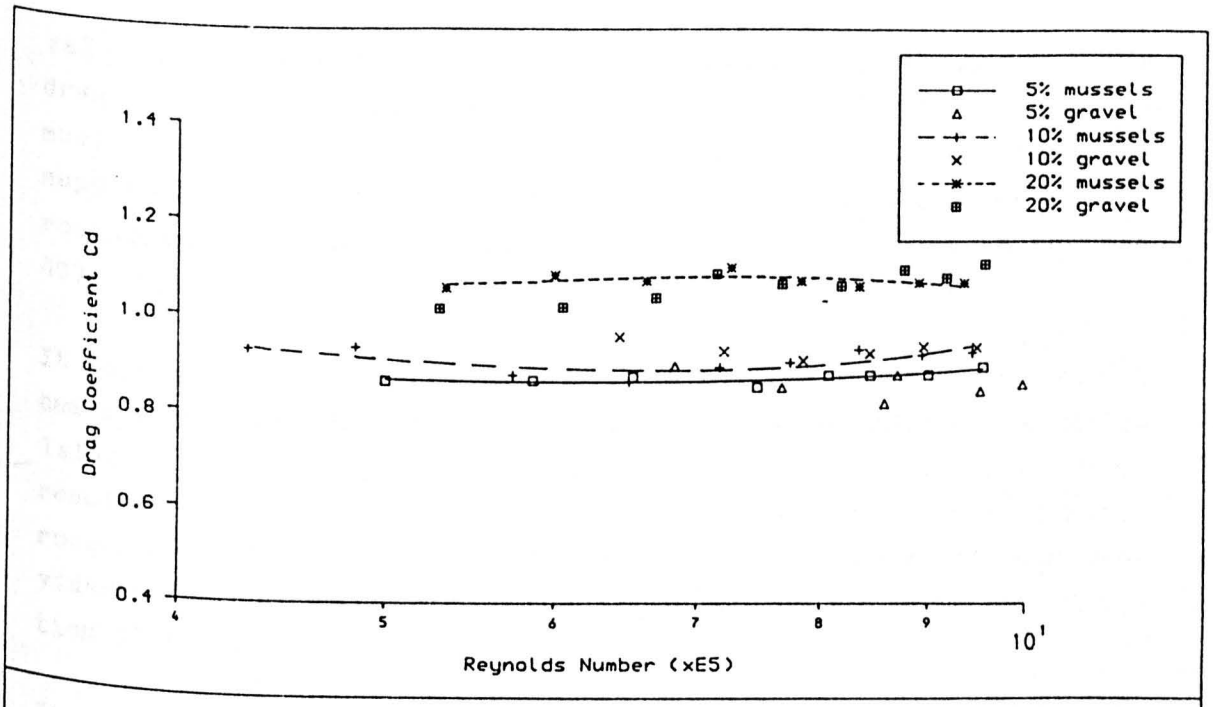

Fig. 8.27 Cd of cylinders partially covered by patches of mussels and gravel.

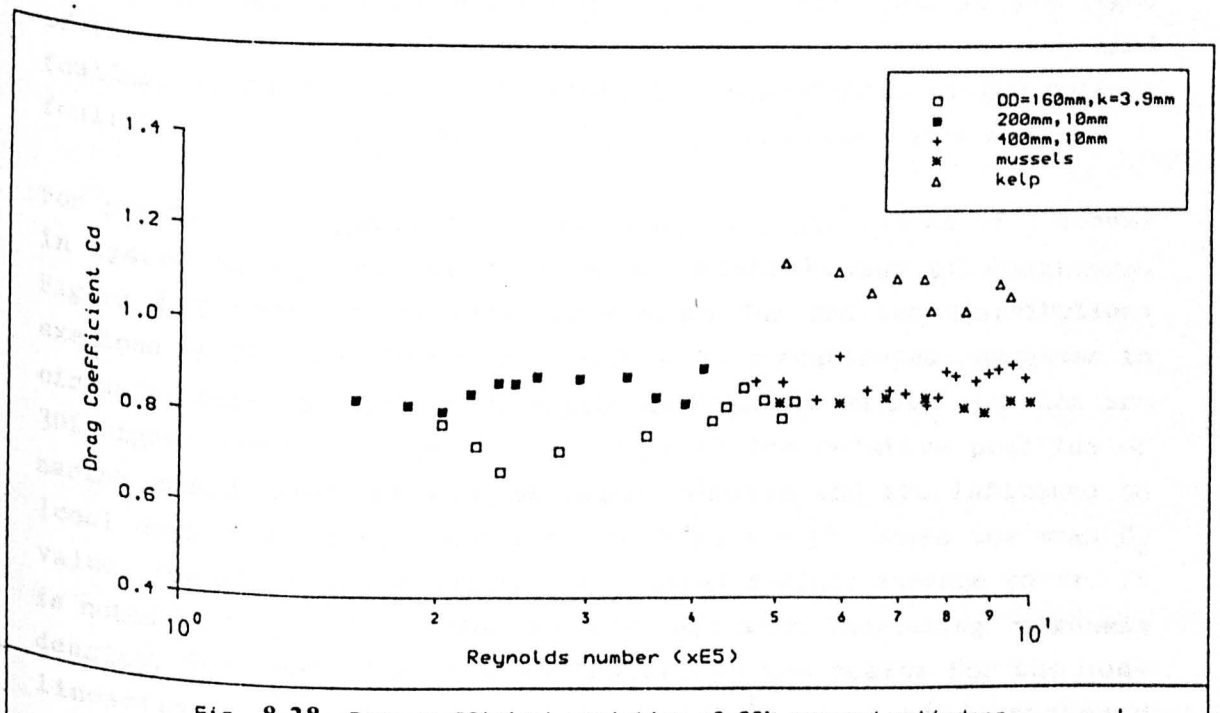

Fig. 8.28 Drag coefficient variation of 20% covered cylinders by strips of mussels, kelp or gravel.

vel; the increase being up to 30% for this set of tests. Again the drag coefficients for gravel roughness are similar to those for mussels despite the difference in roughness height. This trend is supported by the drag coefficents for the 160mm diameter gravel roughened cylinder with the same "local" k/D of 0.025 as for the 400mm cylinder.

It appears that the difference in size between mussels and gravel bears little influence on drag at low roughness densities; the correlation of all the coefficients being consistent. Once again, these results suggest that hard fouling may be represented by artificial roughness with reasonable accuracy at reduced surface covers, provided that roughness distribution is similar relative to the direction of flow.

It may be argued that this conjecture is only valid for hard fouling of uniform thickness over a tubular member, which is hardly the case for offshore structures where large undulations are commonly encountered due to thick mussel clusters. The hydrodynamic significance of such undulations is yet to be fully quantified. Some insight was provided by the data obtained with the multiple layers of mussels which suggested that the difference may be significant. In the light of the reasonable correlation between artificial roughness and hard fouling, it is believed that artificial reproduction of non-uniform fouling would provide good estimates of hydrodynamic drag forces.

For partially roughened cylinders, the principal causes of increase in hydrodynamic drag are density and distribution of roughness. Figure 8.29 presents the drag coefficents for the two distributions examined at 20% surface cover. Compared to concentrated roughness in circumferential strips the drag coefficients for random patches are 30% higher, indicating the significance of the relative position of marine growth over the tubular member surface and its influence on local drag. This is also evident from Figure 8.30, where the mean C_d values for all test conditions are plotted against surface cover. It is noted that C_d again varies non-linearly with increasing roughness density. The variation in distribution is the reason for the non-linearity. The overlap of the curves refering to mussel roughened cylinders with different distributions (Figure 8.19) is due to the same reason. It is conjectured that local flow disturbance depends on the area of patches and their relative position over the cylinder

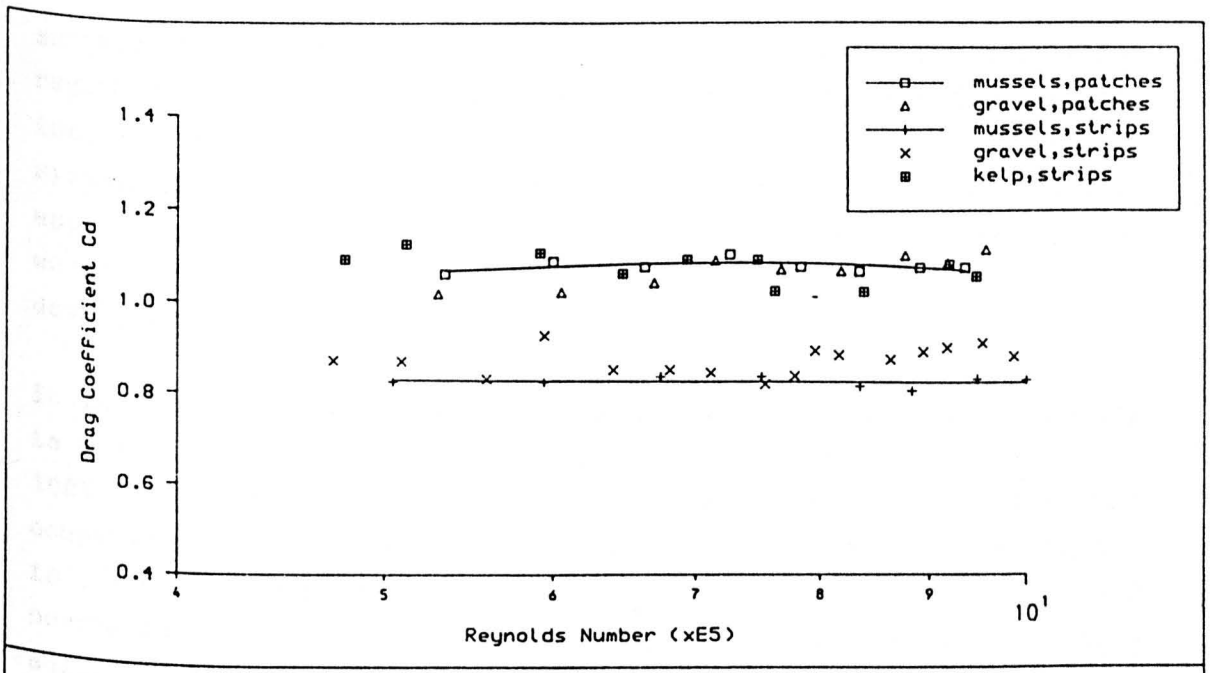

Fig. 8.29 The influence of surface roughness distribution on the drag coefficient of 20% partially covered cylinders.

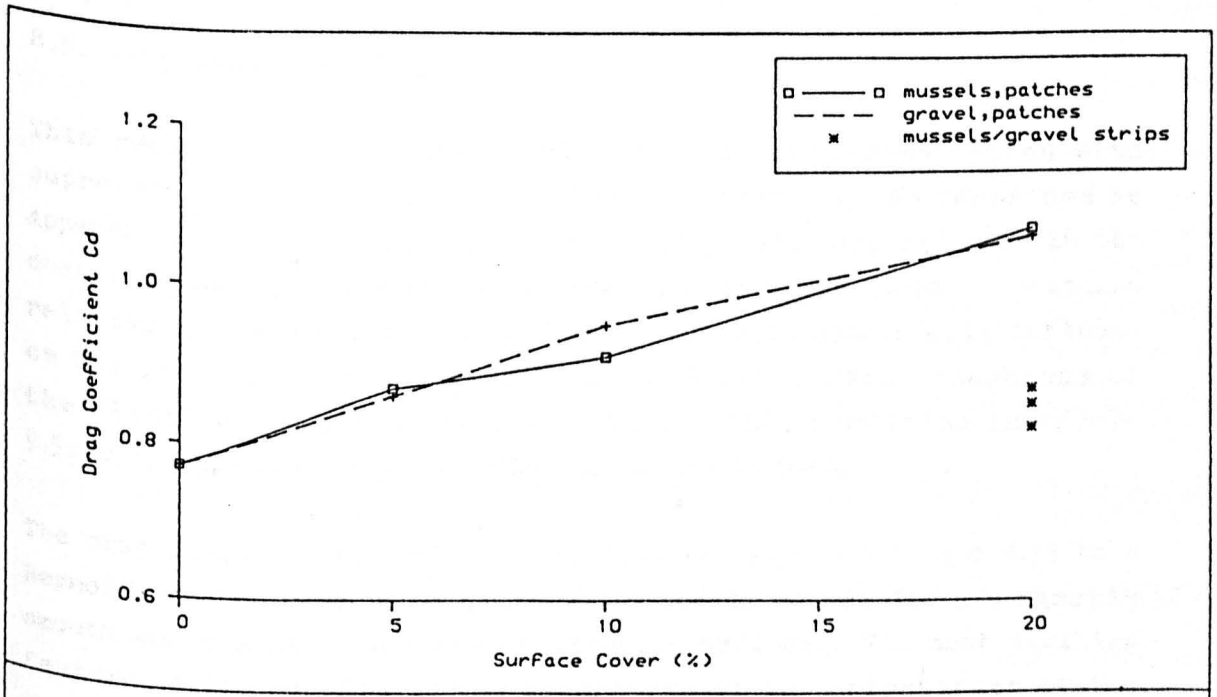

Fig. 8.30 Variation of Cd with % surface cover.

surface. Particularly so, for patches located within the separation region which would cause the local flow to separate earlier and thus induce spanwise pressure fluctuations. Had roughness density been systematically increased by roughness strips one should expect an approximately linear increase in hydrodynamic drag. However, this would be far removed from the realistic representation of the fouling development process.

It is interesting to note that if a cylinder with strips of fouling is treated in three segments, that is as two short cylinders with 100% fouling cover and a longer cylinder which is clean, then the computed drag force using the appropriate C_d values for each segment is close to the measured drag force for the entire cylinder. This occurs for all the cases tested, i.e. circumferential bands of mussels, kelp and gravel. These results suggest that a tubular member in flow orthogonal to its axis may be treated in segments using local force coefficents depending on type, distribution and surface cover of marine growth. Such an approach is particularly relevant to vertical or inclined members where composition and surface cover of marine fouling, being dependent on water depth, discharge outlets etc., vary significantly along the member length.

8.5. Antifouling Cladding

This section presents the results for two cylinders fitted with cupro-nickel based retrofit antifouling cladding. As described in Appendix C, the two prototype versions of panels differed only in the design of the fixing joint which together with the joint orientation relative to the direction of incident flow could potentially influence the drag and lift forces (Figure 8.31(a)). Surface roughness of the cladding was quoted at 30-40 microns [99] resulting in $k/D=7-9.5\times10^{-5}$, excluding the contribution by the joints.

The drag force coefficients are plotted in Figures 8.32 and 8.33 to a Reynolds number base. Also plotted are the C_d curves for a nominally smooth and a lightly abraded calibration cylinder. The most striking feature of the results is the importance of the orientation of the joint relative to the direction of flow. This is true for both the simple angle and the faired joint.

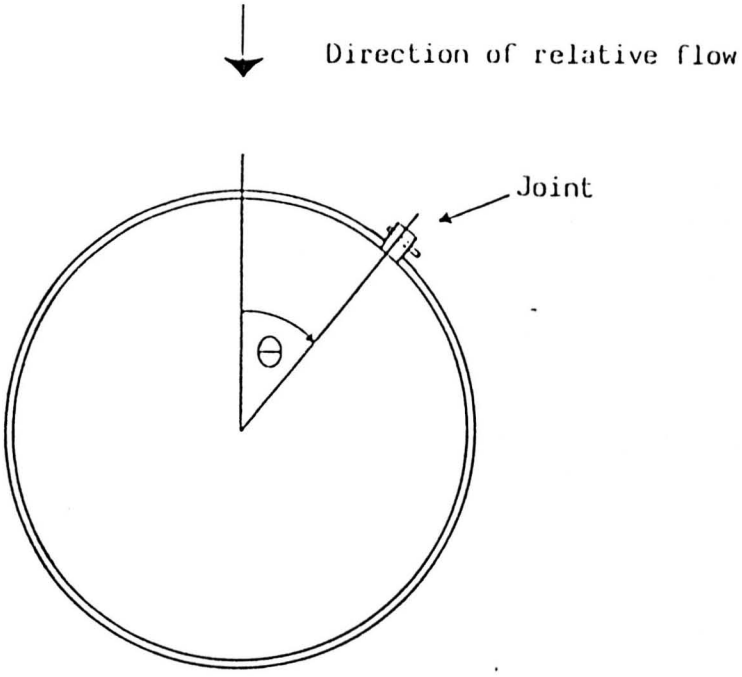

Figure 8.31(a). Definition of joint orientation relative to direction of motion.

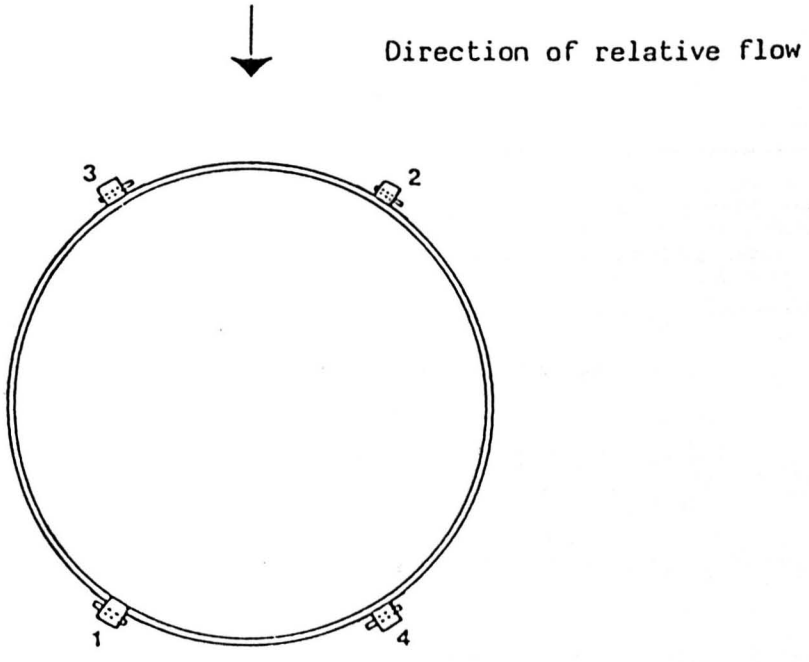

Figure 8.31(b). Pseudo-random positions of segmented joint; numbers indicate sequence of segments from near end of cylinder.

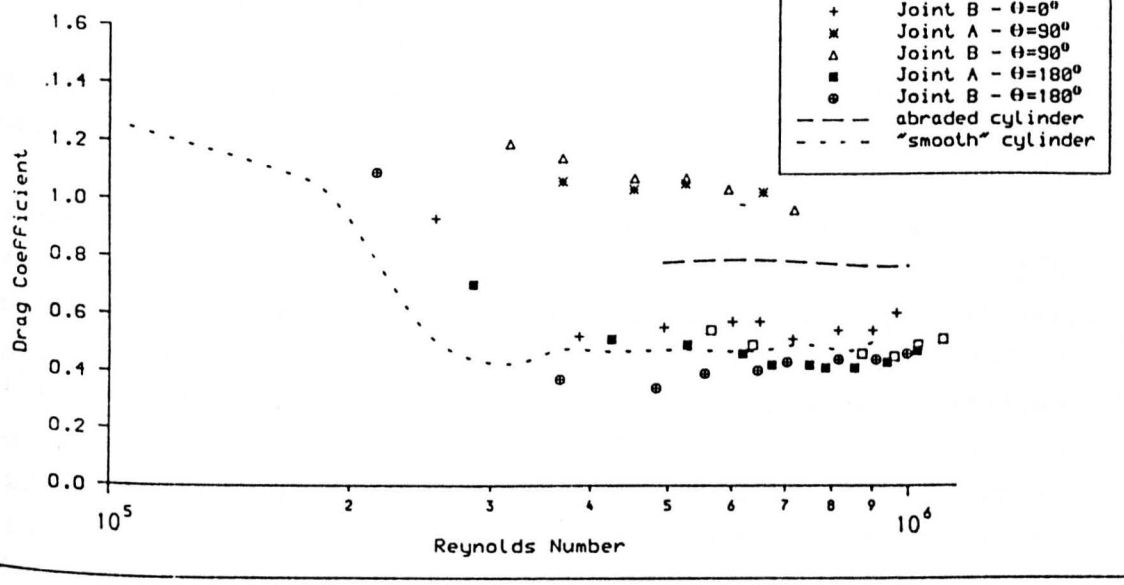

Figure **8.32** Drag of antifouling cladding with angle joint (A) or faired joint (B) at various angles of attack.

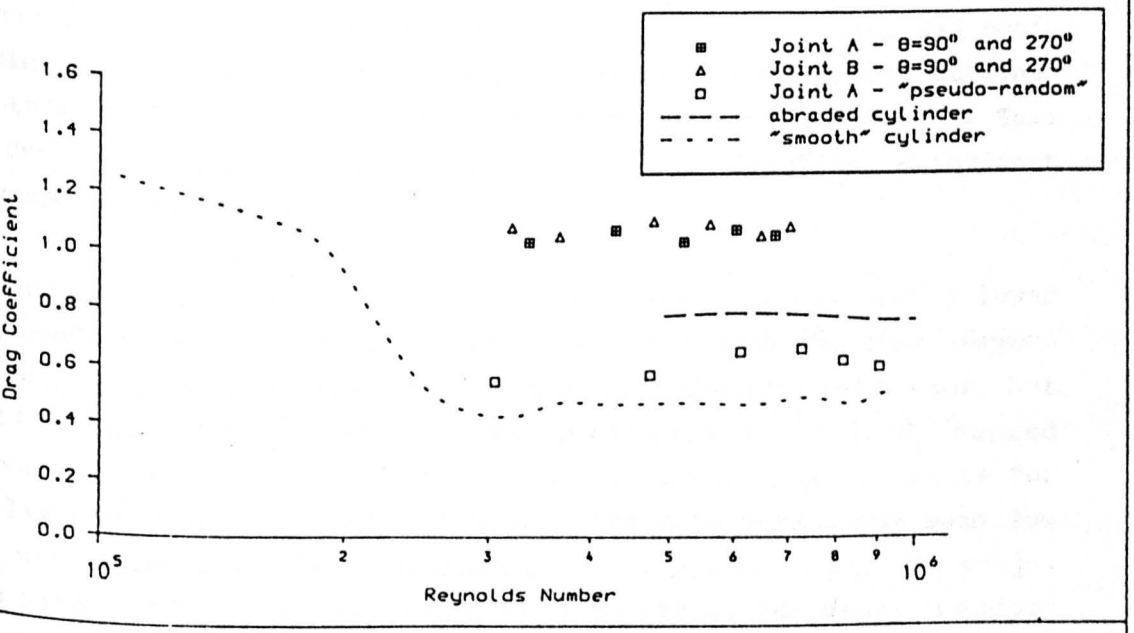

Figure **8.33** Drag of antifouling cladding with diametrically opposite or pseudo-randomly positioned split joints.

For both joint designs tested at $\theta=0^{o}$, C_d was lower than that for the abraded cylinder indicating that any roughness contribution by the joint alone was mitigated by the low surface roughness characteristics of the cladding. No significant differences in C_d were apparent between the two types of joint at that orientation.

With the faired joint positioned at $\theta=180^{o}$, the drag coefficients were similar to those for a smooth cylinder. With the simple angle joint in the wake the results also compared well. They were however slightly higher than those obtained for the faired joint suggesting that the streamlined shape of the latter had some drag reducing effect. Therefore, if the antifouling panels were bonded to the cylinder without a protruding mechanical joint the clad cylinder could be regarded as a nominally smooth cylinder, at least for the surface condition tested.

The most marked increase in C_d occured when the joint spanned one side of the cylinder ($\theta=90^{o}$ or 270^{o}). The steady transverse force affected the magnitude of the measured in-line force and, despite considerable tension in the guide wires, some biased transverse movement occured during the trajectory. The transverse movement was more pronounced for the faired joint which is possibly the reason for greater data scatter.

Although the transverse forces were minimised by splitting and positioning the joints at $\theta=90^{o}$ and $\theta=270^{o}$ the drag coefficients obtained for this configuration were high, ranging between 1.03 and 1.1. This was due to the increased projected area to the direction of incident flow and the higher effective roughness.

In contrast, and despite some transverse movement, considerably lower drag coefficients were obtained from the tests with the four segmented joints "pseudo-randomly" placed around the circumference, but still within the projected diameter (Figure 8.31(b)). C_d ranged between 0.55 and 0.66 which was well below the drag coefficients for the lightly abraded cylinder. However, the main reason for such low drag coefficients was the containment of the joints within the projected diameter and the drag could well be higher for other "random" orientations.

The results of these tests suggested that in retrofit applications offshore the antifouling cladding joints should be pseudo-randomly orientated along the tubular member such that the reduction in drag loading be maximised and assymmetry bias minimised.

D(mm)	k/D	C_d		C_m		Corrected C_m	
		Mean	St.Dev.	Mean	St.Dev.	Mean	St.Dev.
Abraded							
400	0.001	0.78	0.02	2.17	0.21	-	-
Sand							
400	0.005	1.00	0.04	2.04	0.12	2.00	0.18
200	0.0075	1.01	0.04	1.88	0.16	1.80	0.11
160	0.0094	1.03	0.07	1.88	0.30	1.76	0.27
400	0.0097	1.06	0.03	2.22	0.27	2.08	0.10
200	0.0097	1.03	0.04	1.91	0.12	1.75	0.11
150	0.01	1.04	0.02	-	-	-	-
160	0.012	1.19	0.04	1.92	0.19	-	-
315	0.012	1.11	0.02	2.05	0.16	1.94	0.14
400	0.0185	1.12	0.03	2.40	0.23	-	-
200	0.0195	1.10	0.04	1.98	0.11	1.80	0.14
160	0.024	1.16	0.04	1.93	0.27	1.74	0.24
400	0.025	1.19	0.03	2.31	0.08	2.17	0.10
160	0.062	1.20	0.06	2.12	0.28	-	-
Pyramids							
408	0.049	1.17	0.02	1.86	0.20	1.79	0.22
408	0.098	1.29	0.03	1.94	0.19	1.88	0.19

Table 8.1. Summary of results for artificially roughened cylinders.

Test Condition	Surface Cover (%)	k(mm)	k/D	C_d		C_m	
				Mean	S.D.	Mean	S.D.
Random patches	5	8	0.02	0.86	0.04	2.30	0.13
	10	8	0.02	0.95	0.04	2.38	0.19
	20	8	0.02	1.06	0.03	2.43	0.20
	25	7.5	0.018	1.01	0.03	2.11	0.07
	50	7.5	0.018	1.06	0.03	2.12	0.15
Strips	20	10.0	0.025	0.87	0.03	2.08	0.17
	20	4.0	0.025	0.85	0.03	2.22	0.20

Table 8.2. Mean force coefficients for partially roughened cylinders by sand.

Test Condition	Surface Cover (%)	k(mm)	k/D	C_d		C_m	
				Mean	S.D.	Mean	S.D.
"Smooth"	N/A	N/A	N/A	0.49	0.02	2.14	0.24
Abraded	100	0.4	0.001	0.78	0.02	2.17	0.21
Random patches single layer	5	29.5		0.87	0.01	2.24	0.20
	10	29.5		0.91	0.02	2.26	0.24
	20	29.5	0.0	1.07	0.01	2.30	0.18
	25	8.0	0.02	1.09	0.02	2.21	0.15
	25	24.0	0.06	1.00	0.01	2.34	0.10
	25	34.0	0.085	1.05	0.02	2.28	0.10
	50	8.0	0.02	1.12	0.02	2.26	0.22
	50	24.0	0.06	1.09	0.02	2.45	0.15
	50	34.0	0.085	1.11	0.04	2.39	0.15
Full cover single layer	100	8.0	0.02	1.20	0.01	2.41	0.22
	100	24.0	0.06	1.20	0.02	2.41	0.16
	100	27.0	0.675	1.22	0.06	2.32	0.24
	100	34.0	0.085	1.26	0.01	2.48	0.11
Random patches, multiple layers	25	26.0	0.215	1.56	0.02	2.32	0.21
	50	26.0	0.215	1.68	0.07	2.59	0.17
	100	43.0	0.215	1.85	0.02	2.50	0.15
Strips	20	29.5	0.074	0.82	0.01	2.30	0.11

Table 8.3. Summary of mean C_d and C_m for mussel roughness.

Test Condition	Surface Cover (%)	l(mm)	l/D	C_d		C_m	
				Mean	S.D.	Mean	S.D.
"Smooth"	N/A	N/A	N/A	0.49	0.02	2.14	0.24
Abraded	100	0.4	0.001	0.78	0.02	2.17	0.21
Random patches (L.Saccharina)	25	1000	2.5	1.34	0.05	2.40	0.21
	25	500	1.25	1.32	0.04	2.31	0.10
	25	250	0.63	1.20	0.08	2.33	0.11
	50	1000	2.5	1.37	0.03	2.53	0.39
	50	500	1.25	1.39	0.08	2.40	0.23
Strips (L.Digitata)	20	1000	2.5	1.07	0.04	2.41	0.18
Full cover:							
-L. Digitata	100	500	1.25	1.67	0.16	2.99	0.29
-L. Digitata	100	1000	2.5	1.69	0.07	3.29	0.39
-L. Saccharina	100	500	1.25	1.51	0.05	3.37	0.44
-L. Saccharina	100	1000	2.5	1.69	0.04	2.41	0.18

Table 8.4. Summary of mean force coefficients for kelp fouling.

Test Condition	D(mm)	Surface Cover(%)	Mean k(mm)	C_d Mean	C_d S.D.	C_m Mean	C_m S.D.
"Smooth"	400	N/A	N/A	0.49	0.02	2.14	0.24
Abraded	400	100	0.4	0.78	0.02	2.17	0.21
SEA ANEMONES distribution:							
- non-uniform	400	40	60	1.19	0.04	2.17	0.08
- uniform	400	25	60	1.15	0.02	2.16	0.11
MIXED FOULING -Sea anemones and tunicates:							
$\theta=0^o$	315	70	20-80	1.35	0.03	2.08	0.07
$\theta=90^o$	315	70	20-80	1.09	0.07	2.17	0.24
-Barnacles,mussels and seaweed:							
$\theta=0^o$	315	35	24	1.11	0.14	1.98	0.08
$\theta=180^o$	315	35	24	1.03	0.02	2.01	0.05
-Barnacles,mussels and seaweed:							
$\theta=0^o$	400	45	24	0.92	0.04	2.06	0.11
$\theta=0^o$	400	45	24	1.10	0.05	2.07	0.07

Table 8.5. Summary of results for soft and mixed fouling.

CHAPTER 9. WAVE LOADING ON A MACRO-ROUGHENED CYLINDER

Among other findings the steady flow experiments quantitatively established that the drag force increase due to hard marine fouling is similar to that experienced by artificially macro-roughened cylinders. It was also indicated that irregular roughness induces higher local drag than uniformly distributed roughness of similar size. Marine fouling thickness is nothing but irregular and the height of individual species can measure a few centimetres. To realistically reproduce hard fouling one must therefore incorporate such characteristics in the artificial model.

This approach was adopted for the experiments in regular waves on a macro-roughened circular cylinder. The experiments were carried out at the largest possible scale under controlled laboratory conditions in terms of wave kinematics and cylinder/roughness dimensions. As such they provided: firstly, a tangible source of data for design force coefficients at the drag/inertia dominated flow regime; secondly, the opportunity to compare with previous results from planar oscillatory flow and field experiments; and finally, a context to assess the steady flow results for marine roughness.

9.1. Experimental Features

The tests were carried out at the Delta wave flume of the Delft Hydraulics Laboratory with a vertical cylinder of 505mm diameter, at Reynolds numbers from 6×10^4 to 7.7×10^5 and KC numbers up to 29. Figure 9.1 shows a partial view of the Delta flume and the rough cylinder during a test run.

In-line and transverse forces were measured on two 250mm long force elements, their centres located at -1.5m and -2.5m depth elevations. Horizontal and vertical water particle velocities were recorded at the same elevations. More details of the facility, procedures, instrumentation and data acquisition are given in Appendix G.

The roughness consisted of closely packed, randomly orientated and distributed equilateral pyramids of three mean heights; 26.4mm, 19.7mm and 13.5mm. Pyramids were chosen since their geometric features of sharp edges and tapered shape represent reasonably well

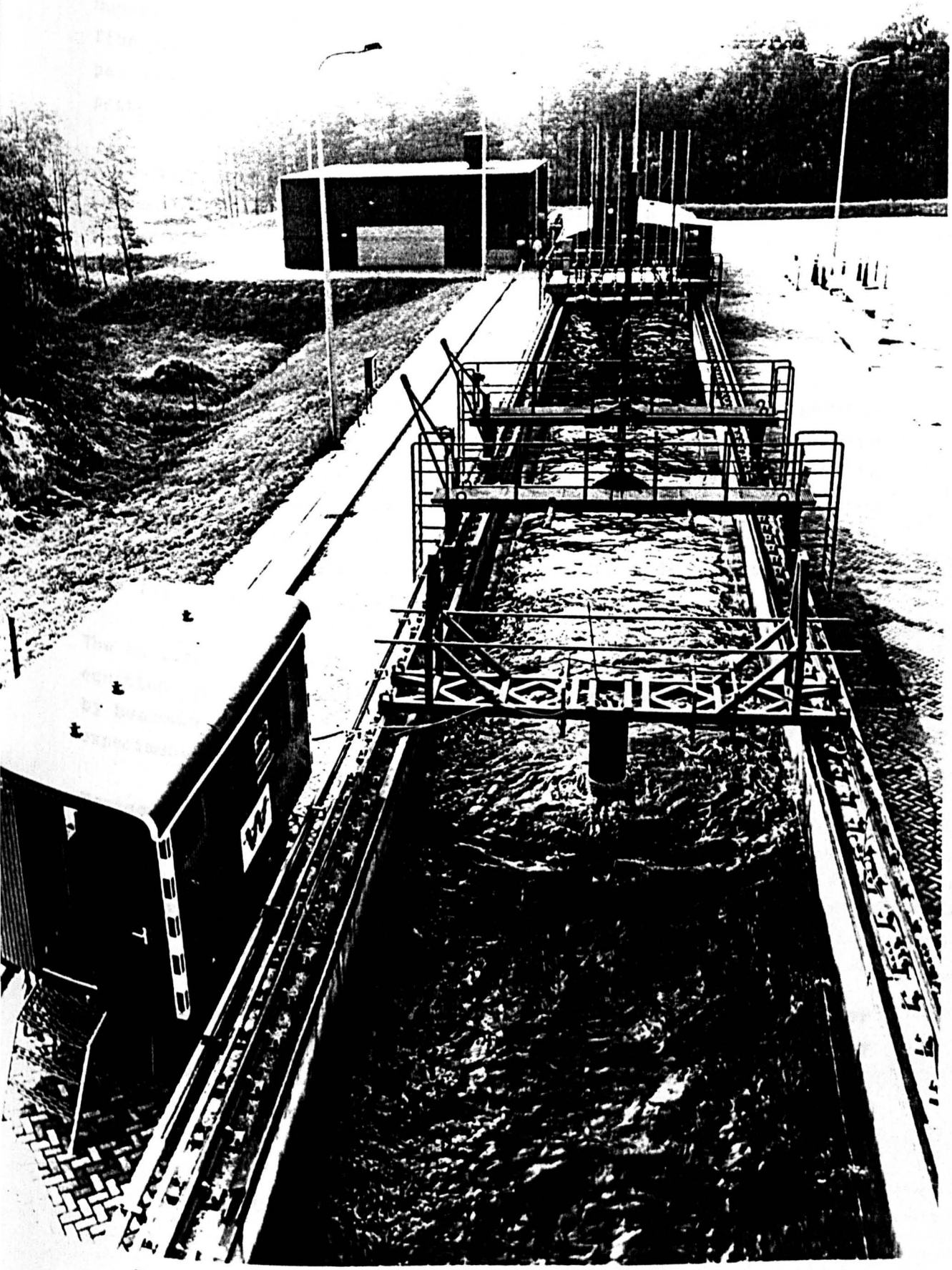

Figure 9.1. Partial aerial view of the Delta wave flume.

mussels and barnacles. The roughness pattern was cast on 250mm long fibreglass shells as described in Appendix G. The shells were strapped around the cylinder over almost its entire length, i.e. the pattern was repeated every 250mm (Figure 9.2).

Allowing for the base shell thickness the cylinder diameter used in the analysis was 521mm. For reference purposes, a relative roughness k/D of 0.038 was assumed (using mean k = 19.7mm).

9.2. Results and Observations

Fifteen runs were performed in waves of nominal heights and periods ranging from 0.6 to 1.9m and 3-10sec respectively. Depending on wave period the regular waves analysed from each run ranged from 77 to 282. A Fourier analysis, described in Appendix G, was carried out on a wave by wave basis for each force element. Since the force and velocity signals contained significant second order components they were fitted using the first six Fourier components.

The in-line force coefficients were determined through a Morison's equation approach described below. The approach was initially adopted by Bearman et al. [113] for the data analysis of smooth cylinder experiments in the same facility.

Morison's equation is expressed as,

$$F(t) = 0.5C_d\rho Du(t)|u(t)| + 0.25C_m\rho\pi D^2\dot{u}(t) \qquad (1)$$

Since the time average $\langle u(t).\dot{u}(t)\rangle$ is zero over each full wave for the fitted u(t) values the following expressions are derived by appropriate manipulation of equation (1),

$$C_d = \frac{2\langle F(t)\,u(t)\rangle}{\rho D\langle u(t)^2\,|u(t)|\rangle} \qquad (2)$$

Figure 9.2. The pyramid roughened cylinder.

and

$$C_m = \frac{4 \langle F(t)\, \dot{u}(t) \rangle}{\rho \pi D^2 \langle \dot{u}(t)^2 \rangle} \qquad (3)$$

The Re and KC numbers and the total force and lift coefficients were evaluated for each wave through various expressions, given in Appendix G, so that direct comparisons could be made with previously published results. In short, C_f, C_{fmax}, C_L, C_{Lmax}, KC and Re were expressed in terms of the maximum horizontal velocity; C'_f and C'_L in terms of the rms velocity; and KC' as a function of the fundamental velocity component (1st harmonic).

No detailed study of Reynolds number effects was warranted. The β values ranged from 23000 to 78000 approximately (β=Re/KC [54]); i.e. well within the post-critical Re regime. It can be safely assumed that all coefficients are independent of Re or β at these ranges, as has been demonstrated by the present steady flow results and through planar oscillatory flow experiments [58].

The coefficients presented are means from 12-14min long records, i.e the averages over all the waves analysed per run excluding wave ramp-up. Their standard deviations are shown in Table G.1, Appendix G. C_d and C_m generally vary less than 11% from their mean values, apart from run P02 which produced variations of 19% and 34% for C_d and C_m respectively. This was attributed to several incoming breaking waves observed during that run (WH=1.12m, T=9.5sec). Some evidence towards this is provided by the higher noise in the velocity time history (Figure G.7) compared to time histories for other runs. The data from run P02 were therefore excluded from further analyses.

Appendix G also includes plots of the mean coefficients for each force element and scatter plots of C_d and C_m for the lower element. Figures G.11-G.13 indicate no differences between the two force elements, hence no further distinction is made herein. Figures G.14 and G.15 suggest that C_d exhibits higher scatter at the inertia dominated regime (KC<5) and low scatter at KC>15, whilst the opposite is noted for C_m. Both coefficients show the same degree of scatter in the intermediate KC range. This scatter is inherent to any wave force data processing in the time domain which involves separating the total force into drag and inertia components. However, good repeatability of wave kinematics throughout each run and large samples

ensured well defined trends and magnitudes of all coefficients.

9.2.1. In-line Forces

The effect of macro-roughness on in-line force coefficients is illustrated by Figures 9.3 to 9.12. Data at typical KC numbers are also shown in Tables 9.1 and 9.2 which indicate the degree of variation with respect to smooth cylinders in wave and planar oscillatory flows and compare with published data for rough cylinders in planar oscillatory flow.

In Figures 9.4-9.6 the results for the pyramid covered cylinder are compared to those reported by Bearman et al. [113] for the same but smooth cylinder. These tests were also performed at the Delta flume and the data from both experiments were analysed by the same method, thus removing potential sources of uncertainty. For an even more direct comparison, only the coefficients for the lower force element are plotted against KC', i.e. consistent with the published smooth cylinder data. Also shown are results by Sarpkaya for smooth and sand roughened cylinders [58]. Sarpkaya's U-tube tests were carried out in planar oscillatory flow at β=11525 and 14200 for the smooth and rough (k/D=0.02) cylinders respectively and the coefficients represent 4.5min means.

A useful comparative measure of the in-line force increase due to roughness is shown in Figures 9.3 and 9.4 in terms of C_{fmax} and C'_f. At low KC numbers the total force coefficients are practically the same, whilst they increasingly diverge from the smooth cylinder values as KC increases. For the wave force data the difference in C'_f at KC'=10.5 is about 50% and rises to 81% at KC'=20. Similar trends are observed for C_{fmax} which tends to be more or less constant at KC>25 approximately.

It must be noted that the total force coefficient obscures the time dependence of forces. In other words it fails to describe the phase differences that exist between in-line forces and water particle velocities and as such, is of limited value to the Morison's equation design approach. The implications are illustrated in Table 9.1. The percentage differences in C_d and C_m over their smooth cylinder values are at variance with the corresponding increase in C'_f. Rough cylin-

	KC'	C'_f	C_d	C_m	C'_L
Pyramids	10.5	3.28	2.16	1.27	2.82
	13.5	2.79	1.85	1.45	1.70
	20.0	2.59	1.64	1.64	1.27
Smooth	10.5	2.20	0.60	1.57	1.38
	13.5	1.76	0.59	1.60	0.62
	20.0	1.43	0.65	1.42	0.74
% Increase	10.5	49	260	-19	104
	13.5	58	213	-10	174
	20.0	81	152	15	72

Table 9.1. Comparison between macro-roughened and smooth vertical cylinder in regular waves.

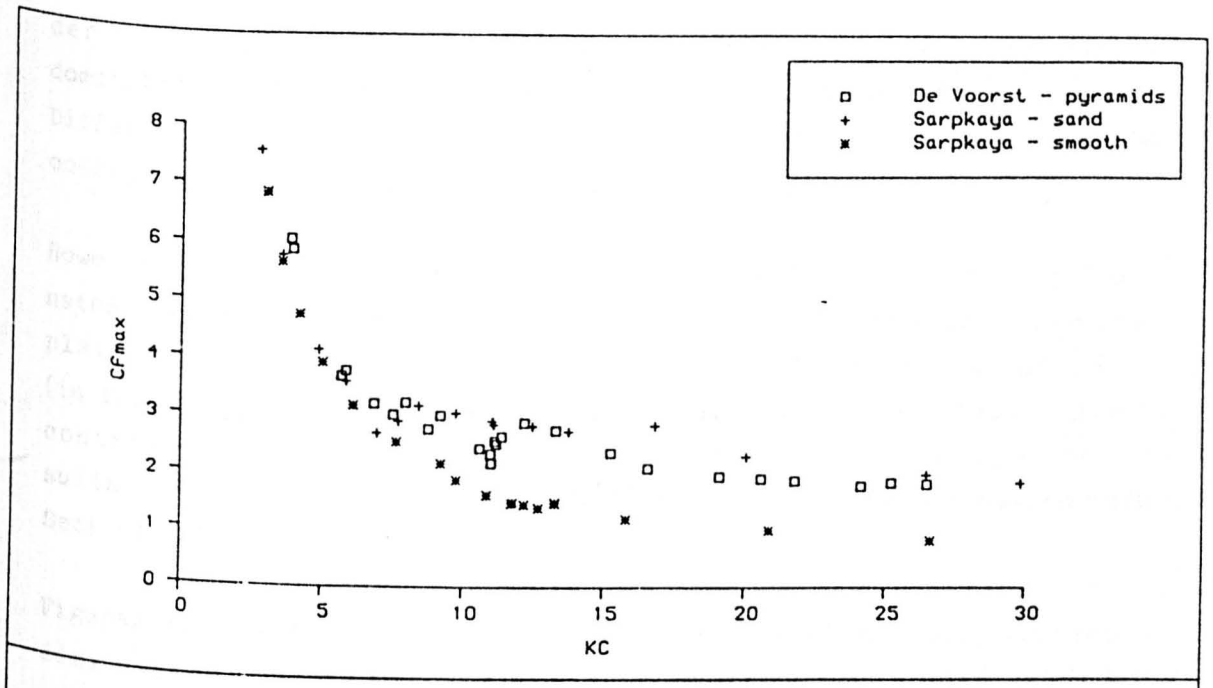

Fig. 9.3. Maximum total force coefficients for pyramid roughened cylinder and comparison with results from tests in harmonic flow.

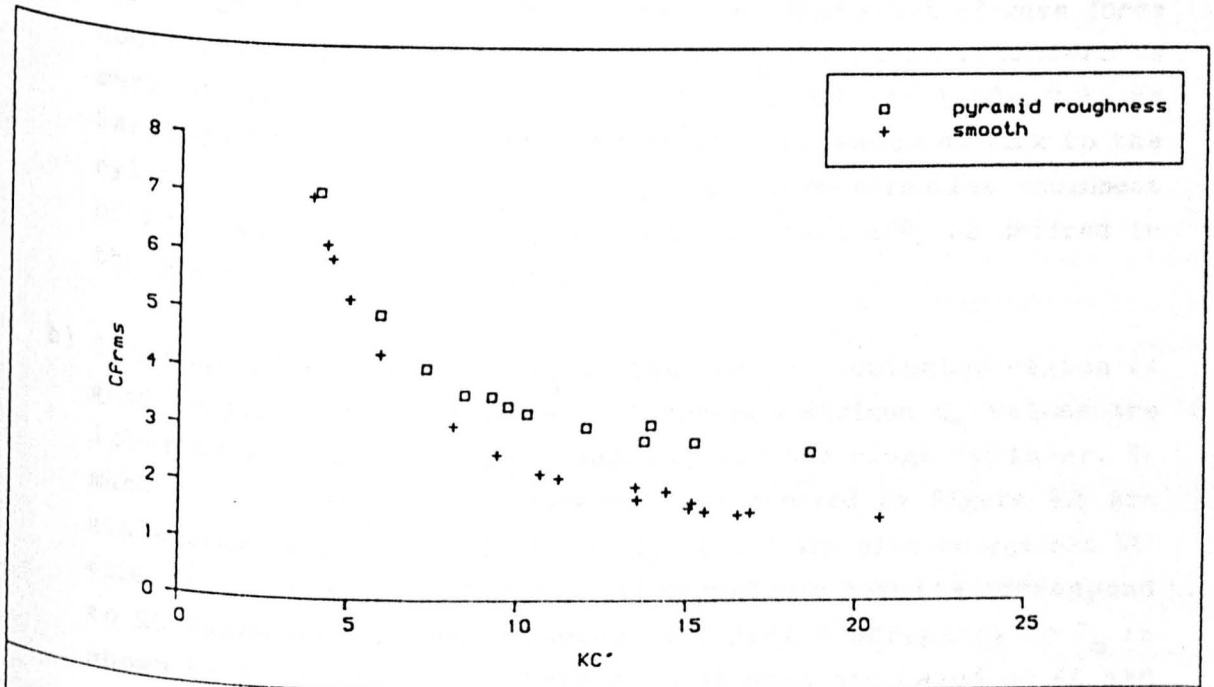

Fig. 9.4. Total force coefficients for pyramid roughened and smooth cylinders in regular waves.

der C_d increases by up to 260% approximately at the drag/inertia dominated regime, the increase being somewhat less (150%) at KC=20. Differences in C_m are small, with a weak trend towards lower inertia coefficients for the rough cylinder.

However, the force-velocity phase lags are reduced at the drag dominated region. This implies that if the maximum C_f reached a constant plateau at high KC, so should C_d both converging to a similar value (in fact C_{fmax} would be slightly higher due to a small inertia force contribution). This is significant in interpreting steady flow results and assessing their applicability to wave force estimation (see Section 9.3 and Chapter 10).

Figures 9.5 and 9.6 show that the "inertia crisis" and the corresponding higher drag at $9<KC<14$ are pronounced for the rough cylinder whilst no evidence of such effect is shown by the smooth cylinder data. This is in broad agreement with Sarpkaya's findings although the following differences are noted between the Delta wave flume and the U-tube results:

a) Sarpkaya's drag coefficients are consistently higher for both smooth and rough cylinders in accordance with his remark that C_d for cylinders in harmonic flow forms the upper bound of wave force coefficients [114]. The difference in C_d for rough cylinders is marginally larger than shown in Figure 9.5 and Table 9.2, as Sarpkaya introduced a roughness height allowance of 1.2k to the cylinder diameter. This presumably implies an effective roughness of 0.6k, an effective k/D of 0.02 and an actual k/D, as defined in the present context, of 0.033.

b) Although correlation for C_m at the inertia dominated region is good irrespective of roughness, Sarpkaya's minimum C_m values are lower at KC around 12, particularly for the rough cylinder. It must be noted that the differences illustrated by Figure 9.6 are misleading since the Delta flume C_m values are plotted against KC' (i.e. based on r.m.s. velocity) and Sarpkaya's results correspond to KC based on maximum velocity. The real discrepancy in C_m is shown in Figure 9.8 where both sets of data are based on KC and signifies firstly, that care should be taken in comparing force coefficients with other published data, and secondly, that there is a need for rationalisation of data analysis procedures.

	KC	C_{fmax}	C_d	C_m	C_L
Pyramids	11.0	2.63	2.29	1.11	1.24
	15.5	2.36	1.85	1.45	0.80
	21.5	1.91	1.79	1.40	0.82
	25.0	1.84	1.64	1.64	0.38
Smooth*	11.0	1.62	0.87	1.44	1.33
	16.0	1.25	0.70	1.68	0.41
	21.0	1.01	0.66	1.70	0.23
	26.5	0.82	0.63	1.71	0.17
% Increase	11.0	62	163	-30	-7
	15.5	89	164	-16	95
	21.5	89	171	-21	256
	25.0	124	160	-4	123
Sand**	11.0	2.90	2.51	0.63	1.51
	16.5	2.90	2.17	1.09	1.11
	20.0	2.29	1.87	1.19	0.84
	26.5	1.94	1.80	1.19	0.68
% Difference	11.0	10	10	76	22
	15.5	23	17	33	39
	21.5	20	4	18	2
	25.0	5	10	38	79

* C_L for smooth cylinder at β=6555.

** C_L for sand roughened cylinder at β=6836.

Table 9.2. Comparison between present data and Sarpkaya's results from planar oscillatory flow tests [58].

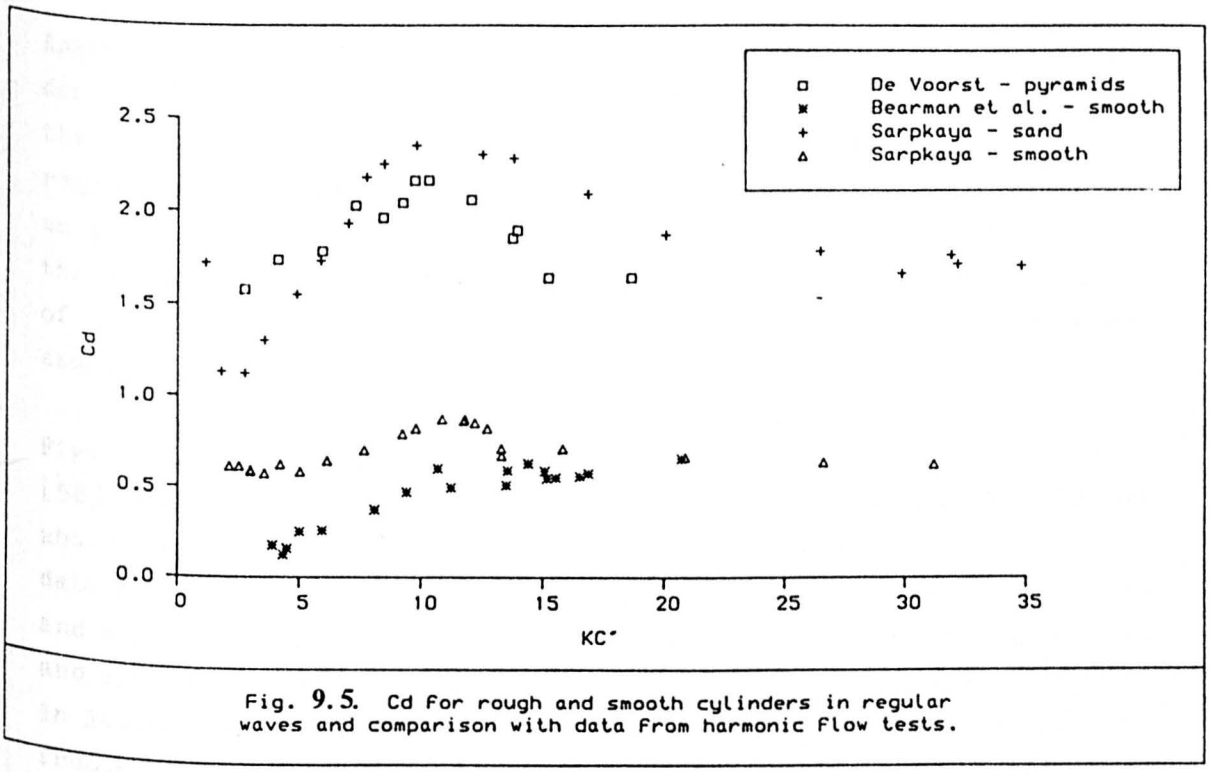

Fig. 9.5. Cd for rough and smooth cylinders in regular waves and comparison with data from harmonic flow tests.

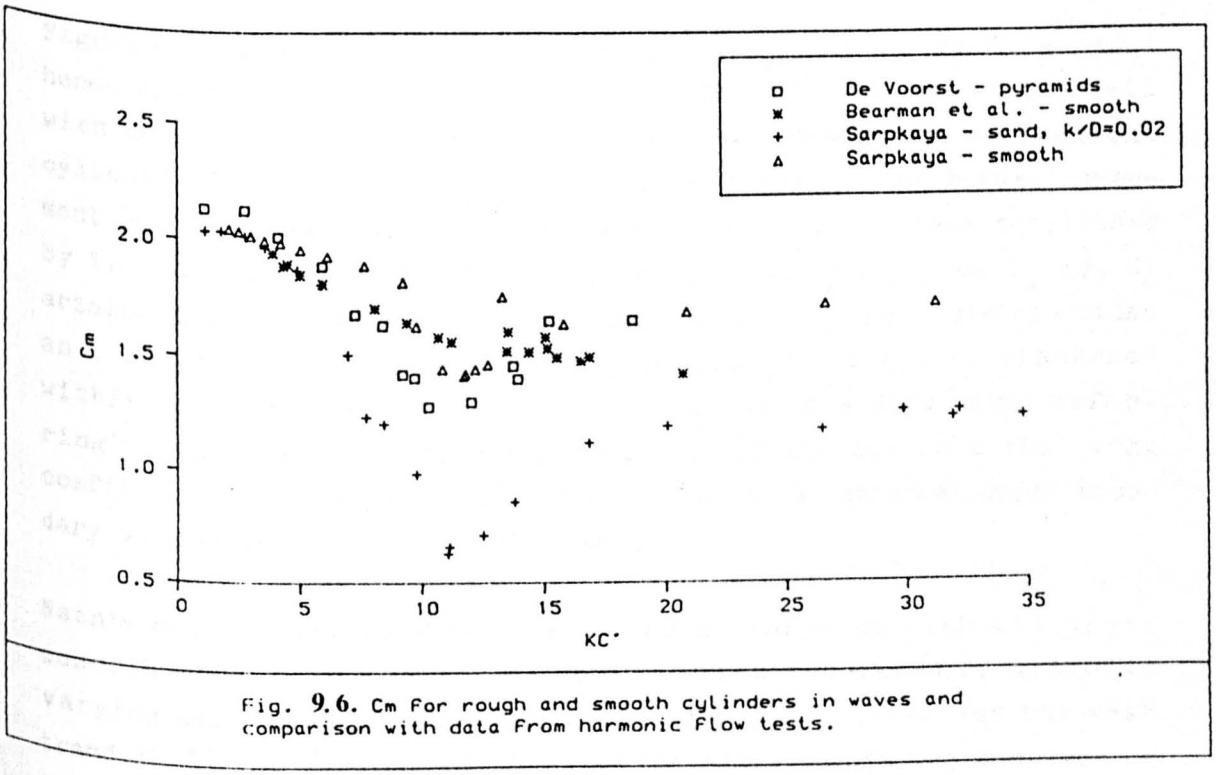

Fig. 9.6. Cm for rough and smooth cylinders in waves and comparison with data from harmonic flow tests.

Apart from the different definitions of relative roughness and cylinder diameter, contributory factors to the remaining discrepancies are the differences in methods of analysis and in phase lags between regular wave and planar oscillatory flows, the effect of lift forces on the resultant force and the orbital versus rectilinear paths of the velocity vector in the two types of flow. In-depth investigation of these interacting factors is outwith the scope of the present study.

Figures 9.7-9.10 compare the present results with those of Sarpkaya [58], Rodenbusch and Gutierrez [59] and Nath [50]. Apart from the above mentioned data by Sarpkaya for a sand roughened cylinder, his data for a barnacle roughened cylinder with clean diameter of 155mm and apparent diameter of 203mm (b=13517) are plotted in Figures 9.9 and 9.10. Rodenbusch and Gutierrez reported on experiments (at SSPA in Sweden) with a 1m diameter cylinder roughened by 20mm high conical frusta (k/D=0.02) which was periodically or randomly oscillated by an X-Y carriage. For brevity, only the data for planar oscillatory motion at $Re=4.4x10^5$ are present here. Nath carried out experiments in regular waves with sand roughened (k/D=0.02) and artificially marine roughened (k/D=0.1) vertical cylinders at Re up to $2x10^5$. Data from his highest Re runs are presented here, i.e. at $Re>1.0x10^5$.

Figures 9.7 and 9.8 show that both C_d and C_m for the pyramid roughened cylinder agree closely with the SSPA data and reasonably well with those by Sarpkaya. Rodenbusch and Gutierrez used an apparent cylinder diameter of (D_{smooth}+2k) and therefore, even better agreement should be expected had their force coefficients been normalised by the "clean" cylinder diameter. Potential effects on C_d and C_m arising from the different hard roughness types, their distributions and, in the case of the SSPA data, actual k/D cannot be discerned within the KC range in question. If anything, the SSPA data, referring to the lower k/D of 0.02, would reiterate the fact that drag coefficients from planar oscillatory flow tests represent upper boundary values of wave drag coefficients.

Nath's results for sand roughness are at variance with all above described data. His data were derived from few waves of slightly varying amplitude. Hence, the high degree of scatter and the weak trend in C_d and C_m with KC. The results shown herein are averages of three consequtive waves past a 200mm cylinder. Although direct velo-

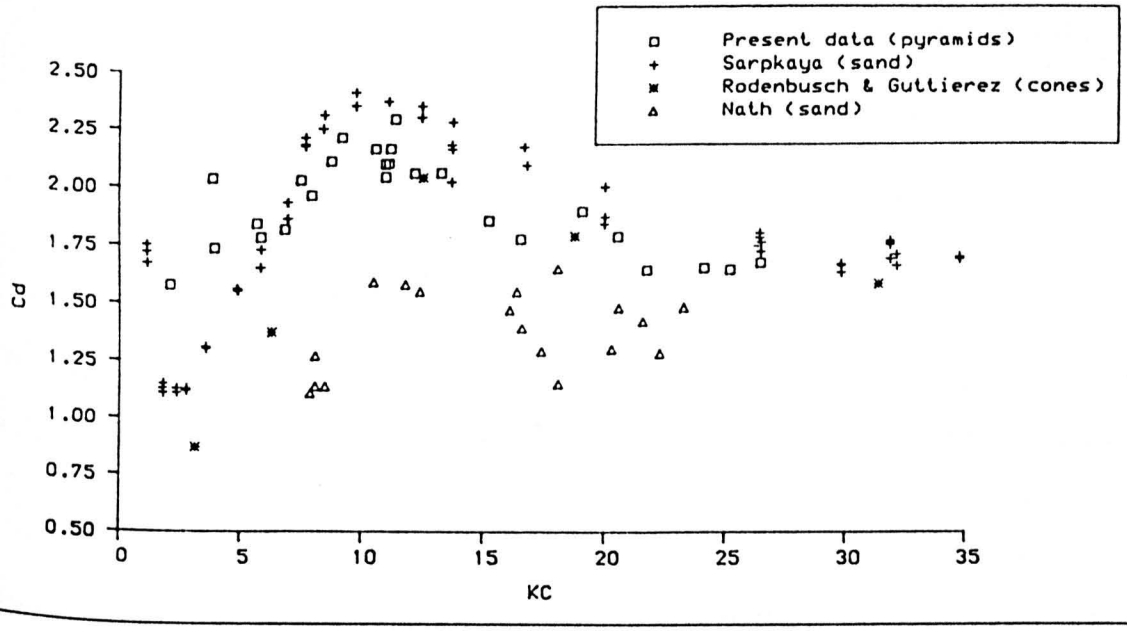

Fig. 9.7. Comparison of present Cd data with previous results for artificially rough cylinders (k/D=0.02).

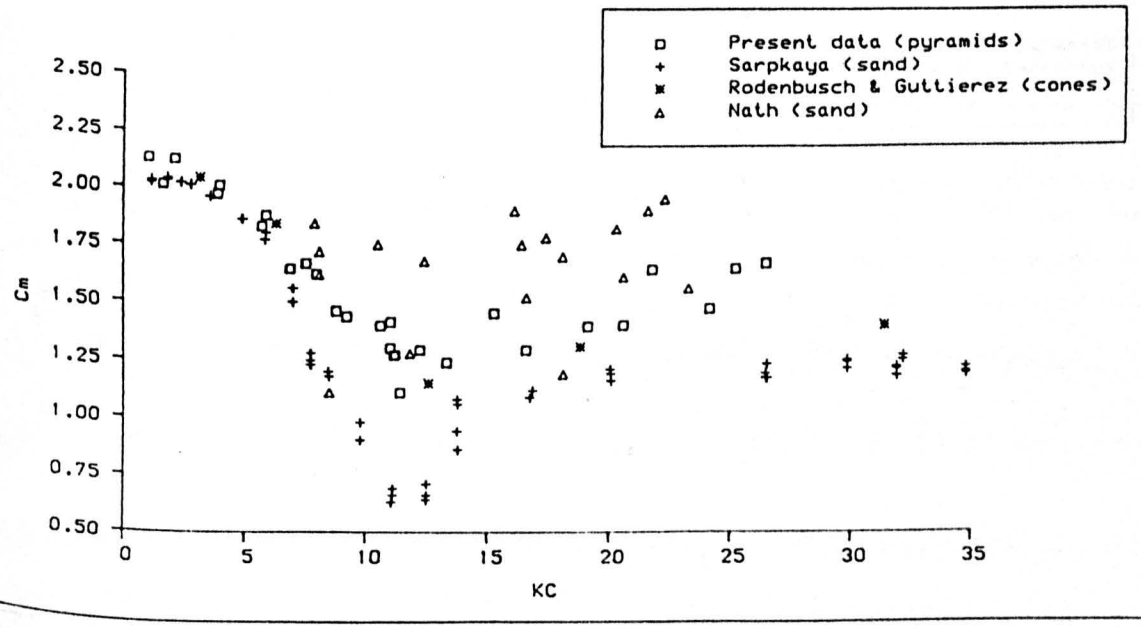

Fig. 9.8. Comparison of present data for Cm with previous results for artificially roughened cylinders (k/D=0.02).

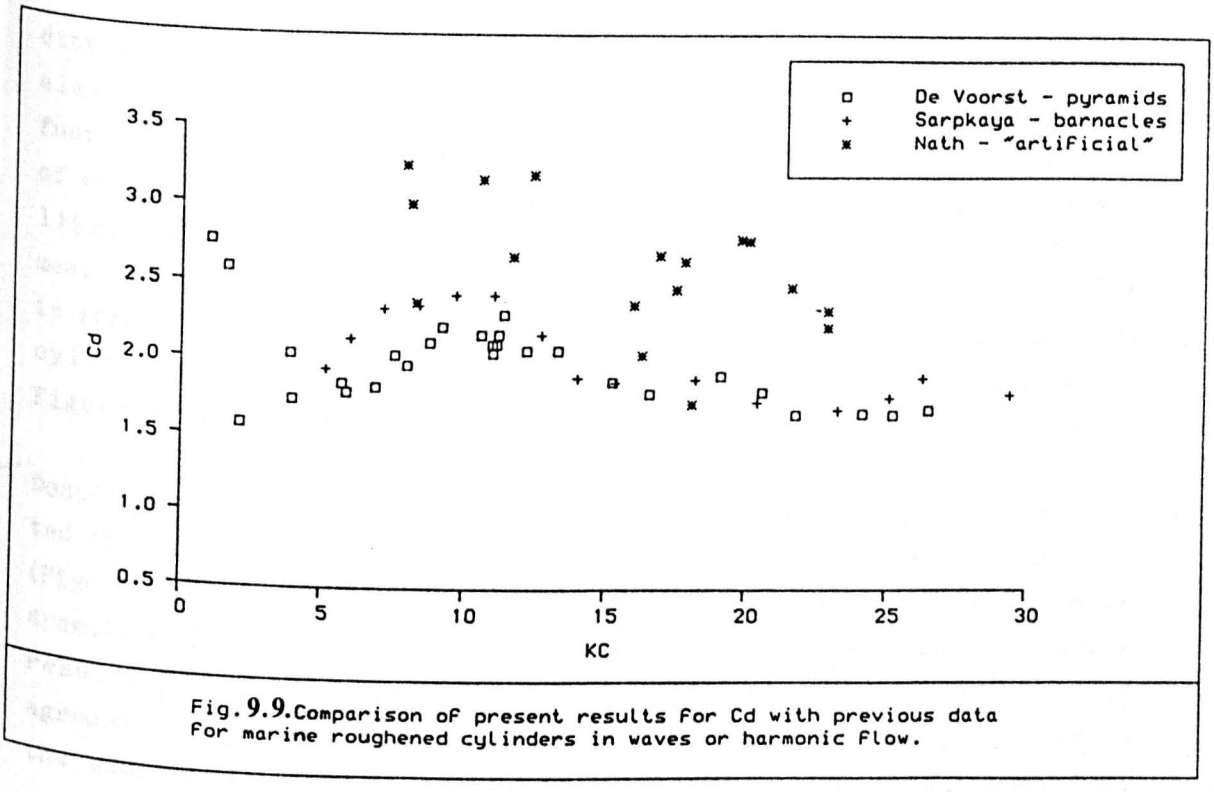

Fig. 9.9. Comparison of present results for Cd with previous data for marine roughened cylinders in waves or harmonic flow.

N.B. The pyramid pattern here is a peudo-random one comprising pyramids of different sizes whereas for the results presented in Figure 8.14 the pyramids are of constant size in a regular pattern. This may be the cause of some of the difference in drag coefficients.

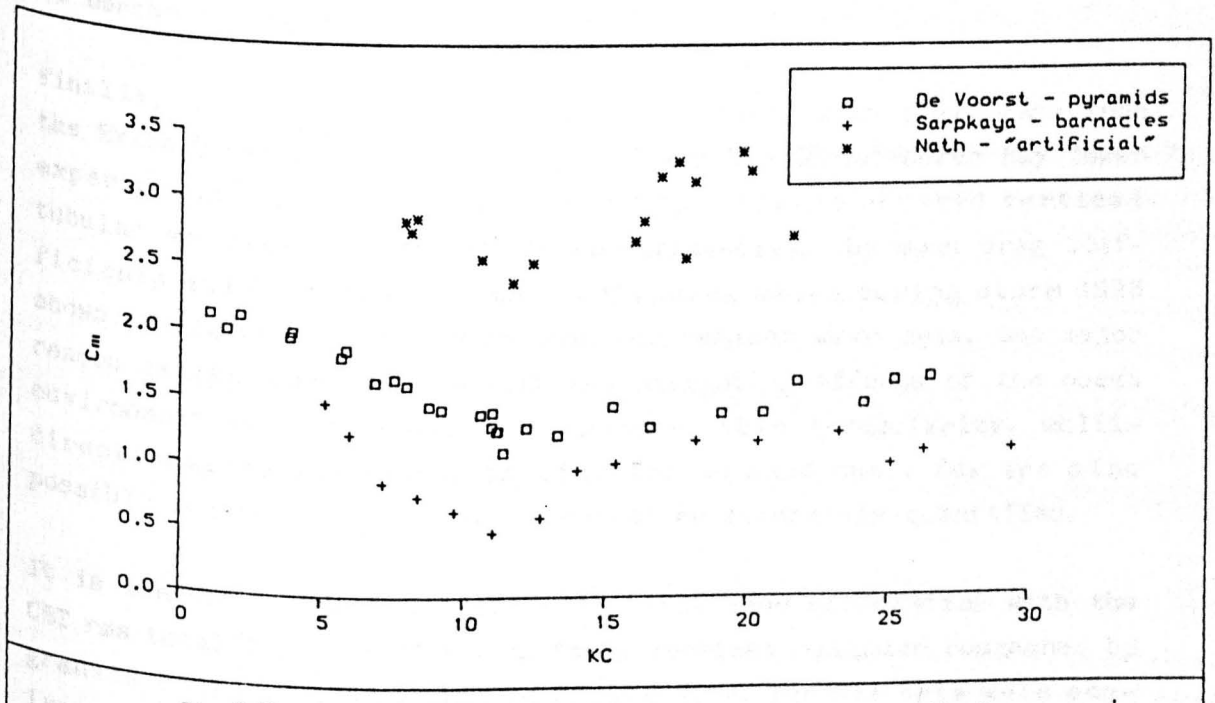

Fig. 9.10 Comparison of present Cm values with previous results for marine roughened cylinders in waves or harmonic flow.

city measurements were taken, the analysis was based on wave surface elevation measurements and predicted kinematics, through the stream function theory, a procedure which may have influenced the magnitude of coefficients. The discrepancies are observed in Figure 9.7 are likely due to such experimental arrangement and procedures as the measurement of forces, filtering and depth parameter corrections. It is recalled that the steady flow C_d values of Nath [49] for the same cylinders are also lower than most other published data shown in Figure 8.13 (Chapter 8).

Despite the above, increases in C_d of the order of magnitude suggested by Nath [50] for a heavily roughened vertical cylinder (k/D=0.1) (Figure 9.9) are likely. However, it is questionable whether C_m would dramatically increase too (Figure 9.10). With respect to Sarpkaya's results for the barnacle roughened cylinder, the apparently good agreement with the present C_d data should once again be qualified by the adopted diameter definitions. According to the definitions used here, k/D for this cylinder would be 0.15 and the apparent increase in diameter would be 30%. If this increase in diameter were accounted for by the drag coefficient, it would bring Sarpkaya's data closer to those of Nath, who used the clean cylinder diameter throughout his analysis, and would indicate the **actual** increase in drag forces due to barnacle roughness.

Finally, the Delta flume results are compared with field data from the Exxon Ocean Test Structure [33,59] and the Christchurch Bay Tower experiments [62]. The OTS data refer to barnacle covered vertical tubular sections ($0.014<k/D<0.024$ approximately). The mean drag coefficients and C_d values for the individual waves during storm SS28 shown in Figure 9.11 are lower than the regular wave data. One major reason is the lower k/D, whilst the mitigating effects of the ocean environment such as presence of currents, wave irregularity, multidirectionality and member inclination to name but a few are also possible reasons whose influence cannot be accurately quantified.

It is therefore remarkable to obtain such good correlation with the CBT rms total force coefficients for a vertical cylinder roughened by granite chips as that shown in Figure 9.12. The CBT data were analysed through the mean square theory developed by Bishop [63] which produces satisfactory time averages of force coefficients. At first sight the agreement may be attributed to similar k/D ratios (0.038

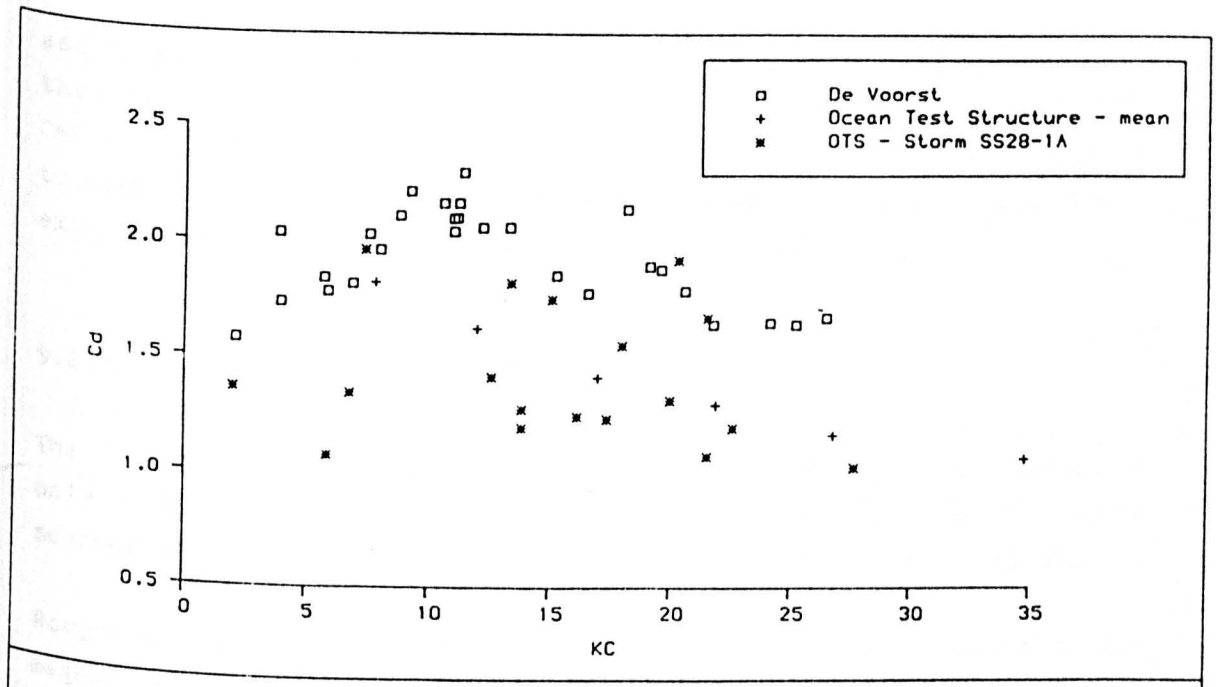

Fig. 9.11. Comparison of De Voorst mean Cd values with data from the OTS field tests.

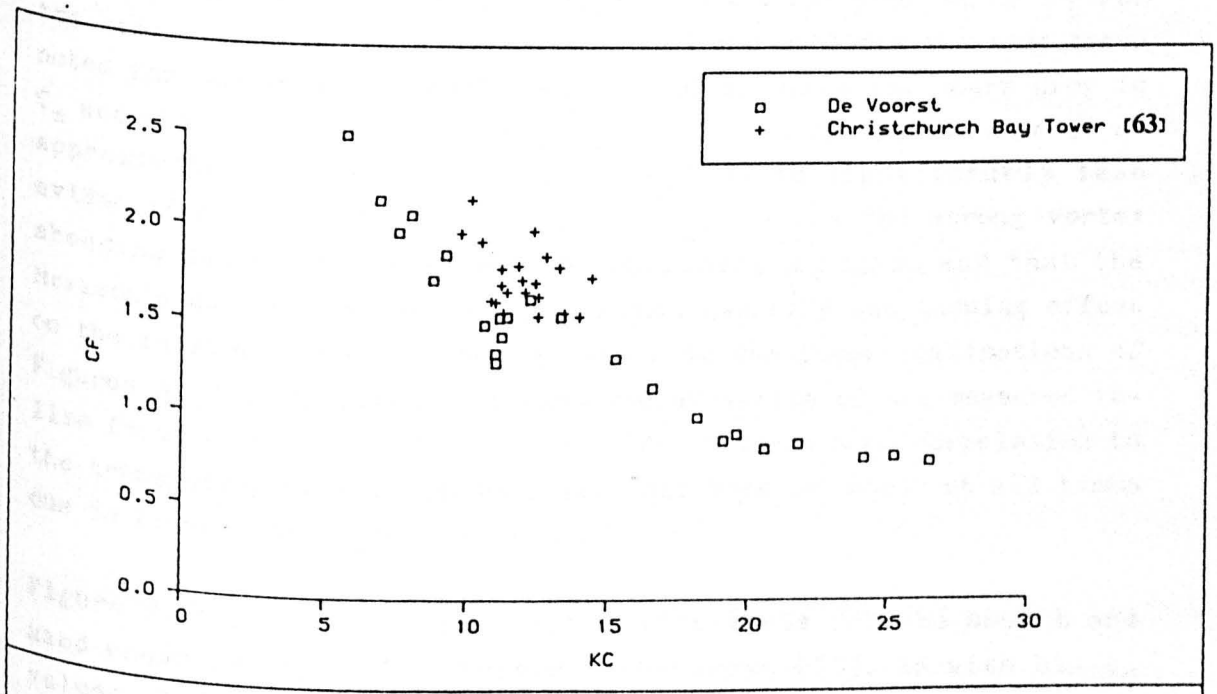

Fig. 9.12. Total force coefficients for pyramid roughened cylinder and for rough force element (k/D=0.033) in field tests.

and 0.033 for the Delta flume and CBT data respectively). However, the comparison is limited by the narrow KC range pertaining to the CBT study (9<KC<14) and more data in terms of C_d and C_m are required to establish trends and to justify the compatibility of large scale experiments with carefully controlled field tests.

9.2.2. Transverse Forces

The lift coefficients for the pyramid roughened cylinder are compared only with laboratory experimental data from the previously refered sources. No field data are available from the OTS or CBT projects.

Roughness induces strong vortex shedding and thus increases the magnitude of transverse force coefficents as illustrated in Figure 9.13. The present data are compared to the smooth cylinder results of Bearman et al. [113] in terms of C'_L and indicate average increases of 175% at the drag/inertia dominated region and of 70% at KC' of about 20 (see Table 9.1). C'_L rises steeply from neglible values at KC'<5 indicating early separation and strong vortex formation. It reaches values of the same order of magnitude as C_d at KC' around 10 and then decreases at a higher rate than C_d. The peaking of C'_L for the smooth cylinder is not as pronounced and exhibits the same trend noted for the in-line coefficients. In other words the sharp drop in C_m and the corresponding peak in C_d for the rough cylinder occur at approximately the same KC. Such behaviour is significantly less evident for the smooth cylinder. This highlights the strong vortex shedding due to roughness at the drag/inertia regime and that the Morison's equation based analysis cannot quantify the ensuing effect on the in-line forces. It can be seen from the force realisations of Figures G.6-G.10 in Appendix G that the deviation of the measured in-line force from the predicted Morison force bears some correlation to the transverse force peaks. However, this does not occur at all times due to transverse force hysterisis.

Figure 9.14 shows the r.m.s. lift coefficients for the smooth and sand roughened cylinders tested by Sarpkaya [58]. As with his C_d values, Sarpkaya's C_{Lrms} data for the rough cylinder are also consistently higher. The trend though is the same with that shown by the pyramid roughness results. Compared to the smooth cylinder the peak value of C_{Lrms} is shifted to lower KC of about 8 - note the differen-

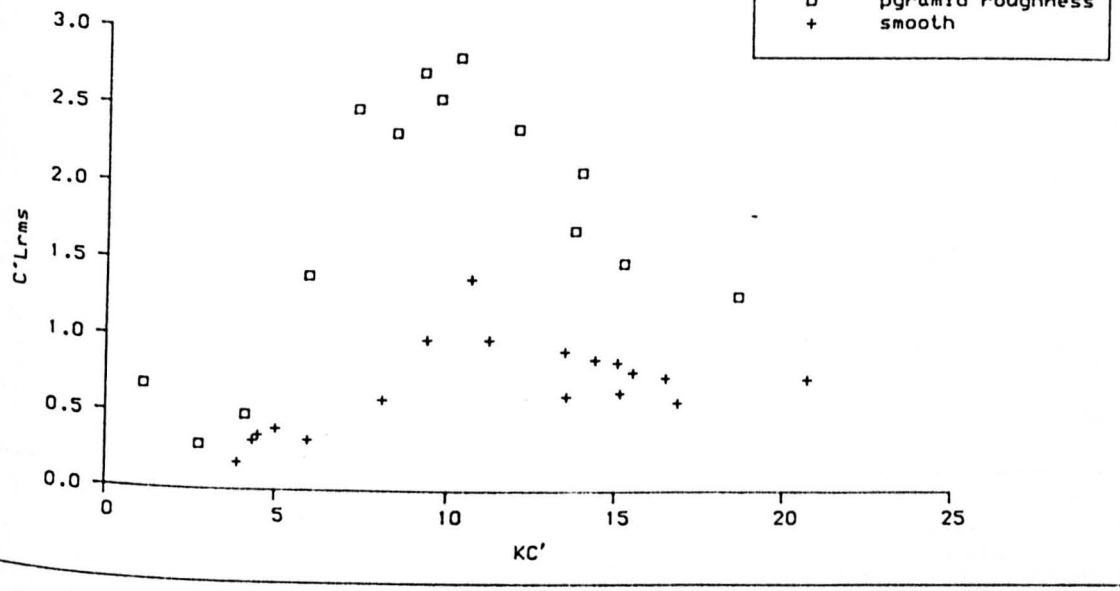

Fig.9.13. RMS lift coefficients for pyramid roughened and smooth [11.3] circular cylinders in regular waves.

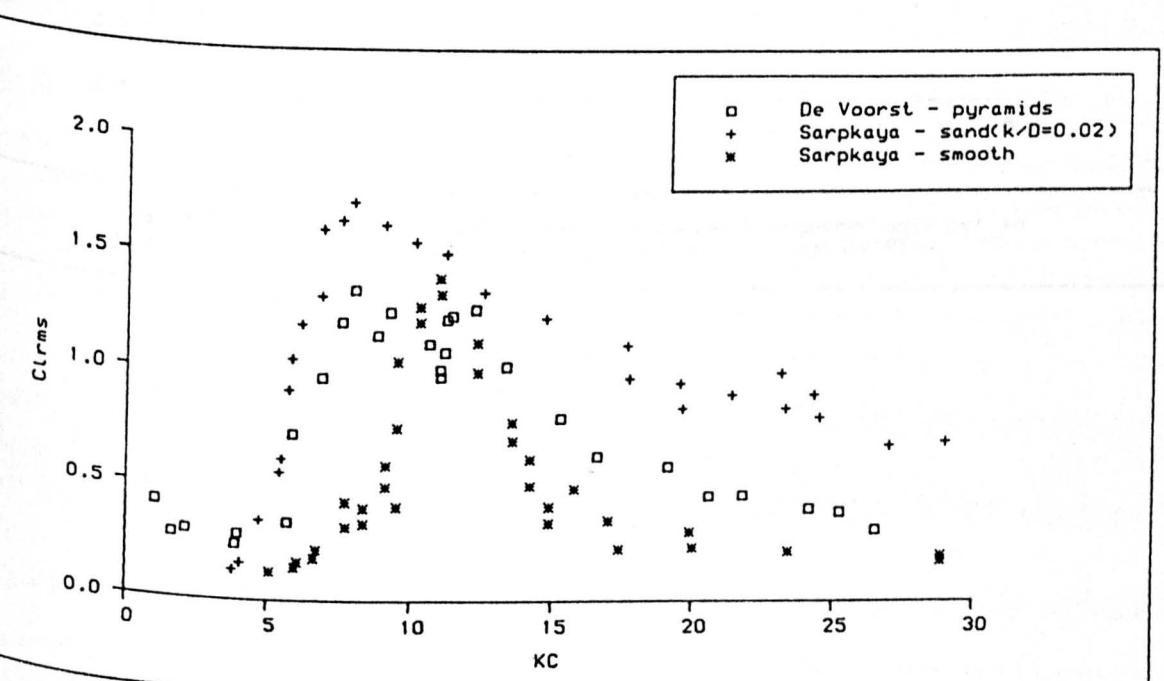

Fig. 9.14. Comparison of rms lift coefficient for pyramid roughened cylinder with data for smooth and rough cylinders in harmonic flow.

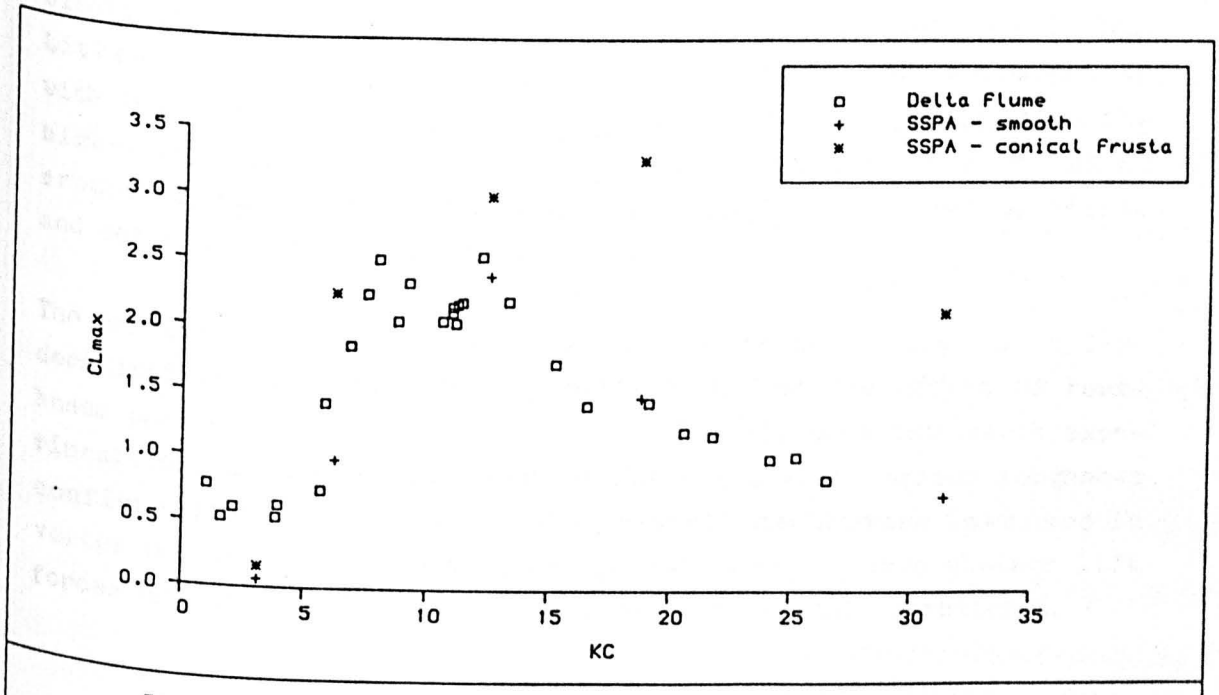

Fig. 9.15. Maximum lift coefficients for pyramid roughened cylinder in regular waves and for smooth and rough cylinder in harmonic flow.

ce with KC' - which conforms with the harmonic flow data. It is surprising however that the peak lift coefficient for the smooth cylinder in harmonic flow is higher than for the pyramid covered cylinder. It is noted in passing that in 1976 Sarpkaya reported higher maximum lift coefficients for the smooth cylinder than for rough cylinders [74]. Those tests were carried out at lower Reynolds numbers than his latest experiments which indicate the opposite being true, bringing them in line with numerous other experimental data.

Although many possible reasons could be cited it is difficult to pinpoint the underlying causes for the differences in lift coefficients derived from experiments in waves and planar oscillatory flow. Little insight is provided by Figure 9.15 which shows a comparison with the SSPA data in terms of C_{Lmax}. The SSPA data are significantly higher than the present maximum C_L values and appear to peak at KC around 18, contrary to established trends. They are however sparse and not much should be read into this trend.

The paucity of reliable experimental data for macro-roughened cylinders inhibits any systematic investigation into the effect of roughness parameters on transverse forces. Clearly more systematic experiments are needed in all types of flows and with various roughness configurations to understand the physical mechanisms involved in vortex induced forces and to quantify how, when, or even whether lift forces are of significance to the design of offshore structures.

9.3. Assessment of Steady Flow Results

It was mentioned at the outset of this chapter that the experiments in regular waves provided a context for assessing the "buoyant cylinder" results. However, in the previous section it was shown that the mean coefficients for the regular wave tests extended to KC numbers of only 26. These are quite low to allow for comparison with steady flow data, assuming that at high KC the latter can represent with reasonable accuracy wave force coefficients.

It should be noted that the above assumption has been seriously questioned due to fundamental differences in the physics of steady and non-linear time dependent wave flows [54]. The apparent agreement

of some drag coefficients obtained in steady flows and in ocean experiments may indeed be fortuitous although the reduced returning wake effects at high KC and the presence of currents - to name but two mitigating effects of the ocean environment - would tend to 'push' the wave drag coefficient to its steady flow value.

One can only speculate that on the basis of the weak indication shown by the present results the time averaged total force and drag coefficients converge to approximately constant values at KC>25. Yet there is no concrete evidence that these constant values should be the same in steady flow. A quick look through the data presented here would show that indeed they are not. Any conclusions must therefore be confined to the effect of hard roughness parameters which were common to both types of experiments reported here. In that respect and subject to the roughness pattern tested in regular waves it is suggested that at the drag dominated region:

a) The percentage increase in wave induced drag forces on vertical macro-roughened cylinders vis-a-vis smooth cylinders is compatible to that observed in steady flow at post-critical Reynolds numbers.

b) Actual roughness height is the overriding roughness parameter and the trend in post-critical C_d variation with relative macro-roughness is similar in both types of flow.

c) Unless the distribution of roughness is strongly biased (e.g. longitudinal strips along one side of cylinder span) its comparative effect on in-line and transverse wave force coefficients would be indistinguishable. This is contrary to steady flow behaviour where variations in C_d and steady lift strongly depend on the relative position of roughness patches with respect to the direction of flow. This is partly due to data scatter, partly due to the rotating velocity vector and the moving separation point and partly to the time averaging process within a wave cycle.

The question that remains is: "What are the appropriate Morison coefficients for design and how should they be selected?". This is addressed in the next chapter where a wave force estimation procedure is proposed based on the state of existing knowledge. Recommendations are also made for the structural re-assessment and maintenance of existing platforms.

CHAPTER 10. RECOMMENDATIONS FOR DESIGN AND MAINTENANCE

In the previous chapters, attention was focused on the quantitative appraisal of the hydrodynamic effects of marine growth through experiments in steady flow and in regular waves which provided an extensive source of data and key findings for the realistic characterisation of marine growth. The following sections deal with the selection of design force transfer coefficients using the current state of knowledge and best available experimental data. Detailed approaches are suggested for the estimation of hydrodynamic loads on marine roughened template platforms for design and maintenance purposes with due consideration of the associated limitations and uncertainties.

10.1. On the Selection of Design Force Coefficients

The hydrodynamic effect of marine growth is one of many factors which affect the choice of the most appropriate force coefficients for the evaluation of wave loads. It is therefore essential to mention those key factors which must be addressed by a rational design approach before moving on to detailed recommendations with respect to marine roughness.

a) Design levels and objectives

It has been firmly established that some unidirectional wave theories overpredict flow kinematics [54] and to compensate lower apparent force coefficients have been recommended by certifying authorities (see Chapter 4). When such wave theories are adopted distinctions are made between the force transfer coefficients used for global and local design. For instance, and without considering their magnitude at this stage, average force coefficients are adopted for global design. In all random sea-states, the spatial correlation of wave forces over the entire structure is less than for unidirectional seas containing the same energy. Since unidirectional wave theories do not account for this effect the application to global design of the same force coefficients as those adopted for local design, where the spatial correlation effect is much less obvious, would lead to overpredicted base shear and overturning moments.

The force coefficients used for the estimation of nominal loads and fatigue damage should again differ from those applied in extreme static wave force calculations. They must reflect the temporal variations in KC and roughness through a range of in-line and transverse force coefficients. On the other hand, static force analysis considers extreme conditions and thus, requires terminal values at high KC, Re and roughness.

b) Evaluation methods of flow kinematics

Methods of estimating combined wave and current flows influence the magnitude of design force coefficients. The effect of currents is to increase the mean flow velocities and consequently the net forces. However, the drag force coefficients will decrease, as currents increase the Keulegan-Carpenter number and quasi-steady flow conditions are approached. Hence steady flow drag coefficients are appropriate for high KC combined flows.

However, vectorial addition of maximum wave and current velocities would overpredict the forces even if steady flow coefficients were adopted. Methods of estimating the joint probability of occurence of waves and currents in storms [118] and random directional wave simulation models [120] improve the estimates of mean flow velocity and hence force, but are subject to availability of statistical ocean measurement records.

c) Compatibility between experimental data and ocean environment

It is highly desirable to model the ocean environment and structural responses as accurately as possible. Yet it must be realised that uncertainties increase as more parameters are introduced in an effort to refine semi-empirical design procedures. To reduce the uncertainties to acceptable levels reliable experimental data and good judgement are necessary. This becomes increasingly feasible as the amount and quality of laboratory and field experimental results is constantly updated and the differences between laboratory and real sea conditions are reduced. The designer has therefore more tangible sources of data at his disposal and what is required is to assess their compatibility with refinements in design procedures through the

following criteria:

- the force coefficients must be selected from results of large scale controlled laboratory experiments with macro-roughened cylinders at high Reynolds and Keulegan-Carpenter numbers;

- the flow kinematics design models must describe with sufficient accuracy real wave flows at the platform location and must correlate with the idealised flow parameters of the experiments;

- realistic characterisations of marine growth as defined at the design stage must be reflected in the adopted values for the force coefficients.

Depending on the wave theory adopted and on the predicted flow and roughness conditions the following sources of force coefficients are suggested:

- The present steady flow drag coefficients for macro-roughened cylinders be used for wave and combined flows at KC>40 regardless of wave theory adopted and consistent with the marine growth types and characteristics they refer to.

- The present data for a vertical macro-roughened cylinder in unidirectional waves be used for waves at 5<KC<30 and for vertical or inclined structural members or member segments fully covered by any form of hard fouling at comparable k/D.

- Bearing in mind that they represent upper limit values the drag and inertia coefficients of Sarpkaya [54,58] for rough cylinders in harmonic flow at $Re>3x10^5$ be tentatively used for high KC wave flows and for hard roughness conditions not covered by the present data.

- The C_d and C_m values by Rodenbusch et al. [59,68,119] for a rough cylinder undergoing random oscillations or combined random and current motions be used in conjunction with random directional wave theory for KC up to 40.

A notable omission from the above are the force coefficients derived from field tests. Obviously such sources of data ought to be the most tangible ones for design since they represent structural responses to real wave flows. However, several uncertainties accompany these data to date and limit their universal applicability. The uncertainties stem from:

- the paucity of reliable and repeatable data from many locations;
- biased wave loading prediction methods which do not account correctly for phase differences between flow kinematics and forces measured at different locations and thus result in large data scatter;
- the inherent nature of the experiments which implies lack of control of the pertinent parameters;
- the potential incompatibility between flow, roughness and structural characteristics related to the experiments and those pertaining to a specific design.

Until further verifications are made it is suggested that field data be used with care and with the above considerations in mind.

On the basis of the foregoing, a detailed procedure is suggested for the selection of design force transfer coefficients for marine roughened template structures. The data requirements are classified with respect to the input and output for global and local design models which are illustrated in Figures 10.1 and 10.2 respectively.

The recommended procedure is as follows:

(i) Using wave and current statistics for the location and suitable wave theories (Stokes 5th order and joint wave/current probability of occurence or random directional) determine the particle kinematics for a 50-year design wave, the current profile and random directional spectra.

(ii) Given the structural configuration and initial estimates of member dimensions and orientation, estimate the variance and maximum values of the local KC and Re for each member with respect to depth. Vertical or inclined members should be segmented and KC be estimated at the mid-point of each segment.

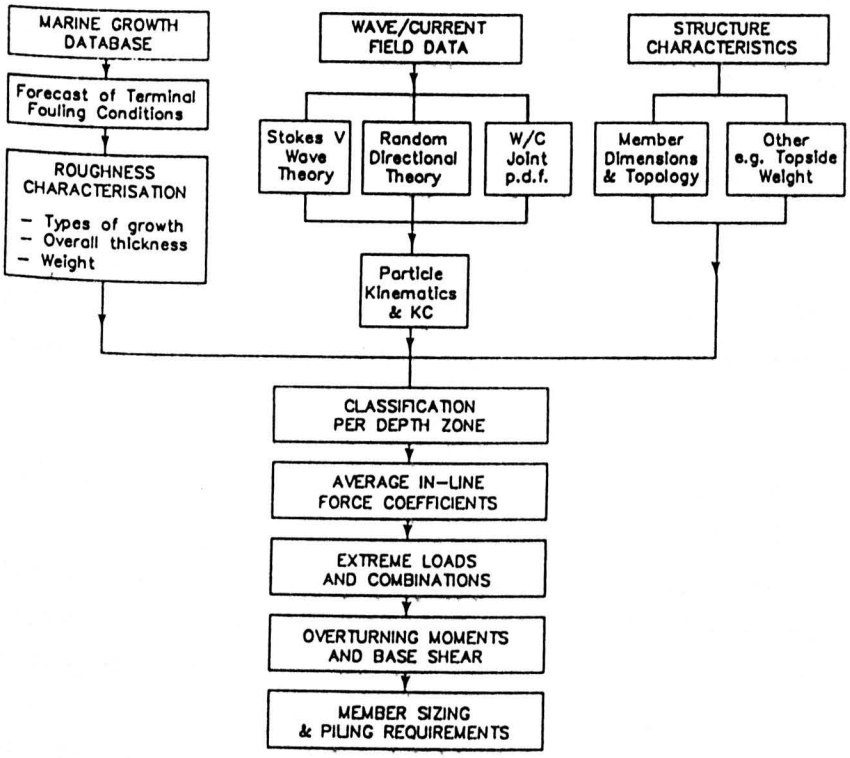

Fig. 10.1. Procedure for global design.

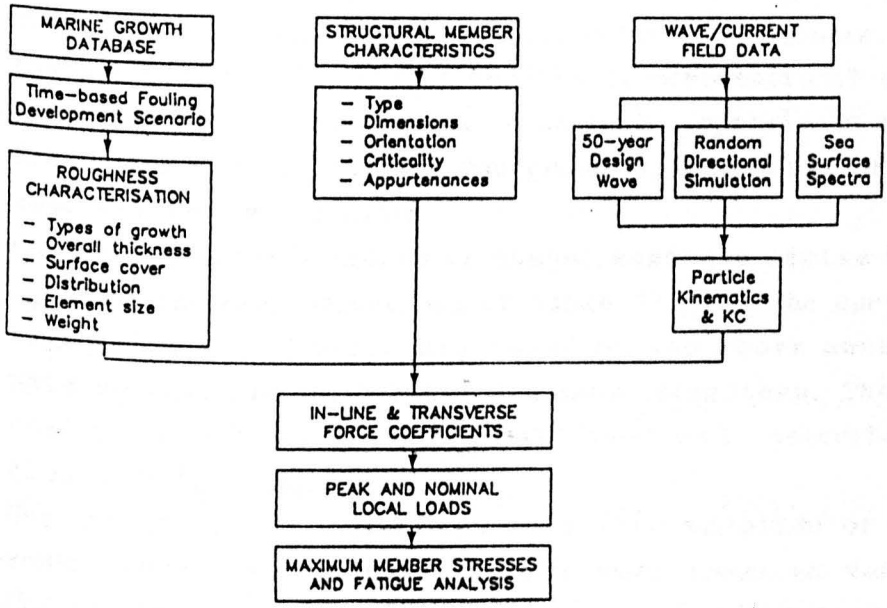

Fig. 10.2. Procedure for local design.

Reynolds number independence may be safely assumed for all members except for kelp covered ones, as kelp tends to be compressed on the member surface at high flow velocities.

(iii) Predict the future levels of marine growth using:

a) historical data from neighbouring platforms;
b) trends on ecology established from marine growth databases, and if available, from samples collected at the particular location.

Develop a time-based marine growth development scenario on an annual basis specifying in probabilistic terms the roughness characterisation parameters shown in Figure 10.2. Possible projected cleaning intervals during the platform life span must be included in the scenario.

(iv) For overall load estimates (global design):

a) Assume terminal roughness conditions ("climax" fouling) and classify the dominant types into hard, soft and seaweed growths.
b) Estimate approximately overall thickness for hard fouling or length (l) for kelp growth and average them over such depth ranges that no significant changes occur in roughness, KC or current velocity to warrant additional computational effort.
c) Using the clean member diameter estimate approximate k/D or l/D ratios for all members and group them in terms of depth zone and average diameter.
d) For each group of members or member segments derive C_d and C_m using the recommendations of Table 10.1 and the curves of Figures 10.3-10.4 which are based on the above mentioned data sources and on "clean" cylinder diameters. The drag coefficient curves H and K should adequately describe most global design conditions.
e) Use the following summation series representation of Morison's equation to estimate overall wave loads on vertical and inclined members:

$$F_T = \sum_{i=1}^{N} \int_{-d_w}^{0} (0.5\rho D C_d \{G_1\} u_i |u_i| + 0.25\rho\pi D^2 C_m \{G_1\} \dot{u}_i) dz \quad [10.1]$$

where, $G_1 = G\{KC, Re, N_i, k/D\}$,
d_w = water depth elevation,
N = total number of members or segments,
N_i = type of fouling on the ith member or segment,
k = mean overall thickness of fouling,
D = "clean" member diameter.

For horizontal members use a vector form of Morison's equation defining velocity and acceleration in terms of their horizontal and vertical instantaneous vectors.

f) Proceed as indicated by Figure 10.1 to estimate maximum overturning moments and base shear for strength analysis and member resizing.

(v) For peak member loads (local design) and fatigue analysis:

a) Consider in detail each member located in the wave affected zone. Follow the roughness characterisation procedure described in (iii) and define the structural characteristics given in Figure 10.2.
b) For each annual projection of the roughness characterisation defined through the fouling development scenario determine statistically the dominant types of fouling and their overall thickness/length, surface cover, distribution and orientation to flow.
c) Segment vertical or inclined members according to the above roughness parameters and derive local KC and Re as in (iv).
d) Assign local drag coefficients to each partially roughened member or segment using the curves of Figure 10.5 which are based on the steady flow results for partially fouled cylinders. For fully roughened members use the data of Table 10.1 or Figure 10.3.
e) Select inertia coefficients from Table 10.1 or Figure 10.4 assuming full roughness conditions.
f) For each annual projection, estimate the total peak in-line force by integrating the local Morison force components over

the member length.

g) For fatigue analysis use a spectral representation of Morison's equation to determine nominal forces and high and low cyclic stresses.

(v) Since Morison's equation underpredicts resultant forces by up to 40% for rough cylinders in vortex flows (see Chapter 9), it is tentatively suggested to estimate the local transverse forces on critical vertical members which are fully roughened by hard fouling. The C_{Lmax} and C_{Lrms} values of Figures 9.14 and 9.15 for the pyramid roughened cylinder in regular waves may be used for peak and nominal load estimates respectively and for representative roughness and flow conditions.

It must be remembered that the above recommendations use the best currently available experimental force coefficients and wave theories and are subject to future revisions. Several uncertainties still exist and not least on the definition of rough member diameter and on the hydrodynamic behaviour of soft fouling and kelp. These and other related issues are discussed in Chapter 11.

10.2. On Structural Assessment and Maintenance

In principle, the suggested procedure can be readily expanded to interact with structural monitoring and maintenance requirements at the detail and work drawings design stage. The basic approach which was outlined in Chapter 5, was adopted in a case study on the sensitivity of structural member characteristics to marine growth variations [121]. Techno-economic criteria and data on fabrication and cleaning-for-structural relief procedures were included in a computer model. Details of the model and results for alternatine designs and fouling scenarios are given in Appendix H.

The study confirmed the earlier findings of Oldfield [9] and Barger et al. [100] that structural weight and material costs increase significantly due to marine growth. However, it indicated that a "clean at regular intervals" design, i.e. a light structure, is not cost-effective in the long run. This conclusion must though be seen in the light of numerous uncertainties involved in data dependent techno-economic models and of strategic objectives and policies of

the operator. Therefore, general conclusions cannot be reached with confidence and design options for a particular platform should be assessed in terms of overall requirements and not just in terms of structural loading effects attributed to marine growth.

For existing platforms the direct application of the research findings is obvious. The experimental results and roughness characterisation procedure relate to most configurations of marine growth encountered offshore and provide ample scope for improved re-assessment of hydrodynamic loads and fatigue damage of joints. However, there are still roughness configurations to which design force coefficients cannot be assigned without some degree of uncertainty as will be shown below.

Consider some typical tubular members of the North Sea platforms reviewed in Chapter 6 and Appendix B, and for which it is required to assign force coefficients for the estimation of peak local loads. The patterns of marine growth on each member are illustrated in Figures 6.1-6.7 (Chapter 6) and their pertinent characteristics and suggested C_d values are summarised in Table 10.2. In all cases KC is in excess of 50 for the following maximum wave and current conditions associated with each platform:

	Platform SNS	**Platforms NCNS and NNS**
Wave height (m) :	16	27.5
Wave period (sec):	12.8	16.8
Current (m/s) :		
surface (MWL):	0.76	0.21
-3m :	0.39	-5m : 0.08
-8m :	0.31	-30m : 0.04

For each member the following are noted:

Member A:

Mussels and sea anemones colonise this leg section at two distinct elevations. In accordance with the previously suggested procedure the member is treated in two segments. The upper segment (-1.5m to -9m depth) is fully covered by mussels of 60mm mean overall thickness; the lower one (-9m to -12m) is 70%

covered in randomly distributed sea anemones ranging in height from 10mm to 80mm. The drag coefficients are obtained using curve H of Figure 10.3 for the mussel covered segment and the "sea anemones" curve of Figure 10.5 for the lower segment at the respective k/D and % surface cover. Whilst the C_d estimate for the upper segment is regarded as accurate, the drag coefficent for the sea anemones is based on experimental data at the higher crude estimate of 0.15 and may be conservative.

Member B:

Marine growth on this horizontal bracing consists of a 30mm thick strip of mussels extending along the top and outer faces, with 200-500mm long kelp and other weeds interspersed among the mussels, whilst sea anemones colonise the bottom half of the member. It is obviously an awsome task to estimate k/D and assign C_d values to this member and the uncertainty in the figures quoted in Table 10.2 is high. For assessment purposes some gross simplifications and assumptions ought to be introduced. If kelp is neglected, and if it assumed that mussel roughness is the dominant species and that sea anemones behave hydrodynamically as hard roughness, then K/D=0.03 and C_d=1.15 may represent base values. However, kelp cannot be ignored altogether and a conservative estimate of 1.28 is in order which is derived from the "kelp" curve of Figure 10.5 at 25% cover.

As marine roughness is profoundly non-uniform, mainly due to kelp plants being present only along the top and outer member faces, biased transverse forces should be expected. It is not possible though to predict their magnitude through the available data and, if required, a conservative estimate of C_{Lmax} must be adopted.

Member C:

This horizontal bracing is fully covered by sea anemones and presents a straightforward application of the "soft fouling" curve of Figure 10.5, even though experimental drag coefficients are only available for 70% surface cover by sea anemones/tunicates. At k/D=0.13 approximately, the member roughness is comparable to the "local" k/D of 0.15 for the cylinder tested in steady flow with the bulk of soft fouling at right angles to

the direction of motion (see Ch. 8, Section 8.3) which is considered as a good approximation of full roughness.

Members D and E:

Hydroids and oher soft weeds apart, the marine roughness on both horizontal members correlates with the fouling cofigurations tested in steady flow at reduced surface covers, albeit at higher "local" k/D. The hydrodynamic effect of hydroids is not known but it is believed to be small. One option is to ignore the hydroids and to treat the members as partially roughened by mussels only. From the "mussels" curve of Figure 10.5 it follows that:

- for member D, which is covered by 80% mussels, C_d=1.14;
- for member E, where the top and outer faces are covered by 70% mussels, the mussel cover over the entire surface averages to 35% approximately, i.e. C_d=1.1;

As the "mussels" curve refers to higher "local" k/D ratios, the above drag coefficients are overestimated. However, they may be interpolated to their "local" k/D of 0.03 and 0.02 using curve H of Figure 10.3. For fully roughened cylinders curve H suggests reductions of 8% and 12% at k/D of 0.03 and 0.02 respectively compared to the mean Cd at 0.06<k/D<0.085. That is, for members D and E C_d is 1.05 and 0.98 respectively. A more conservative option would be to adopt the overestimated coefficients in view of the uncertainty regarding the drag effect of hydroids.

With respect to transverse forces, the arguments given for member B also apply to members D and E as a result of the roughness being concentrated along the top and outer faces of the latter.

Regarding the selection of suitable C_m values for the above members, any uncertainties which arise from the roughness conditions or lack of relevant data would not affect the hydrodynamic loading estimates due to the small inertia force contribution at high KC. The values of Table 10.1 are therefore recommended.

Inspection and maintenance requirements specific to marine growth depend on initial design assumptions and loads pertinent to the particular platform and thus the general recommendations are confined to the following:

- Marine growth should be characterised from good quality general visual inspection records and in terms of the significant roughness parameters identified by the present study.

- Diver surveys should be limited to a minimum and only for cases where detailed information is sought on aspects other than hydrodynamic loading (e.g. corrosion enhancement).

- Cleaning-for-structural relief should be scheduled according to updated marine growth and structural loading scenarios through survey data.

- Preventive anti-fouling measures be taken after experimental verification of their hydrodynamic behaviour and cost-benefit trade-offs.

Notes for Table 10.1 and Figure 10.3:

1. The coefficients for soft fouling are best estimates based upon the steady flow results for sea anemones and tunicates at reduced surface covers.

2. The steady flow drag coefficients for kelp refer to $Re > 7 \times 10^5$; the C_m values for kelp are based on the CBT field tests on horizontal and vertical cylinders [63].

Wave Theory	Marine Growth					
	Hard		Kelp		Soft	
	C_d	C_m	C_d	C_m	C_d	C_m
Stokes V, - 5<KC<30	Curve UD	1.3	1.2-1.7	1.7-2.4	1.3-1.5	1.7
R.D.W., - 5<KC<40	Curve RD	Curve RM	1.2-1.7	1.7-2.4	1.3-1.5	1.7
Either, - KC>40	Curve H	1.3	Curve K	1.7	1.3	1.7

Table 10.1. Recommended design force coefficients for marine roughened structures (refering to Figures 10.3 and 10.4).

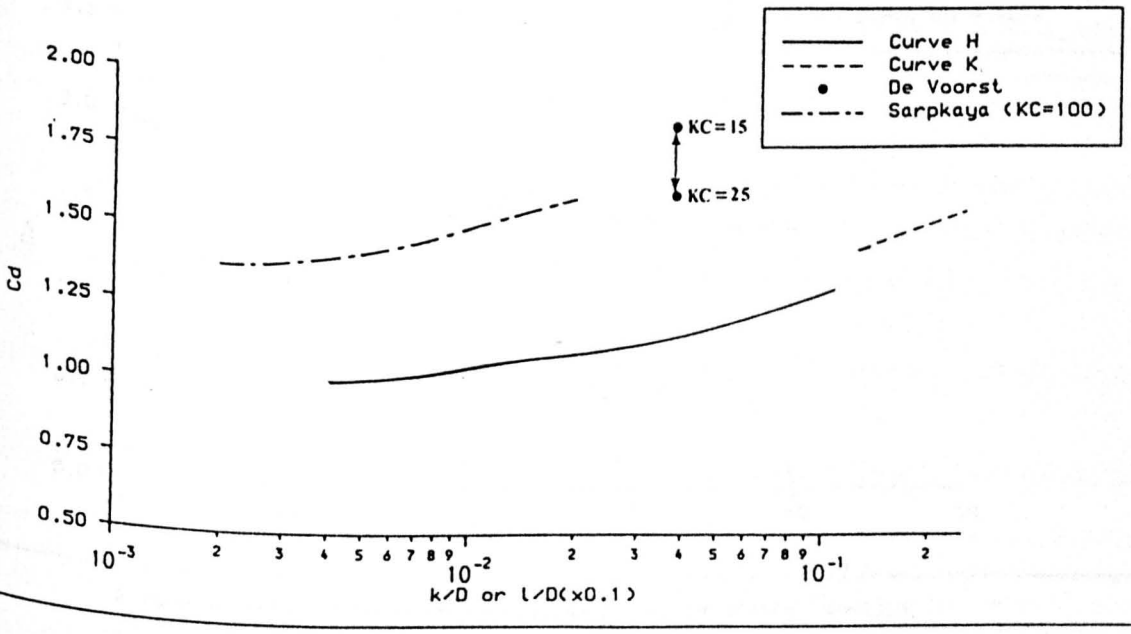

Figure 10.3. Curves for design drag force coefficients of marine roughened offshore structures.

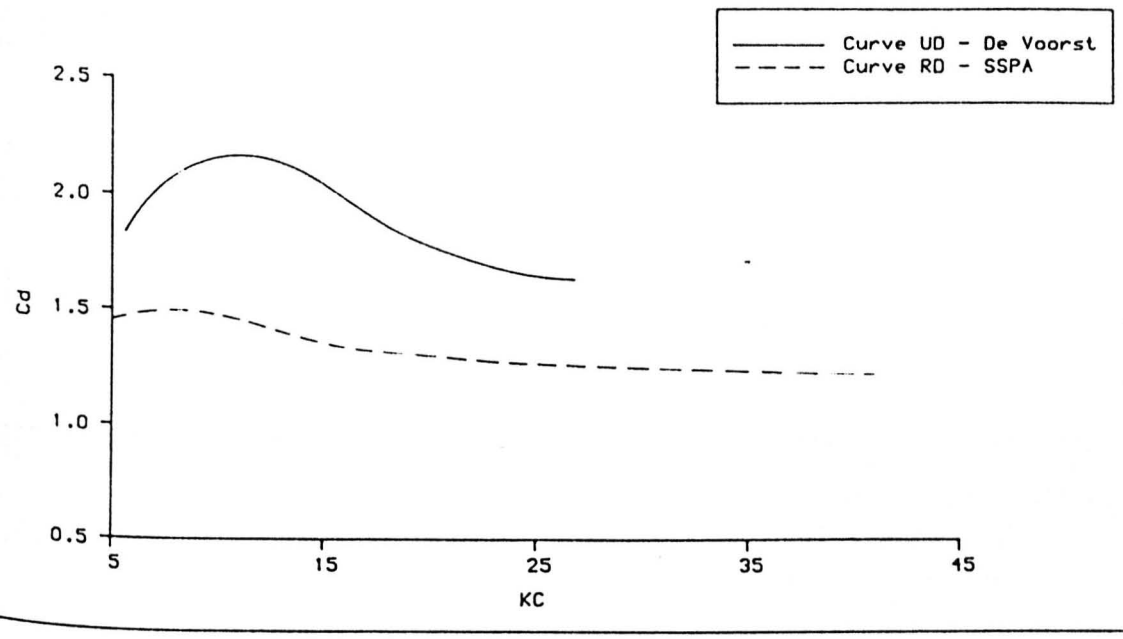

Figure 10.4(a). Design Cd curves for fully roughened tubulars by hard fouling in wave flows up to KC of 40.

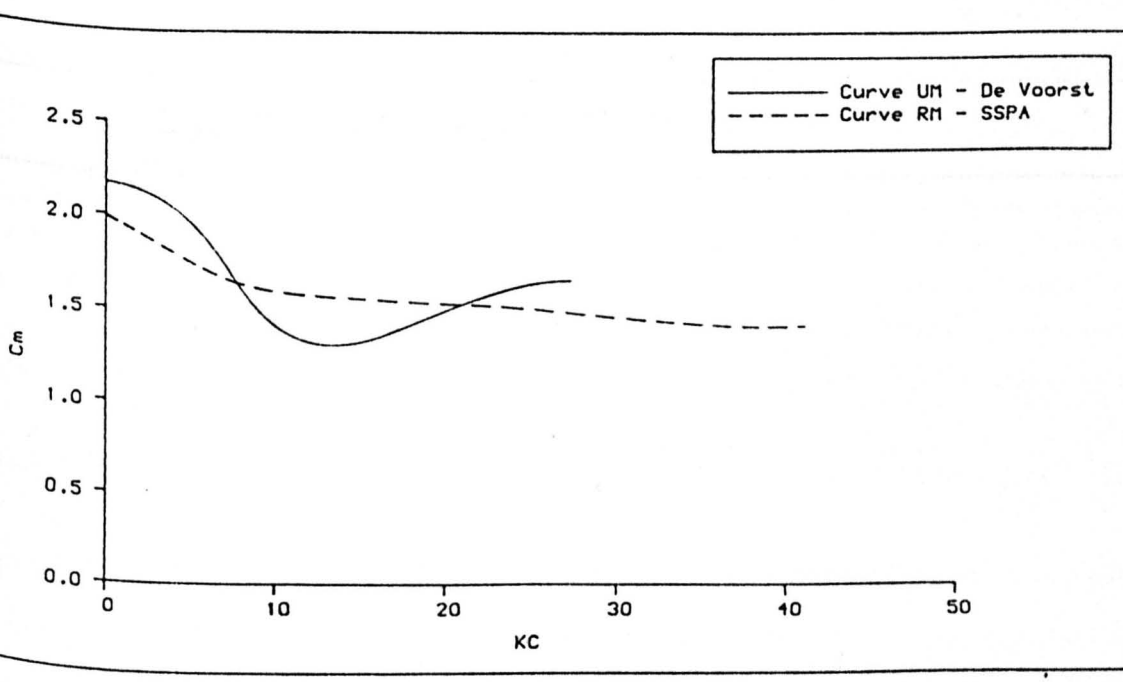

Figure 10.4(b). Design Cm curves for fully roughened tubulars in wave flows up to KC of 40.

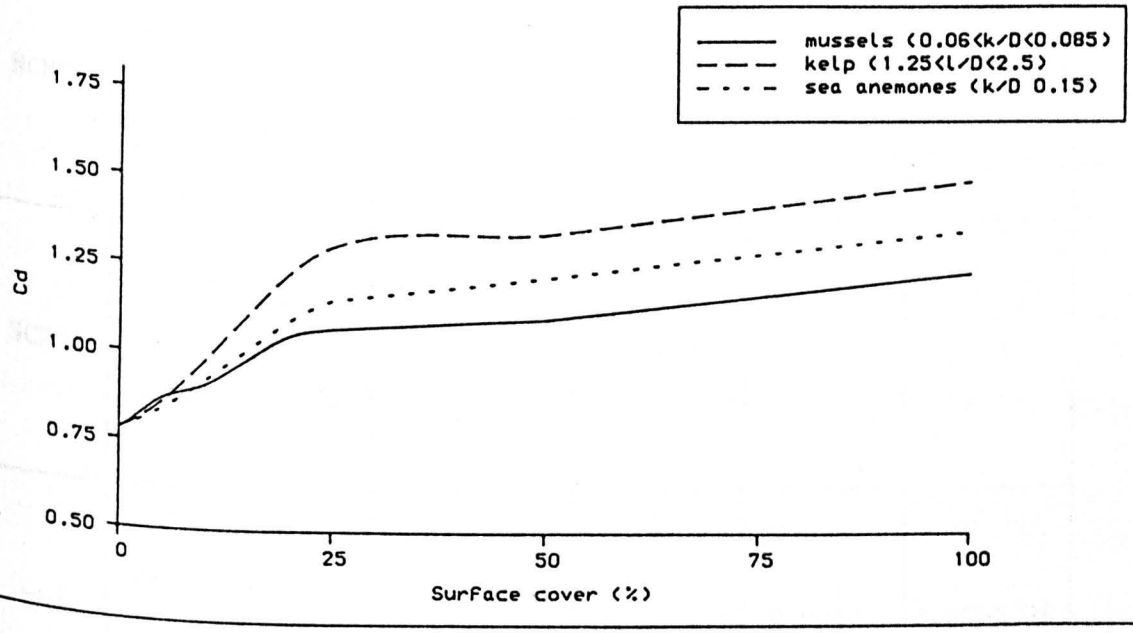

Figure 10.5. Design drag coefficients for partially marine roughened structural members.

Platform	Member	Depth El^{n} (m)	Marine Growth	Approx. k/D	C_d
SNS1	**A** Figs. 6.1-6.2 - North face, - Leg section, - 840mm dia.	-1.5 to -9 -9 to -12	Table B.1 Table B.1	0.07 0.06	1.27 1.20
NCNS1	**B** Figure 6.4, - South face, - Horizontal, - 914mm dia.	-5	Table B.2	0.03(?)	1.15-1.28
NCNS2	**C** Figure 6.5, - West face, - Horizontal, - 762mm dia.	-25	Table B.3	0.13	1.35
NN1	**D** Figure 6.6, - North face, - Horizontal, - 1000mm dia.	-12	Table B.5	0.03(?)	1.05-1.14
NN2	**E** Figure 6.7, - South face, - Horizontal, - 1400mm dia.	-16	Table B.6	0.02(?)	0.98-1.11

Table 10.2 Example applications to marine roughened tubular members.

CHAPTER 11. DISCUSSION

It would be rather ambitious, and that is an understatement, to claim that this research study has provided the offshore engineer with all the answers to the basic problem of hydrodynamic loading on marine roughened template structures. The sheer variability and randomness of the natural phenomena involved will continue to introduce uncertainties in design procedures for some time to come and will present challenging research opportunities. Such areas of research, specific to marine roughness, will be outlined later in this discussion. It would be worthwhile at this stage to review what has been achieved by the present study before moving on to identify what more is required.

11.1. Review of Research Findings

As stated in earlier chapters, the adopted approach was design and maintenance orientated and, as such, it addressed the immediate needs and limitations of current practices. Consideration of the underlying mechanisms of vortex flow about rough circular cylinders extended only as far as validating the experimental procedures and results.

The systematic experiments with macro-roughened cylinders were the focal point of the study. Detailed results and applications to structural design have already been discussed in the previous chapters and only the main points will be drawn here.

As a general comment it may be said that the Reynolds number is of secondary importance to design procedures for estimates of wave loading on marine roughened primary structural members. In all the experiments with macro-roughened cylinders the force coefficients were found to be independent of Reynolds number and variations were only observed with respect to wave amplitude to diameter ratios (i.e. KC numbers).

In terms of hydrodynamic drag, the good correlation found between artificial roughness and hard marine growth removes any ambiguities regarding the modelling of hard fouling by artificial means of similar size and distribution. Sand or gravel is such a suitable form of roughness as it inherently possesses some variability in shape and element size and may model mussel or barnacle growth reasonably well;

albeit over a limited k/D range for large scale tests as the ones carried out within the present study. The range of relative roughness achieved with sand roughened cylinders at high Re (up to 10^6) extended up to 0.025. As such it did not cover the full range of "in-service" hard marine growth.

To achieve higher k/D ratios and at the same time to maintain high Re and KC numbers roughness in the form of pyramids was used. The steady flow results with regular arrays of uniformly sized pyramids established the effect of roughness height and correlated well with the C_d data for mussel roughness. On the basis of these findings an even more realistic pyramid roughness pattern was developed by modelling all the significant characteristics of hard fouling; that is, element size and shape similar to that for mussels and barnacles, non-uniform thickness, and random element distribution. This pattern was used for the De Voorst large scale tests in regular and random uni-directional waves (the results from the latter are the subject of further study) and has also been installed on members of the Christchurch Bay Tower. It has therefore provided a standardised and reproducible means of modelling hard fouling which will allow in due course for unique comparisons to be carried out between data from idealised flows and the real sea environment under the same roughness conditions.

However, the working range of KC numbers for the wave loading experiments extended only up to 29 approximately. The CBT experiments are also limited to KC maxima of around 40. Moreover both investigations are concerned with hard roughness at full surface cover. Data from these studies are useful for applications which fall within the above range of KC and for comparable fouling conditions.

As extreme flow conditions for template structures refer to higher KC numbers and since for a realistic approach to marine fouling one must consider a range of fouling types and configurations, the steady flow drag coefficients presented herein are well conditioned for ultimate loading estimates. The overall agreement between the drag coefficients obtained by the "buoyant cylinder" technique, i.e. in steady flow, and those derived from field experiments or from laboratory simulations of random two-dimensional flows (SSPA tests, Chapter 10, Fig. 10.4) points once again to the conclusion that steady flow drag coefficients are applicable to calculations of extreme design loadings. Undoubtedly there would be no shortage of hydrodynamicists who

would attribute the apparent agreement to the many mitigating factors of the real sea environment. It is known that wave particle orbital motions, yawed flows, currents, reduced spanwise vortex coherence, wave irregularity and multi-directionality contribute to reductions in drag coefficients obtained in random sea-states and to the good correlation with steady flow C_d. Such good correlation is not obvious with drag coefficients obtained in uni-directional periodic wave or oscillatory flows. Whilst the designer should be aware of the above factors and whilst it would be valuable to quantify and understand their effects, it must be realised that such factors cannot as yet be incorporated into a rational design loading estimation procedure. Design must currently remain insensitive to such parameters. Design efficiency, which arises from the necessary simplifications in modelling the environment should not be forsaken by introducing parameters which would simply justify the use of a chosen set of force coefficients derived through steady flow or ocean experiments. Such justification ought to be confined at present to the research level to enhance the limited knowledge available on the effects of the above wave flow phenomena and to explain the variability in data obtained from field tests.

The above argument also applies to the effects of marine growth and their consideration at the design stage. Marine growth was characterised for the purposes of this study through six parameters. For structural assessment of existing platforms it is possible to estimate all of them through inspection records and assign suitable force coefficients. Not so though for the design of new structures. As before, the designer must be aware of the relative effects of all six roughness parameters but, in selecting appropriate force coefficients, he must consider only those ones which can be predicted with reasonable confidence and whose effect can be assessed from available experimental data. For the rest he is forced to make conservative assumptions.

For extreme overall design wave loadings and according to the present results marine growth should be characterised through the type of fouling and the mean overall thickness in the manner suggested in Chapter 10. For peak local loadings or for fatigue analysis of critical members gross estimates of surface cover and distribution of fouling must also be considered. The latter recommendation is tentative as it is based only on the steady flow results. Further verifi-

cation on the effects of each individual parameter is required in time-dependent flows. Until such time and for the sake of design simplification, the distribution of fouling may be incorporated in the surface cover parameter which should be estimated in terms of area of member face and not in terms of the full member area. For similar reasons, non-uniformity in overall thickness of hard growth or mixed fouling should be characterised through the mean overall thickness and dominant fouling types respectively. However, the potential effects on biased transverse forces due to fouling distribution and non-uniform thickness must be recognised at least with respect to induced drag.

In the light of the foregoing, the steady flow results for hard roughness validate in overall terms the force coefficients currently adopted by the industry for purposes of estimating peak member loads, but only with respect to uniform hard fouling. For kelp fouling, the drag and added mass coefficients more than double compared to those for clean members and are about 30-40% higher than the force coefficients for mussel roughness. However, no firm conclusions can be drawn from the "buoyant cylinder" results on the magnitude of inertia coefficients for marine roughness, particularly for kelp. Also, considerable uncertainty is associated with the fluid loading effects of sea anemones and other types of soft growth. It is tentatively, and perhaps conservatively, suggested that the drag effect of sea anemones is similar to that of hard marine growth.

Apart from the undisputed fact that marine growth must be characterised by a combination of roughness parameters, the experimental results offer ample scope for a clearer interpretation of relative roughness for design and experimental purposes. Relative roughness, in the present context, was defined by the mean overall thickness (or length for kelp) and the "clean" cylinder diameter. This is the least uncertain definition for k/D. When coupled by the fact that the experiments were carried out at large scale with real fouling and which covered the most common fouling conditions encountered offshore - at least for hard fouling - the applicability of the results to design and structural assessment is direct. For most practical applications there is no justification to adopt any other definition based on some uncertain and physically insignificant form of "equivalent" roughness thickness. Certainly the traditional practice of normalising marine roughness through some mean C_d versus k/D curve must be

critically revised.

The associated uncertainties regarding the definition of diameter have been repeatedly mentioned in earlier chapters. The increase in force coefficients brought about by the increase in member diameter is profound as demonstrated by the results for the multiple layers of mussels. The same results showed that the "effective" diameter required to bring the drag coefficient in-line with that for single uniform roughness may be larger than the actual diameter of the fouled member. Such exercise may be very misleading in the choice of appropriate force coefficients. The safest alternative is to adopt the "clean" member diameter for loading estimates. It is realised that by using a "clean" diameter the calculated Re and KC numbers and the relative contribution to total loading by the drag and inertia components would differ by a small percentage from the case where a "rough" diameter was adopted. In practice such differences are insignificant because at high KC and Re flows C_d is independent of both parameters and C_m is of limited importance and, in any case, the objective is to estimate the total force acting on members. Therefore, the uncertainties in characterising relative roughness would reduce if the increase in member diameter were included in the force coefficients. This is particularly important for kelp and soft growths and also for partial or mixed fouling.

A comment is in order regarding the application of the research findings to inspection and maintenance. The study showed that the necessary data for characterising fouling may be readily retrieved from high quality general visual inspection records carried out by ROV's and analysed onshore by trained engineers or marine biologists. The interpretation of the data should be carried out according to the procedure described in Chapter 6.

With respect to removal of fouling, the experimental results offer scope for improved forecasting capability in the scheduling of cleaning-for-structural relief intervals for existing platforms. They also provide a measure for assessing the potential benefits of retrofit anti-fouling cladding in terms of reductions in fluid loading and structural weight.

Finally, this research study has formed an intermediate step towards developing an integrated "Design-Construction-Maintenance" enginee-

ring model by formulating the relationship and interactions of the "marine growth" factor to this model. Fluid loading due to marine growth is, however, not the end result and other techno-economic factors must be quantified and integrated within such a concept which addresses strategic engineering objectives.

11.2. Recommendations for Future Research

It is evident from the previous discussion that there is a wealth of areas where further research is needed with respect to marine roughness and hydrodynamic loading. Such areas must be identified not just within the framework of industry needs but also with the aim for improved understanding of the governing flow and roughness phenomena. Inevitably the nature of these phenomena and the limited state of knowledge do not allow for the development of reliable mathematical models without extensive support from experimental data. Hence, the emphasis is still placed on experimental research which, within the context of fluid loading on marine roughened template structures, must be formulated through the following:

- outstanding requirements for marine growth related force coefficients;
- simulation of real sea flow regimes and of in-service marine roughness;
- control of the structural, flow and roughness characteristics to achieve reproducible data at full scale.

According to the above formulation the following are recommended:

a) Enhancement of marine growth database

Despite the extensive laboratory tests with macro-roughened cylinders several issues require verification. The present experiments fell short in fully establishing the effect of kelp and soft fouling. The complex logistics involved in large scale experiments with such forms of growth must be recognised. Therefore a limited range of supplementary tests is proposed with real kelp plants or sea anemones being artificially attached on the cylinder surface. Limited tests are also required with cylinders fully covered in naturally grown multiple layers of mussels and mixed fouling. Such experiments must

be carried out in steady, uniformly accelarating, periodic, and random planar flows at high Re and over the widest possible range of KC numbers. Thus, the present C_d database would be enhanced and extended to include inertia and lift force coefficients. Experiments with other forms of growth (e.g. soft corals and hydroids) would be desirable but are again subject to logistics problems such as the aquisition of fouling and its survival during high velocity tests in fresh water.

However, experiments with marine fouled cylinders cannot guarantee repeatability in roughness conditions nor can they be extended over long testing sessions due to fouling deterioration. Systematic investigations in idealised time-dependent flows must therefore be carried out with artificial macro-roughness. The pyramid roughness pattern developed through the present study should form the basis for such experiments to assess the distribution, orientation and surface cover roughness parameters in quasi-steady and oscillatory flows. Similarly, every attempt should be made to replicate kelp plants with due consideration to their hydroelastic behaviour and dimensional variability. This would allow for maximum flexibilty in designing systematic experiments in all types of flows including regular and random wave flows in facilities such as the large Delta flume at the laboratory De Voorst.

b) Investigation of vortex-induced transverse forces

In design practices formulated around the Morison equation transverse forces are not considered. Yet there is strong experimental evidence that peak lift forces are similar in magnitude to in-line forces, at least for low aspect ratio tubulars. Arguably this effect may be only pronounced in uni-directional periodic flows where vortex lock-in occurs and the shed vortex street is washed back onto the cylinder by the reversed wake. In real seas the vortices disperse in various directions subject to incident wave iregularities and are not coherent over the entire structure or along the span of individual members. However, this has not been substantiated due to the limited knowledge and the paucity of data for macro-roughened cylinders and further research should be of great importance.

Experiments should be carried out at the previously mentioned flows to quantify the roughness distribution and orientation effects to

biased transverse forces. Also, the spanwise vortex coherence must be investigated through oscillatory flow tests with long slender smooth and rough cylinders where their aspect ratio would be systematically varied. The objective should not only be to provide data for extreme loading estimates, but rather to improve on the understanding of such effects in the context of marine roughness and to establish whether transverse loadings ought to be considered for nominal local stresses for fatigue damage purposes, particularly at the drag/inertia dominated regime ($5<KC<25$).

c) Effect of member orientation to flow

It has already been mentioned that yawed flows and water particle orbital paths tend to reduce C_d. To what degree this reduction occurs for marine fouled members is open to speculation. Furthermore there are significant differences in marine growth configurations between vertical, horizontal and inclined members. Large scale experimental work is required in wave flows with horizontal rough cylinders; and also in idealised planar flows with inclined cylinders where the surface cover, distribution and orientation would be systematically varied.

d) Fluid loading on nodes and secondary structure members

Limited data exist for hydrodynamic loads of marine roughened nodes, compliant structures, conductor guide frames and appurtenaces such as fouled anodes. Such experiments call for complex experimental set-ups and data analysis methods and, therefore, are noted here as desirable areas for long term large scale investigations.

The above constitute a considerable amount of research effort which is directly relevant to marine growth and fluid loading. Other research related to the analysis methods of laboratory and field data, the prediction of real sea kinematics, and the overall integration and rationalisation of design and maintenance practices is also required. In the words of Professor Sarpkaya, "...man does not live by experiments alone (i.e. mathematical models are urgently needed) and man cannot resign in face of uncertainties and lump everything into two apparent coefficients".

CHAPTER 12. CONCLUSIONS

The general conclusions drawn from the research study are:

a) Marine growth significantly increases hydrodynamic loading. This increase varies with the type of marine growth. The most severe increase in drag forces is caused by kelp growth which may amount to more than 100% compared to that for a clean member.

b) For any given type of marine growth the increase in drag force depends on the overall thickness and element size of fouling, percentage surface cover, distribution, non-uniform thickness and orientation to direction of flow. The extent of this dependence varies with the type of fouling and is not pronounced for kelp.

c) Marine growth cannot be adequately characterised by a single parameter such as relative roughness (k/D). The following parameters are appropriate when selecting force coefficients for global design: (i) type of dominant fouling; (ii) mean overall thickness.

   For local collapse and fatigue design, forecasts are required of the rates of change of the following parameters during the life of the structure: (i) mean overall thickness of dominant types of fouling; (ii) surface cover per member face; (iii) distribution.

   For the assessment of existing structures, the parameters cited in (b) must be quantified through a multi-disciplinary procedure such as that recommended by the present study.

d) Drag coefficients derived through large scale experiments in steady flow are applicable to design and structural assessment practices for extreme hydrodynamic force estimates on marine roughened tubulars in drag dominated wave or combined wave and current flow regimes. The drag coefficients for uniform hard growth or artificial roughness validate the local design drag coefficients currently adopted by the industry. However, for kelp and soft growths and non-uniform hard growth the latter design coefficients would appear to lead to underprediction of wave forces.

e) At the drag/inertia flow regime, transverse forces on low aspect ratio macro-roughened tubulars are of the same order of magnitude

as in-line forces and are a multiple of flow oscillation frequency. They result in significant increases in total wave loads which are underpredicted through the Morison equation approach.

f) A set of experimental data has been produced which will allow improved estimates to be made of the effect of hard marine growth (and to a lesser extent soft marine growth) upon the hydrodynamic loading of template structures. This data set needs to be expanded to cover the effects of soft fouling and long flapping seaweeds more extensively.

CHAPTER 13. REFERENCES AND BIBLIOGRAPHY

1. **Wolfram,J. and Theophanatos,A.**, "The effects of marine fouling on the fluid loading of cylinders: Some experimental results", Proc. of the 17th Offshore Technology Conference, OTC 4954, Vol. 2, 1985, pp. 517-526.

2. **Wolfram,J.**, "Results from laboratory experiments on the loading of fouled cylinders", Marine Fouling and Structural Loading, S.U.T., October 1985.

3. **Theophanatos,A. and Wolfram,J.**, "Fluid loading on marine fouled and artificially roughened cylinders of various aspect ratios", Proc. of the 6th Int. Symp. on Offshore Mechanics and Arctic Engineering, Vol. 2, 1987.

4. **Theophanatos,A.**, "Fluid loading of marine fouled cylinders in unidirectional flow at high Reynolds numbers", in "Recent developments in offshore hydrodynamics", ed. by P.K. Stansby and M. Isaacson, University of Manchester, August 1986.

5. **Wolfram,J. and Theophanatos,A.**, "Experimental determination of drag and inertia force coefficients for cylinders with marine fouling attached", Research Project Report for SHELL EXPRO (U.K.), Project MASS, University of Strathclyde, 1984.

6. **Theophanatos,A.**, "Fluid loading on circular cylinders with marine growth and artificial roughness in unidirectional flow", Interim Report, Project FLE/6, Marine Technology Centre, Univ. of Strathclyde, March 1986.

7. **Theophanatos,A.**, "Review of marine growth surveys on North Sea platforms and Strathclyde test cylinders", Interim Report, Project FLE/6, Marine Technology Centre, Univ. of Strathclyde, June 1986.

8. **Offshore Marine Studies Unit**, "A guide to marine fouling in the North Sea", Department of Zoology, Aberdeen University, 1980.

9. **Oldfield,D.G.**, "Appraisal of marine fouling on offshore structures", Report OT-R-8003, Dept. of Energy, CIRIA, 1981.

10. **Goodman,K.S. and Ralph,R.**, "Animal fouling on the Forties platforms", Marine Fouling of Offshore Structures, Vol. I, S.U.T., 1981.

11. **Forteath,G.N.R., Picken,G.B., Ralph,R., and Williams,J.**, "Marine growth studies on the North Sea oil platform Montrose Alpha", Marine Ecology Progress Series, Vol.8, 1982, pp. 61-68.

12. **Redfield,A.C., and Deevy,E.S.**, "Quantitative aspects of fouling", Marine Fouling and its Prevention, U.S. Naval Institute, 1952.

13. **Bascom,W., Mearns,A.J., and Moore,M.D.**, "A biological survey of oil platforms in the Santa Barbara Channel", Proc. of the 8th Offshore Technology Conf., OTC 2523, Vol. 2, 1976, pp. 27-36.

14. **Personal communication**, Various oil and gas platform operators, Aberdeen, 1985/6.

15. **Wilkinson,T.G.**, "The influence of the offshore operation on marine fouling of North Sea offshore installations", Marine Fouling of Offshore Structures, Vol. 1, S.U.T., 1981.

16. **Wright,R.A.D. and Bryce,A.A.**, "Assessment of marine growth on offshore structures", Offshore Europe '83, SPE 11904, Society of Petroleum Engineers, 1983, pp. 379-390.

17. **Hama,F.R.**, "Boundary layer characteristics for smooth and rough surfaces", Trans. of SNAME, Vol. 62, 1954, pp.333-368.

18. **Granville,P.S.**, "The frictional resistance and turbulent boundary layer of rough surfaces", Journal of Ship Research, December 1958, pp. 52-74.

19. **Kan,S. et al.**, "Effect of fouling of a ship's hull and propeller upon propulsive performance", Int. Shipbuilding Progress, Vol. 5, No. 41, 1958, pp. 15-34.

20. **Lewthwaite,J.C., Molland,A.F., and Thomas,K.W.**, "An investigation into the variation of ship skin frictional resistance with fouling", Trans. of RINA, 1984, pp. 269-284.

21. **Watson,G.**, "Overview of marine fouling and structural loading", Marine Fouling and Structural Loading, SUT, 1985.

22. **Bolland,J.**, "Resource requirements of inspection", Short Course in Managing Underwater Inspection, Unit 3.4, Project MASS, Univ. of Strathclyde, 1984.

23. **Kingsbury,W.S.M.**, "Marine fouling of North Sea installations", Marine Fouling of Offshore Structures, SUT, 1981.

24. **"Corrosion and marine growth of offshore structures"**, ed. by Lewis,J.R. and Mercer,A.D., Society of Chemical Industry, Ellis Horwood Ltd, 1984.

25. **Kirkwood,D.**, "Marine fouling and corrosion of offshore installations", Marine Fouling of Offshore Structures, SUT, 1981.

26. **Morison,J.R., O'Brien,M.P., Johnson,J.W., and Schaaf,S.A.**, "The force exerted by surface waves on piles", Journal of Petroleum Technology, AIME, Vol. 189, 1950.

27. **Hallam,M.G., Heaf,N.J. and Wooton,L.R.**, "Dynamics of marine structures", Atkins R & D, CIRIA, Report UR8, 1978.

28. **Hogben,N.**, "Fluid loading on offshore structures, A state of the art appraisal: Wave loads", Maritime Technology Monograph No.1, RINA, 1974.

29. **Hoerner,S.F.**, "Fluid dynamic drag", published by the author, 1958.

30. **Keulegan,G.H. and Carpenter,L.H.**, "Forces on cylinders and plates in an oscillating fluid", Journal of Research of National Bureau of Standards, Vol. 60(5), 1958, pp. 423-440.

31. **Lloyd's Register of Shipping**, "Monitoring and assessment of data from offshore platforms", Summary Report OT-0-8356, 1984.

32. **Nath,J.H.**,"Hydrodynamic coefficients for macro-roughnesses", Proc. of the 13th Offshore Technology Conference, OTC 3989, Vol. 1, 1981, pp. 387-407.

33. **Heideman,J.C., Olsen,O.A., and Johansson,P.I.**, "Local wave force coefficients", Civil Engineering in the Oceans IV, American Society of Civil Engineers, Vol. 110, Nov. 1984.

34. **Miller,B.L.**, "The hydrodynamic drag of roughened circular cylinders", The Naval Architect, RINA, Sept. 1976.

35. **Sarpkaya,T.**, "In-line and transverse forces on cylinders in oscillatory flow at high Reynolds numbers", Proc. of the 8th Offshore Technology Conf., OTC 2533, 1976.

36. **Garrison,C.J.**, "A review of drag and inertia forces on circular cylinders", Proc. of the 12th Offshore Technology Conference, OTC 3760, 1980.

37. **Kenley,R.M.**, "Measurement of fatigue performance of Forties Bravo", Proc. of the 14th Offshore Technology Conference, OTC 4402, Vol. 4, 1982, pp. 289-301.

38. **Inglis,R.B., and Kint,T.E.**, "Predicted and measured long term stress range distributions for the Fulmar A platform", Proc. of the 4th Int. Conf. on the Behaviour of Offshore Structures (BOSS '85), Elsevier Science Publishers, Vol. 2, 1985, pp. 153-165.

39. **Achenbach,E.**, "Influence of surface roughness on the cross flow around a circular cylinder", Journal of Fluid Mechanics, Vol. 46, 1971, pp. 321-335.

40. **Roshko,A.**, "Experiments on the flow past a circular cylinder at very high Reynolds number", Journal of Fluid Mechanics, Vol. 10, 1961, pp. 345-356.

41. **Szechenyi,E.**, "Supercrtical Reynolds number simulation for two-dimensional flow around circular cylinders", Journal of Fluid Mechanics, Vol. 70, 1975, pp. 529-542.

42. **Güven,O., Farell,C., and Patel,V.C.**, "Surface roughness effects on the mean flow past circular cylinders", Journal of Fluid Mechanics, Vol. 98, 1980, pp. 673-701.

43. **Jones,G.W., Cincotta,J.J., and Walker,R.W.**, "Aerodynamic forces on a stationary and oscillating circular cylinder at high Reynolds numbers", Technical Report TR-R-300, NASA, Feb. 1969.

44. **Achenbach,E.**, "The effect of surface roughness on the heat transfer from a circular cylinder to the cross flow of air", Int. Journal of Heat and Mass Transfer, Vol. 20, Pergamon Press, 1977, pp. 359-369.

45. **Achenbach,E., and Heinecke,E.**, "On vortex shedding from smooth and rough cylinders in the range of Reynolds numbers $6x10^3$ to $5x10^6$", Journal of Fluid Mechanics, Vol. 109, 1981, pp.239-251.

46. **Fage,A., and Warsap,J.H.**, "The effect of turbulence and surface roughness on the drag of a circular cylinder", R & M No. 1283, Aeronautical Research Council, 1929.

47. **Bearman,P.W.**, "The flow around a circular cylinder in the critical Reynolds number regime", NPL Aero Report 1257, 1968.

48. **Pearcey,H.H., Singh,S., Cash,R.F., and Matten,R.B.**, "Fluid loading on roughened cylindrical members of circular cross section", Report OT-0-8411, NMI Ltd, Jan. 1984.

49. **Nath,J.H.**, "Heavily roughened horizontal cylinders in waves", Proc. of the 3rd Conference on Behaviour of Offshore Structures, Vol. 1, 1982, pp. 387-407.

50. **Nath,J.H.**, "Hydrodynamic coefficients for cylinders with pronounced marine growths", Final Report to API, PRAC Project 80-31B, Oregon State University, Jan. 1983.

51. **Nath,J.H.**, "Marine roughened cylinder wave force coefficients", 19th Int. Conf. on Coastal Engineering, Houston, Sept. 1984.

52. **Nath,J.H. and Wankmuller,R.N.**, "Wave forces on kelp covered horizontal cylinders", Ocean Structural Dynamics Symposium, Oregon State University, Sept. 1984.

53. **Teng,C.C., and Nath,J.H.**, "Forces on horizontal cylinder towed in waves", Journal of Waterway Port Coastal and Ocean Eng., ASCE, Vol. 111, Nov. 1985.

54. **Sarpkaya,T. and Isaacson,M.St.**, "Mehanics of wave forces on offshore structures", Van Nostrand Reinhold Co., 1981.

55. **Matten,R.B.**, "The influence of surface roughness upon the drag of circular cylinders in waves", Proc. of the 9th Offshore Technology Conf., OTC 2902, 1977.

56. **Norton,D.J., and Mallard,W.W.**, "Wind tunnel tests of inclined circular cylinders", Proc. of the 13th Offshore Technology Conf., OTC 4122, Vol. 4, 1981, pp.67-75.

57. **Blumberg,R., and Rigg,A.M.**, "Hydrodynamic drag at supercritical Reynolds numbers", ASME Conference, June 1961.

58. **Sarpkaya,T.**, "In-line and transverse forces on smooth and rough cylinders in oscillatory flow at high Reynolds numbers", Interim Report No. NPS69-86-003, Naval Postgraduate School, Monterey, Ca., 1986.

59. **Rodenbusch,G., and Gutierrez,C.A.**, "Forces on cylinders in two-dimensional flows", Techical Progress Report, BRC 13-83, Shell Develeopment Co., 1983.

60. **Haring,R.E.**, "Ocean Test Structure programme", Ocean Engineering Mechanics, ASME, Vol. I, Dec. 1975.

61. **Bishop,J.R.**, "Wave force investigations at the Second Christchurch Bay Tower", Summary Report R177, OT-0-82100, NMI, 1982.

62. **Bishop,J.R.**, "Experiments offshore to determine the structural loading caused by marine fouling", Marine Fouling and Structural Loading, SUT, Oct. 1985.

63. **Bishop,J.R. and Shipway,J.C.**, "Wave force coefficients for horizontal and vertical cylinders with kelp fouling, measured at the Christchurch Bay Tower", Report OTH-87-268, BMT Ltd, 1988.

64. **Ohmart,R.D., and Gratz,R.L.**, "Drag coefficients from hurricane wave data", Civil Engineering in the Oceans IV, ASCE, 1979, pp. 260-272.

65. **Sarpkaya,T.**, "A critical assessment of Morison's equation", Int.Symposium on Hydrodynamics in Ocean Engineering, Norwegian Hydrodynamic Laboratories, Vol. 1, 1981.

66. **McClelland,B., and Reifel,M.D.**, "Planning and design of fixed offshore platforms", Van Nostrand Reinhold Co., New York, 1986.

67. **Bea,R.G., and Lai,N.W.**, "Hydrodynamic loadings on offshore platforms", Proc. of the 10th Offshore Technology Conf., OTC 3064, 1978, pp.155-168.

68. **Rodenbusch,G.**, "Random directional wave forces on template offshore platforms", Proc. of the 18th Offshore Technology Conf., OTC 5098, Vol. 2, 1986, pp. 147-156.

69. **Harris,D.**, "Views and experience of a Certifying Authority", Marine Fouling and Structural Loading, SUT, 1985.

70. **Det norske Veritas**, "Rules for the design , construction and inspection of offshore structures", Appendix B, 1977.

71. **Bureau Veritas**, "Rules and Regulations for the construction and classification of offshore platforms", 1975.

72. **"Sensitivity study of offshore structures"**, Offshore Research Focus, Department of Energy, No. 52, April 1986.

73. **Abdelradi,M., and Miller,N.S.**, "The effect of variation in hydrodynamic coefficients on the loading on jacket structures and the implications for tank testing", The Naval Architect, RINA, Sept. 1985.

74. **Sarpkaya,T.**, "In-line and transverse forces on smooth and sand roughened cylinders in oscillatory flow at high Reynolds numbers", Interim Report No. NPS-69SL-76062, Naval Postgraduate School, Monterey, Ca., 1976.

75. **Mohamed,F.**, "Consideration of marine fouling at the design stage", Marine Fouling and Structural Loading, SUT, 1985.

76. **Offshore Installations Regulations (Construction and Survey)**, S.I. No. 289, HMSO, 1974.

77. **Guidance on the Design and Construction of Offshore Installations**, Department of Energy, HMSO, 1977.

78. **Department of Energy**, "Report of the Marine Fouling Working Party for the Director of Petroleum Engineering Division", 1979.

79. **Harvey,R.**, "Computer handling of fouling data", Marine Fouling of Offshore Structures, Vol. I, SUT, 1981.

80. **Picken,G.B.**, "The operational assessment of marine growth on offshore structures", Proc. of the 5th Inspection Repair and Maintenance Conf. IRM/AODC, Aberdeen, 1984.

81. **Faulds,E.C.**, "Structural inspection and maintenance in a North Sea environment", Proc. of the 14th Offshore Technology Conf. OTC 4360, 1982.

82. **Wright,R.A.D.**, "Measurement and assessment of marine growth on North Sea structures", Marine Fouling and Structural Loading, SUT, 1985.

83. **Ralph,R.**, "Data from North Sea installations", Marine Fouling of Offshore Structures, SUT, 1981.

84. **Oldfield,D.G.**, "Scale of the problem for U.K. waters", Marine Fouling of Offshore Structures, Vol. II, SUT, 1981.

85. **Short,D. and Bayliss,M.**, "A guide to underwater inspection", ed. by Bax,M., Fort Bovisand Underwater Centre, Plymouth Ocean Projects Ltd., 1982.

86. **"Underwater inspection of offshore installations: Guidance for designers"**, Report UR10, C.I.R.I.A., 1978.

87. **"Down under cutters set to clean up fast"**, Offshore Engineer, May 1987.

88. **Thyson,J.A.G.**, "Hutton production risers - A novel cleaning problem", Proc. of SUBTECH '85, SUT/AODC, Aberdeen, 1985.

89. **Haywood,M.G.**, "Diving considerations", Marine Fouling of Offshore Structures, SUT, 1981.

90. **Wilson,I.**, "The removal of marine fouling", Marine Fouling and Structural Loading, SUT, 1985.

91. **Miller,D.**, "Slippery Paint", Proc. of SUBTECH '85, SUT/AODC, Aberdeen, 1985.

92. **Gaffoglio,C.J.**, "Copper-Nickel sheathing improving jacket performance", Offshore, Nov. 1985, pp. 59-61.

93. **Sell,D.**, "Antifouling techniques", Proc. of SUBTECH '85, SUT/AODC, 1985.

94. **Swain,G.**, "Evaluating antifouling coatings for fixed offshore structures", Proc. of the 7th OMAE Int. Symposium, ASME, Vol. 4, 1987.

95. **"The Hycote underwater painting system"**, Underwater Technology Corproration Ltd., Australia.

96. **Henderson,T. and Rawlings,R.**, "The Henderson Hoop - A marine growth inhibiting device - development and trials", Proc. of IRM '86 Conf., IRM/AODC, Aberdeen, 1986.

97. **Drisko,R.W.**, "Protective coatings and antifouling composite material", Proc. of the 9th Offshore Technology Conf., OTC 3020, Vol. 4, 1977, pp. 419-428.

98. **Miller,K.E.J.**, "Antifouling composite material", Copper Alloys in Marine Environments Seminar, Paper No. 19, Copper Development Association, 1985.

99. **Duncan,J.C.**, "A long term solution to marine fouling", Proc. of the 6th IRM Conf., IRM/AODC, 1986.

100. **Barger,W.R., Danner,L.D., Brown,J.E., and Gaul,T.R.**, "Economic evaluation - Use of Copper-Nickel for sheathing of offshore platforms", INCRA Project No.359, Exxon Production Research Co., 1984.

101. **Wolfram,J., and Theophanatos,A.**, "Experimental determination of drag force coefficients for cylinders covered with marine anti-fouling cladding", Report for ESSO Australia, Project MASS, University of Strathclyde, 1985.

102. **Kim,Y.Y., and Hibbard,H.C.**, "Analysis of simultaneous wave force and water particle velocity measurements", Proc. of the 7th OTC, OTC 2192, Vol. 1, 1975, pp.461-470.

103. **Farell,C., Carrasquell,S., Güven,O., and Patel,V.C.**, "Effect of wind tunnel walls on the flow past circular cylinders and cooling tower models", Journal of Fluids Engineering, ASME, Paper No. 76-WA/FE-20, Sept. 1977, pp. 470-479.

104. **West,G.S., and Apelt,C.J.**, "The effects of tunnel blockage and aspect ratio on the mean flow past a circular cylinder with Reynolds number between 10^4 and 10^5", Journal of Fluid Mechanics, Vol. 114, 1982, pp. 361-337.

105. **Allen,H.J., and Vincenti,W.G.**, "Wall interference in a two-dimensional flow wind tunnel with considerartion of the effect of compressibility", Report No. 782, 1984, National Advisory Committee for Aeronautics.

106. **Maskell,E.C.**, "A theory of the blockage effects on bluff bodies and stalled wings in a closed wind tunnel", R & M No. 3400, Aero. Research Council, 1963.

107. **Goldstein,S.**, ed., "Modern developments in fluid dynamics", Vol. 2, Dover Publications Inc., New York, 1965.

108. **Farivar,Dj.**, "Turbulent uniform flow around cylinders of finite length", AIAA Journal, Vol. 19, No. 3, March 1981.

109. **Stansby,P.K.**, "The effects of end plates on the base pressure coefficient of a circular cylinder", Aeronautical Journal, Vol. 78, 1974, pp. 36-37.

110. **Achenbach,E.**, "Distribution of local pressure and skin friction around a circular cylinder in cross-flow up to $Re=5x10^6$", Journal of Fluid Mechanics, Vol. 34, Part 4, 1968, pp. 625-639.

111. **Engineering Sciences Data Unit**, "Mean forces, pressures and moments for circular cylindrical structures: finite length cylinders in uniform and shear flow", Item No. 81017, June 1981.

112. **Wong,F.Y.F.**, Discussion in "The hydrodynamic drag of roughened circular cylinders", by B.L. Miller, The Naval Architect, RINA, Sept. 1976, pp. 55-70.

113. **Bearman,P.W., Chaplin,J.R., Graham,J.M.R., Kostense,J.K., Hall,P.F., and Klopman,G.**, "The loading on a cylinder in post-critical flow beneath periodic and random waves", Proc. of the 4th BOSS Conf., Elsevier Science Publishers, Vol. 2, 1985, pp.213-225.

114. **Sarpkaya,T.**, "The hydrodynamic resistance of roughened cylinders in harmonic flow", The Naval Architect, RINA, 1977.

115. **Kostense,J.K.**, "Measurements of surf beat and set-down beneath wave groups", Proc. of 19th Int. Conf. on Coastal Engineering, Sept. 1984. (Also Publication No. 338, Delft Hydraulics Laboratory, April 1985).

116. **Seed,R.**, "Ecology", in "Marine mussels; their ecology and physiology", ed. by B.L. Bayne, Cambridge University Press, 1976.

117. **Johnston,C.S.**, "Forecasting of growth patterns - Kelp as an example", Marine Fouling of Offshore Structures, S.U.T., Vol. 1, 1981.

118. **Heideman,J.C. and Padman,L.**, "Bass Strait wind, wave and current joint probability in storms", Workshop on Joint Probability of Metocean Phenomena in Oil Industry's Design Work, London, 1985.

119. **Rodenbusch,G. and Källstrom,C.**, "Forces on a large cylinder in random two dimensional flows", Proc. of the 18th Offshore Tech. Conf., OTC 5096, 1986.

120. **Rodenbusch,G. and Foristall,G.Z.**, "An empirical model for random directional wave kinematics near the free surface", Proc. of the 18th Offshore Tech. Conf., OTC 5097, 1986.

121. **Theophanatos,A.**, "Design for maintenance of jacket structures in the marine fouling context - Results from a research study", Marine Fouling and Structural Loading Seminar, S.U.T, Aberdeen, October 1985.

122. **Kuo,C., MacCallum,K.J., Shenoi,R.A. and Theophanatos,A.**, "Design for production of ship and offshore structures", Proc. of Spring Meeting/STAR Symposium, SNAME, New York, 1983.

123. **Shenoi,R.A.**, "Production orientated structural design appraisal", Ph.D. Thesis, University of Strathclyde, 1981.

124. **Theophanatos,A.**, "Investigation of a production costing method applied to offshore column stabilised units", M.Sc. Thesis, University of Strathclyde, October 1982.

APPENDIX A: Dominant Marine Fouling in the North Sea

A.1. Mussels

One of the most dominant marine organisms on offshore platforms is the mussel. Being circumpolar, mussels are encountered in boreal and temperate seas. Around the British coast the commonest species is the **Mytilus edulis** which can be found on any platform from the southern up to the northernmost North Sea fields. It appears in populations of various densities at shallow waters though occasionally it is present down to -40m water depth.

Significant differences exist among platforms in terms of mussel population depending on whether a platform is located in the path of surface currents carrying planktonic larvae from coastal areas or whether neighbouring platforms act as colonising sources. The mussel, is a robust organism occuring in open water where there is significant water movement, and will survive anywhere provided there is secure anchorage.

Description

Mytilus edulis is a bivalve marine invertebrate protected by a hard calcareous shell of purple-black colour which is essentially triangular in shape. It will attach in large numbers to any hard, rough, preferably discontinuous surface by elastic byssus threads secreted by an associated group of glands in the foot.

Figure A.1 illustrates the shell form and attachment apparatus of the mussel. The threads are planted by the foot such that the individuals are capable of withstanding multi-directional wave forces although they tend to align themselves parallel to the principal direction of flow. The foot retains the capacity for movement particularly in young mussels which are highly mobile. Temporary byssal attachment is made whenever the mussel comes to rest whilst, when moving, threads are attached and then abandoned at every stage in the process. The strength of byssus threads increases both with strong wave or current action and with age of the individuals.

Settlement

Settlement periods for mussels vary with geographic location but it can be generally said that in the North Sea mussels will spawn between March and September [10]. Settlement takes place in two stages. Primary spawning of early plantigrades occurs on filamentous substrata such as members covered by algae or hydroids which subsequently disappear. Secondary settle ment occurs on established mussel beds at any time during the year.

Seed [116] has conclusively demonstrated that mussels attach temporarily on filamentous algae, particularly on the hydroid **Tubularia mytiliflora**, and from those permanently to beds of adult mussels. However the enhancemment to settlement provided by fine filamentous growth is not provided by larger seaweeds (e.g. kelp) which instead inhibit mussel colonisation.

Size and Growth Variation

Shell size is extremely variable and depends on environmental conditions and on the age of the animal. Factors such as growth rate, population density and degree of exposure to waves also influence differential growth producing a considerable array of shell forms.

Disproportionate growth is reflected in a gradual change in body proportions with increasing size and age (Figure A.2). Older mussels generally have heavy, elongate shells where width frequently exceeds shell height. Since growth is defined as increase in body size, weight or volume might be the most appropriate parameters for its measurement. However, the shell is such a prominent feature of the mussel anatomy that growth is generally measured in terms of length. Extreme caution though should be exercised in using singular linear parameters to measure growth. For example, although mussels may be increasing in biomass at approximately equal rates, their growth in terms of other parameters such as length, width or height may vary according to age and local environmental conditions. Even mussels grown under apparently identical conditions can exhibit widely different rates. Variation is such that whilst in ideal conditions mussels may grow very rapidly - sometimes exceeding 60-70mm within a year - under less favourable conditions growth is exceedingly slow with some individuals measuring only 20-30mm long after 15-20 years.

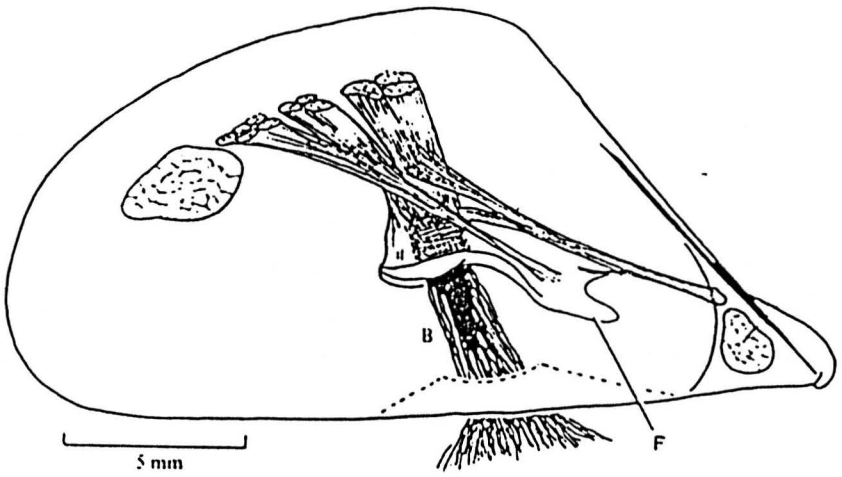

Fig. A.1. Shell shape and attachment mechanism of mussels; (B) byssus threads, (F) foot; (From Seed [116]).

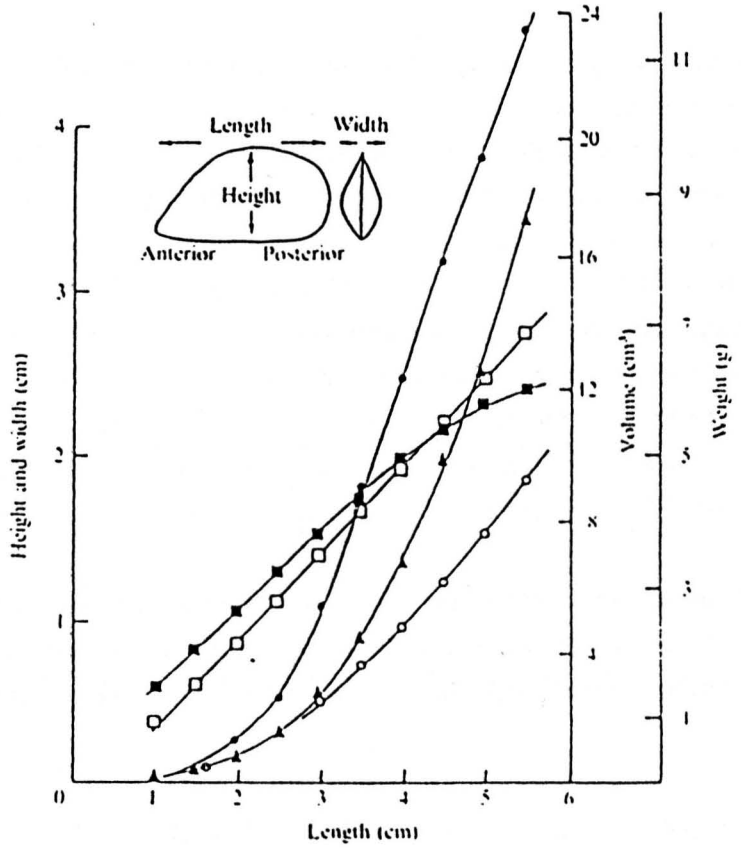

Fig. A.2. Various growth parameters as functions of mussel length; ●, shell weight; o, tissue weight (x10); ▲, volume; ■, height; □, width; (Seed [116]).

Mussel is gregarious and dense settlements are often found around the edges of and between individual mussels in existing populations. Such behaviour has adaptive value since mussels are subjected to wave forces especially on exposed areas. The reduced surface area which is exposed to such forces by animals within dense clusters together with the mutual support of neighbouring individuals makes groups of mussels better adapted to withstand wave action than isolated individuals. Mussel beds increase in dimensions both through gregarious settlement and growth of individual mussels. Typical growth curves for Mytilus from various locations are illustrated in Figure A.3 where it is shown that increasing age is accompanied by a decline in growth rate [10].

Reductions in growth rates are also found in populations of mixed ages where the majority of small mussels amongst the byssus threads of larger individuals are at a disadvantage in the competition for food. It should be expected that growth rate slows down within a densely populated clump of mussels.

Food supply is probably the most important single factor in determining growth rate. If food is scarce the growth is retarded regardless of all other conditions. This factor probably also determines the upper limit of mussel presense on any platform since a point will be reached when the food demand will exceed the supply available during the feeding period. The water depth at which this becomes critical varies from platform to platform depending on local conditions such as tidal level and wave splash. In areas where food is abundant blanket cover up to 250mm thick can develop. However, relatively few of the mussels are actually attached to the substratum. The majority are attached to each other's shell by byssus threads.

Temperature is acknowledged as another important factor in controlling growth rate. Mussel growth occurs between 3^{o} and 25^{o} C with an optimum between 10^{o} and 20^{o} C, whilst growth declines sharply above 20^{o} C.

Mussel mortality and migration may trigger growth variations. Predators such as eider ducks and starfish may reduce thick mussel beds to clusters of empty shells. Intense spatfalls of young plantigrades also constitute a major mortality factor since the underlying mussels suffocate thereby loosening the entire population from the substra-

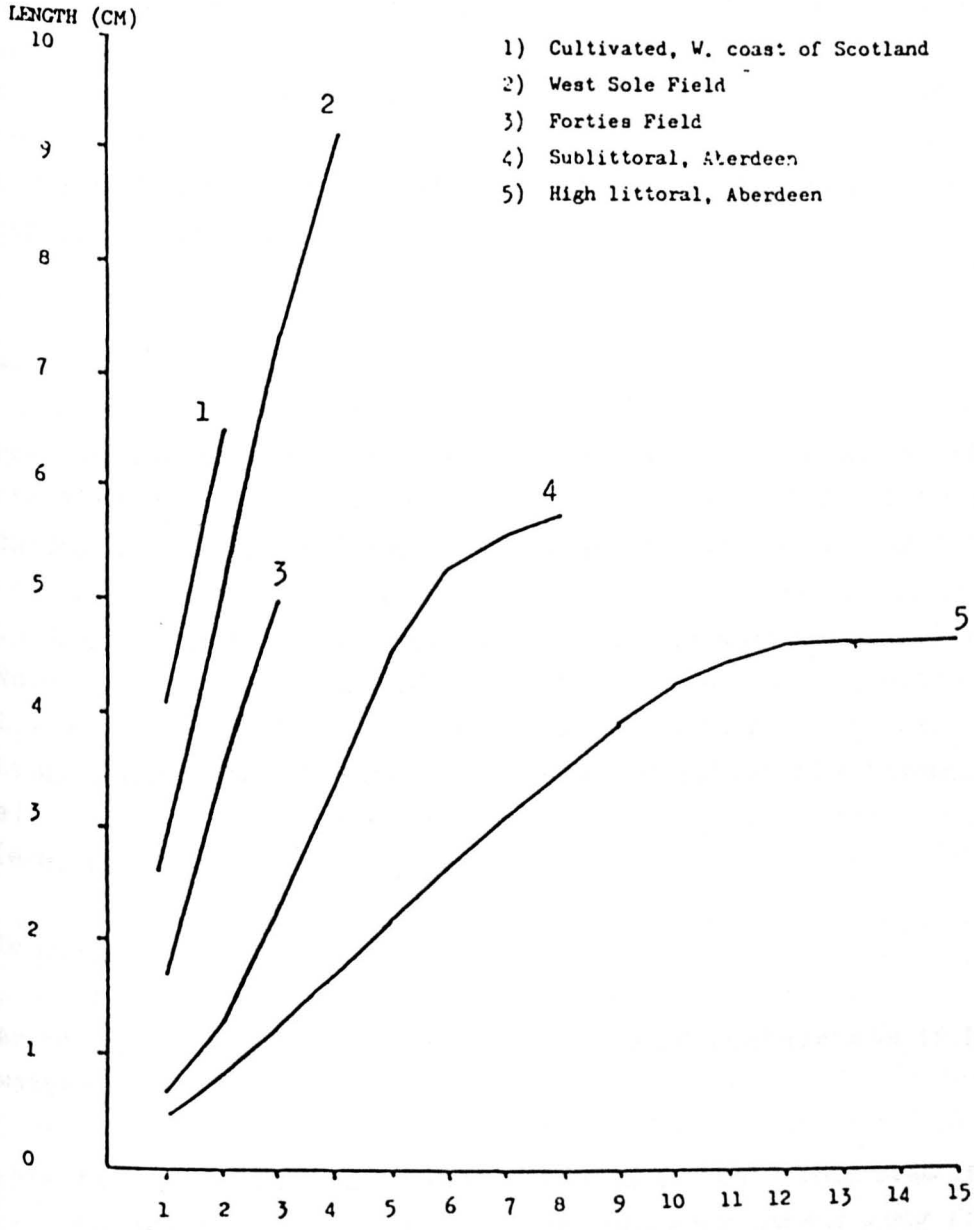

Fig. A.3. Growth rate of mussels at various locations [10].

tum. Alternatively, young mussels becoming attached to older individuals find competition too severe and die.

Competition for space can be strong leading to "hummocking" where mussels being in the centre of the hummock often have no direct contact with the substratum. Much of the population might then be torn off during rough seas. However, in terms of population dynamics some of these mussels will colonise other structural members covered in barnacles and algae. Under such circumstances, mussels are usually the competitive dominants.

A.2. Kelps

Perhaps the most aggressive fouling organisms in the North Sea are the long flapping seaweeds **Laminaria** commonly refered to as kelps. Though occasionally found in the lower 1-2 metres of the inter-tidal zone they are predominantly sub-tidal. All species can extend down to 15-20m water depth or even to 30m in the Norwegian sector of the North Sea . As they thrive in cold water conditions kelps are most likely to cover the top elevations of northern North Sea installations such as the Murchison, Magnus and Hutton platforms. They are also present in limited numbers on some central North Sea platforms (e.g. Forties).

Description

As shown in Figure A.4, the main types of laminarians in North Sea waters are:

- **Laminaria digitata**; distinguished by their long stem (stipe) and palm-like blade which is split into many narrow long fronds.
- **Laminaria hyperborea**; essentially similar in shape to digitata.
- **Laminaria saccharina**; consisting of a single crinkly blade.

All kelps grow on hard substrates from their holdfast, a complex branching system consisting of many haptera tips. The holdfast develops in such manner as to ensure a remarkably strong adhesive action withstanding even the strongest currents or extreme waves. A thick stipe about 20-30mm in diameter supports a broad flexible blade which in the case of L. digitata is split into numerous strip-like fronds

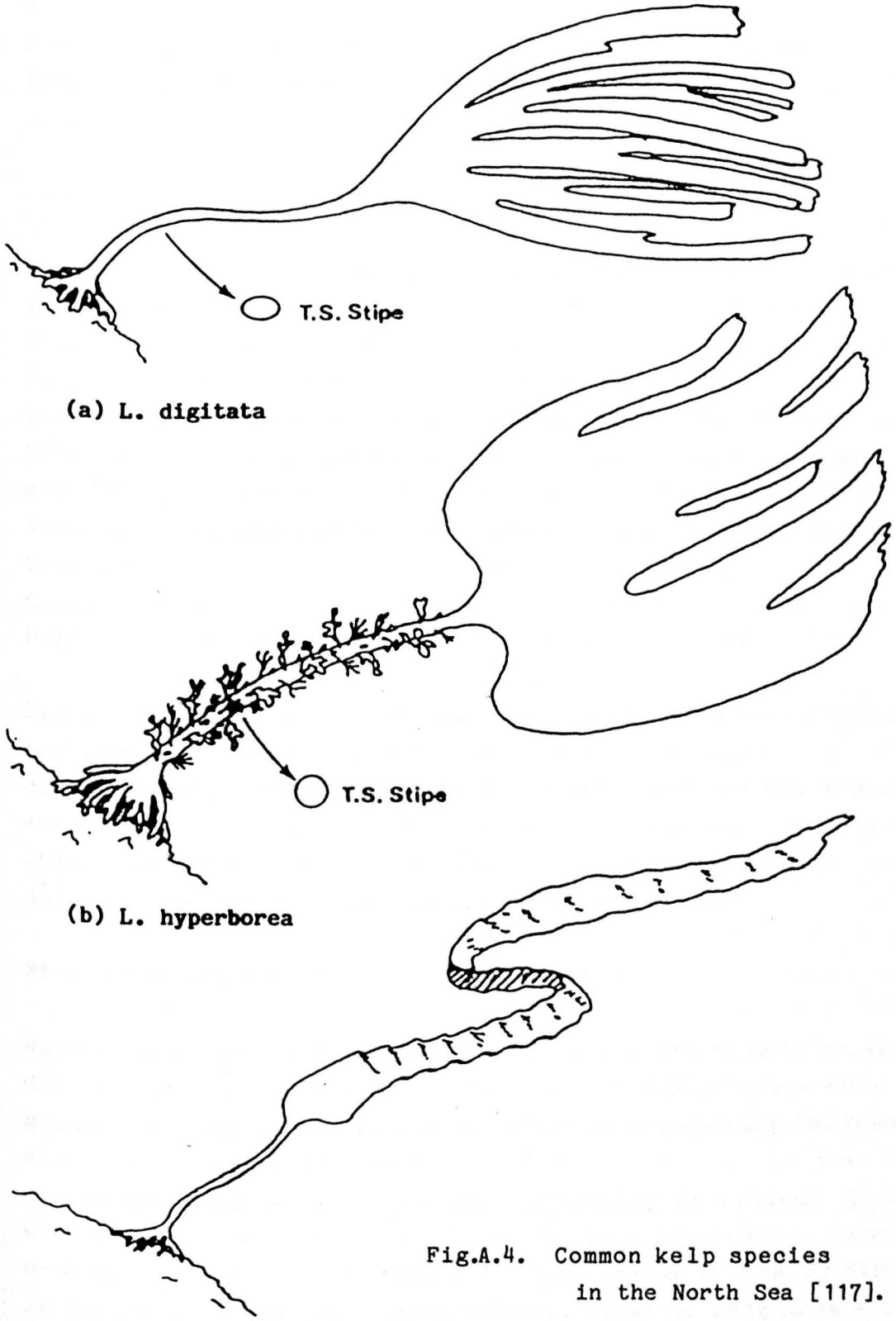

Fig.A.4. Common kelp species in the North Sea [117].

(lamina) of various widths. The plants tend to align with the prevailing current/wave direction and their fronds become thicker in areas of high water turbulence. Elasticity therefore varies not only along the length of each plant (stiff stipe but flexible blade and fronds), but also among different plants depending on their relative position to the predominant direction of flow.

Settlement

Laminarians exhibit a complex life cycle. Mature plants (sporophytes) on the shore or on neighbouring platforms produce spores during the spring which are released into the plankton and carried by water inflows to suitable surfaces. If a spore attaches on a substrate it develops into a gametophyte and becomes fertile at low temperatures (5^{o}-7^{o} C). The female gametophyte then produces fertilised eggs that grow into new sporophytes. This process takes about 2-3 years while the new sporophytes will take a further two years to mature and become fertile. Therefore, kelp growth is not established at least during the first five years after the installation of a platform. Following this period dense populations develop very rapidly.

Light conditons are critical and the optimum water depth range for settlement and growth on North Sea platforms is between -1m to -15m approximately. Inital settlement occurs along the top and outer member faces irrespective of the possible presence of mussels or other hard growth as kelp colonisation is aggressive. In fact mussels and barnacles provide extra anchorage for the plant.

Size and growth rate

Different water regimes produce different forms of kelp growth. **L. digitata** and **L. hyperborea** generally prefer exposed areas where they grow up to lengths of 3m with the stipe alone reaching 1m. They can also adapt to sheltered waters where the stipe will be just a few centimetres long and the blade may not develop into fronds. In areas with strong currents the total length of mature plants may exceed 5m with stipes well over 1m long. **L. saccharina** which usually flourish in sheltered areas grow a single blade about 3m long from a short stipe. They too can adapt to strong currents. Blade width varies with type of laminarians, age of plant and water regime. A 3m long kelp may be 0.5m wide but the proximity of neighbouring plants and its

flapping motion may cause the blade to curl and effectively reduce in width.

Seasonality and water temperature affect growth rates as kelps start growing during the latter half of the winter and peak in the period between April and June. New lamina tissue is produced from the meristem at the proximal region pushing ageing tissue towards the distal region (Figure A.5). The higher summer temperatures result in gradual decay of lamina at the distal region and by late November significant die-back is evident. Johnston [117] quotes the following growth rates:

- L. digitata 11-13mm/day,
- L. saccharina 17-49mm/day.

Kelp density is variable particularly for L. saccharina which may form dense forests with up to 200 plants/m^2 or can be solitary. L. digitata are more consistent at around 45 plants/m^2. In terms of weight the figures quoted by Johnston are [117]:

- L. digitata 6-9 kg/m^2,
- L. saccharina 7-20 kg/m^2.

Kelp plants may live up to fifteen years by regenerating new lamina and shedding the ageing ones. The blades of some plants are however ripped off during storms and since their regeneration system is located at the transition zone between the stipe and the blade they are unable to survive. Also it is preferable to destroy kelps by cutting off the stipe above the holdfast rather than ripping off the whole plant, and possibly damaging the steel surface in the process because of the strong adhesive action by the holdfast.

A.3. Sea Anemones

Classified as climax soft fouling, i.e. not likely to be replaced by other foulers once established, sea anemones are dominant on the central and northern North Sea platforms at water depths between 15m to 120m. The common species is the **Metridium senile**, while the species **Tealia** may also be encountered in isolated form. Abundant growth of Metridium occurs at around -30m to -50m depth, along the bottom

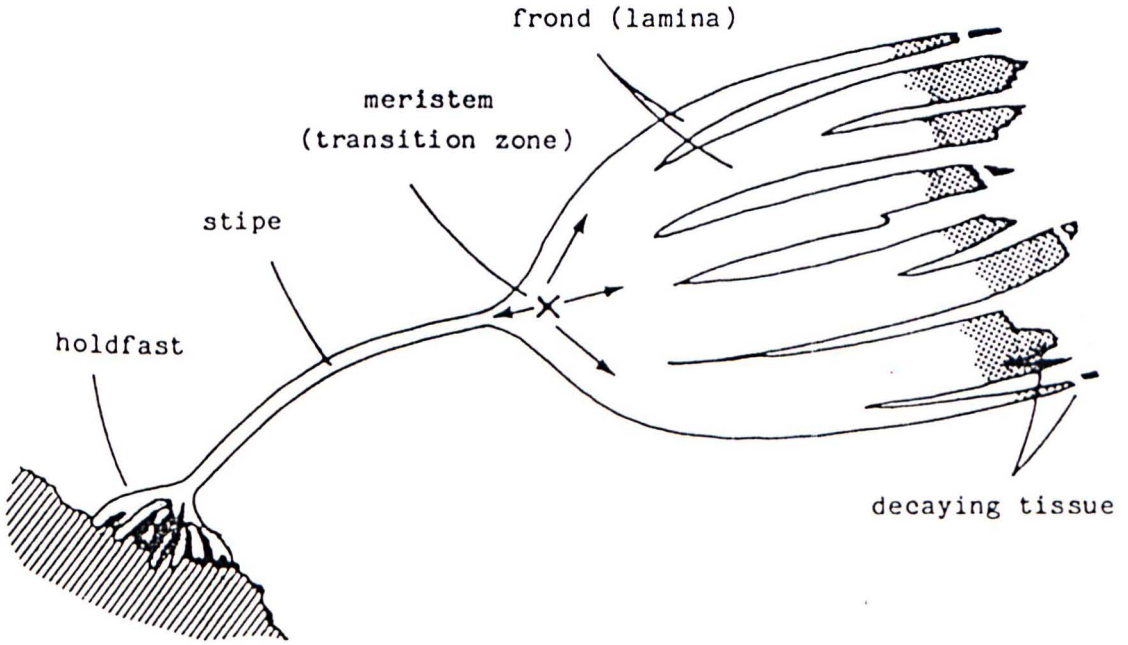

Fig. A.5. The kelp **Laminaria digitata** [117].

faces of tubular members and around anodes and other excrescences. As competition for space becomes acute, the animals propagate over the entire member surface and towards the upper and lower platform elevations overgrowing hard foulers and hydroids.

Description

Metridium senile is a soft orange or white columnar growth with thin tentacles protruding from the top (Figure A.6). It has no rigid skeleton; the water intake filling the column acting as a hydrostatic skeleton. Attachment to the substrate is by means of a basal disc secreting mucus. Strong adhesion is possible but the animal retains the capacity to slowly glide across the substrate.

When disturbed, either by touching the tentacles or by strong water turbulence, the tentacles withdraw into the column which drastically changes in shape becoming much shorter and squat. If removed from its natural environment it loses most of the water intake and changes to blue or purple colour. It can however reattach itself to a new surface provided it is kept in seawater.

Settlement

Metridium breeds during June and July either by releasing larvae into the plankton or by pedal laceration [10]. The latter method, which is very common in the North Sea, involves the release of small pieces from the basal disc of mature animals which quickly develop into small anemones. Thus, blanket cover is achieved with small animals surrounding parent individuals.

Size and growth rate

Due to the method of settlement and reproduction and also because of the dynamic height variation of individuals it is difficult to estimate the thickness of sea anemone cover or the height of individuals. Rough figures of 150-200mm in height and 80-150mm diameter have been quoted, whilst densities of over $400/m^2$ are quite common [8,10]. Growth rate is high once sea anemones are established on a structure as is their resilience to competition from other species and to suspended inorganic matter (e.g. drilling mud and cuttings).

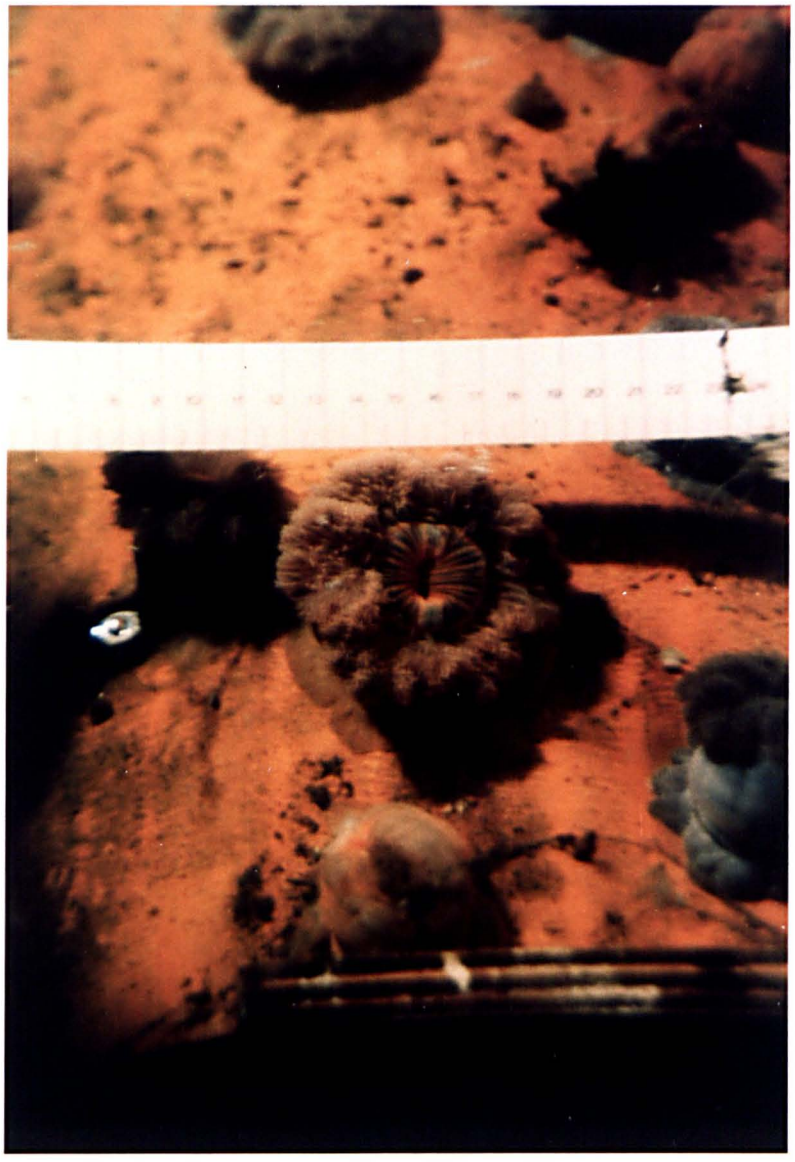

Fig. A.6. Close-up view of sea anemones.

A.4. Tunicates

The **tunicates** or sea squirts, shown in Figure A.7, are common colonisers on most North Sea structures and can be found in all depths preferably in sheltered areas. They have a soft transparent tubular body covered by a cellulose based tunic with two openings. One of the openings is used for adhesion to the substrate. They settle in summer but live only for one year while most animals are washed away during winter storms. Their body is full of water and as they can grow very rapidly in large numbers (about 250/m^2) they entrap large volumes of water.

A.5. Barnacles and Tubeworm

These are two forms of calcareous growth colonising virtually all North Sea platforms at the early stages of their operating life. The main barnacle species are: the **Balanus balanoides** appearing in shallow waters, and the **Balanus hameri** usually found in water depths below 90m. The latter is, therefore, not "hydrodynamically significant".

Balanus balanoides is a white, sharp edged, frustum shaped animal firmly adhering to the substrate via a calcareous disc formed by a cement-like substance. The base remains attached to the steel surface once the rest of the barnacle has been scraped off. Hence if cleaning of bulky growth were carried out, barnacle covered members would remain "rough". Barnacles grow up to 75mm high with a base diameter of 50mm approximately. They settle by releasing larvae and can densely cover large areas but are eventually overgrown by other forms of hard and soft fouling.

Tubeworms or **pomatoceros** behave in a similar manner to barnacles, i.e. initial colonisers which are virtually impossible to remove completely off the substrate. They differ however in shape and dimensions. As the name suggests they are worms living in hard white calcareous tubes of triangular cross-section which are cemented to the substrate in random shapes (Figure A.8). They do not grow more than 10mm high but can cover large areas in the few months following platform installation.

Fig. A.7. Dense population of tunicates on a test cylinder.

Fig. A.8. Pomatoceros (tubeworm) on a test cylinder at Loch Sween, West Coast of Scotland.

A.6. Other Species

In the preceding sections only the species which are considered "hydrodynamically significant" and were tested either exclusively or as part of mixed fouling are described. There are two more fouling organisms which, though not tested for fluid loading, do merit consideration. These are the hydroids and the soft corals.

The hydroid species **Tubularia** is a feathery flower-like animal consisting of stiff stalks up to 150mm long. It appears on platforms at all depths and grows rapidly forming dense forrests. It is very flexible and responds to the slightest wave or current action . Its fluid loading effects are not known.

This is also the situation for the soft coral **Alcyonium digitatum.** Though found in isolated form at depths below 30m on most central North Sea platforms there have been specific cases where abundant growth at the wave affected zone has been recorded. Alcyonium consists of a rubbery tissue mass covered by hundreds of small polyps. Its finger-like shape and its size vary by means of contraction and expansion. Maximum recorded height is about 200mm and density is up to $500/m^2$.

APPENDIX B. Description and Classification of Marine Growth for Six North Sea Platforms.

The state of marine fouling on six fixed steel platforms is described in three sections according to platform location. The study was based on colour videos of ROV general inspections which were carried out during 1985, except for platform NN1 where B/W videos were available. Visual perception was severely impaired in the latter case and also, in some cases, for structural members located near the water surface. Inspection datasheets, structural drawings and member codes provided additional information. The data for each platform are systematically classified in Tables B.1 through B.6.

B.1. Southern North Sea

One platform located in this sector was studied. It is situated in 25m water depth and has been in-service for over 15 years. As shown in Table B.1, the predominant types of marine growth were mussels, which colonised the top half of the jacket, and sea anemones in great profusions over the -12m to -25m depth range. Hydroids and tubeworm were also present at the splash zone.

a) Splash zone

Horizontal members in the splash zone were fully covered by heavy mussel growth. It appeared to be uniform over the entire member surface apart from small areas around appurtenaces (e.g.stubs) where growth was more pronounced. New settlements of 8-10mm mussels were on top of established beds of 25mm mussels. Overall thickness was approximately 60mm. No significant differences were detected between platform faces at that depth range.

b) -1.5m to -12m

The members reviewed in this depth range comprised leg sections and inclined bracings. Therefore, changes in composition, type and surface cover were noticeable due to depth variation. Wide bands and clusters of 25mm mussels were randomly distributed over each inclined member and extended down to -9m depth; the bottom 3m being heavily covered (90%) by 20-40mm long hydroids. Cluster size and thickness

varied between inclined members but no trend could be discerned among platform faces. The larger clusters consisted of multiple mussel layers up to 120mm thick overall. They were genarally located around the anodes on the top and outer member faces. The surface cover gradually reduced from 80% at -1.5m to 30% at -9m, the remaining area being covered by 15mm hydroids or soft green weed. On one diagonal (-5m to -6.5m elevation) a population of starfish was feeding off a 100mm thick mussel bed and, as a result, large amounts of open shells were interspersed among live mussels.

c) -12m to -25m

Sea anemones and hydroids dominated the jacket at that depth range. The North and East face members were 90-100% covered by 100-150mm sea anemones with smaller ones emerging among the established communities, thus indicating new growth. The same pattern applied to South face members with the exception of one nodal area, at -12m, where dense, non-uniform, 25-60mm mussel growth extended along the adjacent horizontal and inclined members. The horizontal member was fully covered by mussels, whilst cover was patchy (20-40%) over the outer and top faces of th inclined member and the leg section down to -21m, the remaining surface area being covered by 50-100mm sea anemones. Mussel size at -18m was 25mm, with apparently new 10-15mm growth stretching down to -21m at 20% cover. Mussels were present only on the South face at that water depth.

Fouling was patchy on all West face horizontals and diagonals consisting primarily of 50-150mm sea anemones, whilst 10-15mm hydroids and 5mm tubeworm covered any free from sea anemones surface. Sea anemones cover did not exceed 30% of the outer faces with the largest and more dense patches situated around the anodes. Also, isolated soft corals, up to 20mm in height, were observed at the bottom face of one diagonal. The distinct reduction in surface cover at the West face at that elevation is attributed to cleaning prior to the installation of a strengthening bracing. It is remarkable that the strengthening member itself was 60% covered by 100mm sea anemones.

B.2. North Central North Sea

The three studied platforms are situated at 100-120m water depth and were installed during 1974/75. Sea anemones were the predominant species an all structures. Although they were found throughout the whole structure in varying densities and thicknesses they covered almost exclusively members in the -24 to -80m depth range. Therefore, the study was concentrated in the MSL to -24m range where fouling composition varied significantly with mussels, kelp and soft green or brown weeds the dominant species.

Platform NCNS1

All horizontal members at the -24m elevation were 90-95% covered by 50-90mm sea anemones with small bare patches randomly distributed along the top face. Anemone layers were thicker at the bottom face of all members suggesting that the communities expand upwards. Isolated 30-40mm soft corals were found among sea anemones along the bottom face of North face bracings.

a) -24m to -5m

The inspected members consisted of leg sections and vertical and inclined bracings. In general, dense populations (70-90%) of sea anemones extended up to -18m. However, size decreased from 40mm at -24m to 20mm at -18m. On one leg section and up to -7.5m, 20mm sea anemones were sparsely distributed over a uniform layer of 10-15mm mussels which extended from -9m to -6m over the outer face only. All other structural members possessed similar characteristics among them, i.e. hydroids between -18m and -5m and 60-100mm long green weeds growing over tubeworms with occasional patches of 20-80mm sea anemones particularly between anodes. Parts of the outer face of some braces were completely free from fouling due to either wire abrasion or cleaning for weld inspection.

b) -5m to MSL

The general pattern for the three platform faces (East face not surveyed at that elevation) consisted of kelp and/or green weeds colonising the top and outer faces. Sea anemones dominated the bottom face of the members. Mussel growth was patchy and outgrown by those

species. Elongated uniform layers of 10-15mm mussels covered the North face horizontal bracings. They spanned the top and outer faces of the LHS member, extended through the node to the adjacent (RHS) member over a 1m span and, over a further 2 or 3m, clusters of mussels were randomly distributed along the outer face. Among the mussels grew 40-60mm long brown weeds which also densely covered any free from mussels areas. The bottom and inner faces of both members were covered by young growth of 10mm sea anemones, in a similar pattern to that described above. However, density increased distinctly in the vicinity of anodes. It should be noted that, at -5m elevation, bracelet anodes are mounted across the circumference and at regular intervals along the member length.

On the South and West faces, kelps were established at the top and outer member faces. They varied in length between 100-500mm and were sparcely distributed over the member span (approximate density of 20-25 plants/m^2). At isolated areas, the kelps grew over 25-40mm thick mussel beds which extended, in elongated strip form, on the top and outer faces of horizontal bracings and around the circumference of the vertical and inclined members. The bottom and inner faces of the horizontals were 80-85% covered by 10-30mm sea anemones, which were also present on the outer faces near the anode bracelets.

Platform NCNS2

Marine growth on platform NCNS2 was broadly similar to platform NCNS1 in species types and their variation with depth. However, some notable differences existed in species size, distribution and composition per member. The North face was less densely covered than the rest. It was virtually free from kelp or green weeds and had patchy colonies of 10-30mm mussels at 20% surface cover on horizontal bracings at the -6m elevation. Sea anemones dominated all members and ranged in height from 20-80mm at -25m to 10-30mm at -5m.

Kelp and 30-40mm long green weeds appeared in low densities (20%) on horizontal members of the East and West faces (-6m elevation). The seaweeds, whose length did not exceed 100mm, were isolated (10-15 plants/m^2) midway along the top faces of both inspected horizontals. The remaining surface areas were 80-90% covered by sea anemones, ranging in size from 100mm at the bottom faces to 50mm at the top. Isolated soft corals (30-50mm) grew among the sea anemones at the

bottom and outer faces of one horizontal. Along the top face of the same bracing, a 100mm high conduit spanning the member, was densely covered by sea anemones and green weeds. It should be expected that significant transverse forces are experienced by this member due to body asymmetry.

South Face

The South face was studied in greater detail since marine growth was significantly heavier. At -25m elevation, both inspected horizontals were 90-100% covered by 30-120mm sea anemones, apart from a 2m span midway along the RHS bracing which was fully covered by 50-70mm soft corals.

a) -25m to -6m

Marine fouling types and composition were similar for the two reviewed inclined members. The LHS member was fully covered by 90-120mm sea anemones and tunicates between -25m and -23m, whilst sea anemones mixed with 15-60mm soft corals covered the member up to -20m in a 70:30 ratio. The top face in the depth range of -20m to -6m was covered by 70-100mm long green weeds with 10-40mm soft corals scattered along the bottom and outer faces up to -15m depth. The RHS inclined bracing was full of 90-120mm sea anemones between -25m and -19m, with occasional, randomly shaped, bare patches on the top face each being about $0.2m^2$. From -19m to -6m, the bottom/outer face was fully covered by 20-60mm anemones and the top one by 100-130mm hydroids and green weeds, except for a circumferential band of 70-80mm soft corals at -16m to -15m.

b) -6m to MSL

The top face of the LHS horizontal brace at -6m had 100mm green weeds and up to 150mm long kelp sparsely distributed along the top face only. Bottom and inner faces were 50% covered by 20-40mm sea anemones. Kelps of similar length were evenly distributed on the top face of the RHS horizontal at 30-40% density, the rest being covered by 20-40mm sea anemones. It is believed that numerous construction points, protruding by about 200mm from the top face, provide a sheltered habitat for the sea anemones.

The partially submerged inclined and vertical bracings were extensively covered by flapping seaweeds, mainly kelp, which ranged in length from 200mm to 900mm. Cover of the top and outer faces was 80%, thinning out at -2m to 30%. Bottom/inner faces were fully covered by 20mm sea anemones at depths up to -2m. Mussels, barnacles or sea anemones grew on top of the kelp holdfasts. Tubeworm was also visible at -2m on the outer face of the South-East corner leg.

Platform NCNS3

The only significant difference from the other two platforms was the strong presence of 40-60mm thick mussel layers on the East and South faces, reaching 80% blanket cover at -5m to MSL. Kelps, growing among mussels, were 600mm long but sparse (10-30%) at the top face of bracings and outer face of leg sections.

B.3. Northern North Sea

Both reviewed platforms were installed in the early '80s and were, therefore, only partially covered by marine growth. The members at depths below 60m were covered by primary settlers such as algae or fine filamentous growth.

Platform NN1

The extent of growth was generally low at all elevations and comprised mussels, hydroids, barnacles, tubeworm and starfish. At depths below 70m down to the seabed, the structure was almost clean, whilst only 20-30mm hydroids and 2-4mm tubeworm were observed in the -15m to -70m range.

At -12m, 15-20mm mussels covered the top half of the horizontals and 20-30mm hydroids colonised the bottom and inner faces. Mussel growth was randomly distributed in patches along the top and outer faces of inclined members resulting in 30% cover. Green weeds, 20-40mm long, covered the remaining surface. Near the nodes, and also around indicator flags and anodes, mussel growth thickened to 40mm approximately. Typical internal braces of the -12m horizontal frame exhibited significant concentrations of 20-30mm around the indicator flags (top face).

Platform NN1 is located in a region where heavy growth of kelp has been recorded [14]. It is therefore likely to be dominated by seaweeds in the wave affected zone with sea anemones prevailing in deeper water.

Platform NN2

The North and South faces of this platform were studied. The most notable differences among the two faces were the kelp presence, at the development stage on the North face, and the comparatively extensive mussel cover of the South face. Mussels, barnacles and hydroids were encountered on all members down to -30m. Solitary tubeworm, hydroids and patches of sea anemones at low density grew in the -30m to seabed region.

The studied splash zone members of the North face comprised one vertical and two inclined bracings. On all three, kelp up to 200mm long was recorded on the top and outer faces, in isolated form (5-10 plants/m^2) and at water depth of about -5m. Hydroids and 60-100mm green weeds grew among the kelps and on top of a tubeworm layer. The outer face of the vertical member was 60% covered by a wide band of 20-30mm mussels, gradually increasing to 80% at -5m. Hydroids and isolated kelp covered the other faces with length reaching 150mm and 300mm respectively at -8.5m.

Within the same depth range (MSL to -16m), the South face horizontals were 60-80% covered by mussels and hydroids colonised the bottom faces. Between -16m and -45m, a mixture of 8-12mm barnacles and 10-20mm mussels was found on the outer faces of inclined bracings in elongated strip form extending down to -30m.

As in the case of platform NN1, kelp is likely to dominate in future at the splash zone, with sea anemones being the main colonisers at deeper water.

KEY TO TABLES	
Member Location	
- Platform Face	N = North S = South E = East W = West HF = Horizontal frame
- Member Type	B = Bracing H = Horizontal V = Vertical I = Inclined
Member Face (Figure B.1)	T = Top O = Outer B = Bottom I = Inner

Notes:

1) Depth ranges are based on ROV water depth indicators at the time of inspection.
2) Mussel size is the estimated height of the species.
3) Thickness of mussels is the estimated average of the overall mussel layer thickness.
4) Length of seaweeds or hydroids refers to the estimated fully extended length of the species.
5) Percentage surface cover estimates are based on the area of **member faces** covered by a particular type of fouling; for example full mussel cover of the top face only is reported as 100% of the top face.

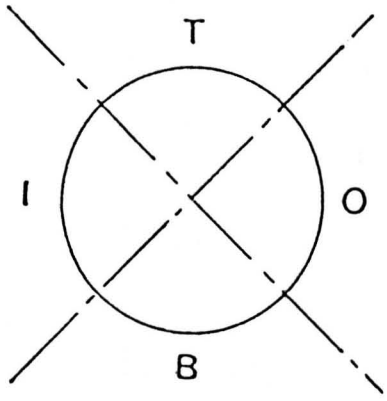

Fig. B.1. Definition of horizontal and inclined tubular member faces.

DEPTH (m)	MEMBER LOCATION		KELP/GREEN WEED				HYDROIDS			MUSSELS					SEA ANEMONES			APPROX. k/d
			LENGTH(mm)		COVER(nos/m2 OR %)		LENGTH	COVER		SIZE	THCK	COVER			THCK	COVER		
	FACE	TYPE	AVE.	MAX	FACE	FORM	(mm)	FACE	%	(mm)	(mm)	FACE	%	FORM	(mm)	FACE	%	
0.5	All	HB								8-25	60	TOBI	100	Heavy				0.17
1.5-9	N	LEG								8-25	60	N	90	Heavy				0.07
9-12							10-50	N	30						10-80	N	70	
1.5-8.5	W	LEG								8-25	80	W	90	Heavy				0.09
8.5-12							20-50	W	20						10-80	W	80	
1.5-6	W	HB								25	80	TOB	60	Patchy				0.16
6-12							20-40	TOBI	90									
3-9	S	HB								25	70	TOB	75	Patchy				
7-8.5	S	HB								25	60	TO	80	Patchy				0.13
8.5-12							60-80	TOBI	90									
12	N	HB					20-50	TOBI	70						30-70	TOB	30	
12	N	HB					20-50	TOBI	50						60-100	TOB	50	
12	W	HB													20-100	TOB	60	
12	S	HB					20-40	TOBI	30						20-90	TOBI	85	
12	S	HB								25-30	50	TOBI	80	Dense				0.15
12	E	HB					20-40	TOBI	20						20-70	TOBI	70	
12-20	N	HB					20-50	TOBI	40						30-90	TOBI	60	
20-25															30-120	TOBII	90	
12-25	W	HB													50-100	TOB	30	
12-18	S	HB					20-40	TOBI	80	25	25	TO	50	Cluster				
18-25										10-15	15	TO	20	Cluster	50-100	TOB	90	
14-17	S	LEG								10-20	15	S	40	Cluster				
17-25															30-60	S	70	
-25	S	HB													50-100	TO	90	

Table B.1. Platform SNS1.

DEPTH (m)	MEMBER LOCATION		KELP/GREEN WEED				HYDROIDS			MUSSELS					SEA ANEMONES			APPROX. k/d
			LENGTH(mm)		COVER(nos/m2 OR %)		LENGTH	COVER		SIZE	THCK	COVER			THCK	COVER		
	FACE	TYPE	AVE.	MAX	FACE	FORM	(mm)	FACE	%	(mm)	(mm)	FACE	%	FORM	(mm)	FACE	%	
MSL-5	S	IB	30	100	I	Light, 40%				20-25	35	IOB	60	Heavy				0.04
MSL-5	S	VB	300	500	0	Isolated k				20-25	30	0	80	Heavy				0.03
MSL-5	S	IB	60	150	IO	Light, 40%				20-25	30	IO	80	Heavy	20-30	B	10	0.03
MSL-5	W	IB	200	400	IO	Cluster				10-20	20	OB	50	Strip				0.02
MSL-5	W	VB	40	200	0	Dense, 70%												
MSL-5	W	VB	50	200	0	Dense, 80%				10-20	20	0	30	Patchy				
MSL-5	W	IB	50	100	IO	Light, 50%												
5	N	HB	40	60	IO	Light, 25%				10-15	15	IO	80	Strip	10-20	IOBI	50	0.016
5	N	HB	40	60	IO	Light, 25%				10-20	15	0	50	Patchy	10-20	0	30	
5	S	HB	200	500	IO	lk:20-25/m²				10-20	25	0	60	Strip	10-20	OBI	85	
5	S	HB	300	500	IO	Light, 40%				15-25	30	IO	75	Heavy	10-30	B	80	0.03
5	W	HB	300	400	IO	Light, 40%									10-30	OBI	60	
5	W	HB	50	150	I	Dense, 80%												
5	W	HB	100	200	I	Dense, 90%									10-20	OBI	60	
5-24	W	IB	50	100	IOBI	Dense, 80%												
5-10	W	IB	50	80	IOBI	Dense, 70%												
10-24			50	60	IOBI	Light, 20%									20-50	IOB	100	
5-10	N	LEG	150	350	E	Isolated k				10-15	15	0	30	Strip				
7.5-24			40	60	0,25%	Patchy GW				10-15	15	0	20	Strip	30-60	0	50	
5-18	N	IB					20-40	IO	70						20-40	B	80	
18-24															30-60	IOBI	80	
18-24	N	VB													30-60	IOBI	90	
5-12	S	IB	50	80	10,25%	Light GW									20-30	IOB	60	
12-24															20-80	IOBI	80	
8-15	S	VB													20-40	0	40	
15-24							20-40	OI	50						30-60	OI	60	
-24	N	HB													50-70	IOBI	90	
-24	S	HB													40-60	IOBI	90	
-24	W	HB													50-90	IOBI	100	
-42	N	HB													50-90	IOBI	100	

Table B.2. Platform NCNS1.

DEPTH (m)	MEMBER LOCATION		KELP/GREEN WEED				HYDROIDS			MUSSELS					SEA ANEMONES			APPROX. k/d
			LENGTH(mm)		COVER(nos/m2 OR %)		LENGTH	COVER		SIZE	THCK	COVER			THCK	COVER		
	FACE	TYPE	AVE.	MAX	FACE	FORM	(mm)	FACE	%	(mm)	(mm)	FACE	%	FORM	(mm)	FACE	%	
MSL-6	S	IB	250	600	TO	Dense, 70%	60	OB	25						10-20	B	90	
MSL-6	S	VB	400	900	O	Dense, 80%									10-20	O	20	
MSL-6	S	IB	250	600	TO	Dense, 70%									10-20	BO	70	
MSL-6	S	LEG	300	600	O	Dense, 65%				10-20	20	O	25	Patchy				
6	S	HB	100	150	TO	Light, 40%									20-40	BI	80	
6	S	HB	100	150	TOB	Light, 25%									20-40	B	50	
6	N	HB					20-50	OB	20	10-30	20	TO	25	Patchy	10-25	TOBI	90	
6	N	HB	150	250	OB	Isolated k				10-30	20	TO	25	Patchy	10-25	TOBI	90	
6	W	HB	80	100	T	Isolated k	30-40	TO	20	10-20	20	T	20	Patchy	50-100	TOBI	80	
6	W	HB	80	100	T	Isolated k									50-100	TOBI	90	
6-9	N	LEG	100	200	N	Isolated k	30-40	N	70									
21-25							30-40	N	40						20-30	N	80	
6-20	S	IB	70	100	TO	Dense, 60%	30-40	TO	50									
20-25															90-120	TOB	90	
6-19	S	IB	100	130	TO	Dense, 60%	100	TO	40						20-60	BO	60	
19-25															90-12	TOBI	80	
25	W	HB													50-120	TOBI	100	
25	S	HB													50-120	TOBI	100	
25	S	HB													50-100	TOBI	90	

Table B.3. Platform NCNS2.

DEPTH (m)	MEMBER LOCATION		KELP/GREEN WEED				HYDROIDS			MUSSELS					SEA ANEMONES			APPROX. k/d
			LENGTH(mm)		COVER(nos/m2 OR %)		LENGTH	COVER		SIZE	THCK	COVER			THCK	COVER		
	FACE	TYPE	AVE.	MAX	FACE	FORM	(mm)	FACE	%	(mm)	(mm)	FACE	%	FORM	(mm)	FACE	%	
MSL-2	S	LEG	250	600	O	Dense, 70%				20-25	40	O	20	Patchy				
2-5			150	400	O	Light, 30%				20-25	40	O	20	Patchy	20-30	O	70	
MSL-2	S	IB	300	600	T	Light, 20%									10-20	BO	60	
2-5										15-25	20	B	10	Cluster	10-30	TOB	80	
MSL-3	S	LEG	200	500	O	Light, 30%												
3-5										20-35	40	O	70		10-30	O	60	
MSL-3	S	VB	200	400	O	Dense, 60%				20-25	40	O	40					
			100	250	O	Light, 20%				20-25	40	O	90					
MSL-2	C	IB	150	200	TOB	Light, 10%												
2-5			150	200	TOB	Light, 30%												
MSL-5	C	IB								20-30	50	TOB	85	Heavy	15-20	OB	40	
MSL-5	C	VB					20-30	TOBI	20	20-30	60	TOBI	95					
MSL-5	C	IB					20-30	TO	20	20-30	60	TO	90		15-30	B	80	
5	S	HB	200	500	TO	Light, 30%									10-20	B	80	
24	C	HB													60-120	TOBI	85	

Table B.4. Platform NCNS3.

DEPTH (m)	MEMBER LOCATION		KELP/GREEN WEED				HYDROIDS			MUSSELS					SEA ANEMONES			APPROX. k/d
			LENGTH(mm)		COVER(nos/m2 OR %)		LENGTH	COVER		SIZE	THCK	COVER			THCK	COVER		
	FACE	TYPE	AVE.	MAX	FACE	FORM	(mm)	FACE	%	(mm)	(mm)	FACE	%	FORM	(mm)	FACE	%	
12	N	HB					20-30	OBI	60	20	30	TOI	80	Strip				
12	E	HB	30	40	0,80%	Dense				15-20	25	I	90	Strip				
			30	40	1,30%	Light												
TML-12	E	.B	20	40	0,60%	Patchy				15-20	20	TO	30	Patchy				
12	HF	IB					20-30	TOBI	20	20-30	35	TOI	50	Patchy				
										15-20	20	B	20	Cluster				
38	N	HB					20-30	TOBI	100									
38	N	HB					20-30	TOBI	90									
38	N	HB					20-30	TOBI	100									
90	N	HB					10-20	TOI	40									
90-108	N	IB					10-20	TOI	30									

Table B.5. Platform NN1.

DEPTH (m)	MEMBER LOCATION		KELP/GREEN WEED				HYDROIDS			MUSSELS					SEA ANEMONES			APPROX. k/d
			LENGTH(mm)		COVER(nos/m2 OR %)		LENGTH	COVER		SIZE	THCK	COVER			THCK	COVER		
	FACE	TYPE	AVE.	MAX	FACE	FORM	(mm)	FACE	%	(mm)	(mm)	FACE	%	FORM	(mm)	FACE	%	
HSL-16	N	IB	100	200	10,60%	k:5-10/m²												
HSL-5	N	VB	100	200	10	Isolated k				20	25	TO	80	Dense				0.015
HSL-9			100	300	1	Isolated k												
6-16							20-40	TO	50	20	25	TO	60	Dense				
6-16							20-80	1	90			1	60	Dense				
HSL-16	N	IB	150	200	TO	Isolated k	20-60	TO	60									
3-9	N	LEG	200	350	N	Isolated k												
16	S	HB	30	50	10,60%	Dense GW	20-60	OB	70	10-20	20	T	70	Dense				0.016
16-40							20-50	1	50	10-20	20	1	60	Dense				
16-48	S	LEG					20-60	S	90	10-20	15	S	10	Cluster				
24-28	S	IB								10-20	20	O	80	Strip				0.01
28-45	S	IB					30-80	TOBI	100									
81							20-50	TOBI	60						20-30	OB	5	
81-110	S	HB					20-40	TOB	80						20	O	2	
	S	IB					20-40	TOBI	90									

Table B.6. Platform NN2.

APPENDIX C. Preparation of Macro-roughened Test Cylinders

Each PVC cylinder was lightly abraded using a disc sander to provide a key for better adhesion of marine growth or artificial roughness. In the case of partially roughened cylinders, a grid of 150mm squares was drawn on the cylinder surface to facilitate the build-up of the desired roughness density through the pseudo-random positioning of roughness patches of arbitrary size and shape. In this way accurate repetition of the same pseudo-random pattern with both fouling and sand was achieved as shown in Figure C.1. Thus, direct correlation between the two types of roughness was possible.

The preparation of test cylinders with either circumferential roughness strips or full cover was less complicated. The former were roughened by two strips of mussels, kelp or gravel, each 150mm wide and located 150mm away from each free cylinder end (Figures C.2-C.3).

C.1. Sand roughness

For fully roughened cylinders, graded sand or gravel chips were glued onto the cylinder to achieve a uniform single layer of roughness. A thin layer of polyester resin was applied to the cylinder surface onto which sand was gradually poured, any excess being shaken off after the resin had set. Typical sand roughened cylinders are shown in Figures C.4 and C.5. The mean height and standard deviation of grains were estimated from a random samples of 30. The roughness measurements are summarised in Appendix D.

Design of End-Plates

To examine the three-dimensional flow effects, rectangular plates were fitted to a 150mm diameter perspex cylinder (Figures C.6 and C.7). The principal dimensions of the end plates, shown in Figure C.8, were adopted from optimisation experiments by Stansby [109] and were as follows:

a) Width of end plate = 6D
b) Distance from cylinder axis to trailing edge of plate = 4.5D
c) Distance from cylinder axis to leading edge of plate = 2.5D.

The leading edge of the plates was chamfered to streamline the flow. Two longitudinal stiffeners were fitted on each plate to prevent distortion and an aluminium strap was recessed along the off-side face, as illustrated in Figure C.7. The straps were strain gauged, at the locations shown in Figure C.8, for measuring the force difference across the test cylinder in the manner described in Chapter 7. The end plates were fixed to the cylinder by means of a threaded rod spanning the logitudinal cylinder axis. The cylinder was fitted with end caps which were recessed into the plates leaving a clearance of 1-2mm around the circumference. Some calibration runs were carried out with the gaps sealed to prevent leakage of flow, but no effect was discernible on drag forces.

C.2. Mussels

Cylinders with mussel roughness were prepared in two ways:

a) To obtain a single layer of live mussels fast setting epoxy resin was used which gave a good bond with a small amount of glue. The mussels were placed in random relative orientations but always with the foot close to the cylinder surface. After testing at a lower percentage cover, each mussel cluster was further built up to achieve a higher overall surface cover thus simulating typical colonisation patterns. Figure C.9 shows a cylinder fully covered by a single layer of mussels.

b) For multiple layers of mussels a different technique was adopted where the attachment mechanism of the mussels was exploited (see Appendix A). A cylinder which had a diameter of 200mm was placed in a mesh bag of live mussels such that the mussels covered the entire outer surface. The bag was left in the Gareloch (sea water) on the west coast of Scotland for several weeks until the mussels had attached themselves naturally on the cylinder by their byssus threads. The mesh bag was removed before the cylinder was tested. It is important to note that the mussels whilst they covered the cylinder, were not uniformly distributed in a layer of constant thickness. In fact, overall thickness varied from one to five or six layers resulting in a mean increase in diameter of 42% or 85mm. In practice this is how they form dense colonies on North Sea structures; in clumps which gradually merge rather than as one

uniformly distributed layer.

After the first set of tests, half the mussels were removed leaving patches of about the same area as the cross section of the cylinder (Figure C.10). The density was again reduced after further tests and the cylinder was finally tested at 25% cover. The distribution of mussels at reduced coverage simulated that observed on mussel dominated North Sea platforms.

Live mussels were obtained from two sources; a mussel farm and a beach in the west coast of Scotland. The latter had barnacle encrusted shells. Both were of the species **Mytilus edulis** which is most commonly encountered in the North Sea. A random sample of 30 was taken from each batch per cylinder and the height, breadth and length were measured. The mean dimensions and standard deviations of the batches are given in Appendix D.

C.3. Kelps (Long flapping seaweeds)

Two kelp species were tested; the kelp **Laminaria digitata**, a common species found on offshore installations, and the kelp **Laminaria Saccharina** usually encountered in sheltered waters (Figure C.11). Both types are described in Appendix A. The kelp plants were collected from the floating pontoons and breakwaters of Rhu Marina on the Clyde estuary. They were carefully scraped off the substrate to preserve their rooting system (holdfast) intact which was cleaned off any parasitic fouling.

After being wiped dry the holdfast of each plant was embedded in a thick layer of fast setting epoxy resin and stapled onto the cylinder. The kelps were distributed such that there were no significant gaps between the holdfasts of adjacent plants. The collection, preparation and testing of kelp roughened cylinders were completed within one to two days per cylinder due to the short life of the species under laboratory conditions. Unlike hard fouling which is more robust, kelp dies in fresh water and its elasticity and "flapping" action alter; factors considered to be important to its hydrodynamic behaviour.

The experimental programme with kelp roughened cylinders included tests with pseudo-randomly distributed patches of approximately 1m long kelp at the percentage surface covers denoted in Chapter 7, Table 7.2. After the build up to 100% cover the plants were cut down to approximately 0.5m and tested in that condition. The surface cover was reduced to 50% for further tests by scraping off some plants and finally to 25%. One set of tests was carried out at 25% cover by kelp stipes about 250mm long after the fronds of the plants had been cut off. Measurements of kelp samples are given in Appendix D.

Throughout the cylinder preparation and testing, care was taken to distribute the kelp plants in roughly equal amounts over the cylinder to avoid large transverse forces induced by non-symmetrical roughness.

C.4. Sea anemones

The sea anemones, predominantly of the species **Metridium senile**, were obtained from a floating pontoon at Garelochead (west coast of Scotland). They were carefully scraped off and transferred to the test cylinder. They were placed along the top surface of a horizontal cylinder which was fixed a few centimetres beneath the water surface in a wire cage and allowed to attach naturally over a period of a day or two. The cylinder was then rotated a few degrees and the new top surface covered with more sea anemones. This process was repeated several times until cover extended over the whole surface. Unfortunately not all the sea anemones remained on the cylinder and several migrated on the wire cage reducing the uniformity of the cover.

The test cylinder shown in Figure C.12, was prepared over a period of several weeks and transported to the laboratory in a sea water tank. The sea anemones did not survive the fresh water of the test tank although they were kept in aerated sea water both before and after the tests. For this reason just one 400mm diameter cylinder was tested at two pecentage covers.

The height and diameter of sea anemones alters when they are disturbed (see also Appendix A). In fact they contracted when attempts were made to measure them and also when they were transferred into fresh water. When contracted the sample on the cylinder had the following

characteristics:

	Height (mm)	Diameter (mm)
Mean	60	70
Range	30-80	30-70

It should be pointed out that the measurement of sea anemones was found to be difficult and the above values may contain errors.

C.5. Naturally Accumulated Mixed Fouling

Several abraded PVC cylinders were deployed in the Clyde Estuary and the West coast of Scotland at various depths in areas renowned for rapid development of fouling. The objective was to accumulate various types of marine growth and test at regular intervals.

Tests were carried out with three cylinders having six-month accumulated growth. One cylinder was covered with sea anemones and sea squirts and the other two were partially covered with barnacles, green seaweed and clumps of very small mussels (Figures C.13 and C.14). All cylinders had been deployed in a horizontal attidude and the roughness distribution around their circumference was not uniform. These distributions are depicted in Figure 8.24, Ch. 6. Similar distributions are encountered on North Sea structures during the first few years of their in-service life (see Ch. 6 and Appendix B).

The sea anemones and tunicates covered about 70% of the cylinder and were largely concentrated in two diametrically opposite strips. The sea anemones ranged in size from 20mm to 80mm and the tunicates from 30mm to 60mm with an average of 50mm. The barnacles and soft fouling covered about 45% and 35% of the other two cylinders respectively. The fouling formed a continuous layer of 24mm average thickness in the areas of cover whilst individual specimens of barnacles averaged 8mm in height. The soft green weeds **ulva** were sparcely distributed on top of the barnacles with some fronds up to 200mm long. Following the tests these cylinders were returned to the sea to allow marine fouling to develop further.

C.6. Pyramid Roughness

The cylinders tested in steady flow were prepared using vacuum formed polystyrene panels of square based pyramids in regular arrays as shown in Figure C.15. The panels were glued on 1500mm long fibreglass sleeves which had been cast from 400mm diameter cylinders. The detachable sleeves were fastened on the test cylinder by means of rivets. The rivets were running along the perimeter at both cylinder ends and also along the longitudinal seam of the sleeve. Care was taken to position the seam along the trailing cylinder edge to minimise possible minor roughness effects by the rivets.

Two pyramid sizes were used, both with 40mm x 40mm bases and with heights of 40mm and 20mm respectively. Roughness density was therefore kept constant at 505 pyramids per square metre.

C.7. Anti-fouling cladding

Two versions of a proprietary make of retrofit copper-nickel based anti-fouling cladding were fitted on 400mm diameter test cylinders. The first had simple aluminium angle sections attached to opposite edges of the flexible panel. These were bolted together on a rubber gasket to form a joint when the panel was wrapped around the cylinder as shown in Figure C.16. The second version had a faired joint with recessed bolts (Figure C.17).

The antifouling panels were initially attached to the 1500mm long cylinder in two 750mm lengths. Each cylinder with a full length joint was tested in three orientations; at $\theta=0^{\circ}$, 90° and 180° as defined in Figure 8.31(a), Ch. 8. With the joint at $\theta=90^{\circ}$, considerable transverse forces were generated due to body asymmetry. The transverse force was eliminated by splitting the panels in four equal segments and positioning the joints of two segments at either end quarter of the cylinder at $\theta=90^{\circ}$ and the joints of the segments spanning the middle half at $\theta=270^{\circ}$. Tests were also undertaken with the non-faired joints on four panel segments located at the pseudo-random orientations depicted in Figure 8.31(b), Ch.8. The particulars of the anti-fouling panels are summarised in Appendix D.

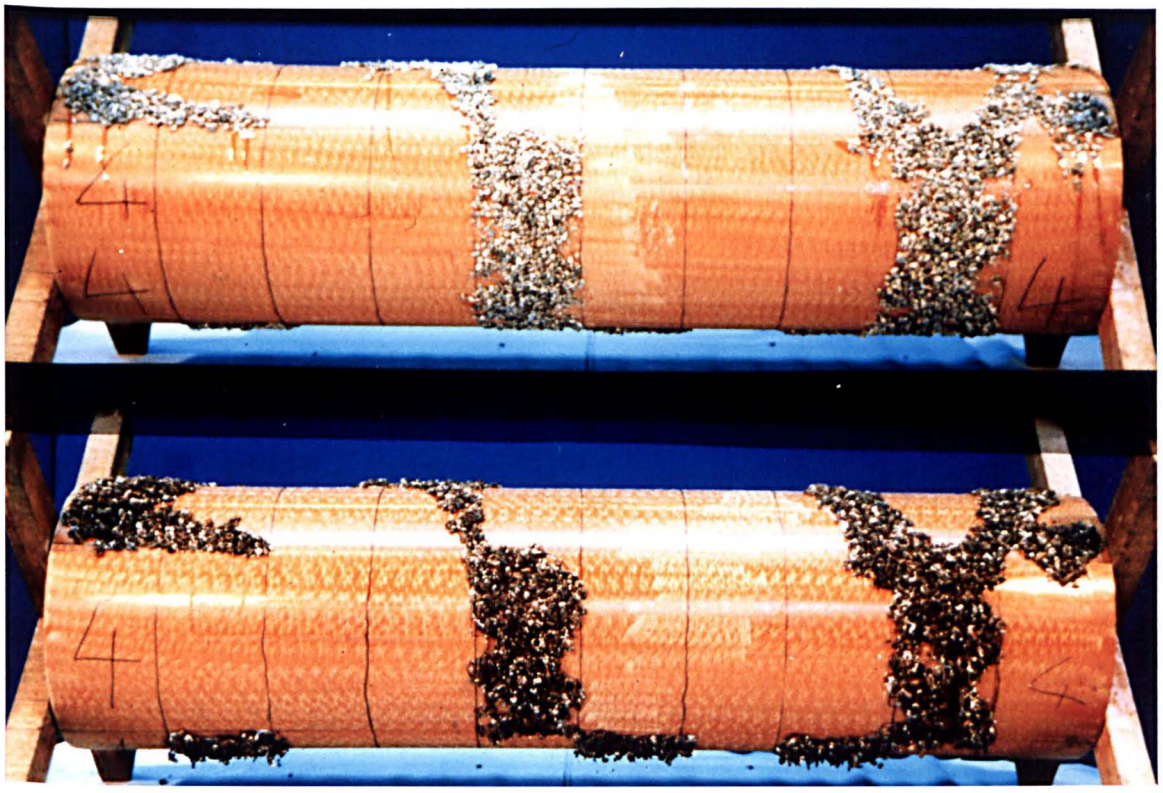

Fig. C.1. Partially covered cylinders by mussels and gravel.

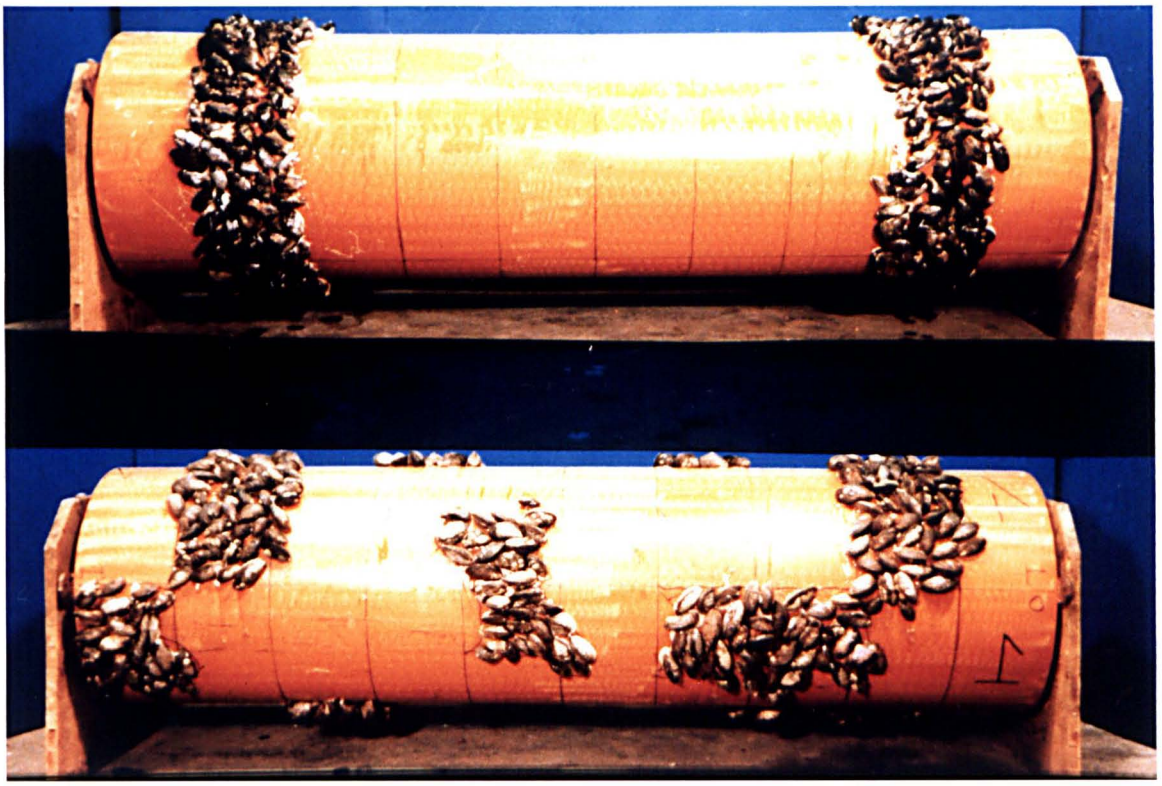

Fig. C.2. Cylinder covered by circumferential strips of mussels.

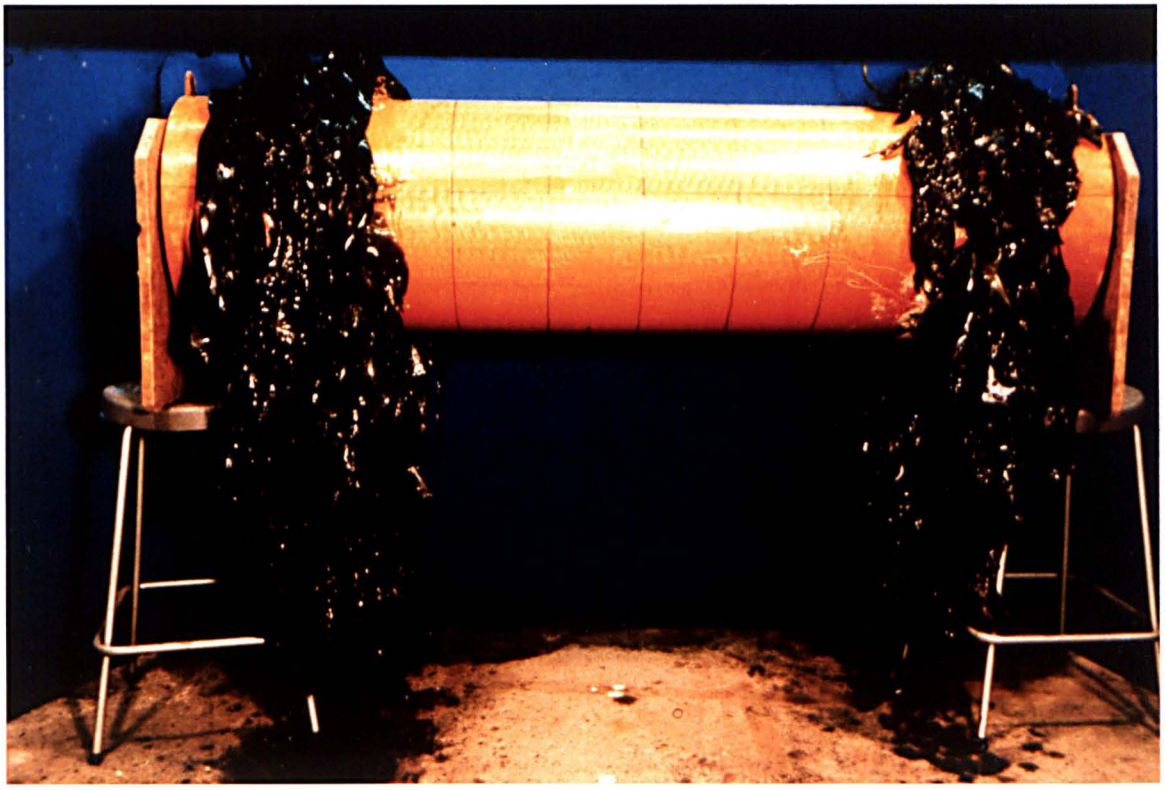

Fig. C.3. Cylinder covered by circumferential strips of kelp.

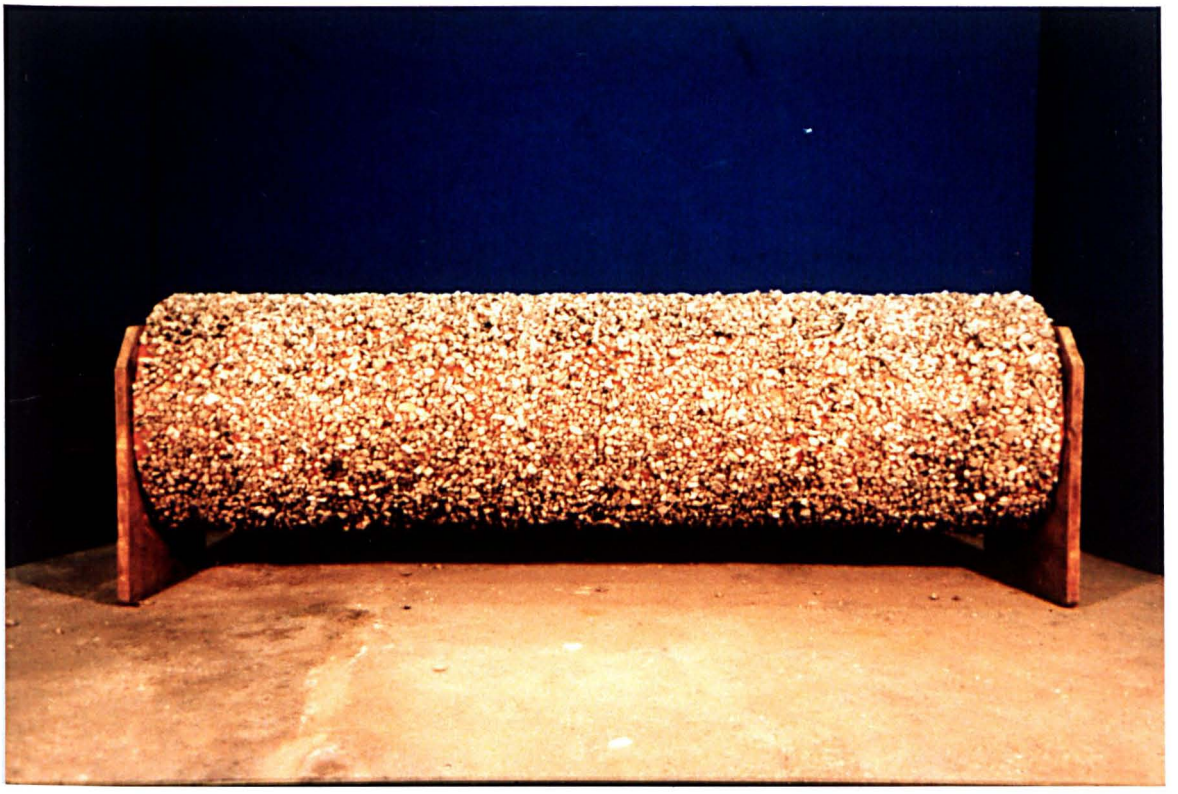

Fig. C.4. Sand roughened cylinder (k=10mm).

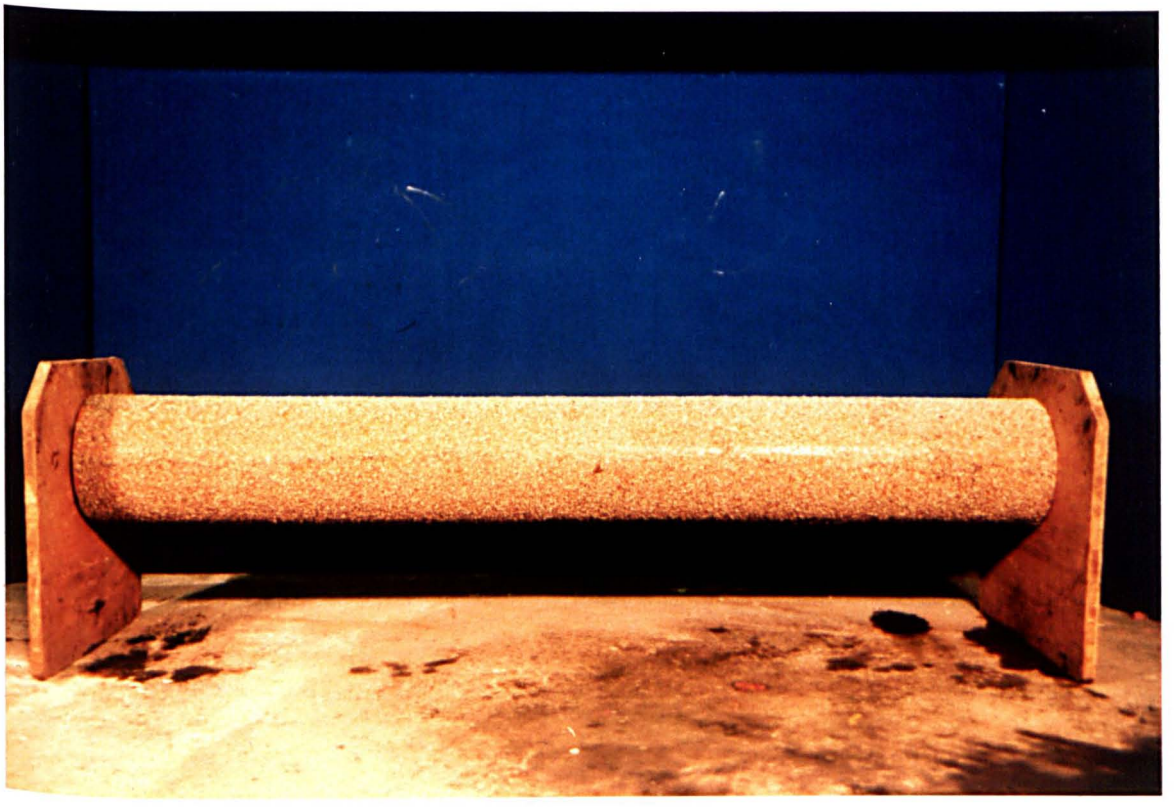

Fig. C.5. Sand roughened cylinder (k=2mm).

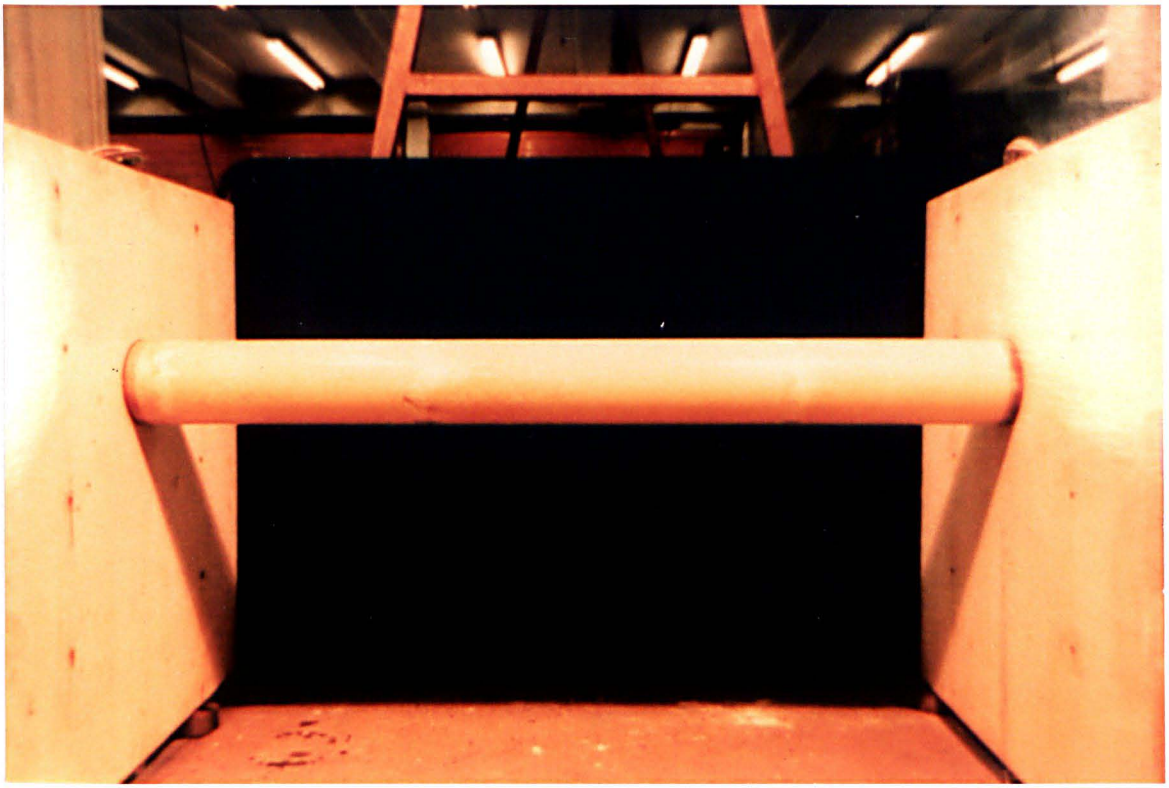

Fig. C.6. 150mm dia. rough cylinder fitted with end plates.

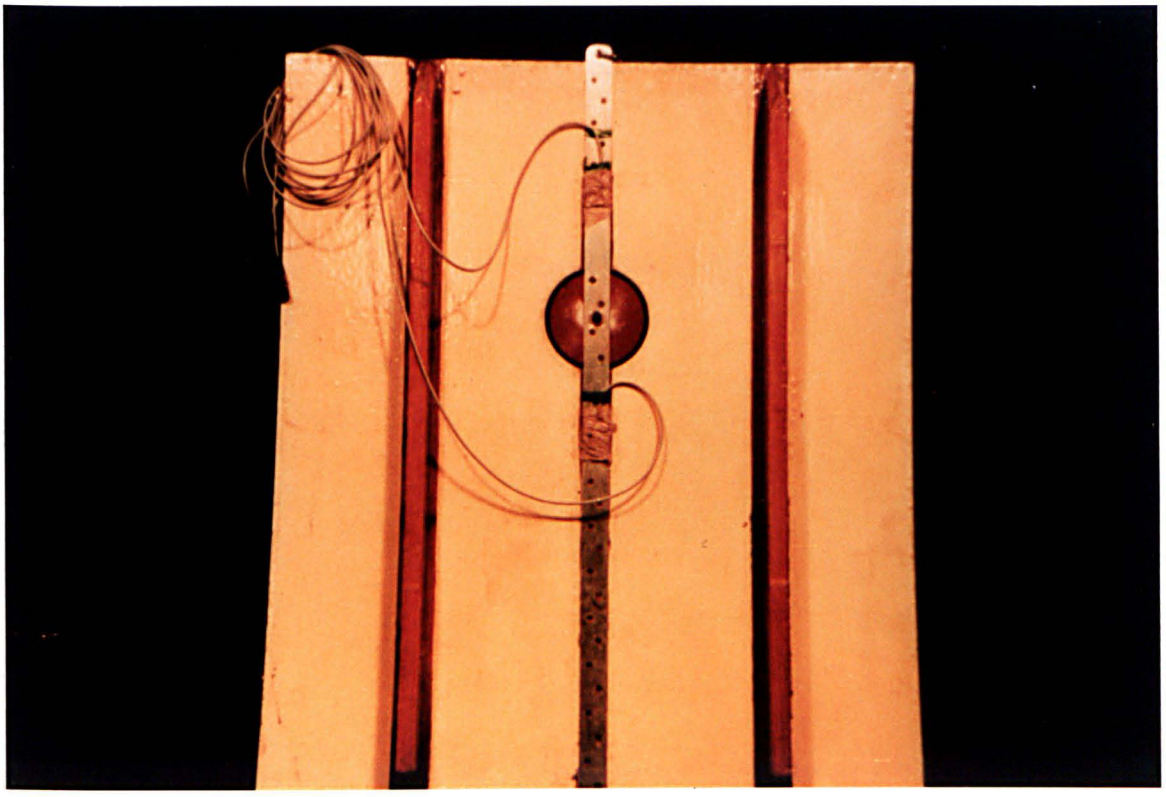

Fig. C.7. Back view of end plate showing strain gauged transducers.

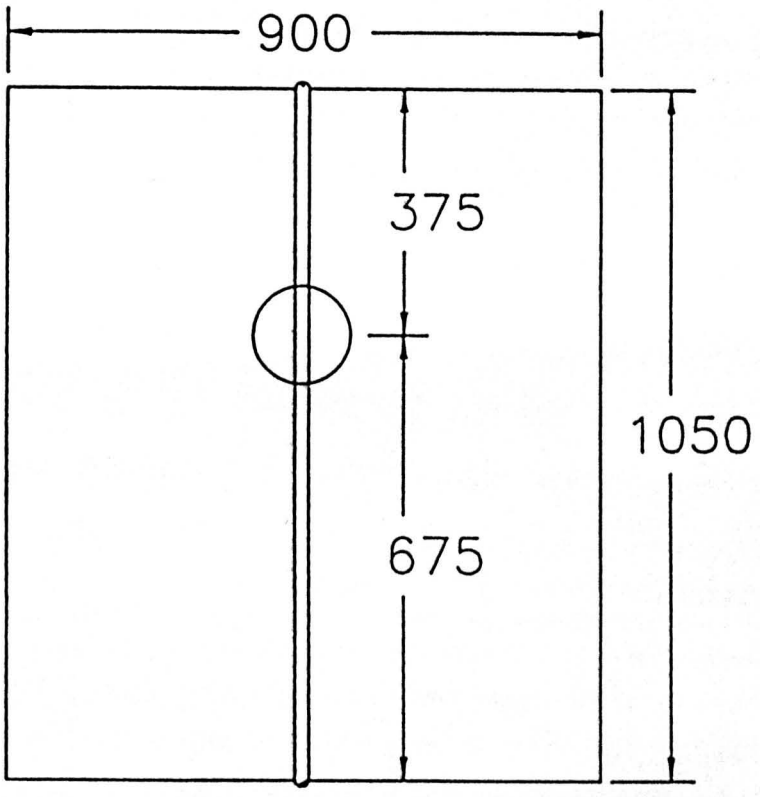

Fig. C.8. The geometry of the end plates.

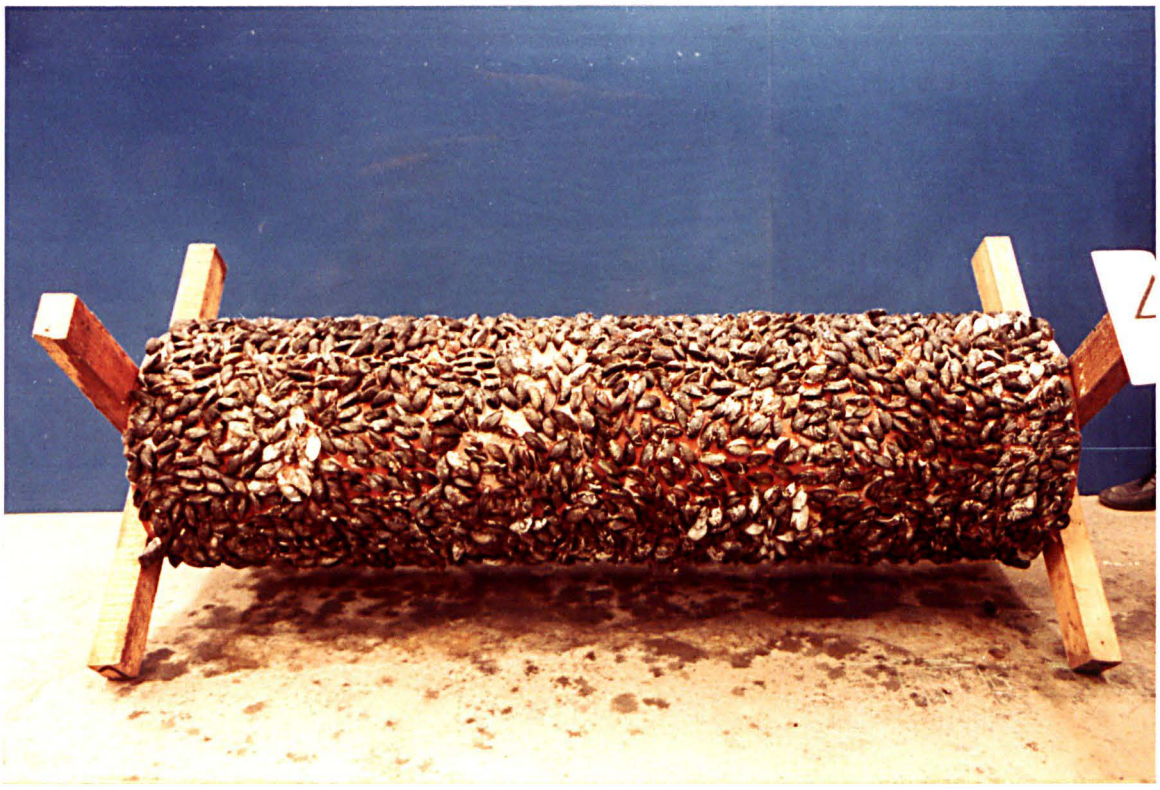

Fig. C.9. 400mm dia. cylinder covered with single layer of mussels.

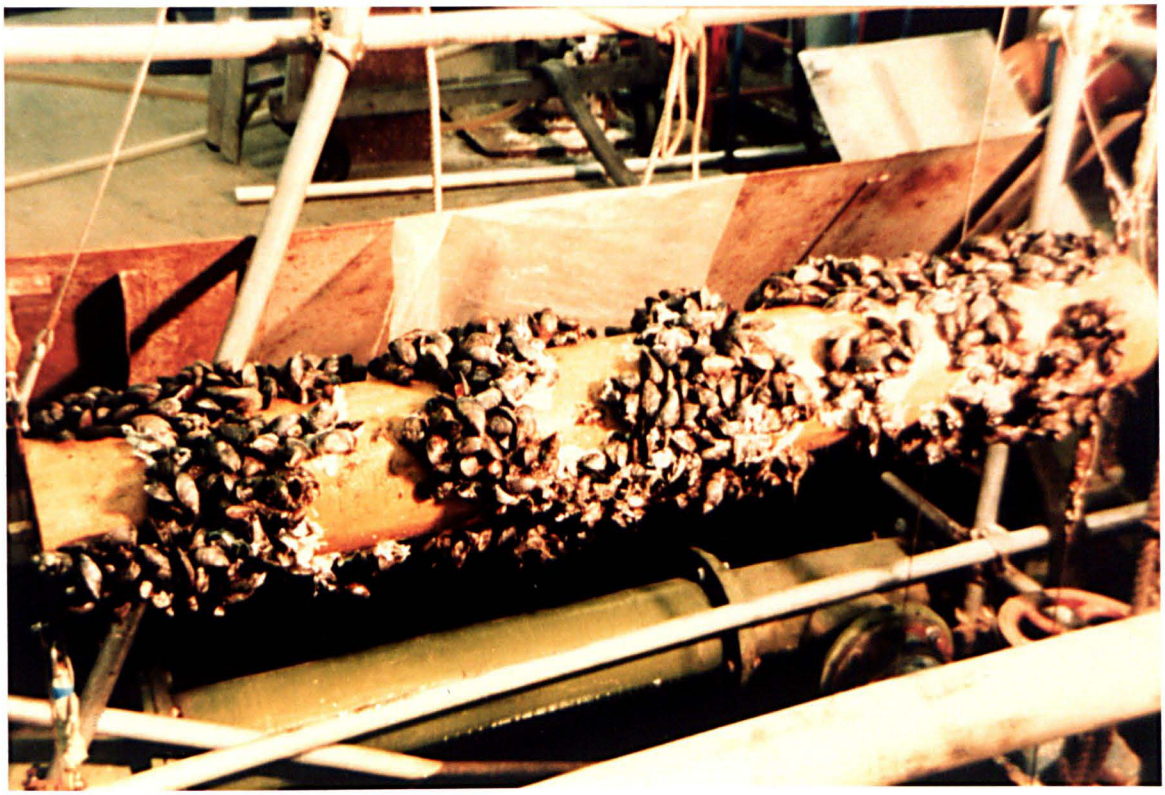

Fig.C.10. Multiple layers of mussels at 50% surface cover.

Fig. C.11. Fully covered cylinder with the kelp L. saccharina.

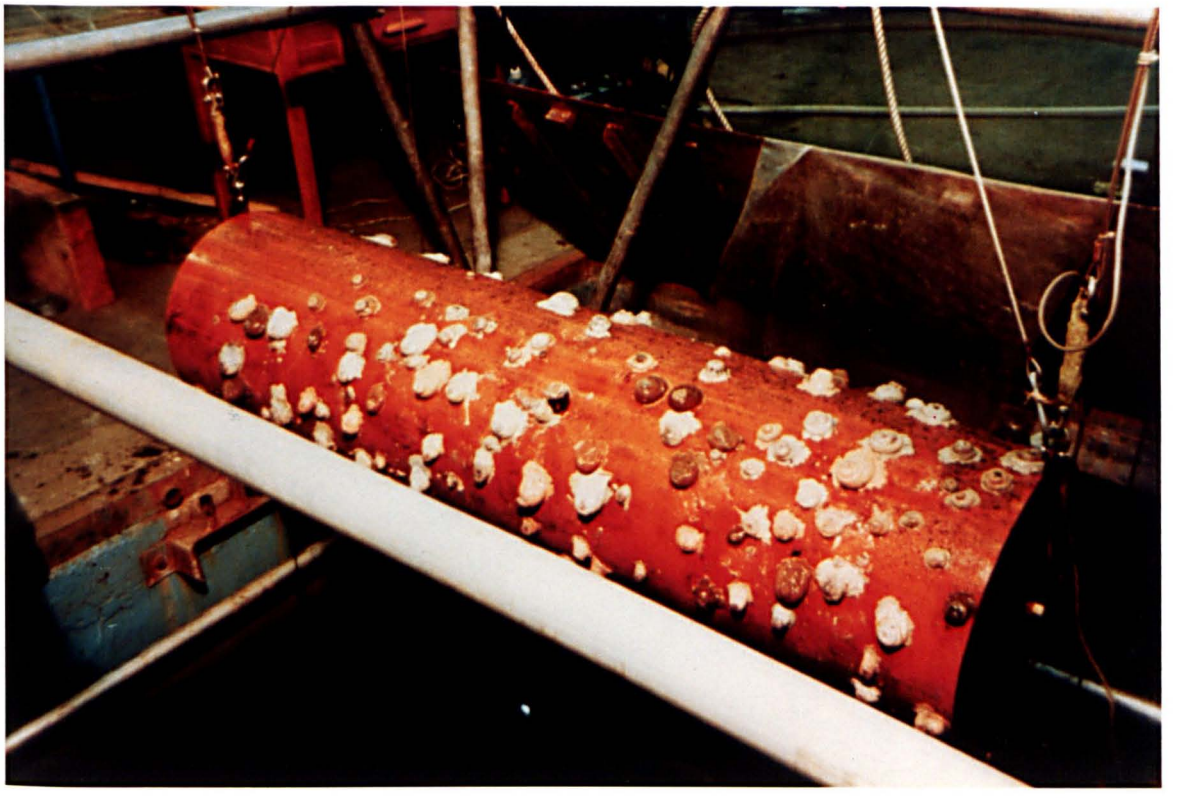

Fig. C.12. Test cylinder partially covered with sea anemones.

Fig. C.13. Strip roughness of mixed hard and soft fouling on 400mm dia. cylinder.

Fig. C.14. Sea anemones and tunicates on 315mm dia cylinder.

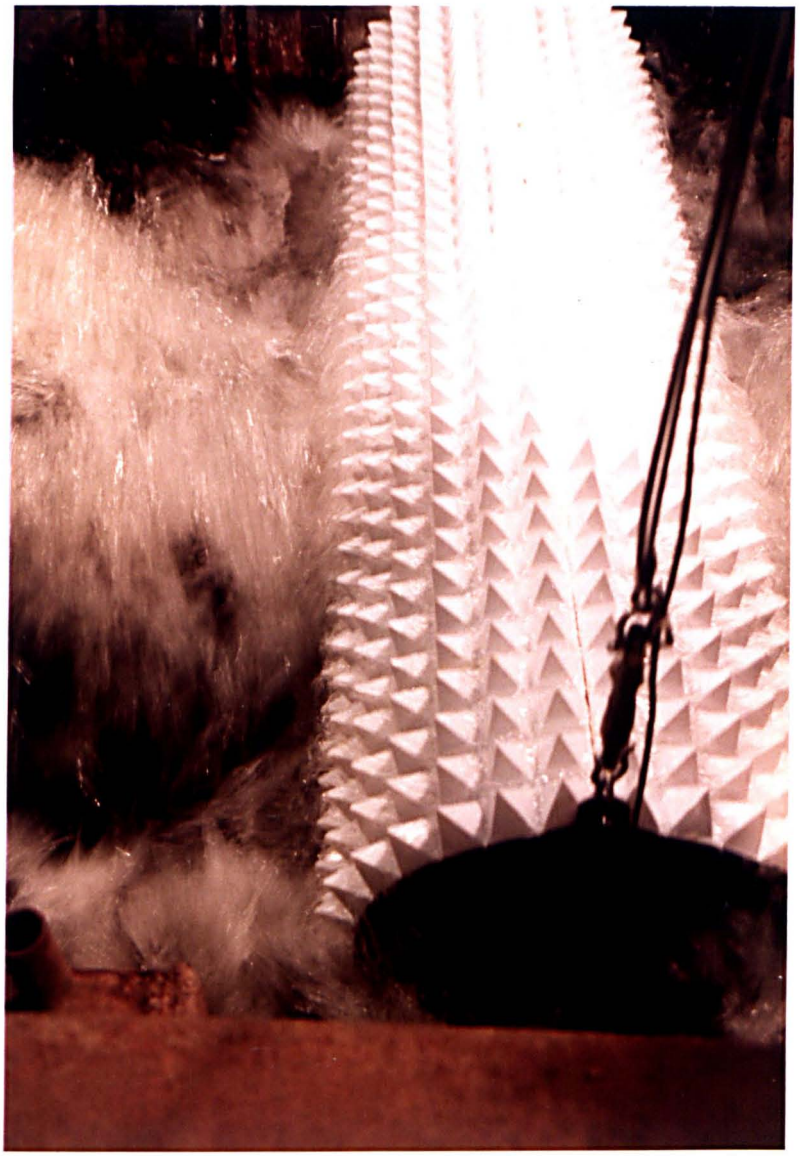

Fig. C.15. Regular arrays of pyramid roughness (k=40mm).

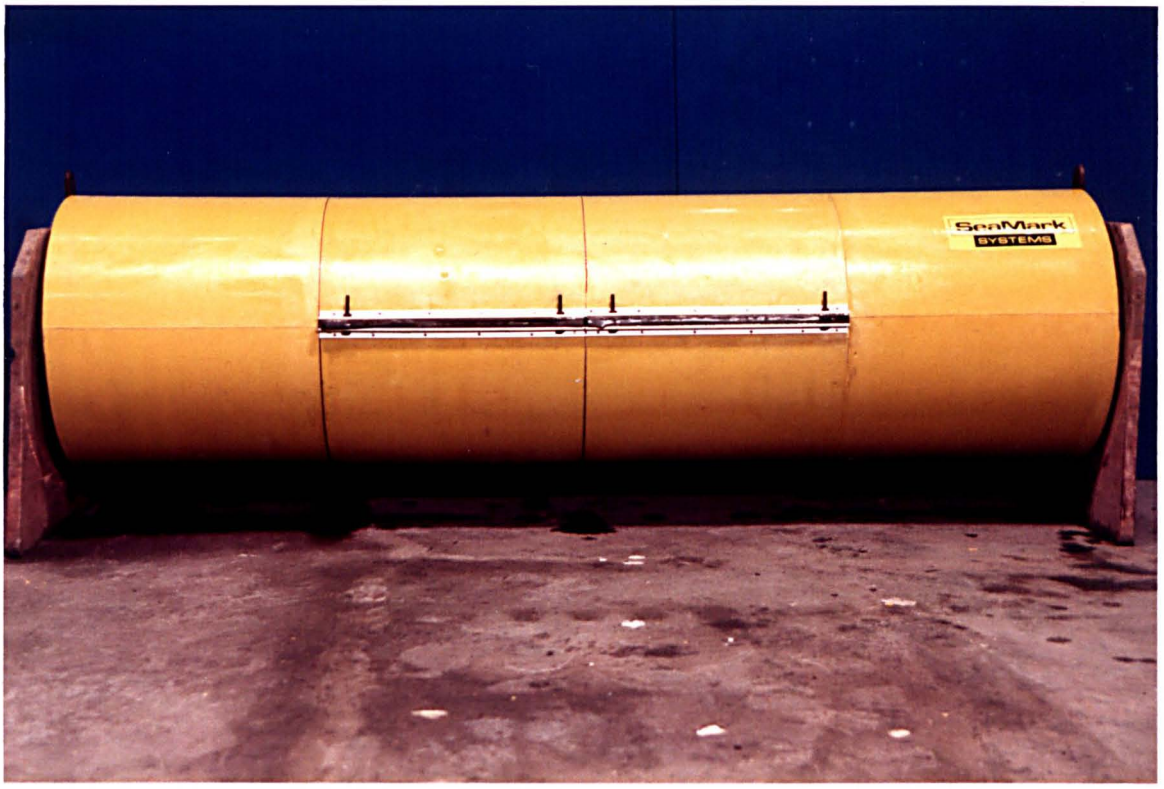

Fig. C.16. Antifouling cladding fitted with aluminium angle joints.

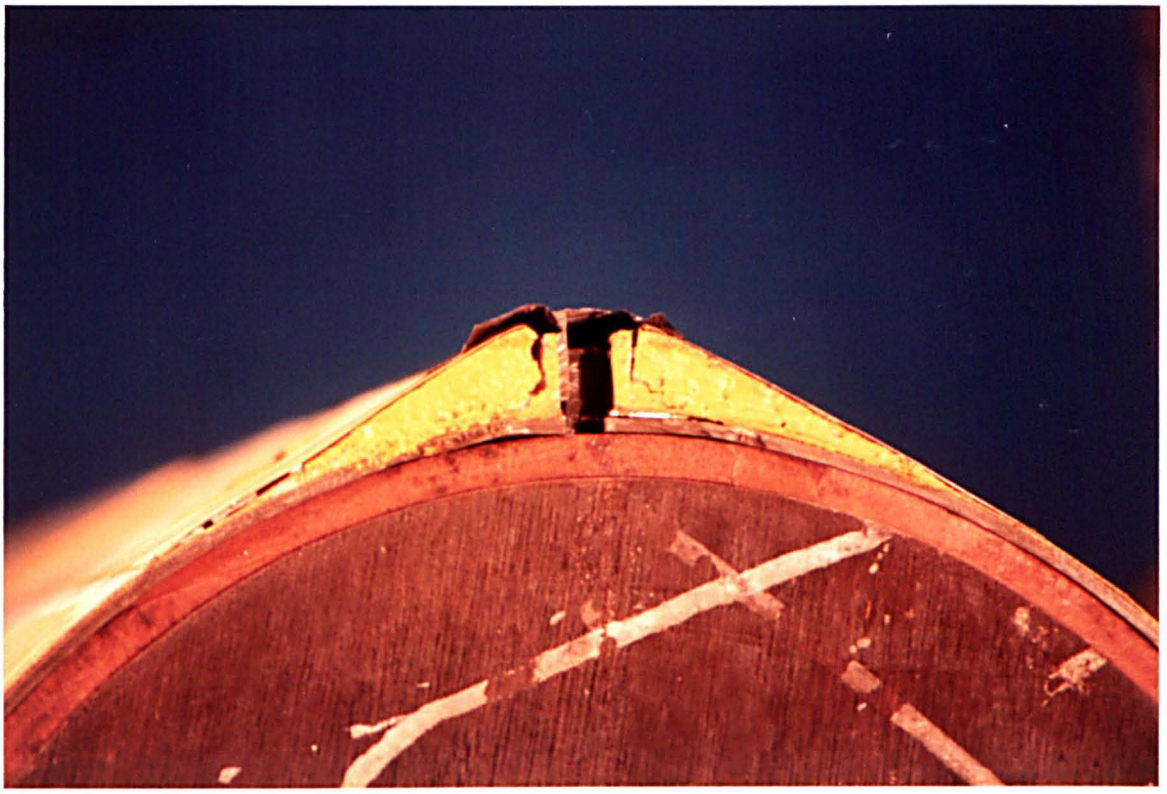

Fig. C.17. Faired joint of antifouling panel.

APPENDIX D. Roughness Measurements

Type	Mean (mm)	Standard Deviation (mm)	Coefficient of Variation (%)
Midross sand			
- sample A	1.48	0.36	24.0
- sample B	1.94	0.31	16.0
Paving stone	3.9	0.80	20.0
Gravel			
- sample A	7.53	1.41	15.1
- sample B	8.05	0.77	9.5
- sample C	9.9	1.28	13.0

N.B. Sample population N=30

Table D.1 Mean height of sand and gravel roughness.

Mussel Sample	Height (mm)		Length (mm)		Breadth (mm)	
	Mean	s.d.	Mean	s.d.	Mean	s.d.
A	7.9	1.3	14.5	2.6	5.9	1.2
B	24.0	2.3	40.0	4.7	17.6	2.0
C	26.0	2.1	47.0	4.7	21.0	2.6
D	27.0	5.1	53.0	2.6	27.0	2.8
E	29.5	2.5	53.0	4.3	24.0	2.3
F	34.0	2.4	58.5	4.0	26.0	1.4

N.B. Sample population N=30

Table D.2 Mean dimensions of mussels.

N	Kelp length (cm)	Kelp width (cm)	Stipe length (cm)	Number of blades
1	92	20	4	16
2	106	12	11	6
3	110	8	21	2
4	106	6	19	1
5	96	11	13	3
6	98	6	16	1
7	107	30	14	30
8	114	18	8	3
9	83	15	6	4
10	124	27	26	5
11	96	15	10	8
12	86	15	14	6
13	98	24	14	15
14	86	13	6	7
15	104	15	10	7
16	100	26	13	11
17	104	18	20	10
18	100	24	14	28
19	107	18	11	13
20	83	11	11	4
21	89	11	6	9
22	101	16	11	18
23	94	14	15	16
24	84	19	17	6
25	117	24	20	20
26	84	17	9	16
27	99	20	16	26
28	103	20	12	11
29	100	18	10	10
30	111	20	12	13
Mean	99.4	17.1	12.6	11
S.D.	10.5	6.1	5.0	7.8
c.o.v.	10.6%	35.7%	40%	71%

Table D.3 Sample of the kelp **Laminaria Digitata.**

Kelp Sample	Surface Cover (%)	Length (cm) Mean	s.d.
L. Digitata	100	99.4	10.5
	100	54.4	8.1
L. Saccharina	100	103.0	22.2
	50	98.0	20.3
	25	93.0	17.1

N.B. Sample population N=30

Table D.4 Summary of length measurements of kelp plants.

Particulars of Antifouling cladding

Panel thickness = 4.5mm
Total height of Al angle joint from base = 25mm
Width of Al angle joint = 8mm
Maximum height of streamlined joint from base = 31mm
Mesh roughness height [99] = 0.03-0.04mm
Mesh size (square woven) [99] = 20 x 20

APPENDIX E: Instrumentation and Sample Outputs of 'Buoyant Cylinder' Experiments

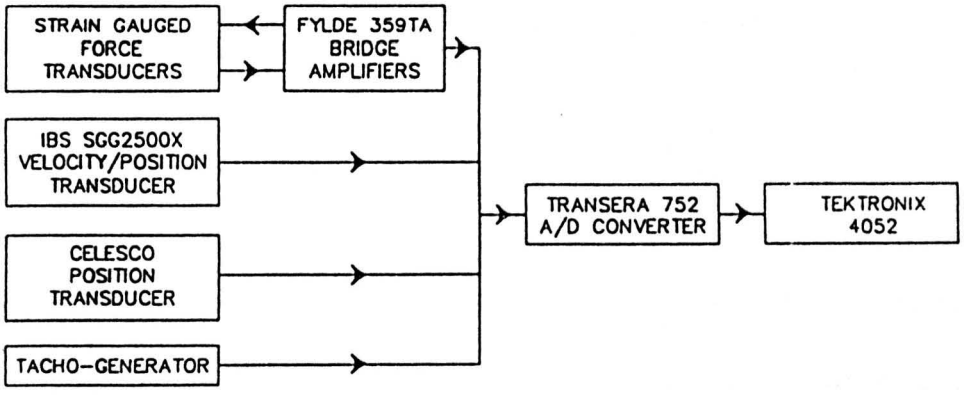

Fig. E.1. Test rig instrumentation.

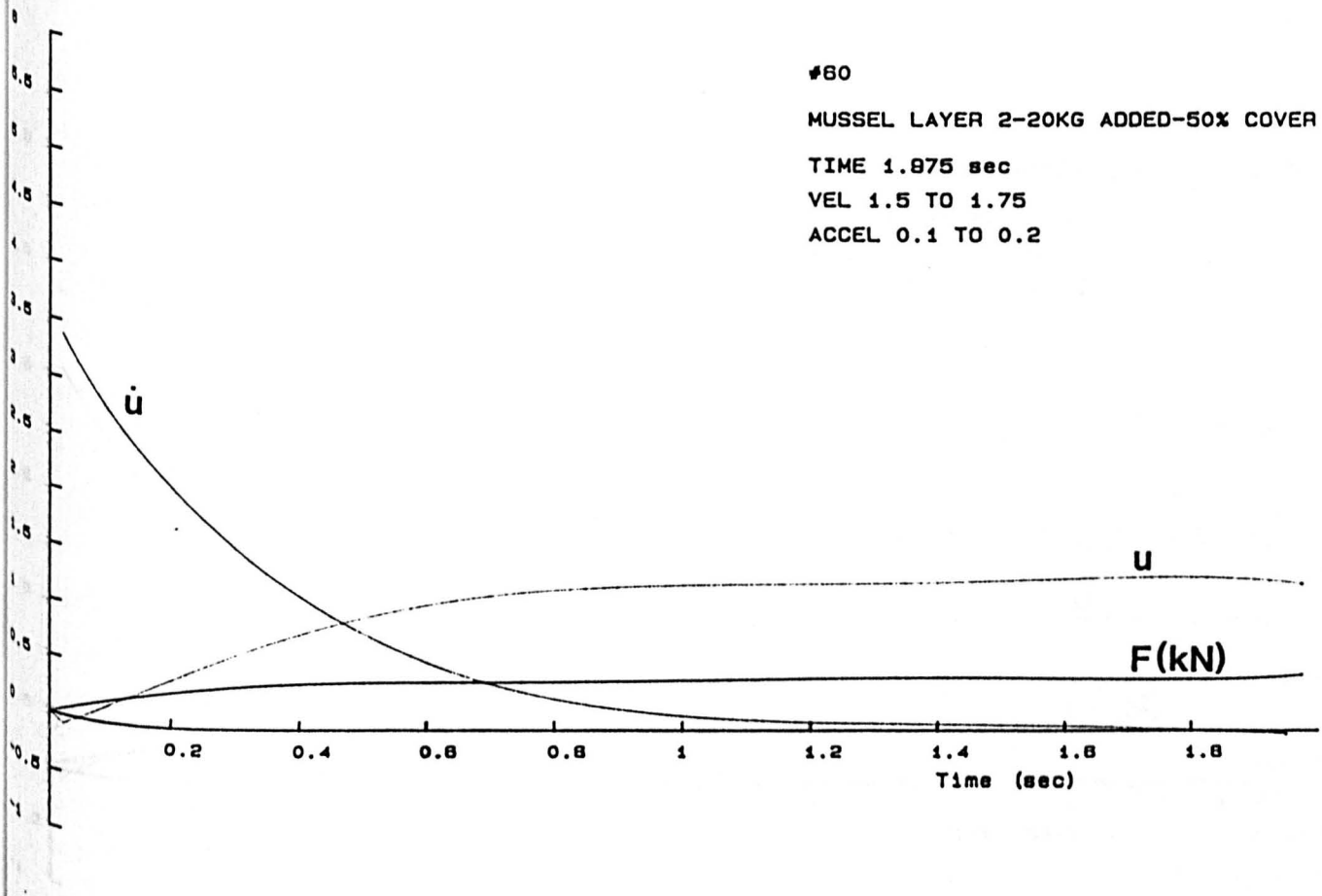

Fig. E.2. 200mm dia. cylinder - Re = 2.37×10^5.

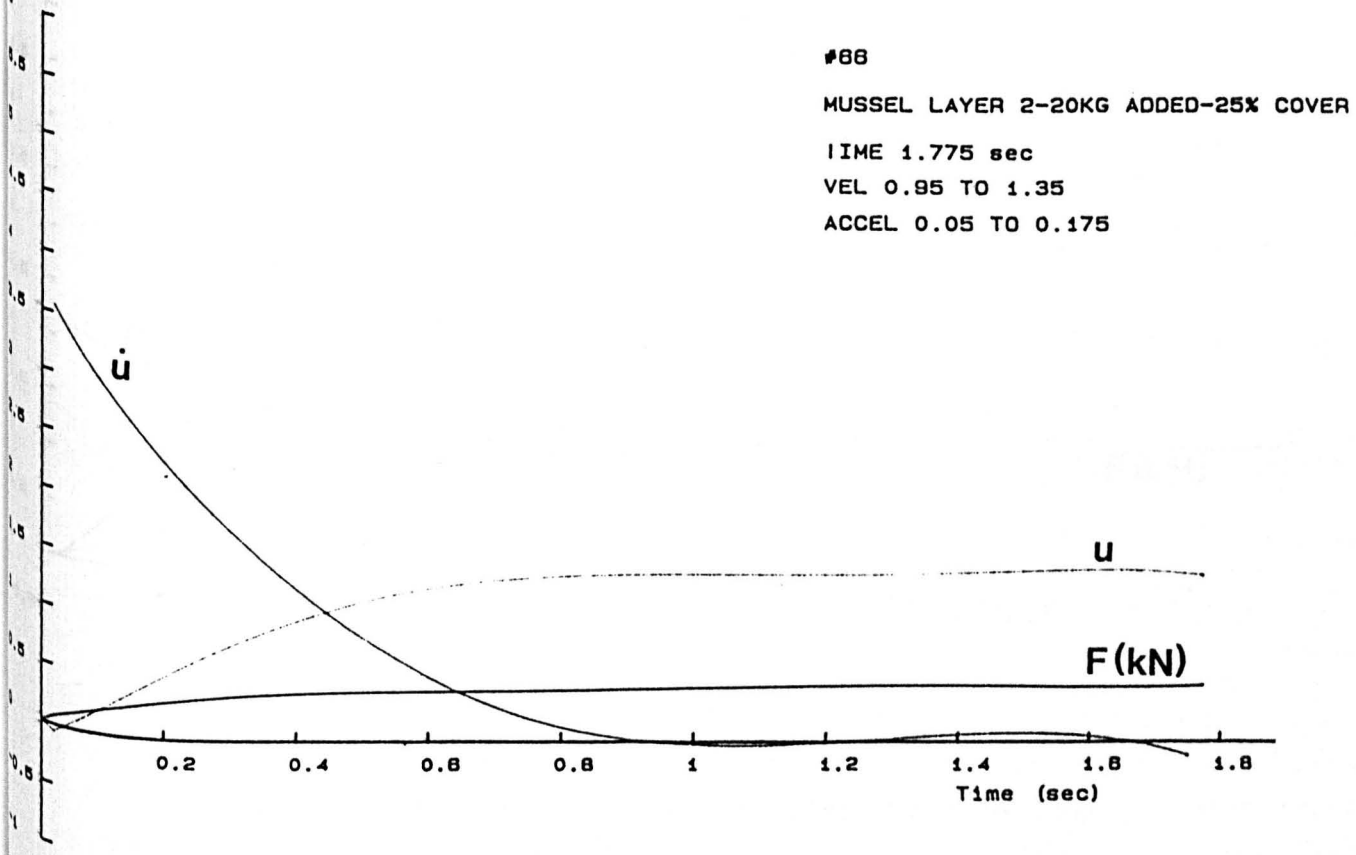

Fig. E.3. 200mm dia. cylinder - Re = 2.5×10^5.

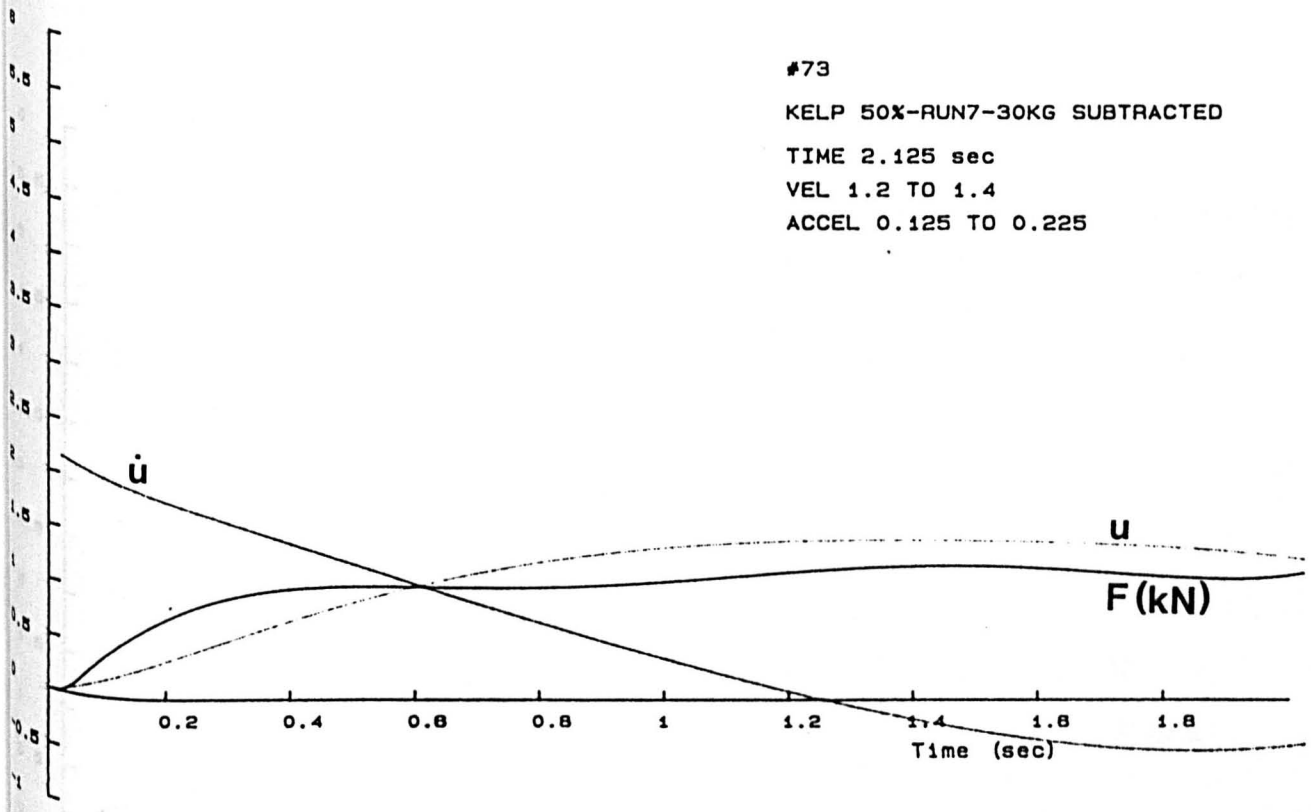

Fig. E.4. 400mm dia cylinder - L. digitata, 0.5m long
Re = 5.16×10^5.

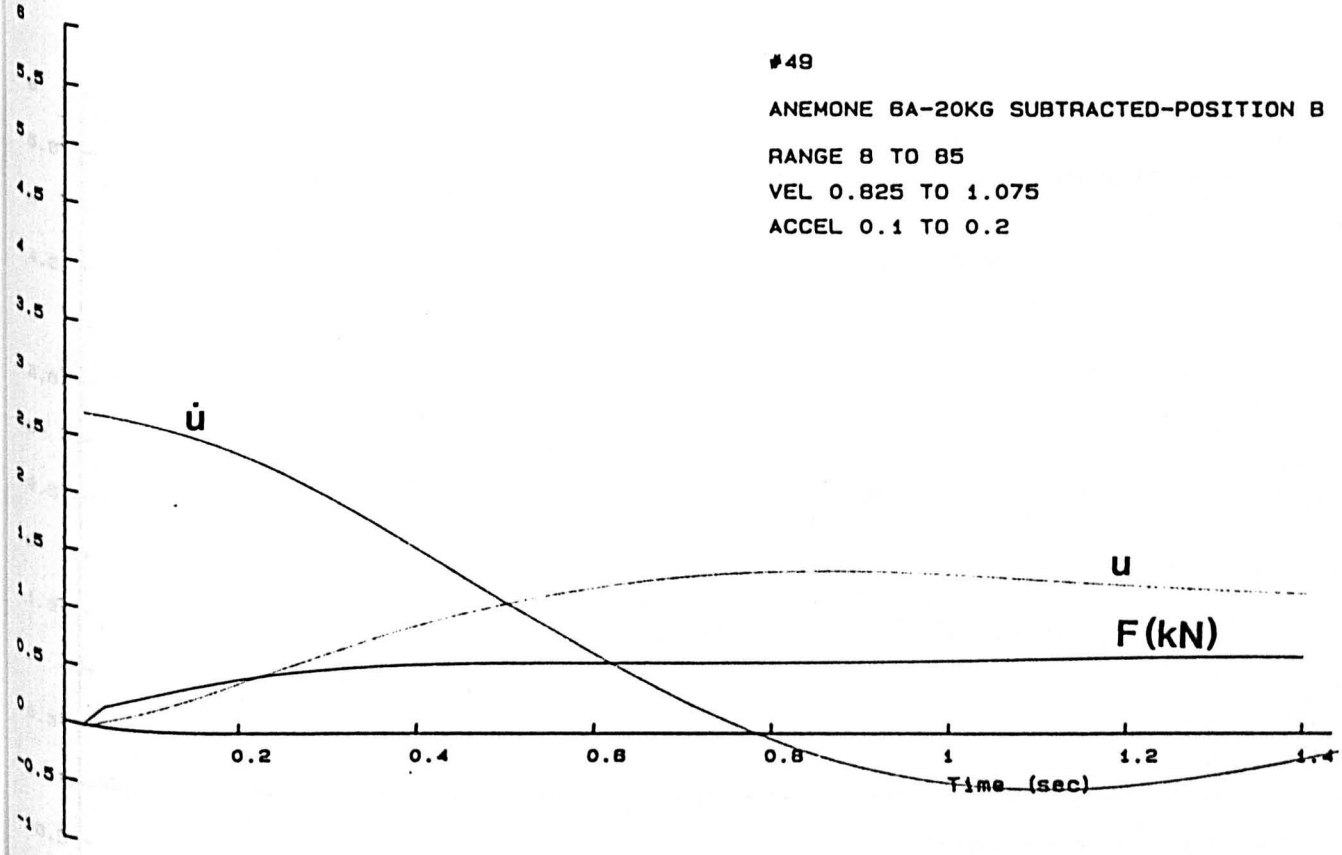

Fig. E.5. 315mm dia cylinder - mixed soft growth along cylinder top and bottom faces - Re = 3.89×10^5.

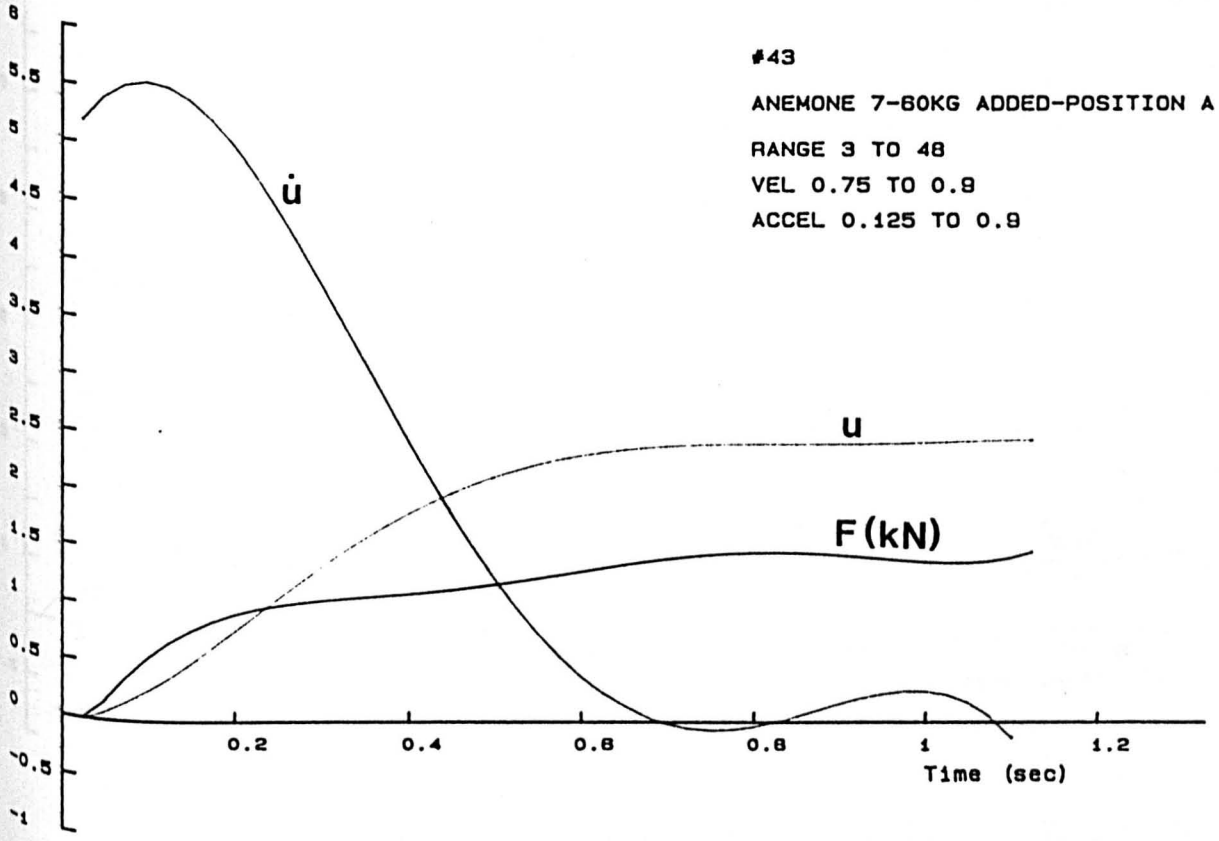

Fig. E.6. 315mm dia cylinder - mixed soft growth along cylinder sides - Re = 6.78×10^5.

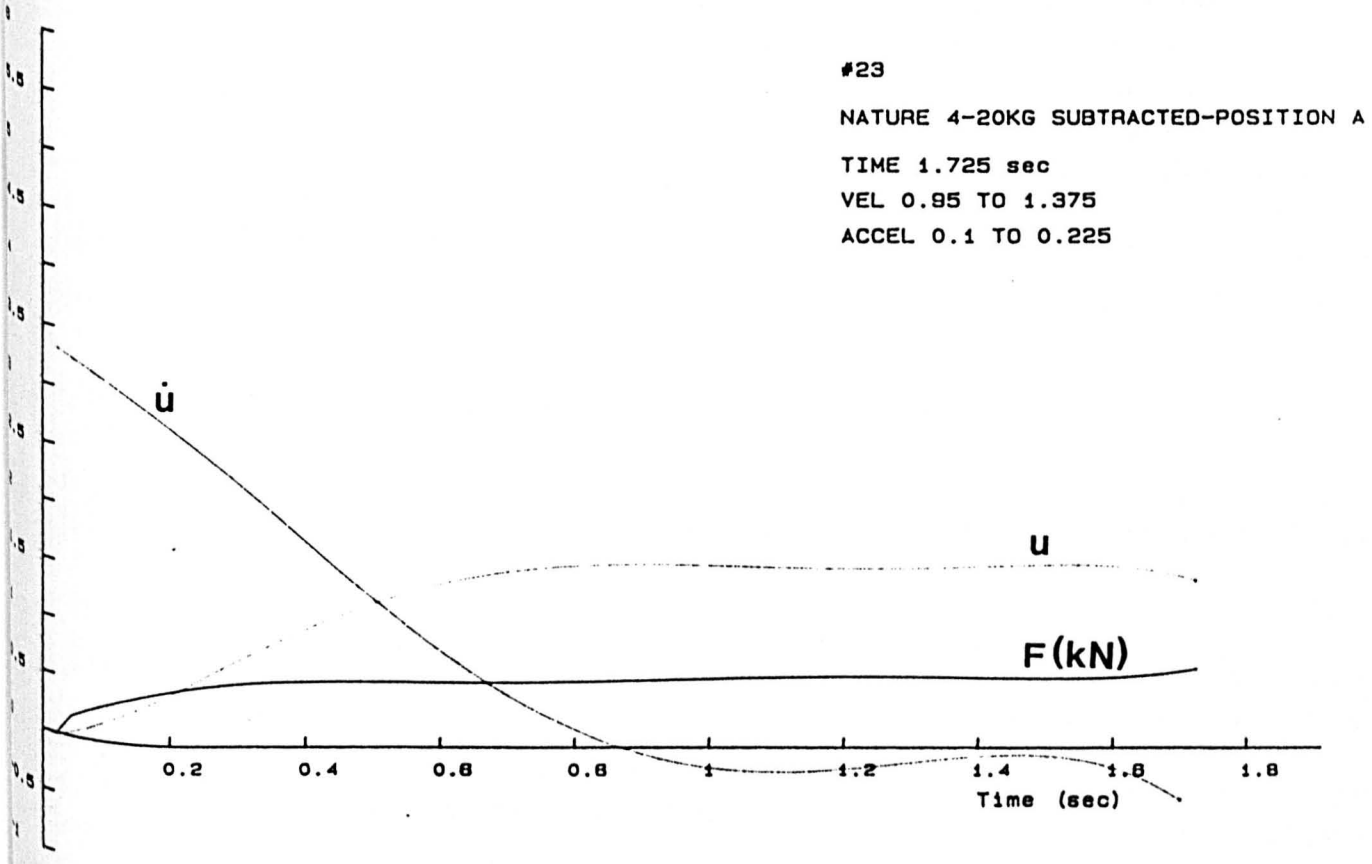

Fig. E.7. 315mm dia cylinder - mixed hard growth along leading edge - Re = 4.33×10^5.

APPENDIX F: Blockage Correction

The Allen and Vincenti correction procedure [105] as applied to circular cylinders is based on the method of images, i.e. the cylinder is represented by a doublet and the infinite series of its images in the wall boundaries. The wake is represented by a source of strength Q such that the pressure difference between two points far upstream and downstream of the cylinder is the same in potential flow as in actual flow. A solution for Q is obtained from the continuity, Bernoulli and momentum equations. Through the method of images an induced velocity, u_s, results at the position of the cylinder representing the solid blockage contribution. The infinite system of sources yields another induced velocity upstream of the model which in order to maintain mass continuity must be cancelled out by a velocity, u_w, of equal magnitude and opposite sign. The resulting expressions for the induced velocities are:

$$u_s = \frac{\pi^2}{12} UB^2 \qquad (1)$$

$$u_w = \frac{C_d}{4} UB \qquad (2)$$

where, B = area blockage ratio,
U = ambient flow velocity,
C_d = drag coefficient.

When the above velocity increments are added to U (in the present context the cylinder velocity) the following expression is obtained for the corrected velocity U_c:

$$\frac{U_c}{U} = 1 + \frac{\pi^2}{12} B^2 + \frac{C_d}{4} B \qquad (3)$$

Therefore, the correction formula for the unblocked drag coefficient C_{dc} is:

$$\frac{C_{dc}}{C_d} = \frac{U^2}{U_c^2} = \frac{1}{(1+u')^2} \qquad (4)$$

where $u' = \frac{\pi^2}{12}B^2 + \frac{C_d}{4}B$

The particulars for the tank and rough cylinders are:

tank length L_t = 3200mm
tank width W_t = 3800mm
cylinder length L = 1500mm
cylinder diameter D = 150-400mm
relative roughness k/D = 0.0094-0.01 and 0.025

Therefore, Area Blockage $B = \frac{LD}{L_t W_t} = \frac{1500D}{12.16 \times 10^6}$

The corrected mean drag coefficients are:

D (mm)	k/D	L/D	C_d	B	C_{dc}/C_d	C_{dc}
400	0.0097	3.75	1.06	0.049	0.97	1.028
200	0.0097	7.5	1.03	0.025	0.99	1.020
160	0.0094	9.375	1.03	0.020	0.99	1.019
150	0.01	10.0	1.04	0.018	0.99	1.029
400	0.025	3.75	1.19	0.049	0.968	1.152
315	0.025	4.76	1.16	0.039	0.975	1.131
160	0.024	9.375	1.16	0.020	0.989	1.146

Table F.1

APPENDIX G. Details of the Wave Loading Experiments

G.1. The Delta Flume

The wave flume is sited at Laboratory De Voorst (Delft Hydraulics Laboratory) in the Netherlands. The flume is 230m long, 5m wide and 7m deep; the water depth for these tests set at 5m. Depending on wave period, up to 2m high second-order waves can be generated by an MTS translatory wavemaker with maximum stroke capability of 5m. Waves are absorbed by a 1:6 beach, the maximum reflection coefficients being 10%. The wavemaker compensates for wave re-reflection through a control feedback system described by Kostense [115]. The facility is depicted in Figure G.1.

G.2. The Test Cylinder

The cylinder, which was designed by BMT Ltd, was located 55m from the wavemaker in a vertical attitude. It had a base diameter of 505mm and overall length of 7165mm consisting of five connected sections as shown in Figure G.2. The bottom section was rigidly mounted on the flume floor and the upper section was supported by a gantry spanning the flume width. The force measuring elements were attached to the adjacent rigid sections by means of transducers mounted along the cylinder longitudinal axis. The clearance between force elements and rigid sections was 1mm approximately.

The cylinder was roughened with equilateral pyramids of three nominal heights, 30mm, 22mm and 15mm. The pyramids were arranged in random distribution and element orientation on 250mm long fibreglass shells (Figure G.3). The amount of pyramids of each size was equivalent to one third of the total panel area. A prototype semi-cylindrical 250mm long panel was constructed and a negative was cast using a high definition flexible moulding compound. Several panels were then reproduced using polyester resin and fiberglass into which stainless steel straps were embedded. Two such panels were hinged together to form a cylindrical one which could be wrapped around the cylinder and securely fastened with recessed buckles attached at the ends of the straps. The shells were strapped around the cylinder, which was clad with 1mm thick sandpaper, such that the buckles were located along the trailing cylinder edge.

Measurements of randomly selected pyramids and base shell were made at regular intervals around the circumference and produced the following averages:

- mean height of pyramids = 26.4mm, 19.7mm, 13.5mm
- mean shell base thickness = 7mm

Thus, allowing for the shell and sandpaper thickness, the mean base diameter was 521mm, i.e the mean k/D was 0.038 (where k is taken as the average of the pyramid heights).

G.3. Instrumentation and Data Acquisition

In-line and transverse forces were measured on each force element by two-component strain-gauged transducers. The force transducers were designed and calibrated by staff of Imperial College, London. Horizontal and vertical water particle velocities were measured by two Colnbrook electromagnetic flow-meters positioned 0.6m away from the flume wall at -1.5m and -2.5m water depth, and at 55m from the wavemaker datum. Two capacitance gauges, suspended at 43.6m and 48m from the wavemaker, recorded wave heights. The flow-meter velocity records were used in the data analysis presented here.

Real time data from ten channels in total were sampled at a rate of 50Hz by a Hewlett-Packard HP1000 computer. The analogue velocity signals were filtered by a 10Hz filter and a 50Hz anti-aliasing filter, resulting in phase lags of 32msec and 4msec respectively which were accounted for in the data analysis. Around 440K data records per run were stored. On-line data analysis of a 75sec time history and graphical outputs of all signals provided a quick check on the validity of the runs. Typical time histories are shown in Figures G.4 and G.5.

G.4. Data Analysis

The data were analysed on a MicroVax II computer at the Marine Technology Centre of Strathclyde University. Spectral and statistical analysis was also carried out for all signals and force coefficients. The data were converted to physical values through the appropriate

calibration factors and the corresponding zero readings averaged over the first 6 seconds of the time series. The zero up-crossings of the raw horizontal velocity signal were used for the full wave and force cycle identification.

The Discrete Fourier Transform (DFT) was applied to obtain an approximation of the Fourier integral series,

$$F(n) = \int_{-\infty}^{\infty} f(t)\, e^{-2\pi int}\, dt$$

which over the region (0,T) becomes,

$$F(k) = \frac{T}{N} \sum_{j=0}^{N-1} f(j)\, e^{-2\pi ijk/N}$$

where, T = time period,
N = number of data points,
k = 0,1,...,N-1.

The DFT is defined by,

$$z_k = \frac{1}{N} \sum_{j=0}^{N-1} z_j\, e^{-2\pi ijk/N}$$

where, $z_k = a_k + ib_k$,
$z_j = x_j + iy_j$

For a sequence of real numbers,

$$z_j = x_j,$$

$$\text{i.e. } z_k = a_k + ib_k = \frac{1}{\sqrt{k}} \sum_{j=0}^{N-1} x_j\, e^{-2\pi ijk/N}$$

The coefficients a_k and b_k were evaluated for the force and velocity arrays of length N for each wave. The realisation of the fitted signals at each point N was expressed by the function,

$$\sum_{n=1}^{n} F = a_o + 2\sum_{n=1}^{n} (a_n \cos(2\pi m/N) - b_n \sin(2\pi n/N))$$

where, n is the order of fit.

The acceleration was derived by differentiating the above expression for the velocity. It was found that a sixth order fit gives satisfactory results with very low residual errors, particularly for the velocity and in-line force realisations. Typical realisations are illustrated in Figures G.6 through G.10.

The dimensionless flow kinematics parameters and total force and lift force coefficients were evaluated through the following expressions:

$$Re = \frac{u_{max}\, D}{\nu} \quad , \quad KC = \frac{u_{max}\, T}{D} \quad , \quad KC' = \frac{u_{h1}\, T}{D}$$

$$C_f = \frac{2\, F_{x(rms)}}{\rho D\, u^2_{max}} \quad , \quad C_{fmax} = \frac{2\, F_{x(max)}}{\rho D\, u^2_{max}}$$

$$C'_f = \frac{2\, F_{x(rms)}}{\rho D\, u^2_{rms}}$$

$$C_L = \frac{2\, F_{y(rms)}}{\rho D\, u^2_{max}} \quad , \quad C_{Lmax} = \frac{2\, F_{y(max)}}{\rho D\, u^2_{max}}$$

$$C'_L = \frac{2\, F_{y(rms)}}{\rho D\, u^2_{rms}}$$

where, u_{max}, u_{rms} and u_{h1} are the maximum, rms and 1st harmonic horizontal velocity components of each wave,

F_x and F_y the in-line and transverse forces per wave,

and T is the actual wave period.

Over 2000 waves were analysed as described above and in Chapter 9 and the C_d and C_m for each wave are plotted in Figures G.14 and G.15.

Run	KC	C_d	S.D.	C_M	S.D.	C_{frms}	S.D.	C_{Lrms}	S.D.
BP15	1.04	2.76	0.39	2.13	0.07	16.10	2.02	0.42	0.15
TP15	1.64	2.59	0.23	2.01	0.06	9.25	0.84	0.81	0.12
BP14	2.11	1.58	0.46	2.12	0.12	11.02	7.63	0.30	0.23
TP14	3.87	2.03	0.23	1.97	0.09	4.37	1.15	0.24	0.10
BP13	3.94	1.73	0.30	2.01	0.10	4.09	0.67	0.29	0.15
TP13	5.71	1.84	0.15	1.83	0.08	2.50	0.32	0.34	0.16
BP12	5.87	1.78	0.21	1.88	0.10	2.57	0.34	0.73	0.30
TP12	6.88	1.81	0.16	1.65	0.11	2.15	0.33	0.97	0.31
BP10	7.55	2.03	0.20	1.67	0.11	1.98	0.27	1.21	0.32
BP11	7.99	1.96	0.19	1.62	0.13	2.07	0.28	1.35	0.35
TP10	8.79	2.11	0.27	1.46	0.13	1.73	0.24	1.15	0.28
TP11	9.22	2.21	0.27	1.44	0.12	1.87	0.26	1.25	0.27
BP08	10.60	2.16	0.21	1.40	0.16	1.49	0.18	1.12	0.25
TP01	11.00	2.10	0.24	1.30	0.16	1.34	0.15	1.01	0.21
BP01	11.02	2.04	0.22	1.42	0.14	1.29	0.16	0.98	0.20
TP08	11.15	2.10	0.23	1.27	0.19	1.53	0.21	1.08	0.24
BP07	11.22	2.16	0.23	1.27	0.18	1.43	0.26	1.22	0.26
TP07	11.40	2.29	0.30	1.11	0.22	1.53	0.28	1.24	0.27
BP09	12.21	2.06	0.22	1.30	0.20	1.63	0.23	1.27	0.26
TP09	13.32	2.06	0.24	1.24	0.21	1.54	0.24	1.02	0.21
BP06	15.27	1.85	0.27	1.45	0.22	1.30	0.25	0.80	0.21
TP06	16.58	1.78	0.27	1.29	0.26	1.15	0.18	0.63	0.15
BP02	18.18	2.14	0.41	1.22	0.41	0.99	0.15	0.54	0.17
TP02	19.59	1.88	0.29	1.34	0.39	0.90	0.12	0.43	0.12
BP04	19.12	1.89	0.15	1.40	0.12	0.86	0.07	0.59	0.07
TP04	20.59	1.79	0.15	1.40	0.11	0.82	0.07	0.45	0.08
BP05	21.79	1.64	0.16	1.64	0.17	0.85	0.09	0.46	0.15
TP05	24.16	1.65	0.18	1.47	0.18	0.77	0.09	0.40	0.14
BP03	25.24	1.64	0.16	1.64	0.18	0.78	0.09	0.38	0.12
TP03	26.51	1.67	0.17	1.67	0.23	0.76	0.08	0.31	0.10

N.B. Run codes TP and BP denote upper and lower force elements respectively.

Table G.1. Summary of mean force coefficients for pyramid roughened cylinder.

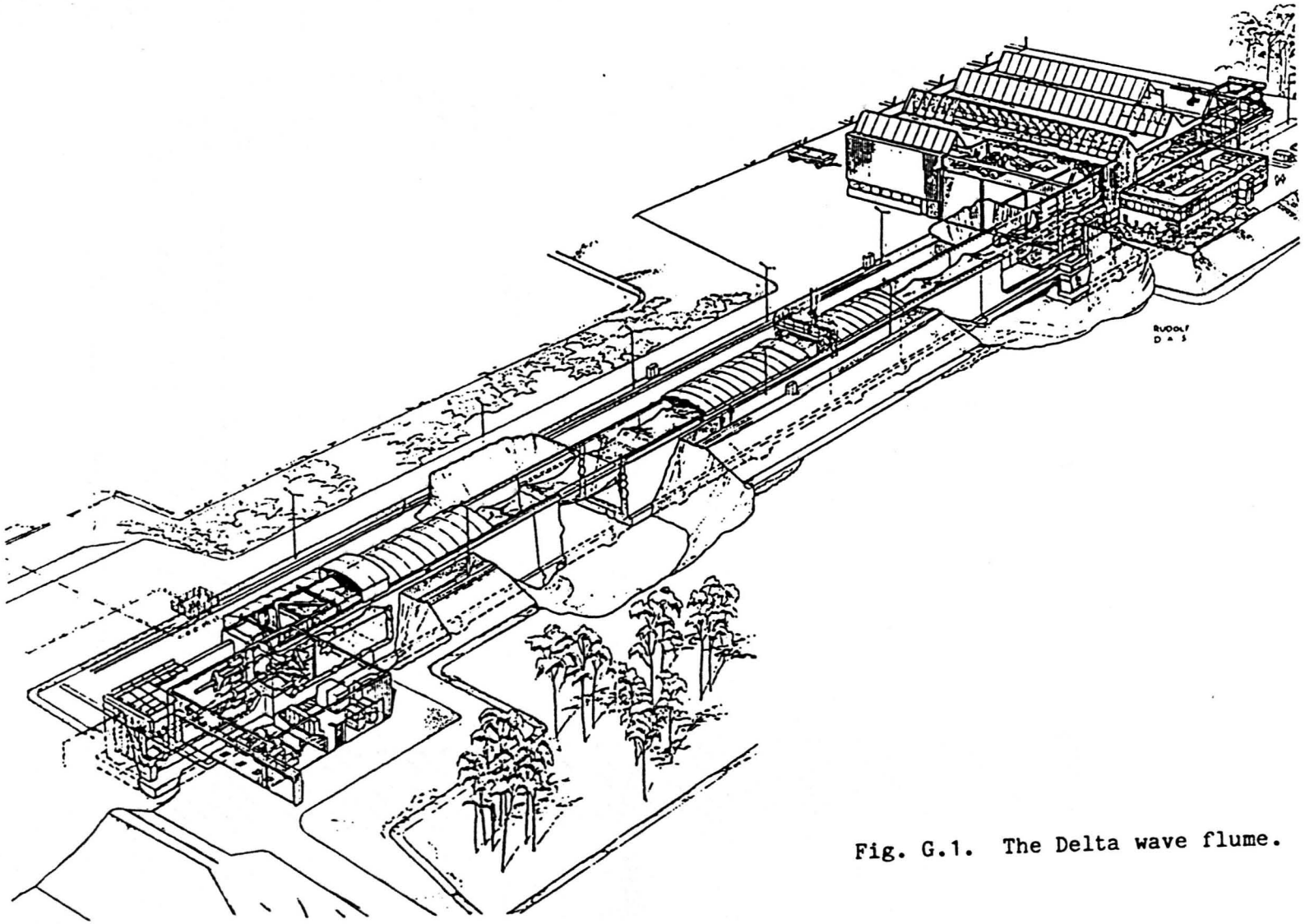

Fig. G.1. The Delta wave flume.

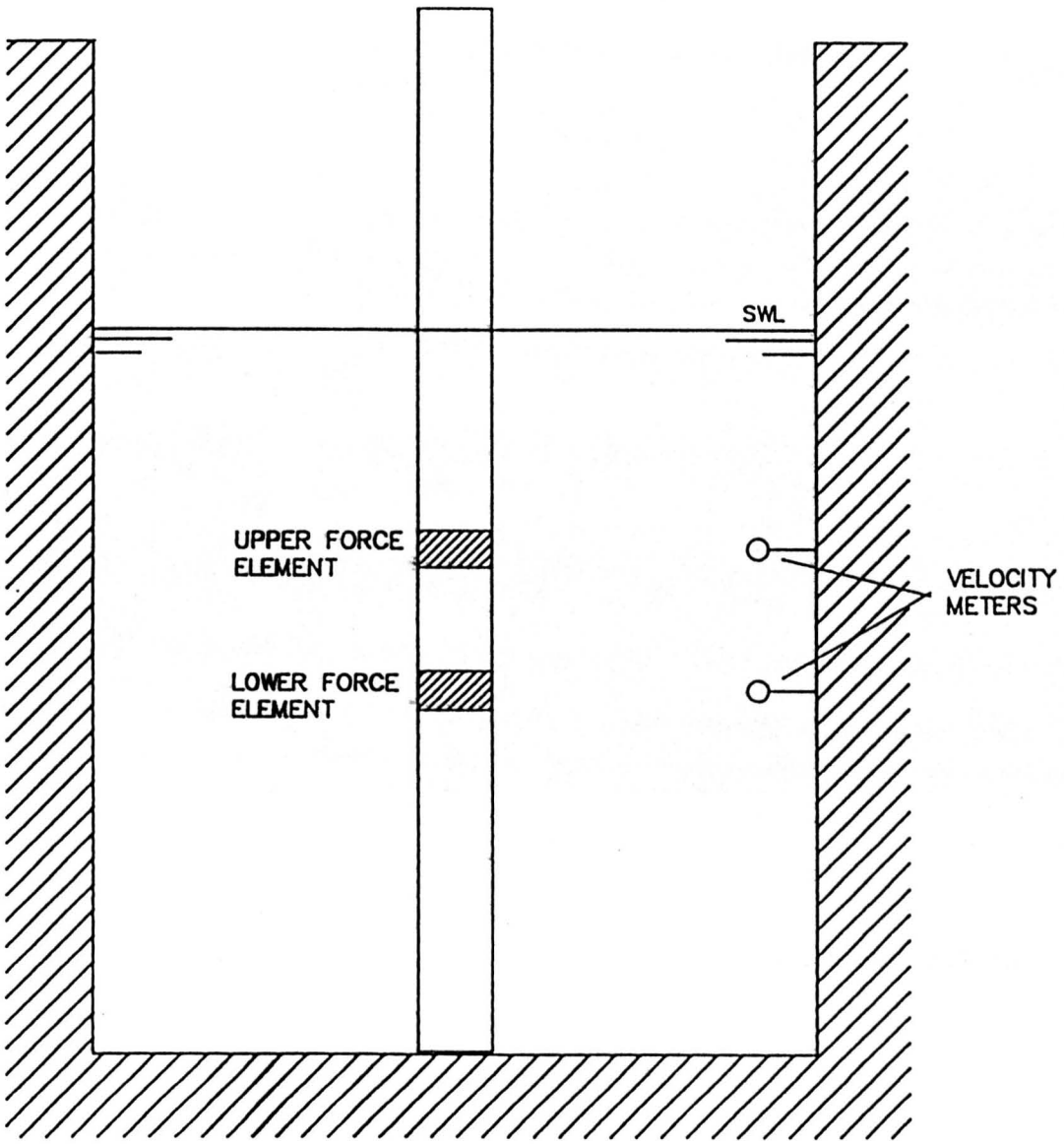

Fig. G.2. Section through the Delta flume.

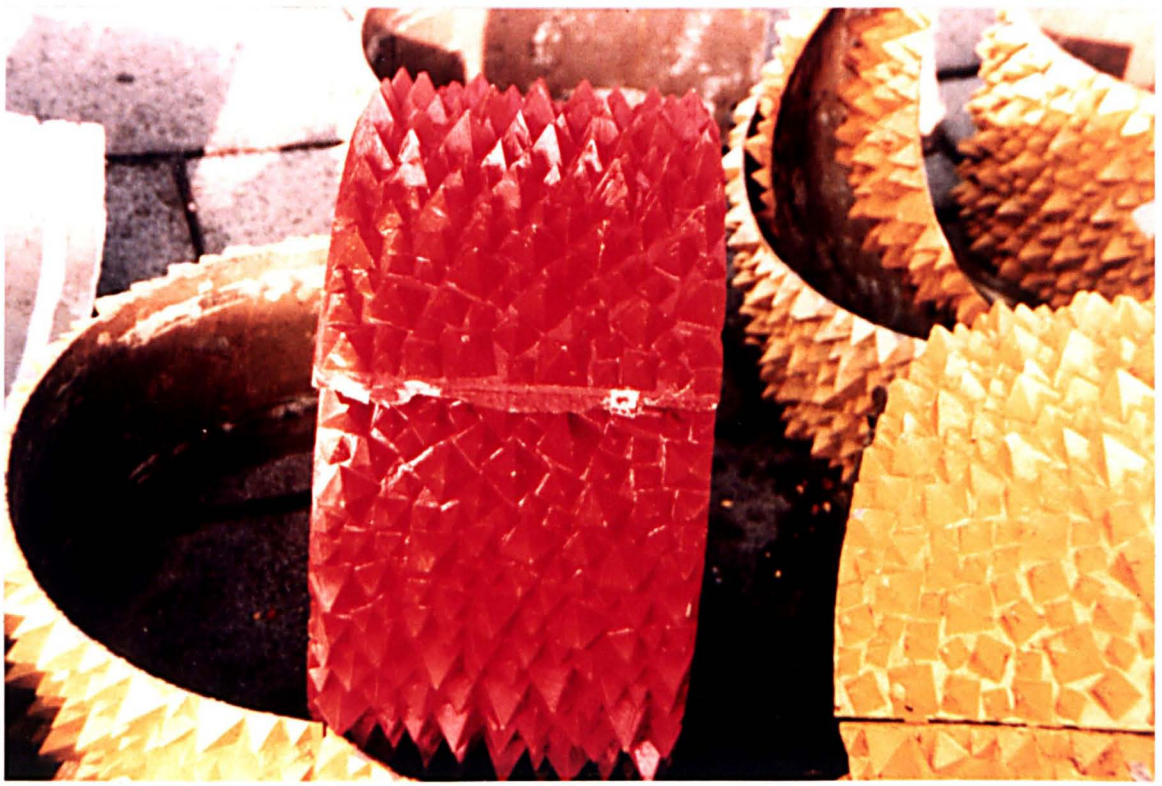

Fig. G.3. Close-up view of pyramid roughened shells.

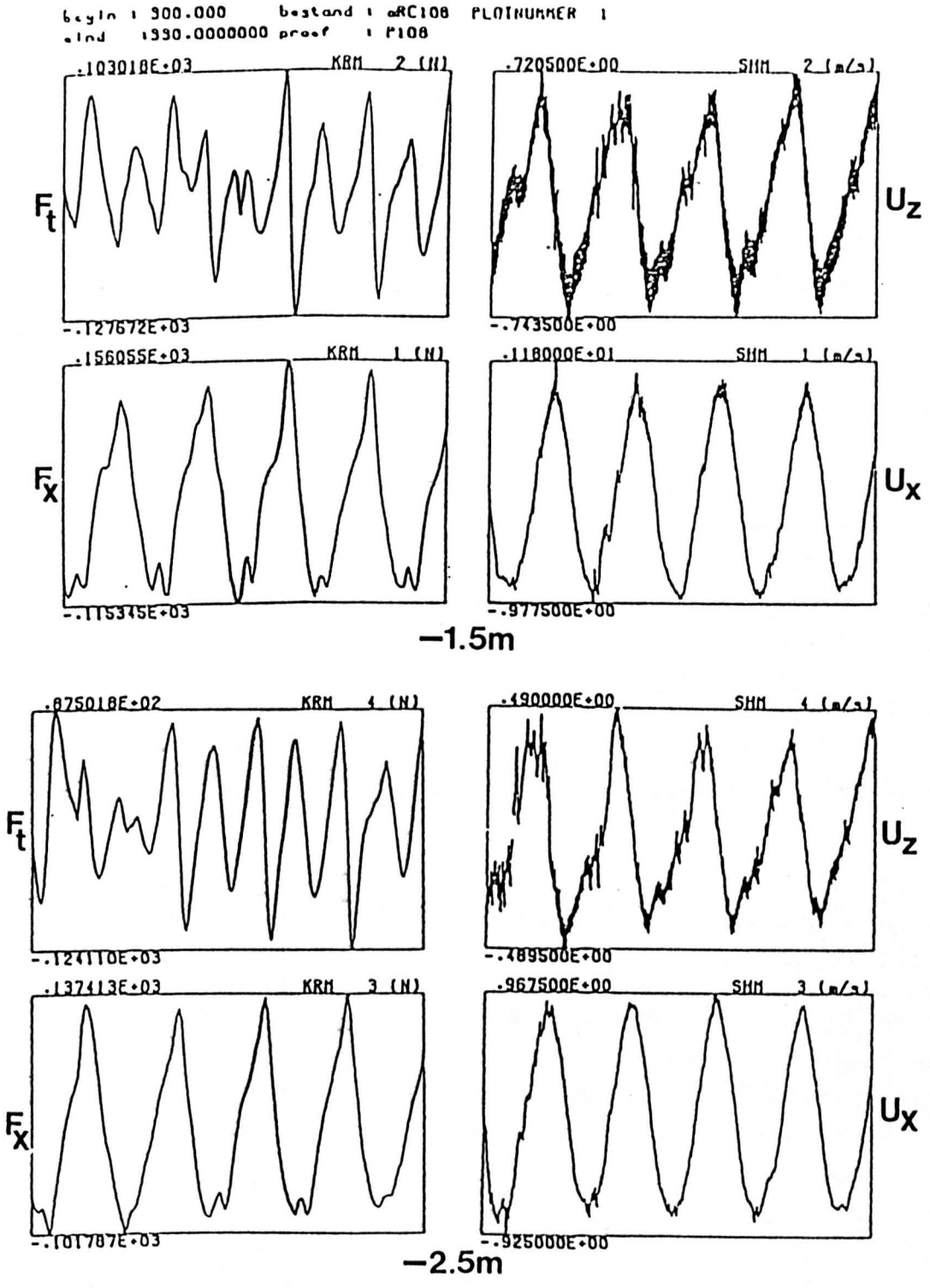

Fig. G.4. A 30sec time history from run P08;
wave height, WH = 1.5m
wave period, T = 6.0sec.

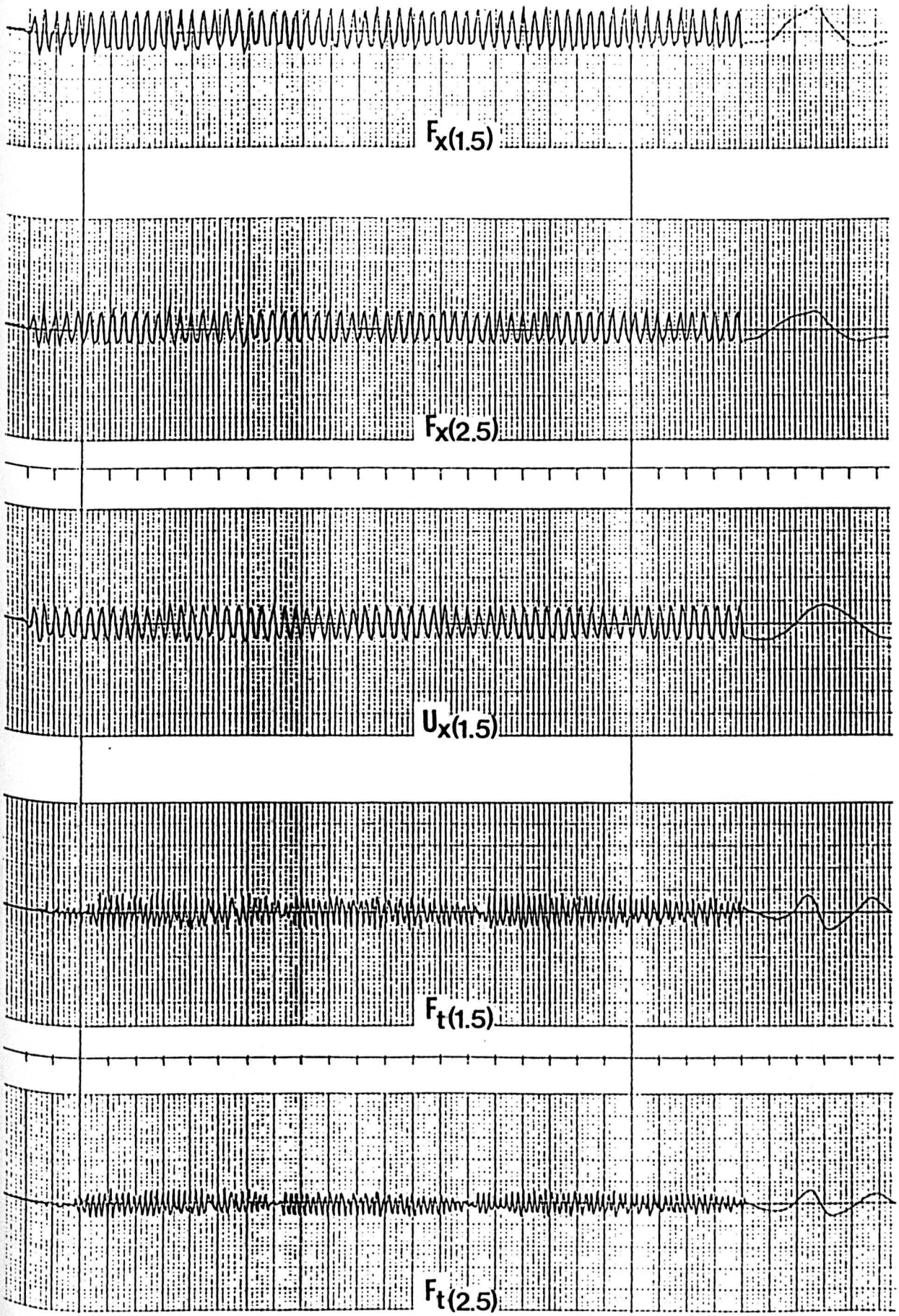

Fig. G.5. Typical time history from run P10.

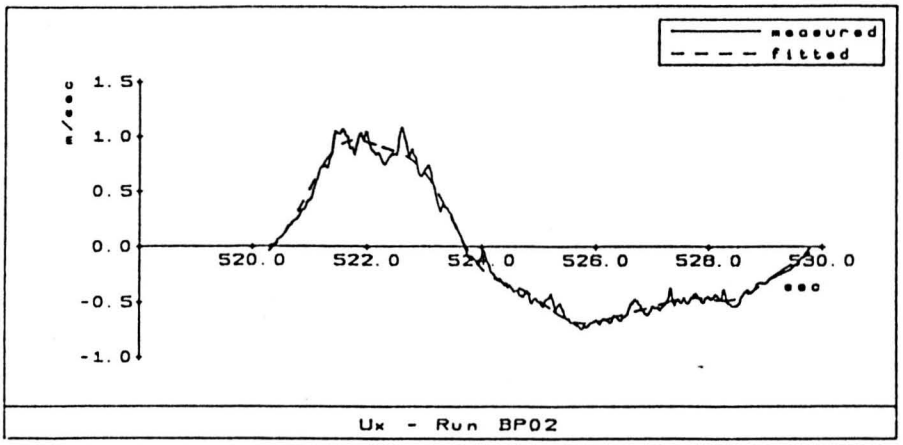

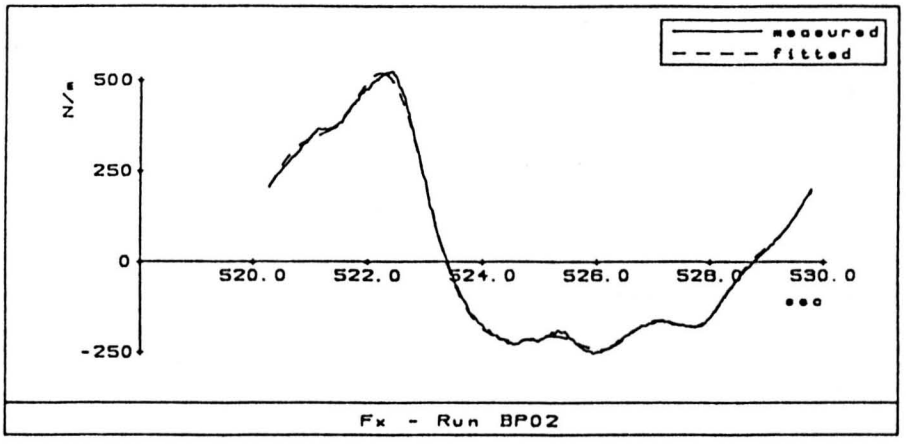

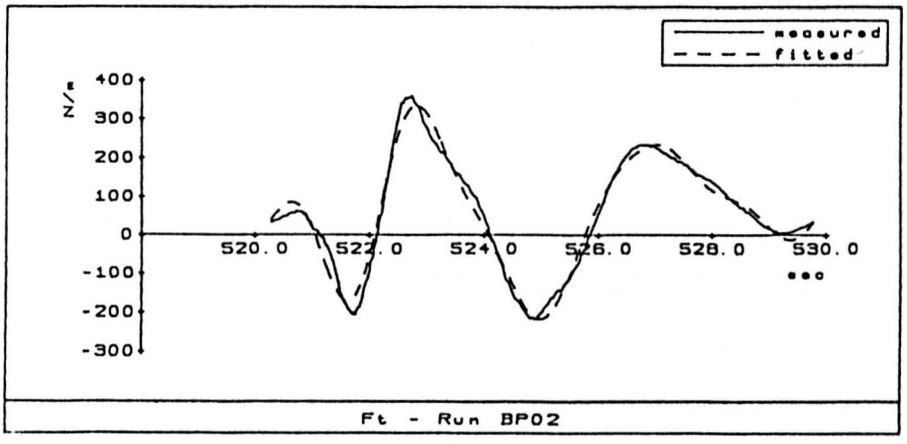

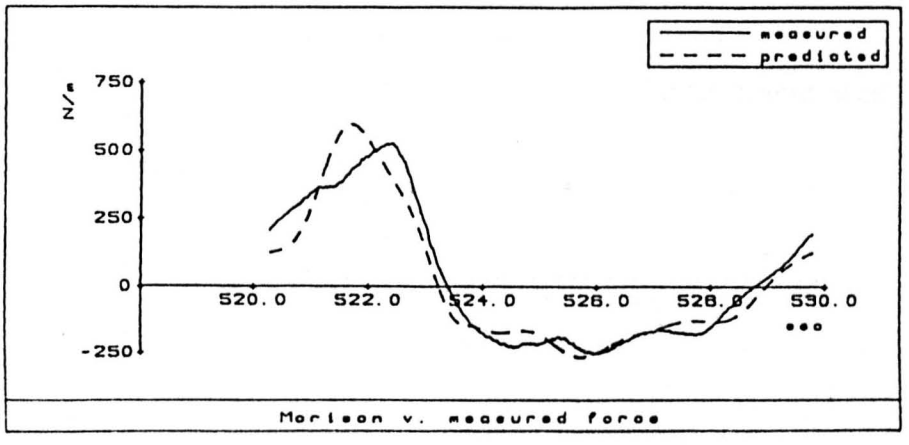

Fig. G.6. Run P02 - lower element; WH=1.12m, T=9.5sec, KC=18.2.

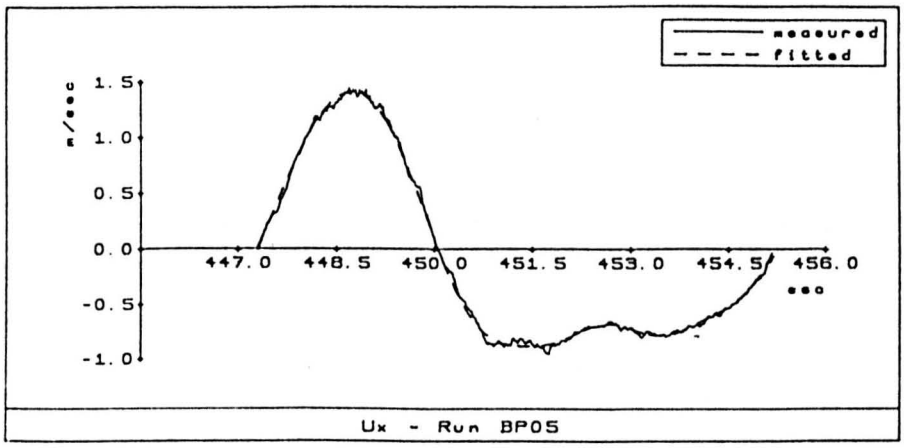

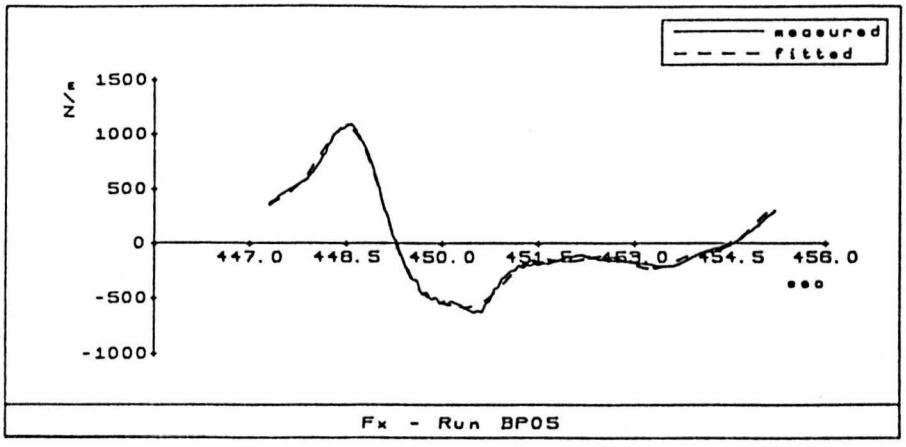

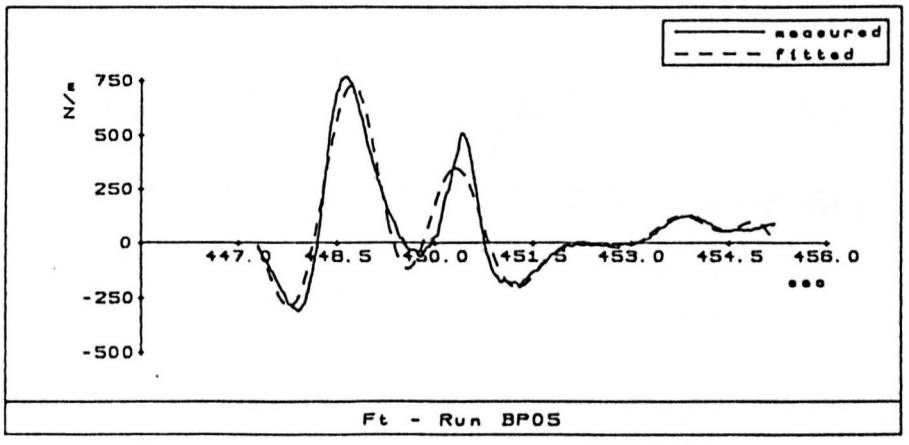

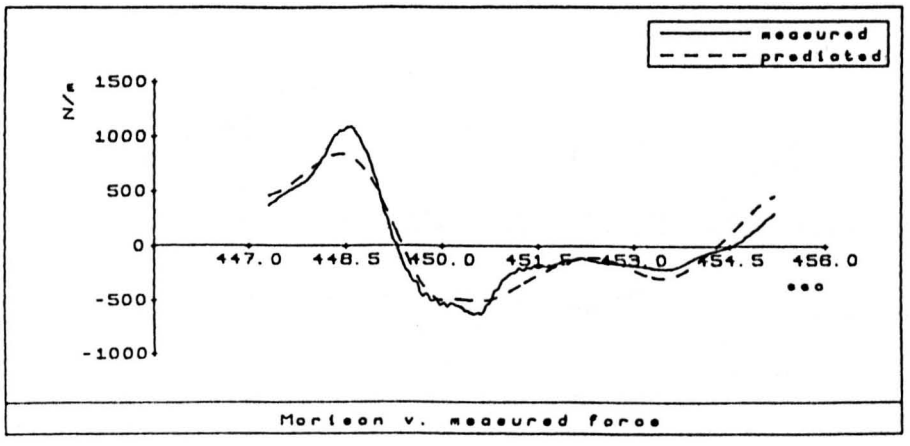

Fig. G.7. Run P05 - lower element; WH=1.84m T=8.0sec, KC=21.8.

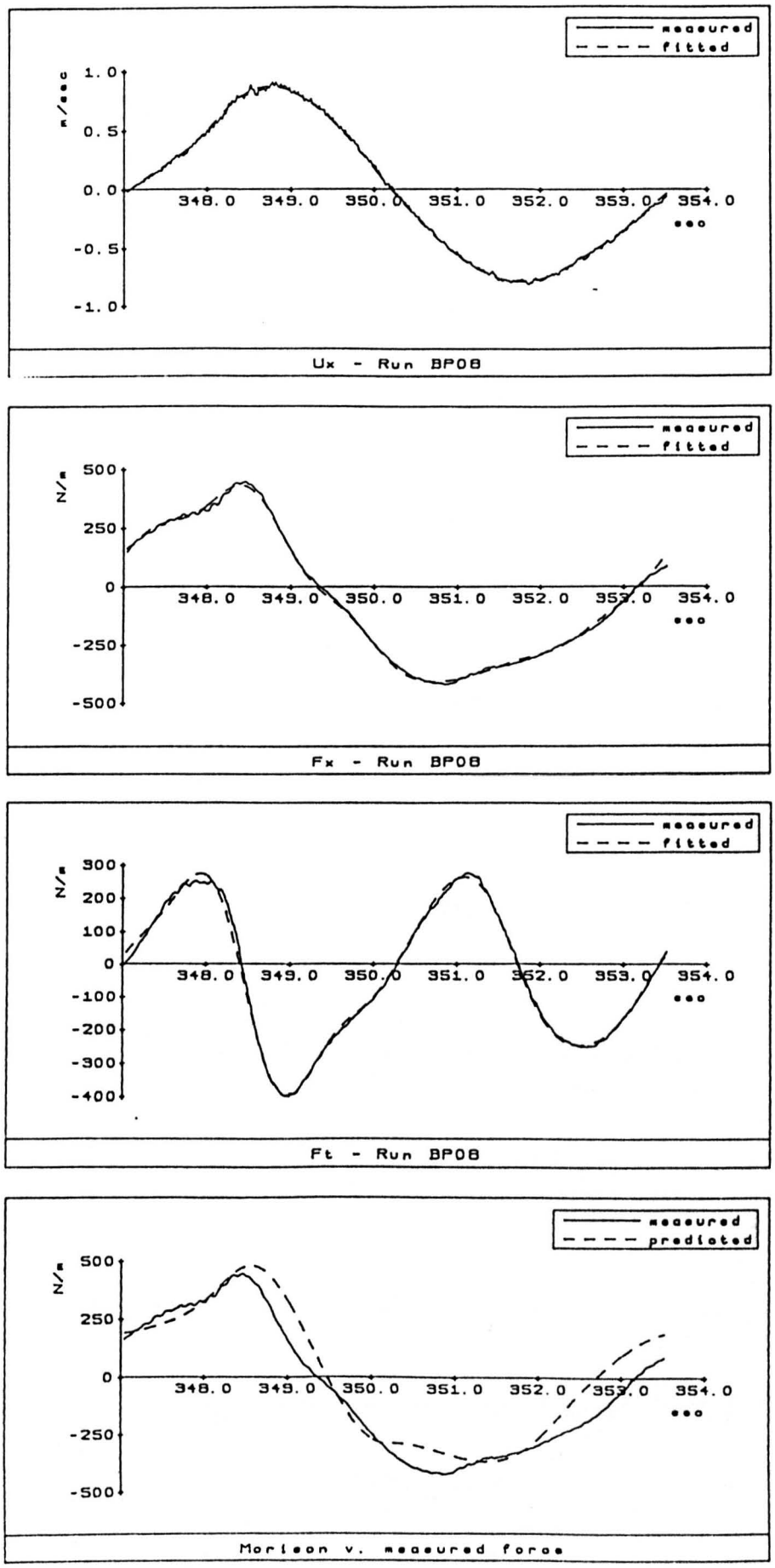

Fig. G.8. Run P08 - lower element; WH=1.5m, T=6.5sec, KC=10.6.

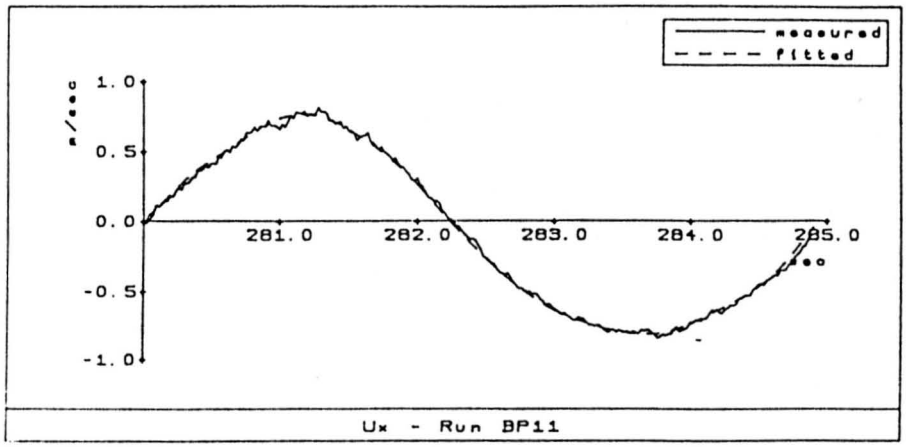

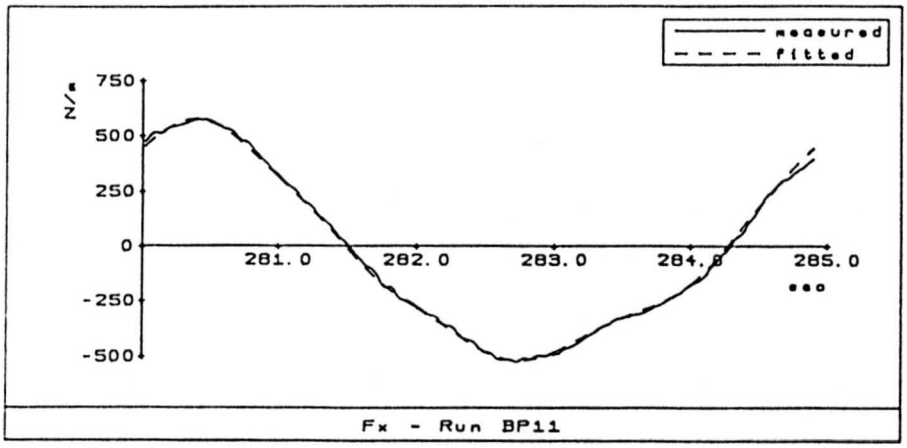

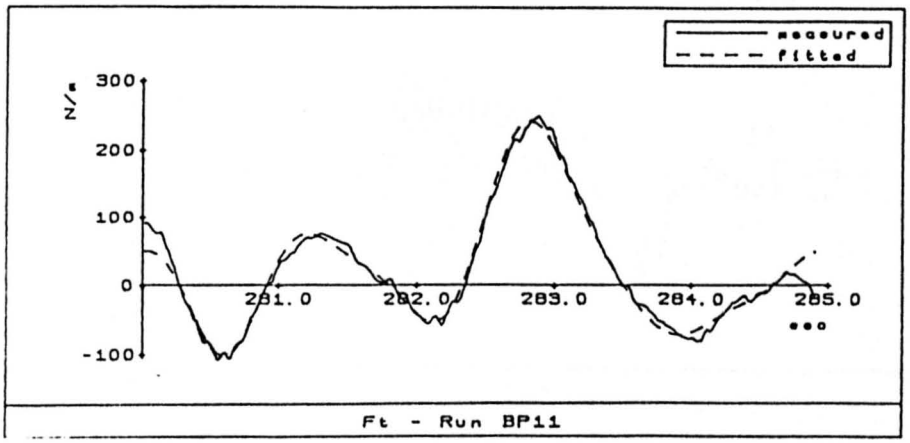

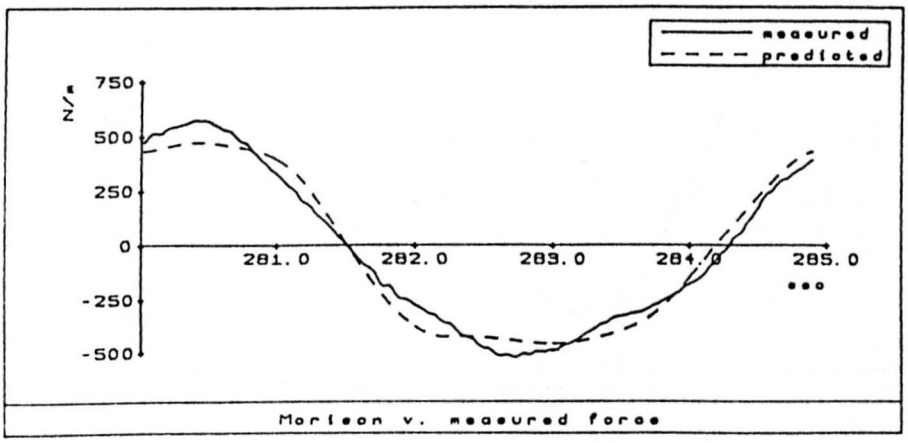

Fig. G.9. Run P11 - lower element; WH=1.73m, T=5.0sec, KC=8.0.

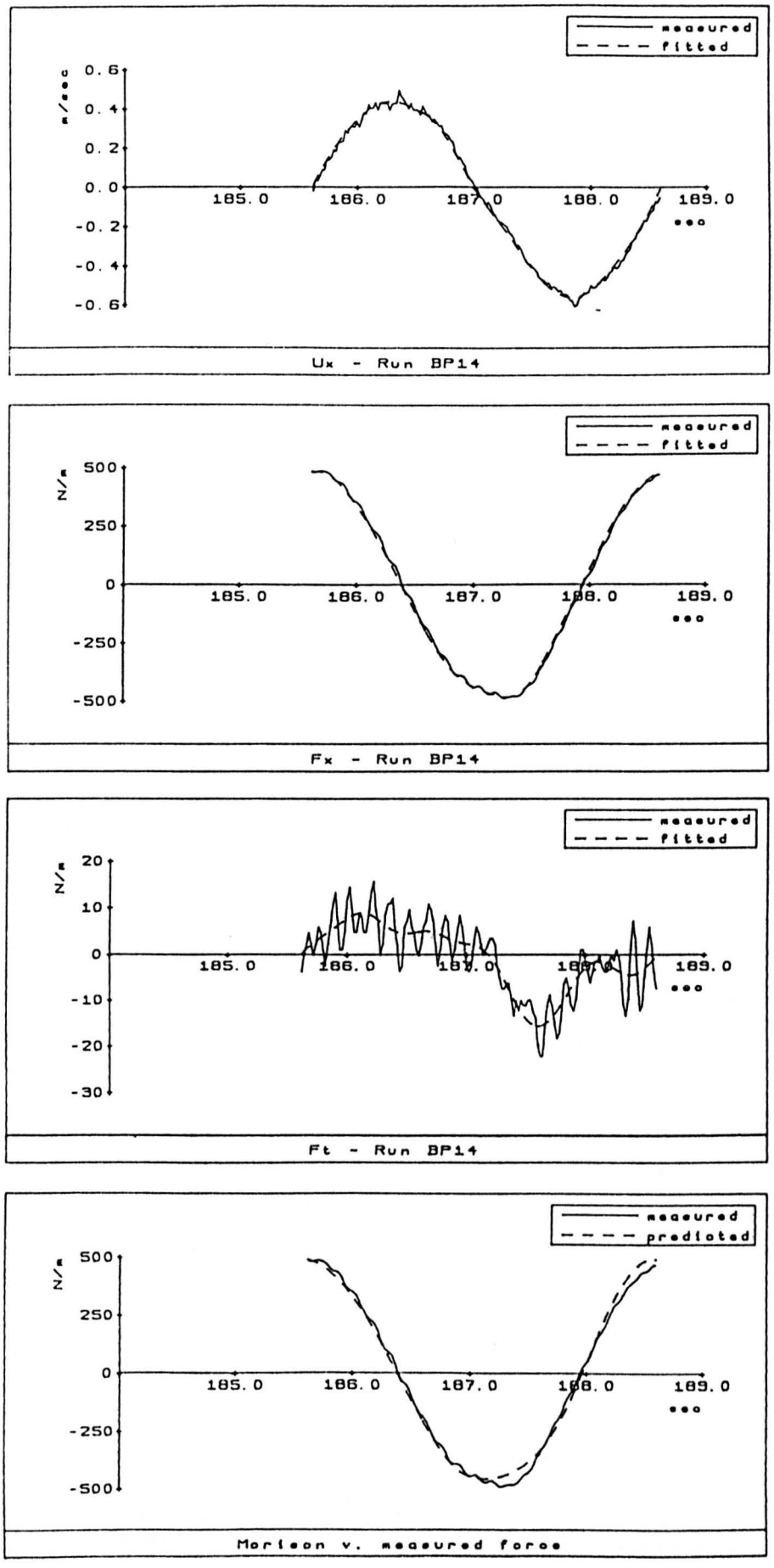

Fig. G.10. Run P14 - lower element; WH=1.49m, T=3.0sec, KC=2.1.

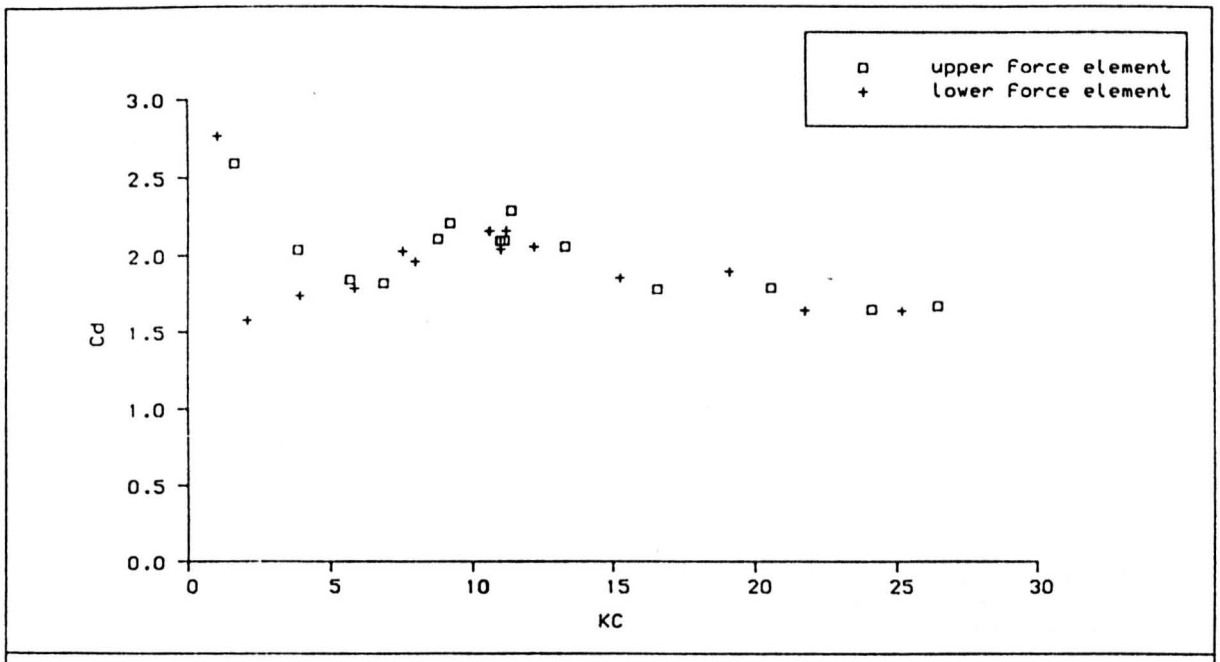

Fig. G.11. Drag coefficient variation with KC for pyramid roughened cylinder in regular waves.

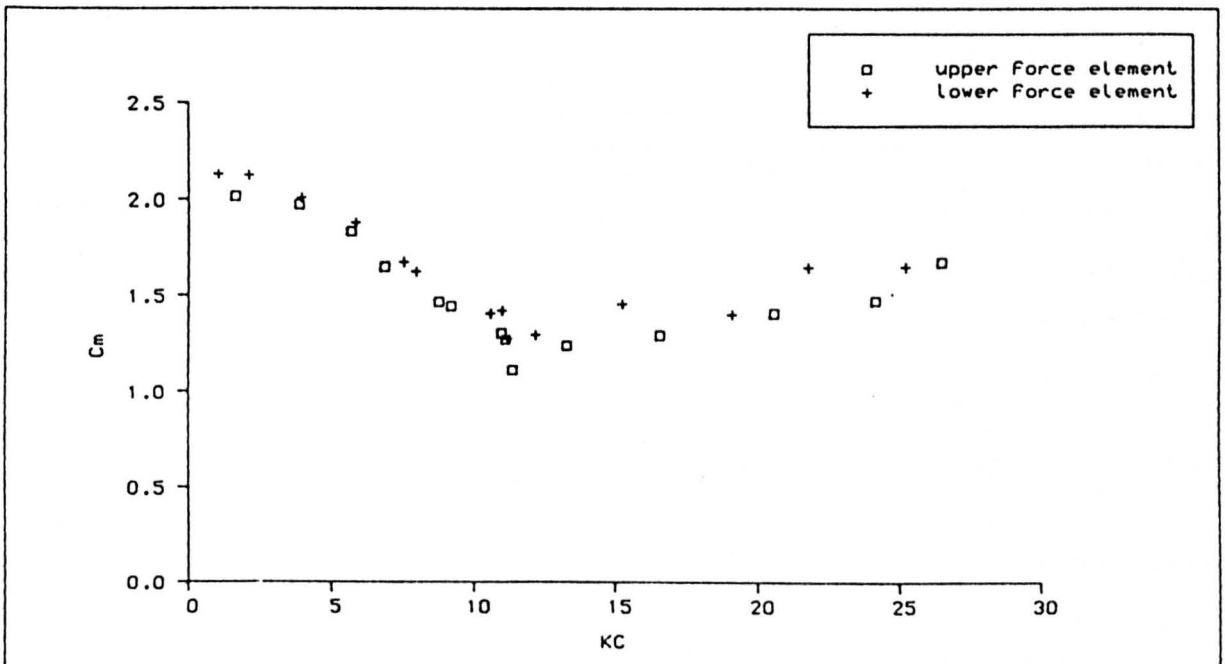

Fig. G.12. Inertia coefficients for the same cylinder.

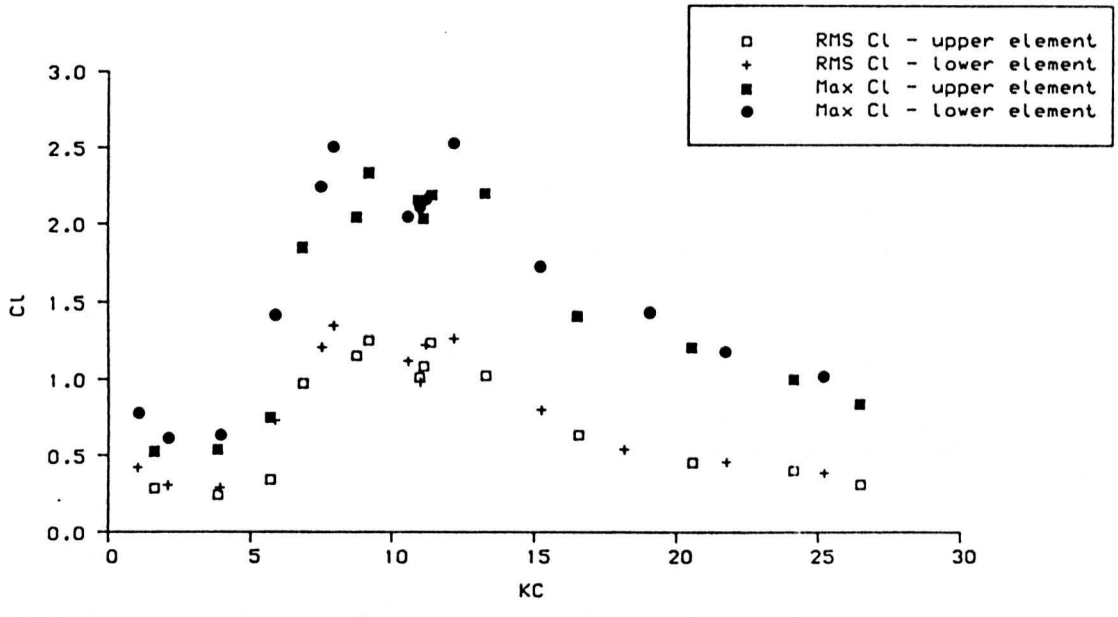

Fig. G.13. Variation of rms and maximum lift force coefficients with KC (Cl normalised by maximum horizontal velocity).

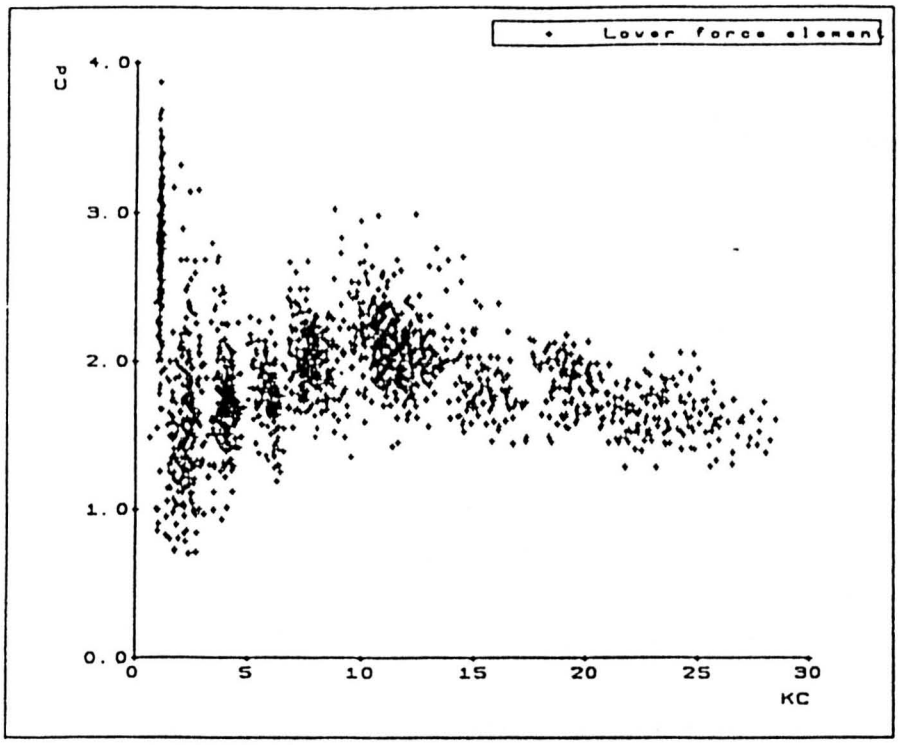

Fig. G.14. C_d for all waves analysed.

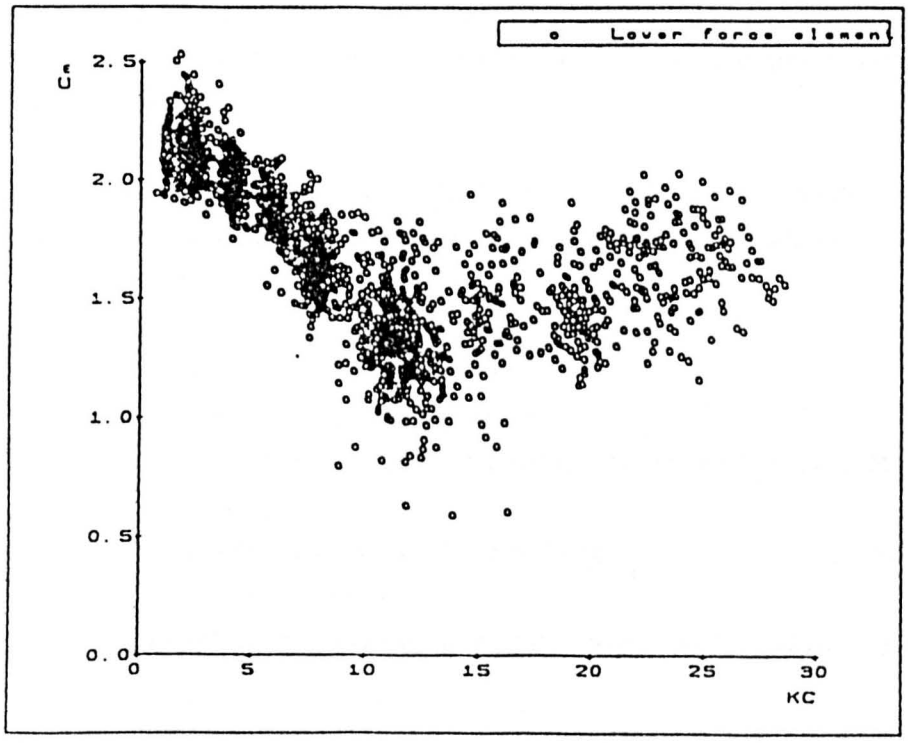

Fig. G.15. C_M for all waves analysed.

APPENDIX H: Computer Modelling and Applications.

As shown in Figure H.1, the computer model for the design and maintenance appraisal of marine growth consists of three interacting modules. These are described below.

H.1. Hydrodynamic Loading and Marine Growth Database

The input data requirements for this module are:

- design wave height and period
- mean current speed and direction
- water depth
- member elevation and orientation
- member length
- initialisation of nominal member diameter
- marine growth characterisation

The drag and inertia forces are derived through Morison's equation using linear wave theory and current superposition. The force coefficients are retrieved from the marine growth database according to the specified mapping of fouling.

The database includes the mean force coefficients obtained from the steady flow experiments and the corresponding roughness characterisation parameters, i.e.

- type of fouling species
- percentage surface cover
- distribution and orientation to principal direction of incident flow
- overall thickness of fouling
- roughness element size
- weight of fouling per unit area per fouling species.

The recommended by the certifying authorities base force coefficients for clean and rough structural members are also included in the database.

By defining a marine growth scenario over a number of years, the history of hydrodynamic loads is determined. Pressure due to waves and hydrostatic pressure are also estimated assuming that the member is watertight. The loading data files are input to the "Design Optimisation" module to determine the direct member stresses.

H.2. Structural Design Optimisation

Each tubular member is designed to withstand extreme environmental and static loads (Ultimate Limit State). These are transformed to combined axial, bending, pressure, shear and torsional stresses. The length, diameter and plate thickness of the member are computed to ensure resistance against buckling and structural collapse. The general stability requirement for tubular members subjected to a combination of forces and moments is expressed by the following interaction formula [70]:

$$\left(\frac{\sigma_n}{R_n} + \frac{\sigma_b}{R_b} + \frac{\sigma_c}{R_c} + \frac{\tau_s + \tau_t}{R_{nc}}\right)^2 \left(\frac{k}{\psi}\right)^2 < \left(\frac{1}{\gamma_m}\right)^2$$

where, σ_n, σ_b, σ_c, τ_s and τ_t are the axial, bending, circumferential, shear and torsional stresses respectively;

R_n, R_b, R_c, and R_{nc} the axial, bending, pressure and shear and torsion resistances;

k and ψ factors depending on type of member and slenderness ratio;

γ_m material coefficient.

Plate thickness is initialised to evaluate gravity and buoyancy forces. Simple beam theory is applied to derive the bending, shear and circumferential stresses. Longitudinal stresses are estimated assuming constant axial loading and torsional effects are neglected. Corresponding resistances are evaluated for a given diameter and a series of weld thicknesses.

Since design stresses and resistances are functions of the member dimensions and materials specifications, equivalent designs are gene-

rated through an optimisation procedure based on simple linear programming techniques. The objective function combines the stability requirement, as expressed by the above interaction formula, and the minimum material weight requirement. The constraints are specified by the D.n.V. rules for the design and construction of fixed steel structures [70].

Through a series of iterations an optimum plate thickness is reached which gives minimum weight whilst satisfying the rules. The model repeats the optimisation cycle over a user defined range of diameters and steps and the generated output comprises designs of equivalent strength to the maximum allowable stress levels.

The variation in member stresses over a range of diameters is shown in Figure H.2. Circumferential and shear stresses increase linearly with increasing diameter, whilst overall bending stress reduces. The net interaction effect is approximately constant for all designs with different diameter and optimum plate thickness.

H.3. The "Costs" Module

Although the alternative designs are minimum weight solutions, material cost alone is not a reliable indicator in selecting a "best", cost-effective design. Fabrication costs and related overheads must also be considered. This has been established from previous research on the structural design and production of floating structures [122]. Fixed steel structures barely resemble floating structures. However, the main cost centres and fabrication-related factors are compatible; only the relative weighting from each centre changes.

The "Costs" module is a modified version of a production costing methodology first developed for ship structures and later adapted to semi-submersible and tension-leg platform designs and fabrication procedures [123,124]. It has been extended to include procedures and cost indices associated with cleaning-for-structural relief. The main features of each "cost centre" are:

a) Materials Cost Centre

Principal diamensions and market prices for seamless and welded hollow tubes form the materials cost database. All plate thic-

knesses are rounded off to the nearest 0.5mm during the design optimisation to comply with standardised steel pipe dimensions. Alternatively, a flat cost per tonne of steel can be adopted.

b) Fabrication Cost Centre

Labour cost and associated overheads are estimated using work study data on tasks such as edge preparation, fairing and tacking, materials handling etc. Welding time is calculated using mean welding rates for automatic submerged arc and manual metal arc (MMA) processes. The rates vary according to joint configuration, welding position, plate thickness, seam length and number of weld passes. Quality control costs are expressed as a function of seam length and plate thickness squared, i.e. approximately proportional to the weld metal volume. Productivity and overheads indices are input by the user and relate to the total manhours.

c) Cleaning Cost Centre

Rates of cleaning for structural relief are adopted for the air diving depth range (0 to -40m). Maximum dive duration is 8-hour bellruns for two divers and a support vessel is available round the clock with adequate number of divers for uninterrupted work. Due to high standard deviations for cleaning rates, maximum, minimum and average rates are included in the database for two cleaning methods; hand scrapers and high pressure water jetting. The total cleaning effort for each design is calculated on the basis of fouled member surface area and is converted to cost using the support vessel hire daily rate. No distinction in rates is made between types of fouling due to lack of data.

H.4. Particulars of Case Study

To assess the marine growth effects on structural design and related costs, two simple 10-year fouling development scenarios were adopted for a tubular bracing. These were as follows:

Scenario A: Mussels

Year 1:	Patchy cover of algae and 8mm barnacles.
Year 2:	Randomly distributed patches of 8mm mussels at 25% surface cover.
Year 3:	New mussel settlement. Older mussels averaging 20mm in height.
Year 5:	50% cover by 40mm thick mussel patches along the top and outer member faces. Other faces covered by fine filamentous growth and tubeworm.
Year 8:	Full cover by 200mm thick layer of mussels.
Year 10:	Same as year 8. Terminal growth has been reached.

Scenario B: Kelp

Years 1-2:	As above.
Year 3:	Isolated 50-100mm green and brown weeds appear on top of 8mm mussels along the top face.
Year 4:	Rapid growth of Laminaria digitata is reported. No new mussel settlement.
Year 6:	Kelp growth covers 50% of the member the older plants being up to 2m long.
Year 8:	Full cover by 3m long kelp with small mussels and barnacles round their holdfast.
Years 9-10:	Apart from some die-back during the winter periods no significant changes occur.

Other data are as follows:

- Max. wave height : 30m
- Assoc. period : 17sec
- Current velocity : 0.5m/sec
- Water depth : 161.5m
- Member elevation : -12m
- Member type : Face to face horizontal bracing
- Range of diameters : 800-1960mm
- Generated designs : 30
- Axial load : 15-25 MN

Figure H.3 illustrates the variation in C_d over the 10-year period for the two scenarios. The initial C_d (year 0) is the recommended value by D.n.V. for k/D=0.01. During the first two years C_d is approximately the same in both cases. Kelp causes higher during years 3 to 5 and from year 6 onwards slightly higher drag forces are experienced by the mussel dominated member. This is due to high relative roughness when the member is covered by multiple layers of mussels. By year 8, a fairly steady state is reached in both scenarios.

Some points of interest that emerged from this case study are as follows:

a) The variation in shell thickness with member diameter is shown in Figure H.4 for several marine growth conditions. As expected, with more severe fouling higher strength is required, hence thicker pipes. For each fouling condition, shell thickness initially decreases with increasing D until it reaches a more or less steady plateau at a certain diameter range. At a larger D the strength constraints are no longer satisfied and stiffening is required to prevent buckling.

b) Drag loading increases linearly with member diameter. Figure H.5 shows that drag increases by 32% for algal and barnacle cover, by 72% for full mussel cover and by up to 142% for kelp. These percentage increases are direct consequences of the higher C_d applied to each roughness condition.

c) Whilst drag load is doubled when diameter is doubled the total hydrodynamic loading is not, simply because the inertia part in Morison's equation includes a square diameter term. The total load variation with C_d is illustrated in Figure H.6 for D=800mm and 1600mm and for various marine growth conditions (it is noted that C_d is normalised by the D.n.V. value). It can be seen that the lower the member diameter, the higher the total load increase.

d) As a result of higher loads thicker tubulars are required and material and fabrication costs are bound to increase. Material cost increases with member diameter despite the fact that shell thickness reduces for equivalent designs (Figure H.7). However, fabrication cost does reduce because the relative effect of thickness, principally on welding cost, is greater than the effect

of larger diameter. For clarity purposes the fabrication cost variation shown in Figure H.7 has been magnified by a factor of 10, but it also implies that in gross percentage terms any savings in fabrication costs would have little impact on total production costs. Figure H.8 clearly illustrates the strong correlation of material and total production costs for three marine growth conditions. The interesting aspect of the total production cost curves is that for each fouling condition there is a minimum cost design. That is, for the D.n.V. force coefficients the "minimum cost" design diameter is 1040mm, whilst for the member fully covered by mussels or kelp the optima are 1160mm and 1120mm respectively.

e) The above apply to designs where projected cleaning requirements were not considered. If cleaning costs were introduced to the model, the total cost, of production and maintenance this time, would increase linearly in percentage terms. This because cleaning is expressed only as a function of surface area. However, it may still provide a fair indicator for asseessing the cost effectiveness of alternative designs. Figure H.9 shows the effects on C_d by of a cleaning strategy for a "clean at regular intervals" design option, i.e. for a light tubular member. According to Scenario A, the maximum design loading would be reached by year 5 or 6 during which time period the member would be cleaned. Over a 25-year platform life the fouling development cycle could be repeated four more times. The total cleaning effort would increase the overall cost by 22%, which if discounted to the time of fabrication would reduce slightly. Alternatively, a "no cleaning" design option, i.e. a heavy tubular member, would have enough loading capacity to ensure that cleaning would be required only in the event of marine fouling exceeding the terminal fouling conditions as stipulated by the marine growth scenario. First costs for the heavier design would be 7% higher than for the "clean at regular intervals" option. However, the latter would incur cleaning costs which would make it a more costly option after one or, if costs were discounted, two cleaning sessions.

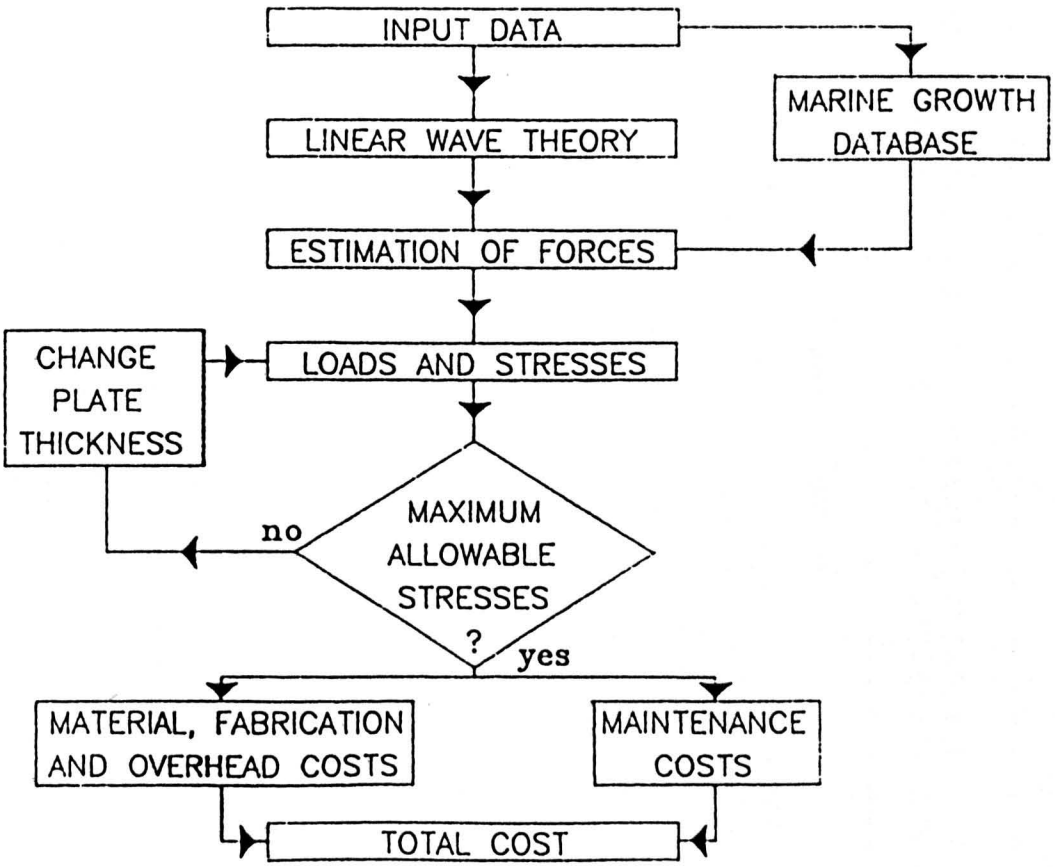

Fig. H.1. Structure of the computer model.

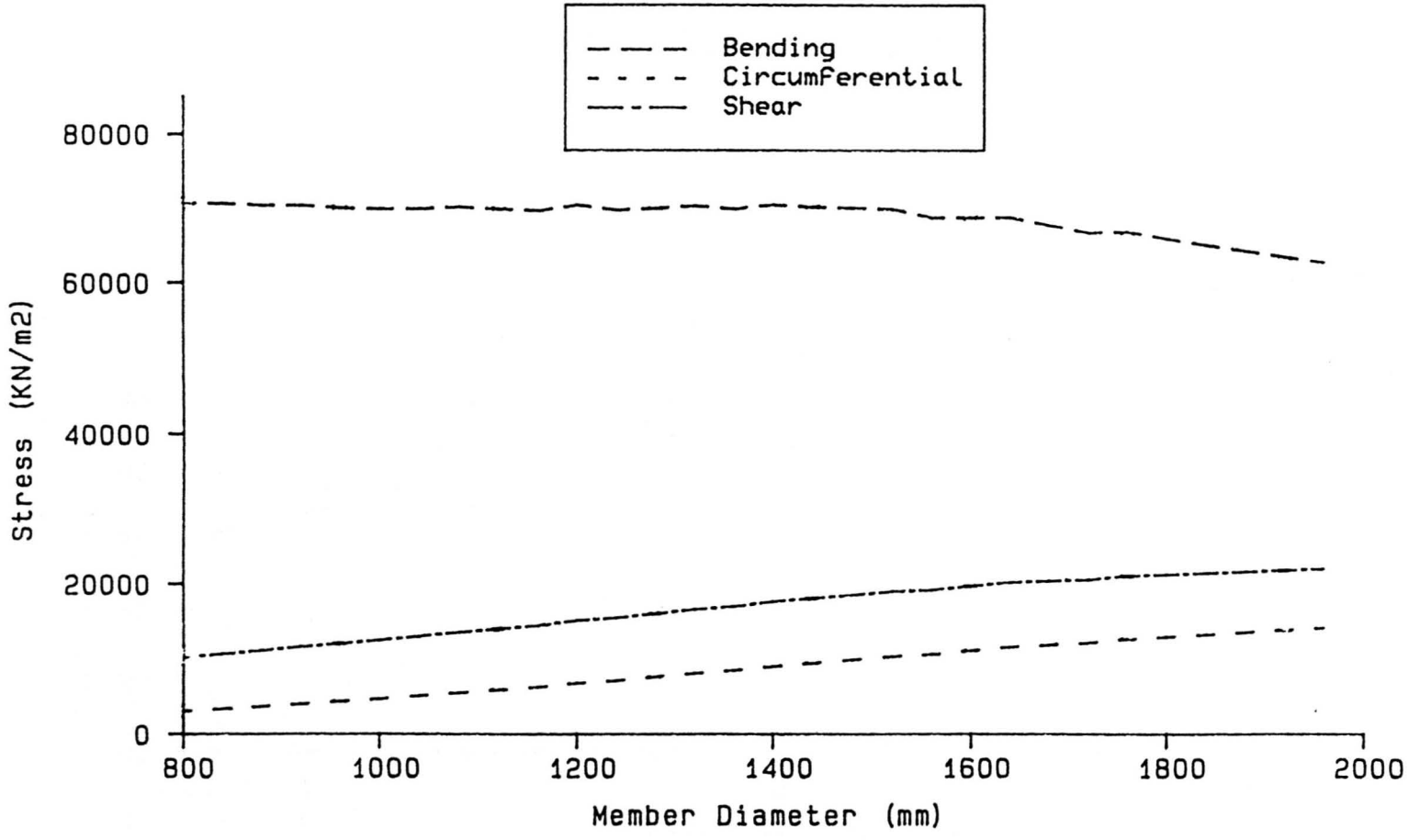

Fig.H.2. Variation of local stresses with member diameter
(variable thickness, axial load = 25 MN)

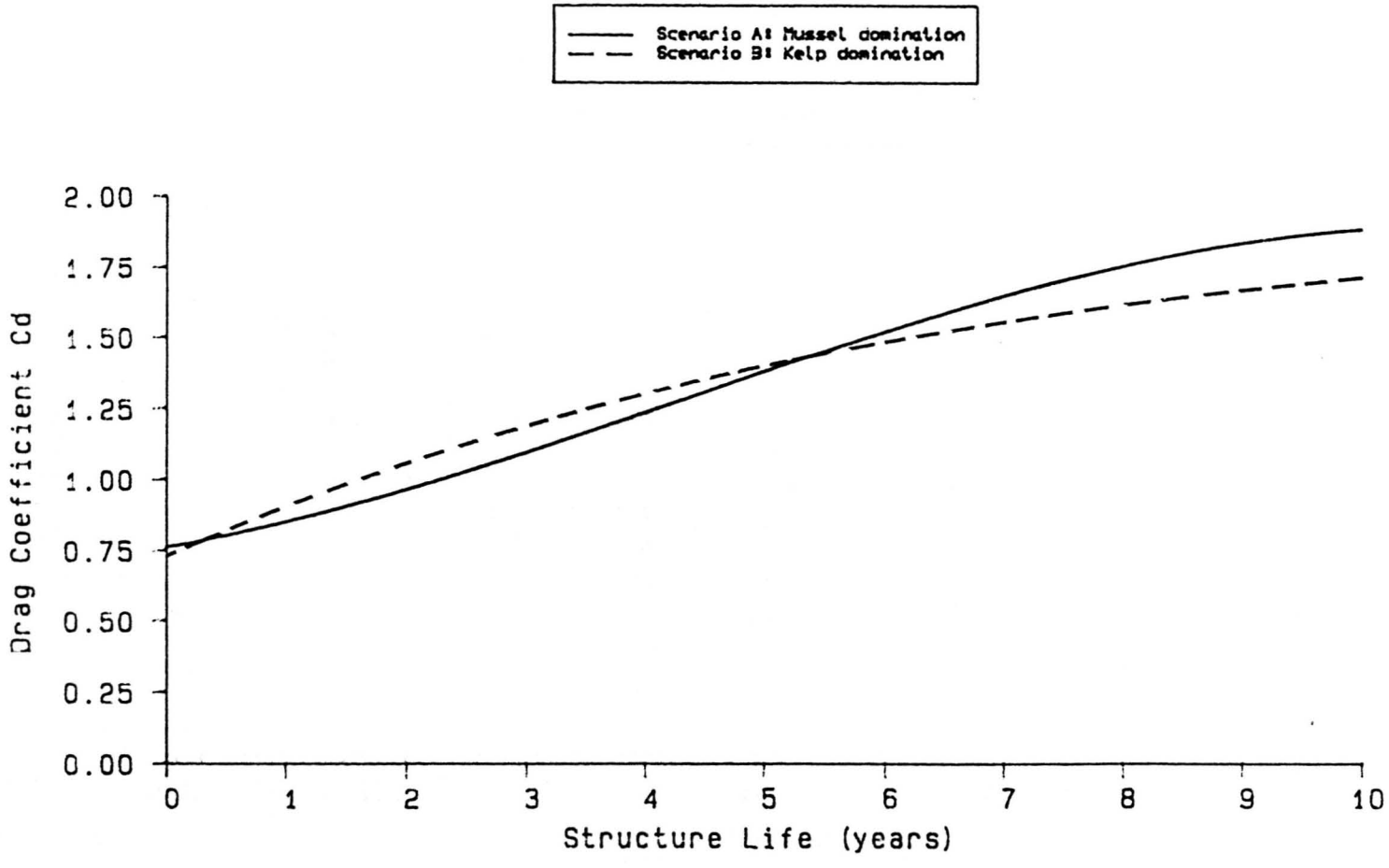

Fig.H.3. Variation of Cd over first ten years of structure life for two dominant marine growth types.

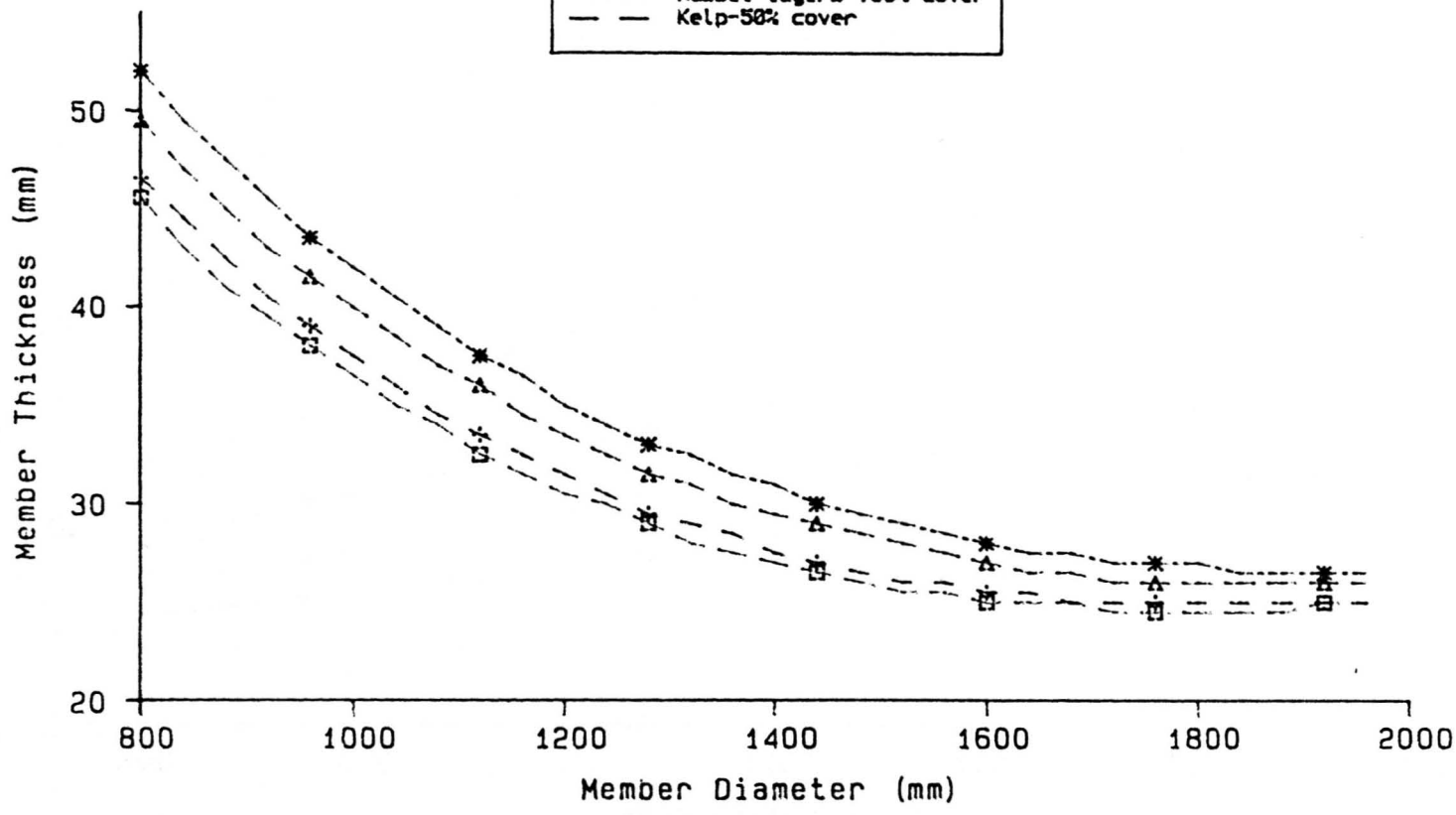

Fig.H.4. Variation of shell thickness with diameter for various marine growth conditions.

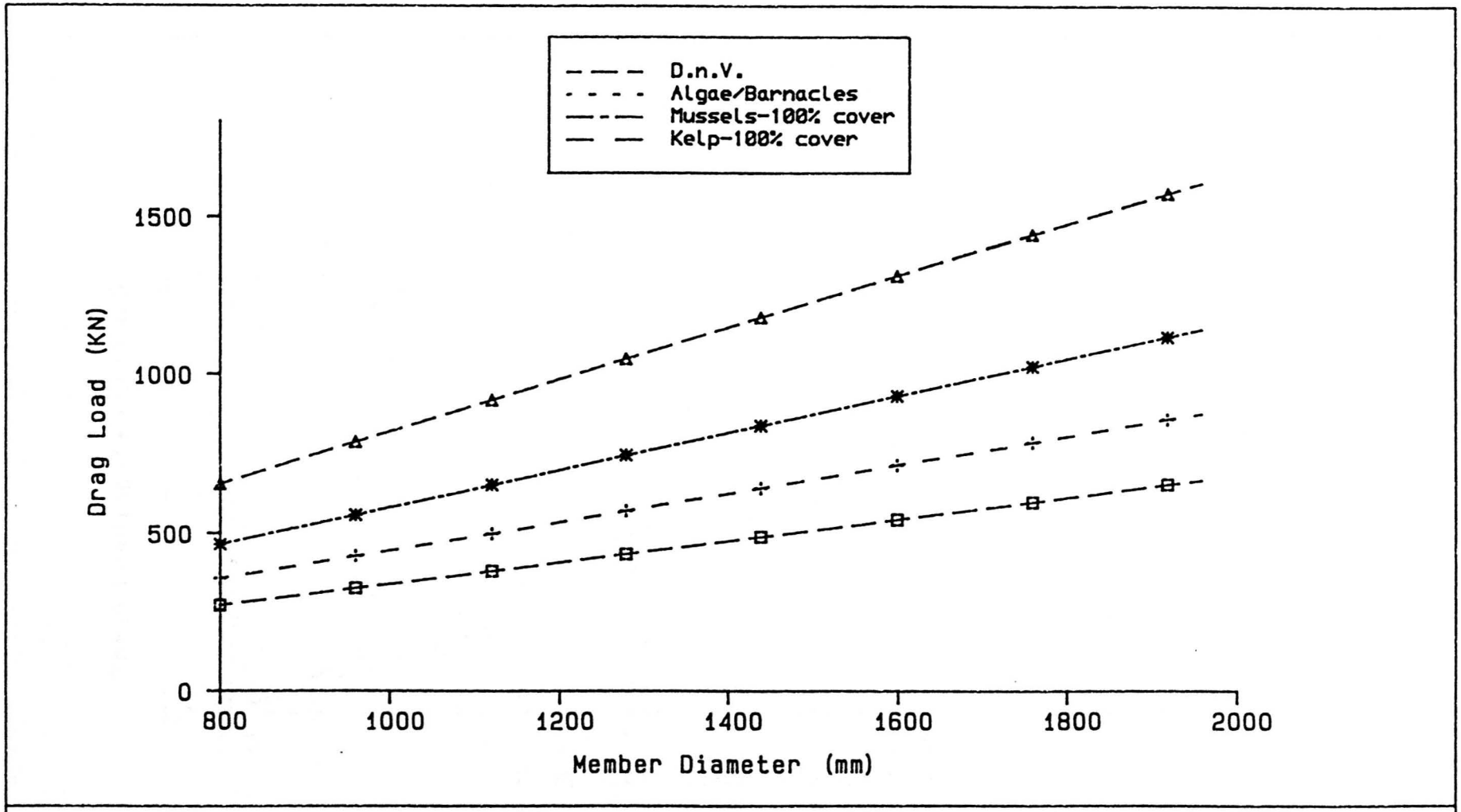

Fig. H.5. Variation of loading due to drag with member diameter.

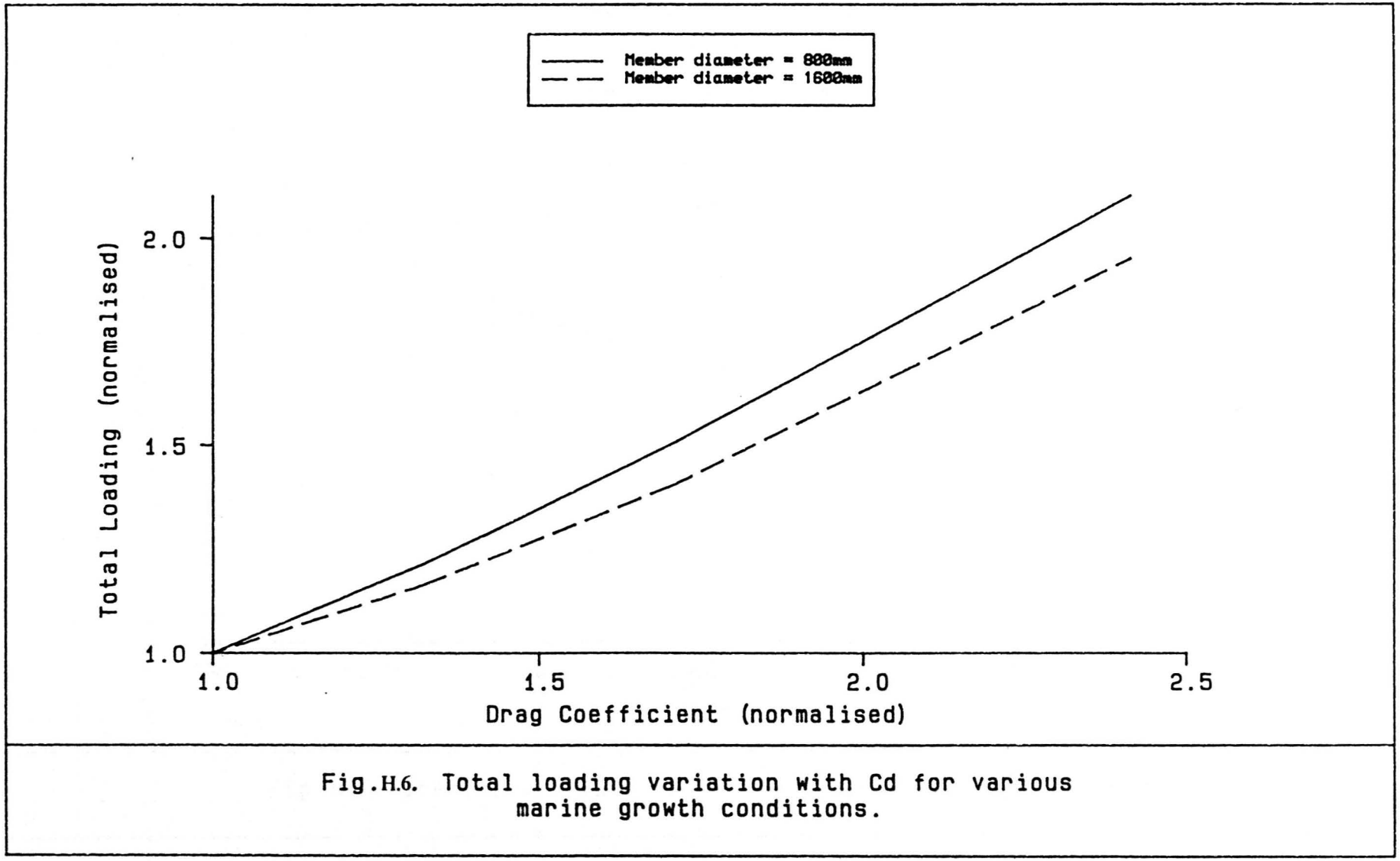

Fig.H.6. Total loading variation with Cd for various marine growth conditions.

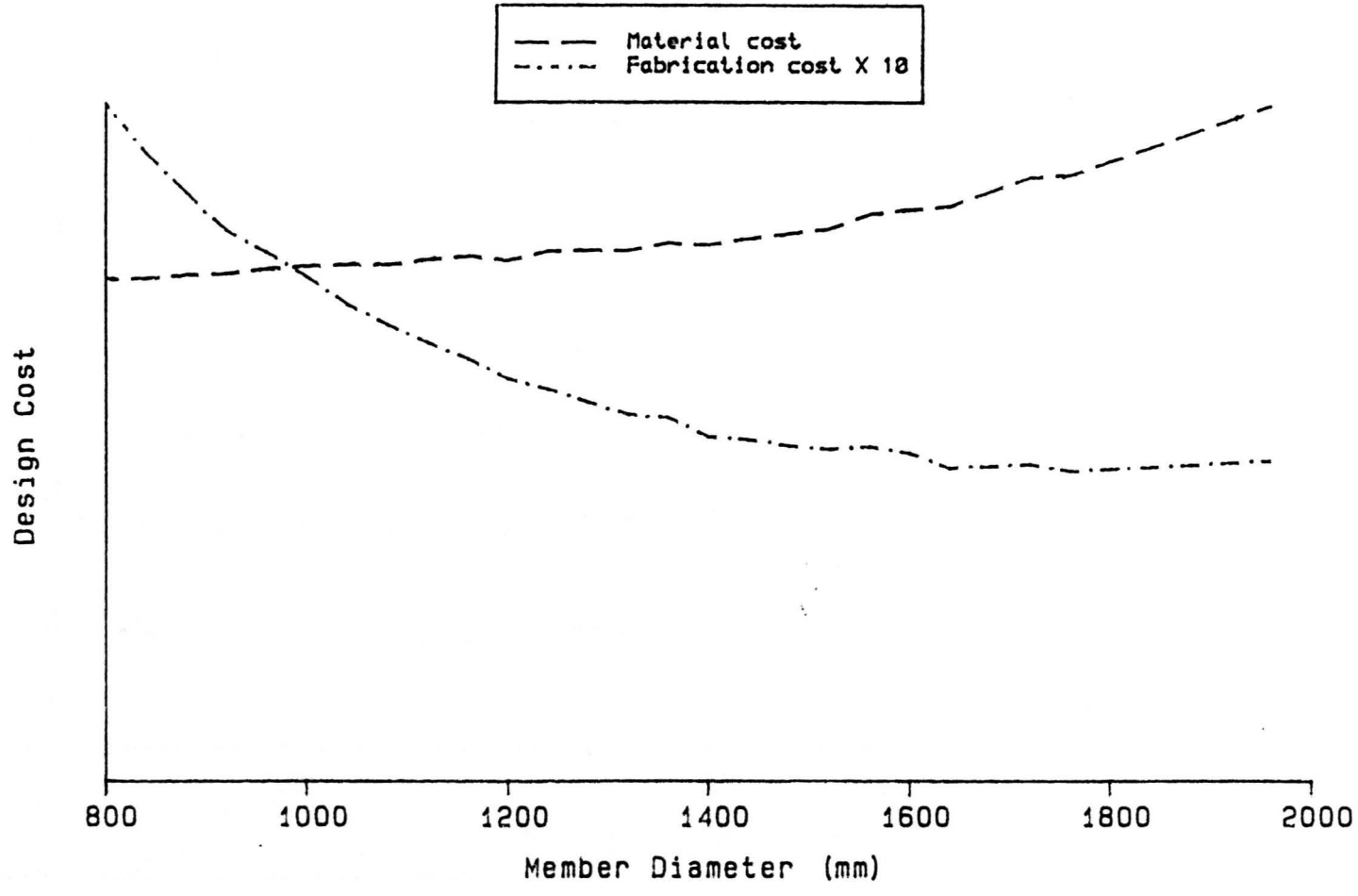

Fig.H.7. Material and fabrication cost variation with diameter.

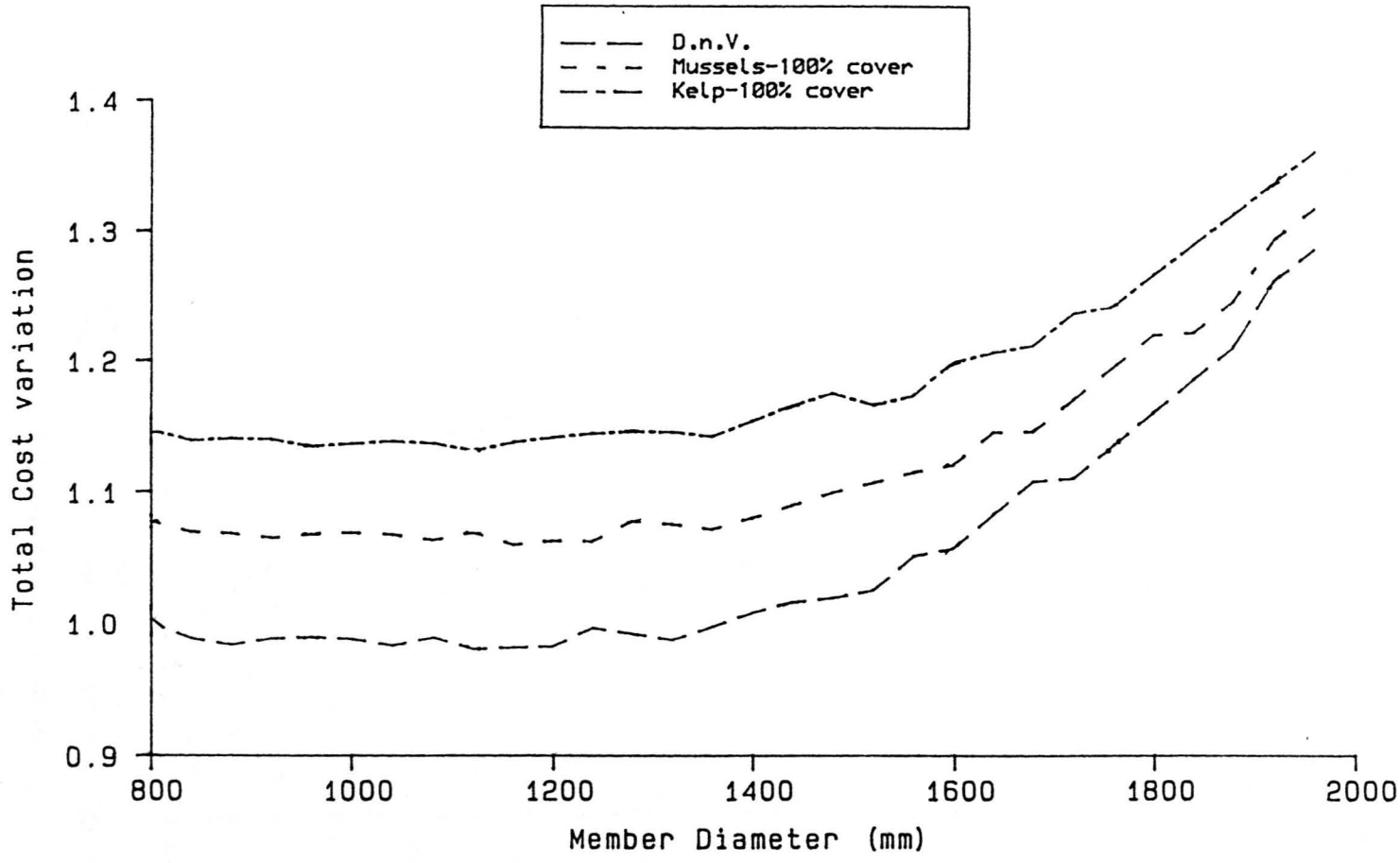

Fig.H.8. Total cost variation with member diameter for three marine growth conditions.

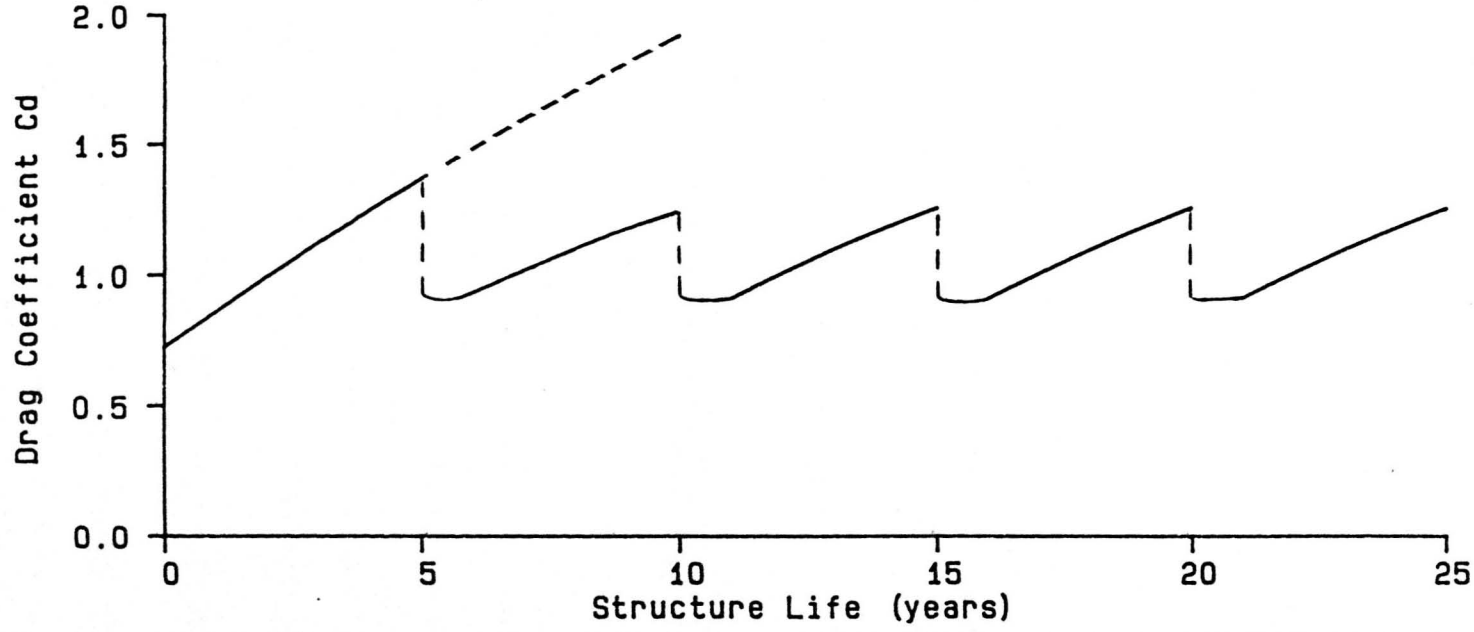

Fig.H.9. Variation in Cd for a regularly cleaned tubular member of a platform with 25 years operational life.